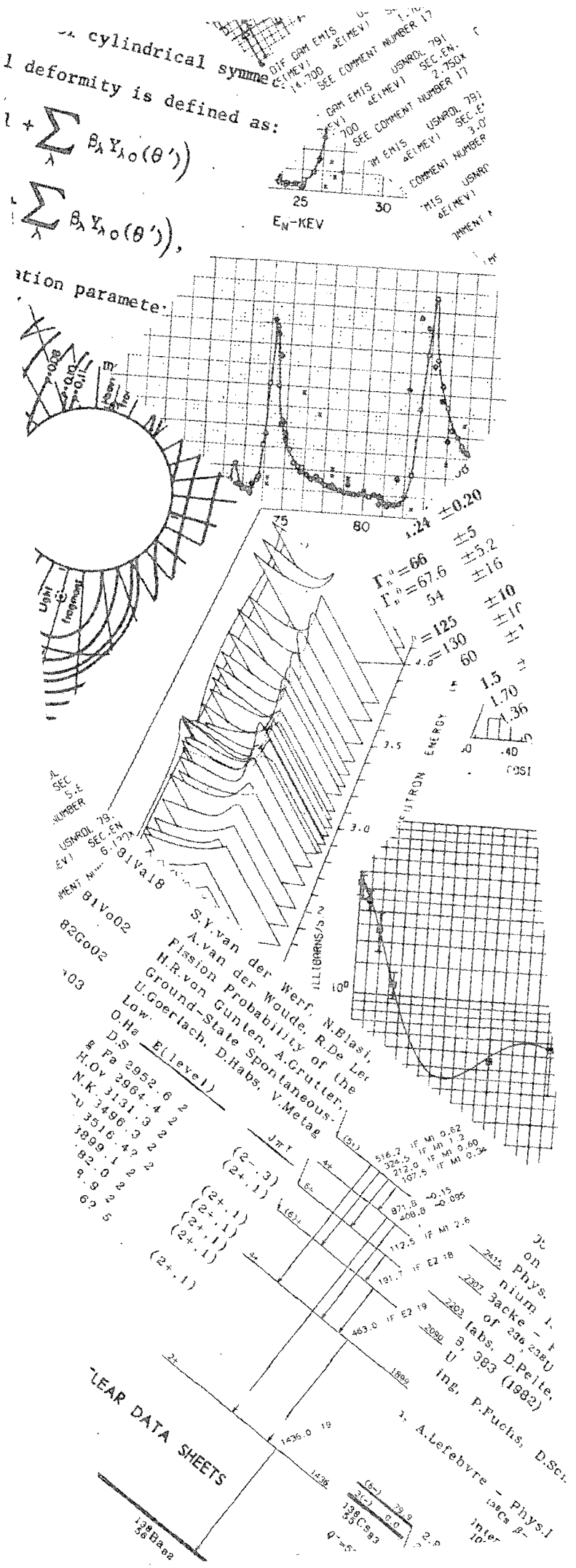

BNL-NCS-34291
DOE/NDC-33/U
NEANDC(US)-218/U
INDC(USA)-93/L
Informal Report
Limited Distribution

REPORTS TO THE DOE NUCLEAR DATA COMMITTEE

Compiled by
NATIONAL NUCLEAR DATA CENTER
for the
U.S. Department of Energy
Nuclear Data Committee

May 1984

BROOKHAVEN NATIONAL LABORATORY
ASSOCIATED UNIVERSITIES
UPTON, LONG ISLAND, NEW YORK 11973

national
nuclear
data
center

BNL-NCS-34291
DOE/NDC-33/U
NEANDC(US)-218/U
INDC(USA)-93/L
Informal Report
Limited Distribution

REPORTS TO

THE DOE NUCLEAR DATA COMMITTEE

MAY 1984

Compiled by the

NATIONAL NUCLEAR DATA CENTER
BROOKHAVEN NATIONAL LABORATORY
ASSOCIATED UNIVERSITIES, INC.

UNDER CONTRACT NO. DE-AC02-76CH00016 WITH THE
UNITED STATES DEPARTMENT OF ENERGY

Printed in the United States of America
Available from
National Technical Information Service
U.S. Department of Commerce
5285 Port Royal Road
Springfield, VA 22161

NTIS price codes:
Printed Copy: A10; Microfiche Copy: A01

TABLE OF CONTENTS

TABLE OF CONTENTS (cont.)

PREFACE

The reports in this document were submitted to the Department of Energy, Nuclear Data Committee (DOE-NDC) in April, 1984. The reporting laboratories are those with a substantial program for the measurement of neutron and nuclear cross sections of relevance to the U.S. applied nuclear energy program.

The authors of the Status Report contributions are responsible for collecting and editing individual contributions from their laboratory and are not necessarily the sole authors of the contributions. The scientists responsible for the work described in each individual contributions are listed at the beginning of the contribution.

The material contained in these reports is to be regarded as comprised of informal statements of recent developments and preliminary data. Persons wishing to make use of these data should contact the individual experimenter for further details. The data which appear in this document should be quoted only by permission of the contributor and should be referenced as private communication, and not by this document number. Appropriate subjects are listed as follows:

1. Microscopic neutron cross sections relevant to the nuclear energy program, including shielding. Inverse reactions where pertinent are included.

2. Charged-particle cross sections, where they are relevant to (1.) above, and where relevant to developing and testing nuclear models.

3. Gamma ray production, radioactive decay, and theoretical developments in nuclear structure which are applicable to nuclear energy programs.

4. Proton and alpha-particle cross sections, at energies of up to 1 GeV, which are of interest to the space program.

These reports cannot be regarded as a complete summary of the nuclear research efforts in the U.S. A number of laboratories whose research is less programmatically oriented do not submit reports; neither do the submitted reports reflect all the work related to nuclear data in progress at the submitting laboratory.

This compilation has been produced almost completely from master copies prepared by the individual contributors listed in the Table of Contents, and reports are reproduced without change from these master copies.

The CINDA-type index which follows the Table of Contents was prepared by Norman E. Holden of the National Nuclear Data Center, Brookhaven National Laboratory, Upton, Long Island, New York.

NEUTRON DATA REFERENCES

Element	Quantity	Energy (eV) Min	Max	Type	Documentation Ref	Page	Date	Lab	Comments
Li	$\sigma_{n,\alpha}$	1.5+7		Expt	DOE-NDC-33	173	Apr84	AI	Kneff+ TBL. EN=14.8 MEV.
^{6}Li	σ_{el}	NDG		Eval	DOE-NDC-33	11	Apr84	ANL	Poenitz. SIMULTANEOUS EVAL. ENDF-VI.
^{6}Li	$\sigma_{el}(\theta)$		6.0+6	Eval	DOE-NDC-33	162	Apr84	OHO	Knox+ R-MATRIX STUDY. NDG.
^{6}Li	$\sigma_{el}(\theta)$	7.0+6	1.5+7	Expt	DOE-NDC-33	177	Apr84	TNL	Byrd+ NDG. PR/C TBP.
^{6}Li	$\sigma_{dif.inl}$		6.0+6	Eval	DOE-NDC-33	162	Apr84	OHO	Knox+ R-MATRIX STUDY. NDG.
^{6}Li	$\sigma_{n,2n}$	1.5+7		Expt	DOE-NDC-33	173	Apr84	AI	Kneff+ TBL. MEAS (N,ALPHA) CS.
^{6}Li	$\sigma_{n,p}$	6.0+7		Expt	DOE-NDC-33	42	Apr84	DAV	Brady+ TBL. ANG DIST.
^{6}Li	$\sigma_{n,nd}$		6.0+6	Eval	DOE-NDC-33	162	Apr84	OHO	Knox+ R-MATRIX STUDY. NDG.
^{6}Li	$\sigma_{n,nd}$	1.5+7		Expt	DOE-NDC-33	173	Apr84	AI	Kneff+ TBL. MEAS (N,ALPHA) CS.
^{6}Li	$\sigma_{n,t}$	1.5+7		Expt	DOE-NDC-33	86	Apr84	LRL	Goldberg+ CS = 515+-26 MB.
^{6}Li	$\sigma_{n,t}$		6.0+6	Eval	DOE-NDC-33	162	Apr84	OHO	Knox+ R-MATRIX STUDY. NDG.
^{6}Li	$\sigma_{n,t}$	1.5+7		Expt	DOE-NDC-33	173	Apr84	AI	Kneff+ TBL. MEAS (N,ALPHA) CS.
^{6}Li	$\sigma_{n,t}$	NDG		Eval	DOE-NDC-33	11	Apr84	ANL	Poenitz. SIMULTANEOUS EVAL. ENDF-VI.
^{7}Li	$\sigma_{el}(\theta)$		4.0+6	Eval	DOE-NDC-33	162	Apr84	OHO	Knox+ R-MATRIX STUDY. NDG.
^{7}Li	$\sigma_{el}(\theta)$	7.0+6	1.5+7	Expt	DOE-NDC-33	177	Apr84	TNL	Byrd+ NDG. PR/C TBP.
^{7}Li	$\sigma_{dif.inl}$		4.0+6	Eval	DOE-NDC-33	162	Apr84	OHO	Knox+ R-MATRIX STUDY. NDG.
^{7}Li	$\sigma_{n,X\gamma}$	2.0+5	4.0+7	Expt	DOE-NDC-33	144	Apr84	ORL	Larson+ ANALYSIS TBC.
^{7}Li	$\sigma_{n,2n}$	1.5+7		Expt	DOE-NDC-33	173	Apr84	AI	Kneff+ TBL. MEAS (N,ALPHA) CS.
^{7}Li	$\sigma_{n,p}$	6.0+7		Expt	DOE-NDC-33	42	Apr84	DAV	Brady+ TBL. ANG DIST.
^{7}Li	$\sigma_{n,nt}$	1.5+7		Expt	DOE-NDC-33	173	Apr84	AI	Kneff+ TBL. MEAS (N,ALPHA) CS.
^{7}Li	$\sigma_{n,\alpha}$	1.5+7		Expt	DOE-NDC-33	86	Apr84	LRL	Goldberg+ CS = 334+-17 MB.
^{9}Be	σ_{tot}	2.0-3	5.0+0	Expt	DOE-NDC-33	139	Apr84	ORL	Harvey+ CRYSTAL EFFECTS.
^{9}Be	$\sigma_{el}(\theta)$	1.1+7	1.7+7	Expt	DOE-NDC-33	177	Apr84	TNL	Byrd+ GRPH.
^{9}Be	$\sigma_{el}(\theta)$	7.0+6	1.5+7	Expt	DOE-NDC-33	177	Apr84	TNL	Byrd+ NDG. PR/C TBP.
^{9}Be	$\sigma_{el}(\theta)$	NDG		Expt	DOE-NDC-33	183	Apr84	TNL	Anderson+ FWD ANG, 1.5-9 DEGS.
^{9}Be	$\sigma_{el}(\theta)$	1.7+7		Expt	DOE-NDC-33	185	Apr84	TNL	Byrd+ NDG.
^{9}Be	$\sigma_{el}(\theta)$	1.5+6	1.0+7	Exth	DOE-NDC-33	2	Apr84	ANL	Smith+ NDG.
^{9}Be	σ_{pol}	1.7+7		Expt	DOE-NDC-33	185	Apr84	TNL	Byrd+ NDG.
^{9}Be	$\sigma_{dif.inl}$	NDG		Expt	DOE-NDC-33	183	Apr84	TNL	Anderson+ FWD ANG, 1.5-9 DEGS.
^{9}Be	$\sigma_{n,\alpha}$	1.5+7		Expt	DOE-NDC-33	173	Apr84	AI	Kneff+ TBL. EN=14.8 MEV.
B	$\sigma_{n,\alpha}$	1.5+7		Expt	DOE-NDC-33	173	Apr84	AI	Kneff+ TBL. EN=14.8 MEV.
^{10}B	σ_{el}	NDG		Eval	DOE-NDC-33	11	Apr84	ANL	Poenitz. SIMULTANEOUS EVAL. ENDF-VI.
^{10}B	$\sigma_{el}(\theta)$	7.0+6	1.5+7	Expt	DOE-NDC-33	177	Apr84	TNL	Byrd+ NDG. PR/C TBP.

NEUTRON DATA REFERENCES

Element	Quantity	Energy (eV) Min	Max	Type	Documentation Ref	Page	Date	Lab	Comments
^{10}B	$\sigma_{n,X\gamma}$	2.0+5	4.0+7	Expt	DOE-NDC-33	144	Apr84	ORL	Larson+ TBD.
^{10}B	$\sigma_{n,\alpha}$	1.0-2	3.0+4	Expt	DOE-NDC-33	146	Apr84	ORL	Gwin+ REL 235U, 239PU (N,F).
^{10}B	$\sigma_{n,\alpha}$	1.5+7		Expt	DOE-NDC-33	173	Apr84	AI	Kneff+ TBL. EN=14.8 MEV.
^{10}B	$\sigma_{n,\alpha}$	NDG		Eval	DOE-NDC-33	11	Apr84	ANL	Poenitz. SIMULTANEOUS EVAL. ENDF-VI.
^{11}B	$\sigma_{el}(\theta)$	7.0+6	1.5+7	Expt	DOE-NDC-33	177	Apr84	TNL	Byrd+ NDG. PR/C TBP.
^{11}B	$\sigma_{n,X\gamma}$	2.0+5	4.0+7	Expt	DOE-NDC-33	144	Apr84	ORL	Larson+ TBD.
^{11}B	$\sigma_{n,\alpha}$	1.5+7		Expt	DOE-NDC-33	173	Apr84	AI	Kneff+ TBL. EN=14.8 MEV.
^{12}C	σ_{tot}	2.0-3	5.0+0	Expt	DOE-NDC-33	139	Apr84	ORL	Harvey+ CRYSTAL EFFECTS.
^{12}C	σ_{el}	1.4+7	1.5+7	Expt	DOE-NDC-33	86	Apr84	LRL	Haight+ EN = 13.5 - 14.6 MEV.
^{12}C	$\sigma_{el}(\theta)$	1.4+7	1.5+7	Expt	DOE-NDC-33	86	Apr84	LRL	Haight+ EN = 13.5 - 14.6 MEV.
^{12}C	$\sigma_{el}(\theta)$	2.0+7	2.6+7	Eval	DOE-NDC-33	163	Apr84	OHO	Meigooni+ CC CALC. NDG.
^{12}C	$\sigma_{el}(\theta)$	2.0+7	2.6+7	Eval	DOE-NDC-33	163	Apr84	OHO	Petler+ OPTMDL ANALYSIS NDG.
^{12}C	$\sigma_{el}(\theta)$	7.0+6	1.5+7	Expt	DOE-NDC-33	177	Apr84	TNL	Byrd+ NDG. PR/C TBP.
^{12}C	$\sigma_{el}(\theta)$	NDG		Expt	DOE-NDC-33	183	Apr84	TNL	Anderson+ FWD ANG, 1.5-9 DEGS.
^{12}C	$\sigma_{el}(\theta)$	1.7+7		Expt	DOE-NDC-33	185	Apr84	TNL	Byrd+ NDG.
^{12}C	σ_{pol}	1.7+7		Expt	DOE-NDC-33	185	Apr84	TNL	Byrd+ NDG.
^{12}C	$\sigma_{dif.inl}$	1.4+7	1.5+7	Expt	DOE-NDC-33	86	Apr84	LRL	Haight+ EN = 13.5 - 14.6 MEV.
^{12}C	$\sigma_{dif.inl}$	2.0+7	2.6+7	Eval	DOE-NDC-33	163	Apr84	OHO	Meigooni+ CC CALC. NDG.
^{12}C	$\sigma_{dif.inl}$	NDG		Expt	DOE-NDC-33	183	Apr84	TNL	Anderson+ FWD ANG, 1.5-9 DEGS.
^{12}C	$\sigma_{n,\alpha}$	1.5+7		Expt	DOE-NDC-33	173	Apr84	AI	Kneff+ TBL. EN=14.8 MEV.
^{12}C	$\sigma_{n,n\alpha}$	1.4+7	1.5+7	Eval	DOE-NDC-33	86	Apr84	LRL	Haight+ FROM SCAT. MEAS. + TOT.
^{13}C	$\sigma_{el}(\theta)$	2.0+7	2.6+7	Eval	DOE-NDC-33	163	Apr84	OHO	Petler+ OPTMDL ANALYSIS NDG.
^{13}C	$\sigma_{el}(\theta)$	7.0+6	1.5+7	Expt	DOE-NDC-33	177	Apr84	TNL	Byrd+ NDG. PR/C TBP.
^{14}N	$\sigma_{el}(\theta)$	1.1+7	1.7+7	Expt	DOE-NDC-33	177	Apr84	TNL	Byrd+ GRPH.
^{16}O	$\sigma_{el}(\theta)$	2.0+7	2.6+7	Expt	DOE-NDC-33	158	Apr84	OHO	Islam+ NDG. ANALYSIS TBC.
^{16}O	$\sigma_{el}(\theta)$	7.0+6	1.5+7	Expt	DOE-NDC-33	177	Apr84	TNL	Byrd+ NDG. PR/C TBP.
^{16}O	$\sigma_{dif.inl}$	2.0+7	2.6+7	Expt	DOE-NDC-33	158	Apr84	OHO	Islam+ NDG. ANALYSIS TBC.
^{16}O	$\sigma_{n,\alpha}$	1.5+7		Expt	DOE-NDC-33	173	Apr84	AI	Kneff+ TBL. EN=14.8 MEV.
^{18}O	$\sigma_{el}(\theta)$	5.0+6	7.5+6	Expt	DOE-NDC-33	158	Apr84	OHO	Koehler+ NDG. 20-160 DEGS.
^{18}O	$\sigma_{el}(\theta)$	5.0+6	7.5+6	Expt	DOE-NDC-33	164	Apr84	OHO	Koehler+ MEAS. R-MATRIX ANAL. NDG.
^{18}O	$\sigma_{dif.inl}$	5.0+6	7.5+6	Expt	DOE-NDC-33	158	Apr84	OHO	Koehler+ NDG. 20-160 DEGS.
^{18}O	$\sigma_{dif.inl}$	8.7+6	1.1+7	Expt	DOE-NDC-33	164	Apr84	OHO	Koehler+ MEAS. R-MATRIX ANAL. NDG.
^{19}F	$\sigma_{n,\alpha}$	1.5+7		Expt	DOE-NDC-33	173	Apr84	AI	Kneff+ TBL. EN=14.8 MEV.

NEUTRON DATA REFERENCES

Element	Quantity	Energy (eV) Min	Max	Type	Documentation Ref	Page	Date	Lab	Comments
^{27}Al	$\sigma_{el}(\theta)$	1.1+7	1.7+7	Expt	DOE-NDC-33	180	Apr84	TNL	Byrd+ ANG DIST. GRPH.
^{27}Al	$\sigma_{dif.inl}$	1.1+7	1.7+7	Expt	DOE-NDC-33	180	Apr84	TNL	Byrd+ ANG DIST. GRPH.
^{27}Al	$\sigma_{n,2n}$	1.4+7	1.5+7	Expt	DOE-NDC-33	8	Apr84	ANL	Smither+ GRPH. PROD.CS. META,GND ST.
^{27}Al	$\sigma_{n,\alpha}$	1.5+7		Expt	DOE-NDC-33	173	Apr84	AI	Kneff+ TBL. EN=14.8 MEV.
Si	σ_{tot}	2.0-3	5.0+0	Expt	DOE-NDC-33	139	Apr84	ORL	Harvey+ CRYSTAL EFFECTS.
^{28}Si	$\sigma_{el}(\theta)$	1.7+7		Expt	DOE-NDC-33	180	Apr84	TNL	Byrd+ NDG. USED IN CC-CALC.
^{28}Si	$\sigma_{el}(\theta)$	1.7+7		Expt	DOE-NDC-33	185	Apr84	TNL	Byrd+ NDG.
^{28}Si	σ_{pol}	1.7+7		Expt	DOE-NDC-33	185	Apr84	TNL	Byrd+ NDG.
^{28}Si	$\sigma_{dif.inl}$	1.7+7		Expt	DOE-NDC-33	180	Apr84	TNL	Byrd+ NDG. USED IN CC-CALC.
^{32}S	$\sigma_{el}(\theta)$	1.7+7		Expt	DOE-NDC-33	180	Apr84	TNL	Byrd+ NDG. USED IN CC-CALC.
^{32}S	$\sigma_{el}(\theta)$	1.7+7		Expt	DOE-NDC-33	185	Apr84	TNL	Byrd+ NDG.
^{32}S	σ_{pol}	1.7+7		Expt	DOE-NDC-33	185	Apr84	TNL	Byrd+ NDG.
^{32}S	$\sigma_{dif.inl}$	1.7+7		Expt	DOE-NDC-33	180	Apr84	TNL	Byrd+ NDG. USED IN CC-CALC.
^{33}S	Res.Params.	NDG		Expt	DOE-NDC-33	143	Apr84	ORL	Coddens+ WN, WG, WA MEAS. NDG.
^{34}S	σ_{tot}	9.0+4	1.5+6	Expt	DOE-NDC-33	138	Apr84	ORL	Carlton+ NDG.
^{34}S	$\sigma_{el}(\theta)$	2.2+7		Expt	DOE-NDC-33	159	Apr84	OHO	Alarcon+ EN=21.7 MEV. NDG.
^{34}S	$\sigma_{dif.inl}$	2.2+7		Expt	DOE-NDC-33	159	Apr84	OHO	Alarcon+ EN=21.7 MEV. NDG.
^{34}S	$\sigma_{n,\gamma}$	3.0+4	1.1+6	Expt	DOE-NDC-33	138	Apr84	ORL	Carlton+ NDG.
Cl	$\sigma_{n,\gamma}$	NDG		Expt	DOE-NDC-33	140	Apr84	ORL	Macklin. NDG.
^{35}Cl	$\sigma_{n,\gamma}$	3.0+4		Expt	DOE-NDC-33	140	Apr84	ORL	Macklin. CALC FROM CL-37, NAT.
^{35}Cl	Res.Params.	4.0+3	2.3+5	Expt	DOE-NDC-33	140	Apr84	ORL	Macklin. 54 RES. NDG.
^{37}Cl	$\sigma_{n,\gamma}$	NDG		Expt	DOE-NDC-33	140	Apr84	ORL	Macklin. NDG. CS(30KEV)=2.15+-.08MB.
^{37}Cl	Res.Params.	8.0+3	1.5+5	Expt	DOE-NDC-33	140	Apr84	ORL	Macklin. 12 RES. NDG.
Ca	σ_{tot}	+3	2.0+7	Expt	DOE-NDC-33	1	Apr84	ANL	Poenitz+ NDG. TB ANALYZED.
^{40}Ca	$\sigma_{el}(\theta)$	2.2+7		Expt	DOE-NDC-33	159	Apr84	OHO	Alarcon+ EN=21.7 MEV. NDG.
^{40}Ca	$\sigma_{el}(\theta)$	1.7+7		Expt	DOE-NDC-33	181	Apr84	TNL	Byrd+ NDG.
^{40}Ca	$\sigma_{el}(\theta)$	1.7+7		Expt	DOE-NDC-33	185	Apr84	TNL	Byrd+ NDG.
^{40}Ca	σ_{pol}	1.7+7		Expt	DOE-NDC-33	185	Apr84	TNL	Byrd+ NDG.
^{40}Ca	$\sigma_{dif.inl}$	2.2+7		Expt	DOE-NDC-33	159	Apr84	OHO	Alarcon+ EN=21.7 MEV. NDG.
^{40}Ca	$\sigma_{dif.inl}$	1.4+7		Expt	DOE-NDC-33	181	Apr84	TNL	Byrd+ NDG.
^{46}Ca	$\sigma_{n,\gamma}$	2.5+4		Expt	DOE-NDC-33	87	Apr84	KFK	Mathews+ CS = 6.4+-0.5 MB.
^{48}Ca	$\sigma_{n,\gamma}$	2.5+4		Expt	DOE-NDC-33	87	Apr84	KFK	Mathews+ CS = 1.9+-0.5 MB.
^{45}Sc	σ_{tot}	2.0+3		Expt	DOE-NDC-33	148	Apr84	ORL	Harvey+ CS = 0.35+-0.03 B.

NEUTRON DATA REFERENCES

Element	Quantity	Energy (eV) Min	Max	Type	Documentation Ref	Page	Date	Lab	Comments
^{45}Sc	σ_{tot}	+3	2.0+7	Expt	DOE-NDC-33	1	Apr84	ANL	Poenitz+ NDG.
Ti	σ_{tot}	+3	2.0+7	Expt	DOE-NDC-33	1	Apr84	ANL	Poenitz+ NDG. TB ANALYZED.
Ti	$\sigma_{n,\alpha}$	1.5+7		Expt	DOE-NDC-33	173	Apr84	AI	Kneff+ TBL. EN=14.8 MEV.
^{51}V	σ_{tot}	+3	2.0+7	Expt	DOE-NDC-33	1	Apr84	ANL	Poenitz+ NDG. TB ANALYZED.
^{51}V	$\sigma_{n,p}$		1.0+7	Expt	DOE-NDC-33	6	Apr84	ANL	Smith+ REPORT TBP.
^{51}V	$\sigma_{n,\alpha}$		1.0+7	Expt	DOE-NDC-33	6	Apr84	ANL	Smith+ ANALYSIS TBD.
Cr	$\sigma_{el}(\theta)$	1.5+6	1.0+7	Exth	DOE-NDC-33	2	Apr84	ANL	Smith+ NDG.
Cr	$\sigma_{n,X\gamma}$	2.0+5	4.0+7	Expt	DOE-NDC-33	144	Apr84	ORL	Larson+ ANALYSIS TBC.
Cr	$\sigma_{n,\alpha}$	1.5+7		Expt	DOE-NDC-33	173	Apr84	AI	Kneff+ TBL. EN=14.8 MEV.
^{52}Cr	σ_{tot}	+4	9.0+5	Expt	DOE-NDC-33	153	Apr84	ORL	Agrawal+ NDG.
^{52}Cr	$\sigma_{n,p}$	1.4+7		Expt	DOE-NDC-33	127	Apr84	MHG	Agrawal+ NDG. TBD.
^{52}Cr	$\langle\Gamma\rangle/D$		9.0+5	Expt	DOE-NDC-33	153	Apr84	ORL	Agrawal+ S0, S1 GIVEN.
^{52}Cr	Lvl Density		9.0+5	Expt	DOE-NDC-33	153	Apr84	ORL	Agrawal+ P-WAVE DENSITY LARGER.
^{53}Cr	$\sigma_{n,X\gamma}$	2.0+5	4.0+7	Expt	DOE-NDC-33	144	Apr84	ORL	Larson+ ANALYSIS TBC.
^{54}Cr	σ_{tot}	+4	9.0+5	Expt	DOE-NDC-33	153	Apr84	ORL	Agrawal+ NDG.
^{54}Cr	$\langle\Gamma\rangle/D$		9.0+5	Expt	DOE-NDC-33	153	Apr84	ORL	Agrawal+ S0, S1 GIVEN.
^{54}Cr	Lvl Density		9.0+5	Expt	DOE-NDC-33	153	Apr84	ORL	Agrawal+ P-WAVE DENSITY LARGER.
^{55}Mn	σ_{tot}	+3	2.0+7	Expt	DOE-NDC-33	1	Apr84	ANL	Poenitz+ NDG. TB ANALYZED.
^{55}Mn	$\sigma_{n,\alpha}$	1.5+7		Expt	DOE-NDC-33	173	Apr84	AI	Kneff+ TBL. EN=14.8 MEV.
Fe	σ_{tot}	2.0-3	5.0+0	Expt	DOE-NDC-33	139	Apr84	ORL	Harvey+ CRYSTAL EFFECTS.
Fe	$\sigma_{el}(\theta)$	1.5+6	1.0+7	Exth	DOE-NDC-33	2	Apr84	ANL	Smith+ NDG.
^{54}Fe	σ_{tot}	NDG		Expt	DOE-NDC-33	5	Apr84	ANL	Smith+ NDG.
^{54}Fe	$\sigma_{el}(\theta)$	8.0+6	1.7+7	Expt	DOE-NDC-33	181	Apr84	TNL	Byrd+ NDG. SIG, ANAL. POWER.
^{54}Fe	$\sigma_{el}(\theta)$	1.7+7		Expt	DOE-NDC-33	185	Apr84	TNL	Byrd+ NDG.
^{54}Fe	$\sigma_{el}(\theta)$	NDG		Expt	DOE-NDC-33	5	Apr84	ANL	Smith+ NDG.
^{54}Fe	σ_{pol}	1.7+7		Expt	DOE-NDC-33	185	Apr84	TNL	Byrd+ NDG.
^{54}Fe	$\sigma_{dif.inl}$	1.1+7	2.6+7	Expt	DOE-NDC-33	160	Apr84	OHO	Mellema+ 2 ENS. NDG.
^{54}Fe	$\sigma_{dif.inl}$	1.1+7	2.6+7	Expt	DOE-NDC-33	164	Apr84	OHO	Mellema+ NDG. DWBA ANALYSIS.
^{54}Fe	$\sigma_{dif.inl}$	8.0+6	1.7+7	Expt	DOE-NDC-33	181	Apr84	TNL	Byrd+ NDG. SIG, ANAL. POWER.
^{54}Fe	$\sigma_{dif.inl}$	NDG		Expt	DOE-NDC-33	5	Apr84	ANL	Smith+ NDG.
^{54}Fe	$\sigma_{n,n'\gamma}$	2.6+6	4.2+6	Expt	DOE-NDC-33	69	Apr84	KTY	Gacsi+ NDG.
^{54}Fe	$\sigma_{n,n'\gamma}$		4.0+6	Expt	DOE-NDC-33	5	Apr84	ANL	Smith+ GRPHS.
^{54}Fe	$\sigma_{n,2n}$	NDG		Expt	DOE-NDC-33	8	Apr84	ANL	Smither+ NDG.

NEUTRON DATA REFERENCES

Element	Quantity	Energy (eV) Min	Max	Type	Documentation Ref	Page	Date	Lab	Comments
^{56}Fe	σ_{tot}	NDG		Expt	DOE-NDC-33	142	Apr84	ORL	Perey+ NDG.
^{56}Fe	$\sigma_{el}(\theta)$	8.0+6	1.7+7	Expt	DOE-NDC-33	181	Apr84	TNL	Byrd+ NDG. SIG, ANAL. POWER.
^{56}Fe	$\sigma_{dif.inl}$	1.1+7	2.6+7	Expt	DOE-NDC-33	160	Apr84	OHO	Mellema+ 2 ENS. NDG.
^{56}Fe	$\sigma_{dif.inl}$	1.1+7	2.6+7	Expt	DOE-NDC-33	164	Apr84	OHO	Mellema+ NDG. DWBA ANALYSIS.
^{56}Fe	$\sigma_{dif.inl}$	8.0+6	1.7+7	Expt	DOE-NDC-33	181	Apr84	TNL	Byrd+ NDG. SIG, ANAL. POWER.
^{56}Fe	$\sigma_{n,n'\gamma}$	3.6+6	4.5+6	Expt	DOE-NDC-33	69	Apr84	KTY	Gacsi+ NDG.
^{56}Fe	$\sigma_{n,X\gamma}$	2.0+5	4.0+7	Expt	DOE-NDC-33	144	Apr84	ORL	Larson+ ANALYSIS TBC.
^{56}Fe	Res.Params.	1.2+3		Expt	DOE-NDC-33	142	Apr84	ORL	Perey+ E0, WG, WN GIVEN.
^{59}Co	σ_{tot}	+3	2.0+7	Expt	DOE-NDC-33	1	Apr84	ANL	Poenitz+ NDG. TB ANALYZED.
^{59}Co	$\sigma_{n,X\gamma}$	2.0+5	4.0+7	Expt	DOE-NDC-33	144	Apr84	ORL	Larson+ TBD.
^{59}Co	$\sigma_{n,\alpha}$	1.4+7		Expt	DOE-NDC-33	127	Apr84	MHG	Agrawal+ NDG. TBD.
Ni	σ_{tot}	+3	2.0+7	Expt	DOE-NDC-33	1	Apr84	ANL	Poenitz+ NDG. TB ANALYZED.
Ni	$\sigma_{el}(\theta)$	1.5+6	1.0+7	Exth	DOE-NDC-33	2	Apr84	ANL	Smith+ NDG.
Ni	$\sigma_{n,X\gamma}$	2.0+5	4.0+7	Expt	DOE-NDC-33	144	Apr84	ORL	Larson+ ANALYSIS TBC.
^{58}Ni	$\sigma_{el}(\theta)$	8.0+6	1.7+7	Expt	DOE-NDC-33	181	Apr84	TNL	Byrd+ NDG. NP TBP.
^{58}Ni	$\sigma_{el}(\theta)$	1.7+7		Expt	DOE-NDC-33	185	Apr84	TNL	Byrd+ NDG.
^{58}Ni	σ_{pol}	1.7+7		Expt	DOE-NDC-33	185	Apr84	TNL	Byrd+ NDG.
^{58}Ni	$\sigma_{dif.inl}$	8.0+6	1.7+7	Expt	DOE-NDC-33	181	Apr84	TNL	Byrd+ NDG. NP TBP.
^{58}Ni	$\sigma_{n,X\gamma}$	2.0+5	4.0+7	Expt	DOE-NDC-33	144	Apr84	ORL	Larson+ ANALYSIS TBC.
^{58}Ni	$\sigma_{n,p}$	6.0+7		Expt	DOE-NDC-33	43	Apr84	DAV	Ullmann+ TBL. SPECTRA, ANG DIST.
^{60}Ni	$\sigma_{el}(\theta)$	8.0+6	1.7+7	Expt	DOE-NDC-33	181	Apr84	TNL	Byrd+ NDG. NP TBP.
^{60}Ni	$\sigma_{dif.inl}$	8.0+6	1.7+7	Expt	DOE-NDC-33	181	Apr84	TNL	Byrd+ NDG. NP TBP.
^{60}Ni	$\sigma_{n,p}$	6.0+7		Expt	DOE-NDC-33	43	Apr84	DAV	Ullmann+ TBL. SPECTRA, ANG DIST.
^{62}Ni	$\sigma_{n,p}$	6.0+7		Expt	DOE-NDC-33	43	Apr84	DAV	Ullmann+ TBL. SPECTRA, ANG DIST.
^{64}Ni	$\sigma_{n,\gamma}$	1.4+4	3.4+4	Expt	DOE-NDC-33	141	Apr84	KFK	Wisshak+ RES. CAPT. NDG.
^{64}Ni	$\sigma_{n,p}$	6.0+7		Expt	DOE-NDC-33	43	Apr84	DAV	Ullmann+ TBL. SPECTRA, ANG DIST.
^{64}Ni	Res.Params.	1.4+4	3.4+4	Expt	DOE-NDC-33	141	Apr84	KFK	Wisshak+ WG(13.9KEV),WG(33.8KEV)GVN.
Cu	σ_{tot}	2.0-3	5.0+0	Expt	DOE-NDC-33	139	Apr84	ORL	Harvey+ CRYSTAL EFFECTS.
Cu	σ_{tot}	+3	2.0+7	Expt	DOE-NDC-33	1	Apr84	ANL	Poenitz+ NDG.
^{63}Cu	σ_{tot}	NDG		Expt	DOE-NDC-33	5	Apr84	ANL	Smith+ NDG.
^{63}Cu	$\sigma_{el}(\theta)$	8.0+6	1.7+7	Expt	DOE-NDC-33	181	Apr84	TNL	Byrd+ NDG. SIG, ANAL. POWER.
^{63}Cu	$\sigma_{el}(\theta)$	NDG		Expt	DOE-NDC-33	5	Apr84	ANL	Smith+ NDG.
^{63}Cu	$\sigma_{dif.inl}$	8.0+6	1.7+7	Expt	DOE-NDC-33	181	Apr84	TNL	Byrd+ NDG. SIG, ANAL. POWER.

NEUTRON DATA REFERENCES

Element	Quantity	Energy (eV) Min	Max	Type	Documentation Ref	Page	Date	Lab	Comments
^{63}Cu	$\sigma_{dif.inl}$	NDG		Expt	DOE-NDC-33	5	Apr84	ANL	Smith+ NDG.
^{63}Cu	$\sigma_{n,n'\gamma}$		2.0+6	Expt	DOE-NDC-33	5	Apr84	ANL	Smith+ NDG.
^{65}Cu	σ_{tot}	NDG		Expt	DOE-NDC-33	5	Apr84	ANL	Smith+ NDG.
^{65}Cu	$\sigma_{el}(\theta)$	8.0+6	1.7+7	Expt	DOE-NDC-33	181	Apr84	TNL	Byrd+ NDG. SIG, ANAL. POWER.
^{65}Cu	$\sigma_{el}(\theta)$	NDG		Expt	DOE-NDC-33	5	Apr84	ANL	Smith+ NDG.
^{65}Cu	$\sigma_{dif.inl}$	8.0+6	1.7+7	Expt	DOE-NDC-33	181	Apr84	TNL	Byrd+ NDG. SIG, ANAL. POWER.
^{65}Cu	$\sigma_{dif.inl}$	NDG		Expt	DOE-NDC-33	5	Apr84	ANL	Smith+ NDG.
^{65}Cu	$\sigma_{n,n'\gamma}$		2.0+6	Expt	DOE-NDC-33	5	Apr84	ANL	Smith+ NDG.
Zn	σ_{tot}	+3	2.0+7	Expt	DOE-NDC-33	1	Apr84	ANL	Poenitz+ NDG.
^{64}Zn	$\sigma_{n,2n}$	1.4+7		Expt	DOE-NDC-33	127	Apr84	MHG	Agrawal+ NDG. TBD.
^{70}Zn	Res.Params.	1.0+4	4.0+5	Expt	DOE-NDC-33	138	Apr84	ORL	Garg+ NDG.
^{70}Zn	$\langle\Gamma\rangle/D$	1.0+4	4.0+5	Expt	DOE-NDC-33	138	Apr84	ORL	Garg+ S0, S1 GIVEN.
Ge	σ_{tot}	+3	2.0+7	Expt	DOE-NDC-33	1	Apr84	ANL	Poenitz+ NDG. TB ANALYZED.
^{76}Se	$\sigma_{el}(\theta)$	8.0+6	1.0+7	Expt	DOE-NDC-33	165	Apr84	OHO	Finlay+ 2 ENS. NDG. CC-ANALYSIS.
^{76}Se	$\sigma_{dif.inl}$	8.0+6	1.0+7	Expt	DOE-NDC-33	165	Apr84	OHO	Finlay+ 2 ENS. NDG. CC-ANALYSIS.
^{80}Se	$\sigma_{el}(\theta)$	8.0+6	1.0+7	Expt	DOE-NDC-33	165	Apr84	OHO	Finlay+ 2 ENS. NDG. CC-ANALYSIS.
^{80}Se	$\sigma_{dif.inl}$	8.0+6	1.0+7	Expt	DOE-NDC-33	165	Apr84	OHO	Finlay+ 2 ENS. NDG. CC-ANALYSIS.
^{89}Y	σ_{tot}	+3	2.0+7	Expt	DOE-NDC-33	1	Apr84	ANL	Poenitz+ GRPH CFD OTH. EXPT.
^{89}Y	σ_{tot}	5.0+5	4.2+6	Expt	DOE-NDC-33	2	Apr84	ANL	Budtz-Jorgensen+ NDG.
^{89}Y	σ_{tot}	8.0+5	4.5+6	Eval	DOE-NDC-33	15	Apr84	ANL	Smith+ MEAS. CS ANALYZE. OPTMDL
^{89}Y	$\sigma_{el}(\theta)$	8.0+6	1.7+7	Expt	DOE-NDC-33	182	Apr84	TNL	Byrd+ NDG.
^{89}Y	$\sigma_{el}(\theta)$	1.7+7		Expt	DOE-NDC-33	185	Apr84	TNL	Byrd+ NDG.
^{89}Y	$\sigma_{el}(\theta)$	1.5+6	4.0+6	Expt	DOE-NDC-33	2	Apr84	ANL	Budtz-Jorgensen+ NDG.
^{89}Y	$\sigma_{el}(\theta)$	1.5+6	4.0+6	Eval	DOE-NDC-33	15	Apr84	ANL	Smith+ MEAS. CS ANALYZE. OPTMDL.
^{89}Y	σ_{pol}	1.7+7		Expt	DOE-NDC-33	185	Apr84	TNL	Byrd+ NDG.
^{89}Y	$\sigma_{dif.inl}$	8.0+6	1.7+7	Expt	DOE-NDC-33	182	Apr84	TNL	Byrd+ NDG.
^{89}Y	$\sigma_{dif.inl}$	1.5+6	4.0+6	Expt	DOE-NDC-33	2	Apr84	ANL	Budtz-Jorgensen+ GRPH CFD CALC.
^{89}Y	$\sigma_{n,n'\gamma}$	1.6+6	3.8+6	Expt	DOE-NDC-33	2	Apr84	ANL	Budtz-Jorgensen+ GRPH CFD CALC.
^{89}Y	$\sigma_{n,\alpha}$	1.5+7		Expt	DOE-NDC-33	173	Apr84	AI	Kneff+ TBL. EN=14.8 MEV.
Zr	σ_{tot}	NDG		Expt	DOE-NDC-33	142	Apr84	ORL	Salah+ NDG.
Zr	σ_{tot}	+3	2.0+7	Expt	DOE-NDC-33	1	Apr84	ANL	Poenitz+ GRPH CFD OTH. EXPT.
Zr	σ_{tot}	8.0+5	4.5+6	Eval	DOE-NDC-33	15	Apr84	ANL	Smith+ MEAS. CS ANALYZE. OPTMDL.
Zr	$\sigma_{el}(\theta)$	1.5+6	4.0+6	Eval	DOE-NDC-33	15	Apr84	ANL	Smith+ MEAS. CS ANALYZE. OPTMDL.

NEUTRON DATA REFERENCES

Element	Quantity	Energy (eV) Min	Max	Type	Documentation Ref	Page	Date	Lab	Comments
^{91}Zr	Res.Params.	2.9+2		Expt	DOE-NDC-33	142	Apr84	ORL	Salah+ E0, WN, WG GIVEN.
^{96}Zr	Res.Params.	3.0+2		Expt	DOE-NDC-33	142	Apr84	ORL	Salah+ E0, WN, WG GIVEN.
^{93}Nb	σ_{tot}	+3	2.0+7	Expt	DOE-NDC-33	1	Apr84	ANL	Poenitz+ GRPH CFD OTH. EXPT.
^{93}Nb	σ_{tot}		2.0+7	Expt	DOE-NDC-33	5	Apr84	ANL	Smith+ NDG.
^{93}Nb	σ_{tot}	8.0+5	4.5+6	Eval	DOE-NDC-33	15	Apr84	ANL	Smith+ MEAS. CS ANALYZE. OPTMDL.
^{93}Nb	$\sigma_{el}(\theta)$	8.0+6	1.7+7	Expt	DOE-NDC-33	182	Apr84	TNL	Byrd+ NDG.
^{93}Nb	$\sigma_{el}(\theta)$	NDG		Expt	DOE-NDC-33	183	Apr84	TNL	Anderson+ FWD ANG, 1.5-9 DEGS.
^{93}Nb	$\sigma_{el}(\theta)$	1.7+7		Expt	DOE-NDC-33	185	Apr84	TNL	Byrd+ NDG.
^{93}Nb	$\sigma_{el}(\theta)$		1.0+7	Expt	DOE-NDC-33	5	Apr84	ANL	Smith+ NDG.
^{93}Nb	$\sigma_{el}(\theta)$	1.5+6	4.0+6	Eval	DOE-NDC-33	15	Apr84	ANL	Smith+ MEAS. CS ANALYZE. OPTMDL.
^{93}Nb	σ_{pol}	1.7+7		Expt	DOE-NDC-33	185	Apr84	TNL	Byrd+ NDG.
^{93}Nb	$\sigma_{dif.inl}$	8.0+6	1.7+7	Expt	DOE-NDC-33	182	Apr84	TNL	Byrd+ NDG.
Mo	σ_{tot}	+3	2.0+7	Expt	DOE-NDC-33	1	Apr84	ANL	Poenitz+ GRPH CFD OTH. EXPT.
Mo	σ_{tot}	8.0+5	4.5+6	Eval	DOE-NDC-33	15	Apr84	ANL	Smith+ MEAS. CS ANALYZE. OPTMDL.
Mo	$\sigma_{el}(\theta)$	1.5+6	4.0+6	Eval	DOE-NDC-33	15	Apr84	ANL	Smith+ MEAS. CS ANALYZE. OPTMDL.
Mo	σ_{nem}	3.0+6	2.1+7	Expt	DOE-NDC-33	144	Apr84	ORL	Bell. NDG.
^{92}Mo	$\sigma_{el}(\theta)$	1.1+7		Expt	DOE-NDC-33	165	Apr84	OHO	Finlay+ NDG.
^{92}Mo	$\sigma_{dif.inl}$	1.1+7		Expt	DOE-NDC-33	165	Apr84	OHO	Finlay+ NDG.
^{96}Mo	$\sigma_{el}(\theta)$	1.1+7		Expt	DOE-NDC-33	165	Apr84	OHO	Finlay+ NDG.
^{96}Mo	$\sigma_{dif.inl}$	1.1+7		Expt	DOE-NDC-33	165	Apr84	OHO	Finlay+ NDG.
^{98}Mo	$\sigma_{el}(\theta)$	1.1+7		Expt	DOE-NDC-33	165	Apr84	OHO	Finlay+ NDG.
^{98}Mo	$\sigma_{dif.inl}$	1.1+7		Expt	DOE-NDC-33	165	Apr84	OHO	Finlay+ NDG.
^{100}Mo	$\sigma_{el}(\theta)$	1.1+7		Expt	DOE-NDC-33	165	Apr84	OHO	Finlay+ NDG.
^{100}Mo	$\sigma_{dif.inl}$	1.1+7		Expt	DOE-NDC-33	165	Apr84	OHO	Finlay+ NDG.
^{103}Rh	σ_{tot}	+3	2.0+7	Expt	DOE-NDC-33	1	Apr84	ANL	Poenitz+ GRPH CFD OTH. EXPT.
^{103}Rh	σ_{tot}	8.0+5	4.5+6	Eval	DOE-NDC-33	15	Apr84	ANL	Smith+ MEAS. CS ANALYZE. OPTMDL.
^{103}Rh	$\sigma_{el}(\theta)$	1.5+6	4.0+6	Eval	DOE-NDC-33	15	Apr84	ANL	Smith+ MEAS. CS ANALYZE. OPTMDL.
Pd	σ_{tot}	+3	2.0+7	Expt	DOE-NDC-33	1	Apr84	ANL	Poenitz+ GRPH CFD OTH. EXPT.
Pd	σ_{tot}	8.0+5	4.5+6	Eval	DOE-NDC-33	15	Apr84	ANL	Smith+ MEAS. CS ANALYZE. OPTMDL.
Pd	$\sigma_{el}(\theta)$	1.5+6	4.0+6	Eval	DOE-NDC-33	15	Apr84	ANL	Smith+ MEAS. CS ANALYZE. OPTMDL.
Ag	σ_{tot}	+3	2.0+7	Expt	DOE-NDC-33	1	Apr84	ANL	Poenitz+ GRPH CFD OTH. EXPT.
Ag	σ_{tot}	8.0+5	4.5+6	Eval	DOE-NDC-33	15	Apr84	ANL	Smith+ MEAS. CS ANALYZE. OPTMDL.
Ag	$\sigma_{el}(\theta)$	1.5+6	4.0+6	Eval	DOE-NDC-33	15	Apr84	ANL	Smith+ MEAS. CS ANALYZE. OPTMDL.

NEUTRON DATA REFERENCES

Element	Quantity	Energy (eV) Min	Max	Type	Documentation Ref	Page	Date	Lab	Comments
Ag	$\sigma_{n,\alpha}$	1.5+7		Expt	DOE-NDC-33	173	Apr84	AI	Kneff+ TBL. EN=14.8 MEV.
Cd	σ_{tot}	+3	2.0+7	Expt	DOE-NDC-33	1	Apr84	ANL	Poenitz+ GRPH CFD OTH. EXPT.
Cd	σ_{tot}	8.0+5	4.5+6	Eval	DOE-NDC-33	15	Apr84	ANL	Smith+ MEAS. CS ANALYZE. OPTMDL.
Cd	$\sigma_{el}(\theta)$	1.5+6	4.0+6	Eval	DOE-NDC-33	15	Apr84	ANL	Smith+ MEAS. CS ANALYZE. OPTMDL.
In	σ_{tot}	+3	2.0+7	Expt	DOE-NDC-33	1	Apr84	ANL	Poenitz+ NDG.
In	σ_{tot}	8.0+5	4.5+6	Expt	DOE-NDC-33	2	Apr84	ANL	Smith+ NDG. TBP.
In	σ_{tot}	8.0+5	4.5+6	Eval	DOE-NDC-33	15	Apr84	ANL	Smith+ MEAS. CS ANALYZE. OPTMDL.
In	$\sigma_{el}(\theta)$	1.5+6	3.8+6	Expt	DOE-NDC-33	2	Apr84	ANL	Smith+ NDG. TBP.
In	$\sigma_{el}(\theta)$	1.5+6	4.0+6	Eval	DOE-NDC-33	15	Apr84	ANL	Smith+ MEAS. CS ANALYZE. OPTMDL.
In	$\sigma_{dif.inl}$	8.6+5	2.4+6	Expt	DOE-NDC-33	2	Apr84	ANL	Smith+ NDG. TBP.
In	$\sigma_{n,n'\gamma}$	8.6+5	2.4+6	Expt	DOE-NDC-33	2	Apr84	ANL	Smith+ NDG. TBP.
^{115}In	$\sigma_{el}(\theta)$	1.5+6	1.0+7	Exth	DOE-NDC-33	2	Apr84	ANL	Smith+ NDG.
Sn	σ_{tot}	+3	2.0+7	Expt	DOE-NDC-33	1	Apr84	ANL	Poenitz+ NDG.
Sn	σ_{tot}	8.0+5	4.5+6	Eval	DOE-NDC-33	15	Apr84	ANL	Smith+ MEAS. CS ANALYZE. OPTMDL.
Sn	$\sigma_{el}(\theta)$	1.5+6	4.0+6	Eval	DOE-NDC-33	15	Apr84	ANL	Smith+ MEAS. CS ANALYZE. OPTMDL.
^{116}Sn	$\sigma_{el}(\theta)$	1.0+7	1.7+7	Expt	DOE-NDC-33	182	Apr84	TNL	Byrd+ NDG.
^{116}Sn	$\sigma_{el}(\theta)$	1.0+6	4.0+6	Expt	DOE-NDC-33	70	Apr84	KTY	Zhou+ 3 ENS, 1.,1.6,4.MEV. NDG.
^{116}Sn	$\sigma_{dif.inl}$	1.0+7	1.7+7	Expt	DOE-NDC-33	182	Apr84	TNL	Byrd+ NDG.
^{116}Sn	$\sigma_{dif.inl}$	1.0+6	4.0+6	Expt	DOE-NDC-33	70	Apr84	KTY	Zhou+ 3 ENS, 1.,1.6,4.MEV. NDG.
^{116}Sn	$\sigma_{n,n'\gamma}$	1.9+6	4.5+6	Expt	DOE-NDC-33	68	Apr84	KTY	Gacsi+ NDG.
^{118}Sn	$\sigma_{el}(\theta)$	1.0+6	4.0+6	Expt	DOE-NDC-33	70	Apr84	KTY	Zhou+ 3 ENS, 1.,1.6,4.MEV. NDG.
^{118}Sn	$\sigma_{dif.inl}$	1.0+6	4.0+6	Expt	DOE-NDC-33	70	Apr84	KTY	Zhou+ 3 ENS, 1.,1.6,4.MEV. NDG.
^{120}Sn	$\sigma_{el}(\theta)$	1.0+7	1.7+7	Expt	DOE-NDC-33	182	Apr84	TNL	Byrd+ NDG.
^{120}Sn	$\sigma_{el}(\theta)$	1.7+7		Expt	DOE-NDC-33	185	Apr84	TNL	Byrd+ NDG.
^{120}Sn	$\sigma_{el}(\theta)$	1.0+6	4.0+6	Expt	DOE-NDC-33	70	Apr84	KTY	Zhou+ 3 ENS, 1.,1.6,4.MEV. NDG.
^{120}Sn	σ_{pol}	1.7+7		Expt	DOE-NDC-33	185	Apr84	TNL	Byrd+ NDG.
^{120}Sn	$\sigma_{dif.inl}$	1.0+7	1.7+7	Expt	DOE-NDC-33	182	Apr84	TNL	Byrd+ NDG.
^{120}Sn	$\sigma_{dif.inl}$	1.0+6	4.0+6	Expt	DOE-NDC-33	70	Apr84	KTY	Zhou+ 3 ENS, 1.,1.6,4.MEV. NDG.
^{120}Sn	$\sigma_{n,n'\gamma}$	2.1+6	4.5+6	Expt	DOE-NDC-33	69	Apr84	KTY	Shi+ NDG.
^{122}Sn	$\sigma_{el}(\theta)$	1.0+6	4.0+6	Expt	DOE-NDC-33	70	Apr84	KTY	Zhou+ 3 ENS, 1.,1.6,4.MEV. NDG.
^{122}Sn	$\sigma_{dif.inl}$	1.0+6	4.0+6	Expt	DOE-NDC-33	70	Apr84	KTY	Zhou+ 3 ENS, 1.,1.6,4.MEV. NDG.
^{124}Sn	$\sigma_{el}(\theta)$	1.0+6	4.0+6	Expt	DOE-NDC-33	70	Apr84	KTY	Zhou+ 3 ENS, 1.,1.6,4.MEV. NDG.
^{124}Sn	$\sigma_{dif.inl}$	1.0+6	4.0+6	Expt	DOE-NDC-33	70	Apr84	KTY	Zhou+ 3 ENS, 1.,1.6,4.MEV. NDG.

NEUTRON DATA REFERENCES

Element	Quantity	Energy (eV) Min	Max	Type	Documentation Ref	Page	Date	Lab	Comments
^{124}Sn	$\sigma_{n,n'\gamma}$	2.6+6	3.5+6	Expt	DOE-NDC-33	69	Apr84	KTY	Weil+ NDG.
Sb	σ_{tot}	+3	2.0+7	Expt	DOE-NDC-33	1	Apr84	ANL	Poenitz+ NDG.
Sb	σ_{tot}	8.0+5	4.5+6	Eval	DOE-NDC-33	15	Apr84	ANL	Smith+ MEAS. CS ANALYZE. OPTMDL.
Sb	$\sigma_{el}(\theta)$	1.5+6	4.0+6	Eval	DOE-NDC-33	15	Apr84	ANL	Smith+ MEAS. CS ANALYZE. OPTMDL.
^{129}I	$\sigma_{n,\gamma}$	6.0+3	4.0+5	Eval	DOE-NDC-33	46	Apr84	HED	Mann+ GRPH. CFD MEAS. CS.
^{142}Nd	$\sigma_{n,\gamma}$	3.0+4		Expt	DOE-NDC-33	87	Apr84	KFK	Mathews+ CS = 51+-4 MB.
^{143}Nd	$\sigma_{n,\gamma}$	3.0+4		Expt	DOE-NDC-33	87	Apr84	KFK	Mathews+ CS = 258+-11 MB.
^{144}Nd	$\sigma_{n,\gamma}$	3.0+4		Expt	DOE-NDC-33	87	Apr84	KFK	Mathews+ CS = 123+-6 MB.
Sm	σ_{tot}	+3	2.0+7	Expt	DOE-NDC-33	1	Apr84	ANL	Poenitz+ NDG. TB ANALYZED.
Gd	σ_{tot}	+3	2.0+7	Expt	DOE-NDC-33	1	Apr84	ANL	Poenitz+ NDG. TB ANALYZED.
^{165}Ho	σ_{tot}	+3	2.0+7	Expt	DOE-NDC-33	1	Apr84	ANL	Poenitz+ NDG. TB ANALYZED.
Er	σ_{tot}	+3	2.0+7	Expt	DOE-NDC-33	1	Apr84	ANL	Poenitz+ NDG. TB ANALYZED.
Yb	σ_{tot}	+3	2.0+7	Expt	DOE-NDC-33	1	Apr84	ANL	Poenitz+ NDG. TB ANALYZED.
^{175}Lu	$\sigma_{n,\gamma}$	1.0+4	2.5+7	Theo	DOE-NDC-33	97	Apr84	LRL	Gardiner+ GRPH.ISOMER RATIO CFD EXPT
^{175}Lu	$\sigma_{n,2n}$	NDG		Theo	DOE-NDC-33	97	Apr84	LRL	Gardiner+ ISOMER RATIO. NDG.
Hf	σ_{tot}	+3	2.0+7	Expt	DOE-NDC-33	1	Apr84	ANL	Poenitz+ NDG.
^{178}Hf	$\sigma_{n,\gamma}$	2.6+3	2.0+6	Expt	DOE-NDC-33	142	Apr84	ORL	Beer+ NDG.
^{178}Hf	Res.Params.		1.0+4	Expt	DOE-NDC-33	142	Apr84	ORL	Beer+ NDG.
^{179}Hf	$\sigma_{n,\gamma}$	2.6+3	2.0+6	Expt	DOE-NDC-33	142	Apr84	ORL	Beer+ NDG.
^{179}Hf	Res.Params.		1.0+4	Expt	DOE-NDC-33	142	Apr84	ORL	Beer+ NDG.
^{180}Hf	$\sigma_{n,\gamma}$	2.6+3	2.0+6	Expt	DOE-NDC-33	142	Apr84	ORL	Beer+ NDG.
^{180}Hf	Res.Params.		1.0+4	Expt	DOE-NDC-33	142	Apr84	ORL	Beer+ NDG.
^{180}Ta	σ_{tot}	4.3-1		Expt	DOE-NDC-33	139	Apr84	ORL	Harvey+ CRYSTAL EFFECTS.
^{181}Ta	σ_{tot}	2.0-3	5.0+0	Expt	DOE-NDC-33	139	Apr84	ORL	Harvey+ CRYSTAL EFFECTS.
^{181}Ta	σ_{tot}	+3	2.0+7	Expt	DOE-NDC-33	1	Apr84	ANL	Poenitz+ NDG.
^{181}Ta	$\sigma_{n,\gamma}$	2.6+3	1.9+6	Expt	DOE-NDC-33	141	Apr84	ORL	Macklin. NDG.
^{181}Ta	$\sigma_{n,\alpha}$	1.5+7		Expt	DOE-NDC-33	173	Apr84	AI	Kneff+ TBL. EN=14.8 MEV.
^{181}Ta	Res.Params.	2.6+3	4.0+3	Expt	DOE-NDC-33	141	Apr84	ORL	Macklin. NDG.
^{182}W	$\sigma_{el}(\theta)$	5.0+6	6.0+6	Expt	DOE-NDC-33	160	Apr84	OHO	Annand+ NDG. 2 ENS.
^{182}W	$\sigma_{dif.inl}$	5.0+6	6.0+6	Expt	DOE-NDC-33	160	Apr84	OHO	Annand+ NDG. 2 ENS.
^{184}W	$\sigma_{el}(\theta)$	5.0+6	6.0+6	Expt	DOE-NDC-33	160	Apr84	OHO	Annand+ NDG. 2 ENS.
^{184}W	$\sigma_{dif.inl}$	5.0+6	6.0+6	Expt	DOE-NDC-33	160	Apr84	OHO	Annand+ NDG. 2 ENS.
^{187}Os	σ_{tot}	2.7+1	5.0+2	Expt	DOE-NDC-33	140	Apr84	ORL	Winters+ NDG.

NEUTRON DATA REFERENCES

Element	Quantity	Energy (eV) Min	Max	Type	Documentation Ref	Page	Date	Lab	Comments
^{187}Os	σ_{el}	6.1+4		Expt	DOE-NDC-33	74	Apr84	KTY	Hershberger+ CS = 11 B.
^{187}Os	$\sigma_{dif.inl}$	6.1+4		Expt	DOE-NDC-33	74	Apr84	KTY	Hershberger+ CS(9.75 KEV LVL)=1.13 B
^{187}Os	Res.Params.	NDG		Expt	DOE-NDC-33	140	Apr84	ORL	Winters+ NDG.
^{187}Os	$\langle\Gamma\rangle/D$		5.0+2	Expt	DOE-NDC-33	140	Apr84	ORL	Winters+ S0 = 3.9X(10)-4.
^{188}Os	σ_{el}	6.1+4		Expt	DOE-NDC-33	74	Apr84	KTY	Hershberger+ NDG.
^{189}Os	σ_{el}	6.0+4	+5	Expt	DOE-NDC-33	74	Apr84	KTY	Hershberger+ NDG.
^{189}Os	$\sigma_{dif.inl}$	6.0+4	+5	Expt	DOE-NDC-33	74	Apr84	KTY	Hershberger+ NDG.
^{190}Os	σ_{tot}	3.0+5	3.0+6	Expt	DOE-NDC-33	70	Apr84	KTY	Hicks+ NDG.
^{190}Os	$\sigma_{dif.inl}$	3.0+5	3.0+6	Expt	DOE-NDC-33	70	Apr84	KTY	Hicks+ NDG.
^{192}Os	σ_{tot}	3.0+5	3.0+6	Expt	DOE-NDC-33	70	Apr84	KTY	Hicks+ NDG.
^{192}Os	$\sigma_{dif.inl}$	3.0+5	3.0+6	Expt	DOE-NDC-33	70	Apr84	KTY	Hicks+ NDG.
Pt	σ_{tot}	+3	2.0+7	Expt	DOE-NDC-33	1	Apr84	ANL	Poenitz+ NDG.
^{194}Pt	σ_{tot}	3.0+5	4.5+6	Expt	DOE-NDC-33	72	Apr84	KTY	Mirzaa+ TBD.
^{194}Pt	$\sigma_{el}(\theta)$	2.5+6		Expt	DOE-NDC-33	72	Apr84	KTY	Mirzaa+ NDG.
^{194}Pt	$\sigma_{dif.inl}$	2.5+6		Expt	DOE-NDC-33	72	Apr84	KTY	Mirzaa+ NDG.
^{197}Au	Evaluation	1.0+4	3.0+7	Eval	DOE-NDC-33	109	Apr84	LAS	Young+ NDG.
^{197}Au	σ_{tot}	+3	2.0+7	Expt	DOE-NDC-33	1	Apr84	ANL	Poenitz+ NDG.
^{197}Au	$\sigma_{n,\gamma}$	NDG		Eval	DOE-NDC-33	11	Apr84	ANL	Poenitz. SIMULTANEOUS EVAL. ENDF-VI.
Pb	$\sigma_{el}(\theta)$	NDG		Expt	DOE-NDC-33	183	Apr84	TNL	Anderson+ FWD ANG, 1.5-9 DEGS.
^{204}Pb	σ_{tot}	4.0+2	1.1+5	Expt	DOE-NDC-33	139	Apr84	ORL	Horen+ NDG.
^{204}Pb	$\sigma_{dif.inl}$	NDG		Expt	DOE-NDC-33	71	Apr84	KTY	Hanly+ NDG.
^{204}Pb	$\sigma_{n,\gamma}$	2.6+3	8.6+4	Expt	DOE-NDC-33	139	Apr84	ORL	Horen+ CS(30KEV)= 89.5+-4.5 MB.
^{204}Pb	$\sigma_{n,n'\gamma}$		4.0+6	Expt	DOE-NDC-33	71	Apr84	KTY	Hanly+ NDG.
^{204}Pb	Res.Params.	NDG		Expt	DOE-NDC-33	139	Apr84	ORL	Horen+ NDG.
^{204}Pb	$\langle\Gamma\rangle/D$		1.1+5	Expt	DOE-NDC-33	139	Apr84	ORL	Horen+ S0 = 0.93X(10)-4.
^{206}Pb	$\sigma_{dif.inl}$	NDG		Expt	DOE-NDC-33	71	Apr84	KTY	Hanly+ NDG.
^{206}Pb	$\sigma_{n,n'\gamma}$		4.0+6	Expt	DOE-NDC-33	71	Apr84	KTY	Hanly+ NDG.
^{208}Pb	$\sigma_{el}(\theta)$	4.0+6	6.0+6	Expt	DOE-NDC-33	160	Apr84	OHO	Annand+ NDG.
^{208}Pb	$\sigma_{el}(\theta)$	4.0+6	7.0+6	Expt	DOE-NDC-33	165	Apr84	OHO	Annand+ NDG. OPTMDL ANALYSIS.
^{208}Pb	$\sigma_{el}(\theta)$	7.0+6	5.0+7	Expt	DOE-NDC-33	166	Apr84	OHO	Finlay+ NDG. OPTMDL ANALYSIS.
^{208}Pb	$\sigma_{el}(\theta)$	1.0+7	1.7+7	Expt	DOE-NDC-33	182	Apr84	TNL	Byrd+ NDG.
^{208}Pb	$\sigma_{dif.inl}$	4.0+6	6.0+6	Expt	DOE-NDC-33	160	Apr84	OHO	Annand+ NDG.
^{208}Pb	$\sigma_{dif.inl}$	4.0+6	7.0+6	Expt	DOE-NDC-33	165	Apr84	OHO	Annand+ NDG. OPTMDL ANALYSIS.

NEUTRON DATA REFERENCES

Element	Quantity	Energy (eV) Min	Max	Type	Documentation Ref	Page	Date	Lab	Comments
^{209}Bi	σ_{tot}	2.0-3	5.0+0	Expt	DOE-NDC-33	139	Apr84	ORL	Harvey+ CRYSTAL EFFECTS.
^{209}Bi	$\sigma_{el}(\theta)$	4.0+6	6.0+6	Expt	DOE-NDC-33	160	Apr84	OHO	Annand+ NDG.
^{209}Bi	$\sigma_{el}(\theta)$	4.0+6	7.0+6	Expt	DOE-NDC-33	165	Apr84	OHO	Annand+ NDG. OPTMDL ANALYSIS.
^{209}Bi	$\sigma_{dif.inl}$	4.0+6	6.0+6	Expt	DOE-NDC-33	160	Apr84	OHO	Annand+ NDG.
^{209}Bi	$\sigma_{dif.inl}$	4.0+6	7.0+6	Expt	DOE-NDC-33	165	Apr84	OHO	Annand+ NDG. OPTMDL ANALYSIS.
^{227}Th	Fiss.Yield	2.5-2		Eval	DOE-NDC-33	47	Apr84	LAS	England+ ENDF-VI. TBD.
^{229}Th	Fiss.Yield	2.5-2		Eval	DOE-NDC-33	47	Apr84	LAS	England+ ENDF-VI. TBD.
^{230}Th	$\sigma_{n,f}$	NDG		Expt	DOE-NDC-33	5	Apr84	ANL	Meadows. REL 235U NDG.
^{232}Th	σ_{tot}	NDG		Revw	DOE-NDC-33	147	Apr84	ORL	Olsen. NDG.
^{232}Th	σ_{tot}	+3	2.0+7	Expt	DOE-NDC-33	1	Apr84	ANL	Poenitz+ NDG.
^{232}Th	$\sigma_{el}(\theta)$	1.4+7		Expt	DOE-NDC-33	88	Apr84	LRL	Hansen+ NDG.
^{232}Th	$\sigma_{el}(\theta)$	5.0+5	2.5+6	Expt	DOE-NDC-33	115	Apr84	LTI	Beghian+ NDG.
^{232}Th	$\sigma_{dif.inl}$	1.4+7		Expt	DOE-NDC-33	88	Apr84	LRL	Hansen+ NDG.
^{232}Th	$\sigma_{dif.inl}$	5.0+5	2.5+6	Expt	DOE-NDC-33	115	Apr84	LTI	Beghian+ NDG.
^{232}Th	$\sigma_{dif.inl}$	1.2+6	2.2+6	Expt	DOE-NDC-33	115	Apr84	LTI	Beghian+ GRPH. ANG DIST.
^{232}Th	$\sigma_{dif.inl}$	NDG		Theo	DOE-NDC-33	119	Apr84	LTI	Sheldon. NDG.
^{232}Th	$\sigma_{n,\gamma}$	2.3+4	9.6+5	Expt	DOE-NDC-33	125	Apr84	MHG	Wilderman+ NDG.
^{232}Th	$\sigma_{n,\gamma}$	NDG		Revw	DOE-NDC-33	147	Apr84	ORL	Olsen. NDG.
^{232}Th	$\sigma_{n,f}$	NDG		Expt	DOE-NDC-33	5	Apr84	ANL	Meadows. REL 235U NDG.
^{232}Th	Fiss.Yield	FAST		Eval	DOE-NDC-33	47	Apr84	LAS	England+ ENDF-VI. TBD.
^{232}Th	Fiss.Yield	1.4+7		Eval	DOE-NDC-33	47	Apr84	LAS	England+ ENDF-VI. TBD.
^{232}Th	Frag Spectra	7.0+5	1.0+7	Expt	DOE-NDC-33	87	Apr84	LRL	Becker+ FF. ANGDIST. GRPH. LEG COEF.
^{231}Pa	Fiss.Yield	FAST		Eval	DOE-NDC-33	47	Apr84	LAS	England+ ENDF-VI. TBD.
^{232}U	Fiss.Yield	FAST		Eval	DOE-NDC-33	47	Apr84	LAS	England+ ENDF-VI. TBD.
^{233}U	σ_{tot}	+3	2.0+7	Expt	DOE-NDC-33	1	Apr84	ANL	Poenitz+ NDG.
^{233}U	$\sigma_{n,f}$	1.4+7		Expt	DOE-NDC-33	126	Apr84	MHG	Agrawal+ NDG.
^{233}U	$\sigma_{n,f}$	NDG		Expt	DOE-NDC-33	5	Apr84	ANL	Meadows. REL 235U NDG.
^{233}U	ν_p	5.0-3	1.0+1	Expt	DOE-NDC-33	146	Apr84	ORL	Gwin. REL TO 252CF NU.
^{233}U	ν_p	2.5-2		Revw	DOE-NDC-33	147	Apr84	ORL	Olsen. NU=2.490+-0.009.
^{233}U	Fiss.Yield	1.4+7		Expt	DOE-NDC-33	126	Apr84	MHG	Agrawal+ FF. ANG DIST. NDG.
^{233}U	Fiss.Yield	FAST		Eval	DOE-NDC-33	47	Apr84	LAS	England+ ENDF-VI. TBD.
^{233}U	Fiss.Yield	2.5-2	1.4+7	Eval	DOE-NDC-33	47	Apr84	LAS	England+ ENDF-VI. TBD. 2 ENS ONLY.
^{233}U	Frag Spectra	1.4+7		Expt	DOE-NDC-33	126	Apr84	MHG	Agrawal+ NDG. ANG DIST. TBC.

NEUTRON DATA REFERENCES

Element	Quantity	Energy (eV) Min	Max	Type	Documentation Ref	Page	Date	Lab	Comments
^{234}U	$\sigma_{n,f}$	NDG		Expt	DOE-NDC-33	5	Apr84	ANL	Meadows. REL 235U NDG.
^{234}U	Fiss.Yield	FAST		Eval	DOE-NDC-33	47	Apr84	LAS	England+ ENDF-VI. TBD.
^{234}U	Fiss.Yield	1.4+7		Eval	DOE-NDC-33	47	Apr84	LAS	England+ ENDF-VI. TBD.
^{235}U	σ_{tot}	+3	2.0+7	Expt	DOE-NDC-33	1	Apr84	ANL	Poenitz+ NDG.
^{235}U	$\sigma_{el}(\theta)$	2.0+5		Expt	DOE-NDC-33	119	Apr84	LTI	Beghian+ TBD.
^{235}U	$\sigma_{dif.inl}$	2.0+5		Expt	DOE-NDC-33	119	Apr84	LTI	Beghian+ TBD.
^{235}U	$\sigma_{n,f}$	3.0+5	3.0+6	Expt	DOE-NDC-33	128	Apr84	NBS	Carlson+ ANALYSIS TBC.
^{235}U	$\sigma_{n,f}$	2.0+6	6.0+6	Expt	DOE-NDC-33	129	Apr84	NBS	Dias+ ANALYSIS TBD.
^{235}U	$\sigma_{n,f}$	FISS		Expt	DOE-NDC-33	129	Apr84	NBS	Schroeder+ FISS. AVG CS = 1218 MB.
^{235}U	$\sigma_{n,f}$	1.0+5	2.0+7	Eval	DOE-NDC-33	99	Apr84	LRL	Howerton+ ENDL LIB. EVAL. NDG.
^{235}U	$\sigma_{n,f}$	1.4+7		Expt	DOE-NDC-33	126	Apr84	MHG	Agrawal+ NDG.
^{235}U	$\sigma_{n,f}$	1.0-2	3.0+4	Expt	DOE-NDC-33	146	Apr84	ORL	Gwin+ REL 10B (N,A).
^{235}U	$\sigma_{n,f}$	2.0+1	1.0+5	Expt	DOE-NDC-33	147	Apr84	ORL	Weston+ CFD ENDF-V. AGREES.
^{235}U	$\sigma_{n,f}$	NDG		Eval	DOE-NDC-33	11	Apr84	ANL	Poenitz. SIMULTANEOUS EVAL. ENDF-VI.
^{235}U	ν_p	2.5-2	2.0+7	Eval	DOE-NDC-33	99	Apr84	LRL	Howerton+ ENDL LIB. EVAL. NDG.
^{235}U	ν_p	5.0-3	1.0+1	Expt	DOE-NDC-33	146	Apr84	ORL	Gwin. REL TO 252CF NU.
^{235}U	ν_d	2.5-2		Expt	DOE-NDC-33	121	Apr84	LTI	Couchell+ GRPH SPECTRUM. 0.1-2. MEV.
^{235}U	Fiss.Yield	2.5-2		Expt	DOE-NDC-33	170	Apr84	BNW	Reeder+ 90RB, 138CS NDG.
^{235}U	Fiss.Yield	1.4+7		Expt	DOE-NDC-33	126	Apr84	MHG	Agrawal+ FF. ANG DIST. NDG.
^{235}U	Fiss.Yield	FAST		Eval	DOE-NDC-33	47	Apr84	LAS	England+ ENDF-VI. TBD.
^{235}U	Fiss.Yield	2.5-2	1.4+7	Eval	DOE-NDC-33	47	Apr84	LAS	England+ ENDF-VI. TBD. 2 ENS ONLY.
^{235}U	Fiss.Yield	FAST		Expt	DOE-NDC-33	49	Apr84	HED	Rawlins+ 13 FPROD. NDG.
^{235}U	Frag Spectra	1.4+7		Expt	DOE-NDC-33	126	Apr84	MHG	Agrawal+ NDG. ANG DIST.
^{236}U	$\sigma_{n,f}$	NDG		Expt	DOE-NDC-33	5	Apr84	ANL	Meadows. REL 235U NDG.
^{236}U	Fiss.Yield	NDG		Theo	DOE-NDC-33	136	Apr84	NBS	Behrens. NDG.
^{236}U	Fiss.Yield	FAST		Eval	DOE-NDC-33	47	Apr84	LAS	England+ ENDF-VI. TBD.
^{236}U	Fiss.Yield	1.4+7		Eval	DOE-NDC-33	47	Apr84	LAS	England+ ENDF-VI. TBD.
^{237}U	Fiss.Yield	FAST		Eval	DOE-NDC-33	47	Apr84	LAS	England+ ENDF-VI. TBD.
^{238}U	σ_{tot}	1.5+3	4.0+3	Eval	DOE-NDC-33	155	Apr84	ORL	Olsen.
^{238}U	σ_{tot}	+3	2.0+7	Expt	DOE-NDC-33	1	Apr84	ANL	Poenitz+ NDG.
^{238}U	$\sigma_{el}(\theta)$	1.4+7		Expt	DOE-NDC-33	88	Apr84	LRL	Hansen+ NDG.
^{238}U	$\sigma_{el}(\theta)$	5.0+5	9.0+5	Expt	DOE-NDC-33	115	Apr84	LTI	Beghian+ NDG.
^{238}U	$\sigma_{dif.inl}$	1.4+7		Expt	DOE-NDC-33	88	Apr84	LRL	Hansen+ NDG.

NEUTRON DATA REFERENCES

Element	Quantity	Energy (eV) Min	Max	Type	Documentation Ref	Page	Date	Lab	Comments
^{238}U	$\sigma_{dif.inl}$	5.0+5	9.0+5	Expt	DOE-NDC-33	115	Apr84	LTI	Beghian+ NDG.
^{238}U	$\sigma_{dif.inl}$	1.5+6	2.2+6	Expt	DOE-NDC-33	115	Apr84	LTI	Beghian+ GRPHS, ANG DIST, SIG.
^{238}U	$\sigma_{dif.inl}$	NDG		Theo	DOE-NDC-33	119	Apr84	LTI	Sheldon. NDG.
^{238}U	$\sigma_{n,\gamma}$	2.3+4	9.6+5	Expt	DOE-NDC-33	125	Apr84	MHG	Wilderman+ TBD.
^{238}U	$\sigma_{n,\gamma}$	NDG		Eval	DOE-NDC-33	11	Apr84	ANL	Poenitz. SIMULTANEOUS EVAL. ENDF-VI.
^{238}U	$\sigma_{n,f}$	1.4+7		Expt	DOE-NDC-33	126	Apr84	MHG	Agrawal+ NDG.
^{238}U	$\sigma_{n,f}$	NDG		Expt	DOE-NDC-33	5	Apr84	ANL	Meadows. REL 235U NDG.
^{238}U	$\sigma_{n,f}$	NDG		Eval	DOE-NDC-33	11	Apr84	ANL	Poenitz. SIMULTANEOUS EVAL. ENDF-VI.
^{238}U	Fiss.Yield	1.4+7		Expt	DOE-NDC-33	126	Apr84	MHG	Agrawal+ FF. ANG DIST. NDG.
^{238}U	Fiss.Yield	SPON		Eval	DOE-NDC-33	47	Apr84	LAS	England+ ENDF-VI. TBD.
^{238}U	Fiss.Yield	FAST		Eval	DOE-NDC-33	47	Apr84	LAS	England+ ENDF-VI. TBD.
^{238}U	Fiss.Yield	1.4+7		Eval	DOE-NDC-33	47	Apr84	LAS	England+ ENDF-VI. TBD.
^{238}U	Fiss.Yield	FAST		Expt	DOE-NDC-33	49	Apr84	HED	Rawlins+ 13 FPROD. NDG.
^{238}U	Frag Spectra	1.4+7		Expt	DOE-NDC-33	126	Apr84	MHG	Agrawal+ NDG. ANG DIST. TBC.
^{237}Np	σ_{tot}	1.0+0	6.0+2	Expt	DOE-NDC-33	148	Apr84	ORL	Auchampaugh+ NDG.
^{237}Np	$\sigma_{n,2n}$	NDG		Theo	DOE-NDC-33	97	Apr84	LRL	Gardiner+ ISOMER RATIO. NDG.
^{237}Np	$\sigma_{n,f}$	1.4+7		Expt	DOE-NDC-33	126	Apr84	MHG	Agrawal+ NDG.
^{237}Np	$\sigma_{n,f}$	1.0+0	6.0+2	Expt	DOE-NDC-33	148	Apr84	ORL	Auchampaugh+ NDG.
^{237}Np	Fiss.Yield	1.4+7		Expt	DOE-NDC-33	126	Apr84	MHG	Agrawal+ FF. ANG DIST. NDG.
^{237}Np	Fiss.Yield	1.4+7		Eval	DOE-NDC-33	47	Apr84	LAS	England+ ENDF-VI. TBD.
^{237}Np	Fiss.Yield	FAST		Eval	DOE-NDC-33	47	Apr84	LAS	England+ ENDF-VI. TBD.
^{237}Np	Fiss.Yield	FAST		Expt	DOE-NDC-33	49	Apr84	HED	Rawlins+ 13 FPROD. NDG.
^{237}Np	Frag Spectra	1.4+7		Expt	DOE-NDC-33	126	Apr84	MHG	Agrawal+ NDG. ANG DIST. TBC.
^{238}Np	Fiss.Yield	FAST		Eval	DOE-NDC-33	47	Apr84	LAS	England+ ENDF-VI. TBD.
^{238}Pu	Fiss.Yield	FAST		Eval	DOE-NDC-33	47	Apr84	LAS	England+ ENDF-VI. TBD.
^{239}Pu	σ_{tot}	+3	2.0+7	Expt	DOE-NDC-33	1	Apr84	ANL	Poenitz+ NDG.
^{239}Pu	$\sigma_{el}(\theta)$	1.4+7		Expt	DOE-NDC-33	88	Apr84	LRL	Hansen+ NDG.
^{239}Pu	$\sigma_{dif.inl}$	1.4+7		Expt	DOE-NDC-33	88	Apr84	LRL	Hansen+ NDG.
^{239}Pu	$\sigma_{n,f}$	1.0+5	2.0+7	Eval	DOE-NDC-33	99	Apr84	LRL	Howerton+ ENDL LIB. EVAL. NDG.
^{239}Pu	$\sigma_{n,f}$	1.4+7		Expt	DOE-NDC-33	126	Apr84	MHG	Agrawal+ NDG.
^{239}Pu	$\sigma_{n,f}$	1.0-2	6.0+1	Expt	DOE-NDC-33	146	Apr84	ORL	Gwin+ REL 10B (N,A).
^{239}Pu	$\sigma_{n,f}$	2.0+1	1.0+5	Expt	DOE-NDC-33	147	Apr84	ORL	Weston+ CFD ENDF-V.LOWER ABOVE25KEV.
^{239}Pu	$\sigma_{n,f}$	NDG		Expt	DOE-NDC-33	5	Apr84	ANL	Meadows. REL 235U NDG.

NEUTRON DATA REFERENCES

Element	Quantity	Energy (eV) Min	Max	Type	Documentation Ref	Page	Date	Lab	Comments
^{239}Pu	$\sigma_{n,f}$	NDG		Eval	DOE-NDC-33	11	Apr84	ANL	Poenitz. SIMULTANEOUS EVAL. ENDF-VI.
^{239}Pu	ν_p	2.5-2	2.0+7	Eval	DOE-NDC-33	99	Apr84	LRL	Howerton+ ENDL LIB. EVAL. NDG.
^{239}Pu	ν_p	5.0-3	1.0+1	Expt	DOE-NDC-33	146	Apr84	ORL	Gwin. REL TO 252CF NU.
^{239}Pu	Fiss.Yield	1.4+7		Expt	DOE-NDC-33	126	Apr84	MHG	Agrawal+ FF. ANG DIST. NDG.
^{239}Pu	Fiss.Yield	FAST		Eval	DOE-NDC-33	47	Apr84	LAS	England+ ENDF-VI. TBD.
^{239}Pu	Fiss.Yield	2.5-2	1.4+7	Eval	DOE-NDC-33	47	Apr84	LAS	England+ ENDF-VI. TBD. 2 ENS ONLY.
^{239}Pu	Fiss.Yield	FAST		Expt	DOE-NDC-33	49	Apr84	HED	Rawlins+ 13 FPROD. NDG.
^{239}Pu	Frag Spectra	1.4+7		Expt	DOE-NDC-33	126	Apr84	MHG	Agrawal+ NDG. ANG DIST.
^{240}Pu	σ_{tot}	1.1+0		Expt	DOE-NDC-33	139	Apr84	ORL	Harvey+ CRYSTAL EFFECTS.
^{240}Pu	σ_{tot}	+3	2.0+7	Expt	DOE-NDC-33	1	Apr84	ANL	Poenitz+ NDG.
^{240}Pu	$\sigma_{dif.inl}$	NDG		Theo	DOE-NDC-33	119	Apr84	LTI	Sheldon. NDG.
^{240}Pu	$\sigma_{n,f}$	2.0+1	1.0+5	Expt	DOE-NDC-33	147	Apr84	ORL	Weston+ REL 10B (N,A),6LI (N,A).
^{240}Pu	$\sigma_{n,f}$	NDG		Expt	DOE-NDC-33	5	Apr84	ANL	Meadows. REL 235U NDG.
^{240}Pu	Fiss.Yield	FAST		Eval	DOE-NDC-33	47	Apr84	LAS	England+ ENDF-VI. TBD.
^{240}Pu	Fiss.Yield	1.4+7		Eval	DOE-NDC-33	47	Apr84	LAS	England+ ENDF-VI. TBD.
^{240}Pu	Res.Params.	2.0+1	5.7+3	Expt	DOE-NDC-33	147	Apr84	ORL	Weston+ NDG.
^{241}Pu	ν_p	5.0-3	1.0+1	Expt	DOE-NDC-33	146	Apr84	ORL	Gwin. REL TO 252CF NU.
^{241}Pu	Fiss.Yield	2.5-2		Eval	DOE-NDC-33	47	Apr84	LAS	England+ ENDF-VI. TBD.
^{241}Pu	Fiss.Yield	FAST		Eval	DOE-NDC-33	47	Apr84	LAS	England+ ENDF-VI. TBD.
^{242}Pu	$\sigma_{dif.inl}$	NDG		Theo	DOE-NDC-33	119	Apr84	LTI	Sheldon. NDG.
^{242}Pu	$\sigma_{n,f}$	NDG		Expt	DOE-NDC-33	5	Apr84	ANL	Meadows. REL 235U NDG.
^{242}Pu	Fiss.Yield	FAST		Eval	DOE-NDC-33	47	Apr84	LAS	England+ ENDF-VI. TBD.
^{241}Am	$\sigma_{n,\gamma}$	NDG		Theo	DOE-NDC-33	97	Apr84	LRL	Gardiner+ ISOMER RATIO. NDG.
^{241}Am	Fiss.Yield	FAST		Eval	DOE-NDC-33	47	Apr84	LAS	England+ ENDF-VI. TBD.
^{241}Am	Fiss.Yield	2.5-2	1.4+7	Eval	DOE-NDC-33	47	Apr84	LAS	England+ ENDF-VI. TBD. 2 ENS ONLY.
^{242}Am	Fiss.Yield	2.5-2		Eval	DOE-NDC-33	47	Apr84	LAS	England+ ENDF-VI. TBD.
^{243}Am	$\sigma_{n,\gamma}$	NDG		Theo	DOE-NDC-33	97	Apr84	LRL	Gardiner+ ISOMER RATIO. NDG.
^{243}Am	Fiss.Yield	FAST		Eval	DOE-NDC-33	47	Apr84	LAS	England+ ENDF-VI. TBD.
^{242}Cm	Fiss.Yield	FAST		Eval	DOE-NDC-33	47	Apr84	LAS	England+ ENDF-VI. TBD.
^{243}Cm	Fiss.Yield	2.5-2		Expt	DOE-NDC-33	147	Apr84	ORL	Merriman. 12 CUM. YIELDS.
^{244}Cm	Fiss.Yield	SPON		Eval	DOE-NDC-33	47	Apr84	LAS	England+ ENDF-VI. TBD.
^{245}Cm	Fiss.Yield	2.5-2		Eval	DOE-NDC-33	47	Apr84	LAS	England+ ENDF-VI. TBD.
^{248}Cm	Fiss.Yield	SPON		Eval	DOE-NDC-33	47	Apr84	LAS	England+ ENDF-VI. TBD.

Element	Quantity	Energy (eV) Min	Max	Type	Documentation Ref	Page	Date	Lab	Comments
^{249}Cf	Fiss.Yield	2.5-2		Eval	DOE-NDC-33	47	Apr84	LAS	England+ ENDF-VI. TBD.
^{250}Cf	Fiss.Yield	SPON		Eval	DOE-NDC-33	47	Apr84	LAS	England+ ENDF-VI. TBD.
^{251}Cf	Fiss.Yield	2.5-2		Eval	DOE-NDC-33	47	Apr84	LAS	England+ ENDF-VI. TBD.
^{252}Cf	ν_p	SPON		Theo	DOE-NDC-33	111	Apr84	LAS	Madland+ NU = 3.810
^{252}Cf	Spect.fiss n	SPON		Theo	DOE-NDC-33	111	Apr84	LAS	Madland+ GRPH CFD EXPT.
^{252}Cf	Fiss.Yield	SPON		Eval	DOE-NDC-33	47	Apr84	LAS	England+ ENDF-VI. TBD.
^{253}Es	Fiss.Yield	SPON		Eval	DOE-NDC-33	47	Apr84	LAS	England+ ENDF-VI. TBD.
^{254}Es	Fiss.Yield	2.5-2		Eval	DOE-NDC-33	47	Apr84	LAS	England+ ENDF-VI. TBD.
^{254}Fm	Fiss.Yield	SPON		Eval	DOE-NDC-33	47	Apr84	LAS	England+ ENDF-VI. TBD.
^{255}Fm	Fiss.Yield	2.5-2		Eval	DOE-NDC-33	47	Apr84	LAS	England+ ENDF-VI. TBD.
^{256}Fm	Fiss.Yield	SPON		Eval	DOE-NDC-33	47	Apr84	LAS	England+ ENDF-VI. TBD.

ARGONNE NATIONAL LABORATORY

A. NEUTRON CROSS SECTION MEASUREMENTS AND EVALUATIONS

1. Total Neutron Cross Section Measurements
(W. P. Poenitz and J. F. Whalen)

Astounding discrepancies of neutron total cross sections for the actinides were evident at the time of the evaluation of ENDF/B-V. A lack of data and/or discrepancies between existing data were apparent when such data were needed for nuclear model calculations of capture cross sections for fission products[1]. Consequently, a program was started to measure a large number of isotopic and elemental total neutron cross sections in the keV-to-MeV energy range. Such measurements[2,3] were recently extended to 20 MeV. The data analysis has been completed for Sc, Cu, Zn, Y, Zr, Nb, Mo, Rh, Pd, Ag, Cd, In, Sn, Sb, Hf, Ta, Pt, Au, Th, U, ^{233}U, ^{235}U, ^{239}Pu, and ^{240}Pu[4], and corresponding numerical values are available from the National Nuclear Data Center, BNL. Fig. A-1 shows the present results for some of the lighter nuclei. New measurements have been made for Ca, Ti, V, Mn, Co, Ni, Cu, Ge, Sm, Gd, Ho, Er, and Yb. These data are being analyzed.

---

[1] W. P. Poenitz, Proc. Neutr. Cross Sections of Fission Product Nuclei, Bologna 1978, NEANDC(E) 209 "L", p. 85.
[2] W. P. Poenitz et al., NSE 68, 358 (1978).
[3] W. P. Poenitz et al., NSE 78, 333 (1981).
[4] W. P. Poenitz and J. F. Whalen, ANL/NDM-80 (1983).

2. Fast-Neutron Total, Elastic- and Inelastic-scattering Cross Sections of Elemental Indium
(A. Smith, P. Guenther, J. Whalen, I. van Heerden[a] and W. McMurray[b])

Broad-resolution neutron total cross sections of elemental indium have been measured from 0.8 to 4.5 MeV, at intervals of $\leq$ 50 keV and with accuracies of 1-2%. Differential neutron-elastic-scattering cross sections have been measured from 1.5 to 3.8 MeV, at intervals of $\leq$ 50 to 100 keV and at 10-20 scattering angles distributed between 20 and 160°. Furthermore, (n,n'γ) measurements have been made from 0.86 to 2.4 MeV, at intervals of $\approx$ 100 keV and at a gamma-ray emission angle of 55°. The gamma-ray results were associated with the excitation of 36 levels in indium up to excitations of 2.5 MeV. Inelastic-neutron-scattering cross sections were deduced from the gamma-ray measurements for levels to 1.9 MeV. The experimental results are discussed in terms of the optical-statistical, vibrational, rotational and unified nuclear models. The results of this study are being prepared for journal publication.

[a] University of Western Cape, Republic of South Africa.
[b] National Accelerator Center, Republic of South Africa.

3. Fast-neutron Scattering Over the Energy Range 4.0-10.0 MeV

(A. Smith and P. Guenther)

For a number of years the FNG group has experimentally studied the fast-neutron-scattering process; first below 1.5 MeV and more recently at energies in the 1.5-4.0 MeV range. This program has now been extended to 10.0 MeV. Measurements are made at 20 or more scattering angles distributed between 20-160°, and at incident-neutron-energy intervals of $\lesssim$ 0.5 MeV. At present, the mass range of targets extends from A=9(Be) to $\sim$A=115(In). Particular attention is given to the structural materials, Cr, Fe and Ni, including elemental and isotopic results. Model development is presented concurrently with the measurements, including both conventional optical-statistical and coupled-channels models.

4. Neutron Total, Scattering and Inelastic-gamma-ray Cross Sections of Yttrium

(C. Budtz-Jörgensen[a], P. Guenther, A. Smith, J. Whalen, W. McMurray[b], M. Renan[b], and I. van Heerden[c])

Neutron total, scattering and (n,n'γ) cross sections of yttrium have been measured in the few-MeV region. The neutron total cross sections were measured with broad resolutions over the range 0.5 to 4.2 MeV, in steps of $\lesssim$ 0.1 MeV. Neutron elastic- and inelastic-scattering cross sections were measured from $\approx$ 1.5 to 4.0 MeV at incident energy intervals of 50 keV. Inelastic-scattering cross sections were also determined using the (n,n'γ) reaction, at incident neutron energies from 1.6 to 3.8 MeV and at intervals of 0.1 MeV. Gamma-rays and/or inelastically-scattered neutrons were observed corresponding to the excitation of levels at: 909.0±0.5, 1507.4±0.3, 1744.5±0.3, 2222.6±0.5, 2530.2±0.8, 2566.4±1.0, 2622.5±1.0, 2871.9±1.5, 2880.6±2.0, 3067.0±2.0, 3107.0±2.0, 3140.0±2.0, 3410±2.0, 3450.0±2.0, 3504.0±1.5, 3514.0±2.0, 3556.0±2.0, 3619.0±3.0, 3629.0±3.0, 3715.0±3.0 keV. Some of the experimental results are indicated in Fig. A-2. The measured values were examined in terms of the spherical-optical-statistical, coupled-channels, and core-coupling models. The results are particularly relevant to an important fission product.

[a] On leave from the Central Bureau for Nuclear Measurements, Geel, Belgium.
[b] National Accelerator Center, Republic of South Africa.
[c] University of Western Cape, Republic of South Africa.

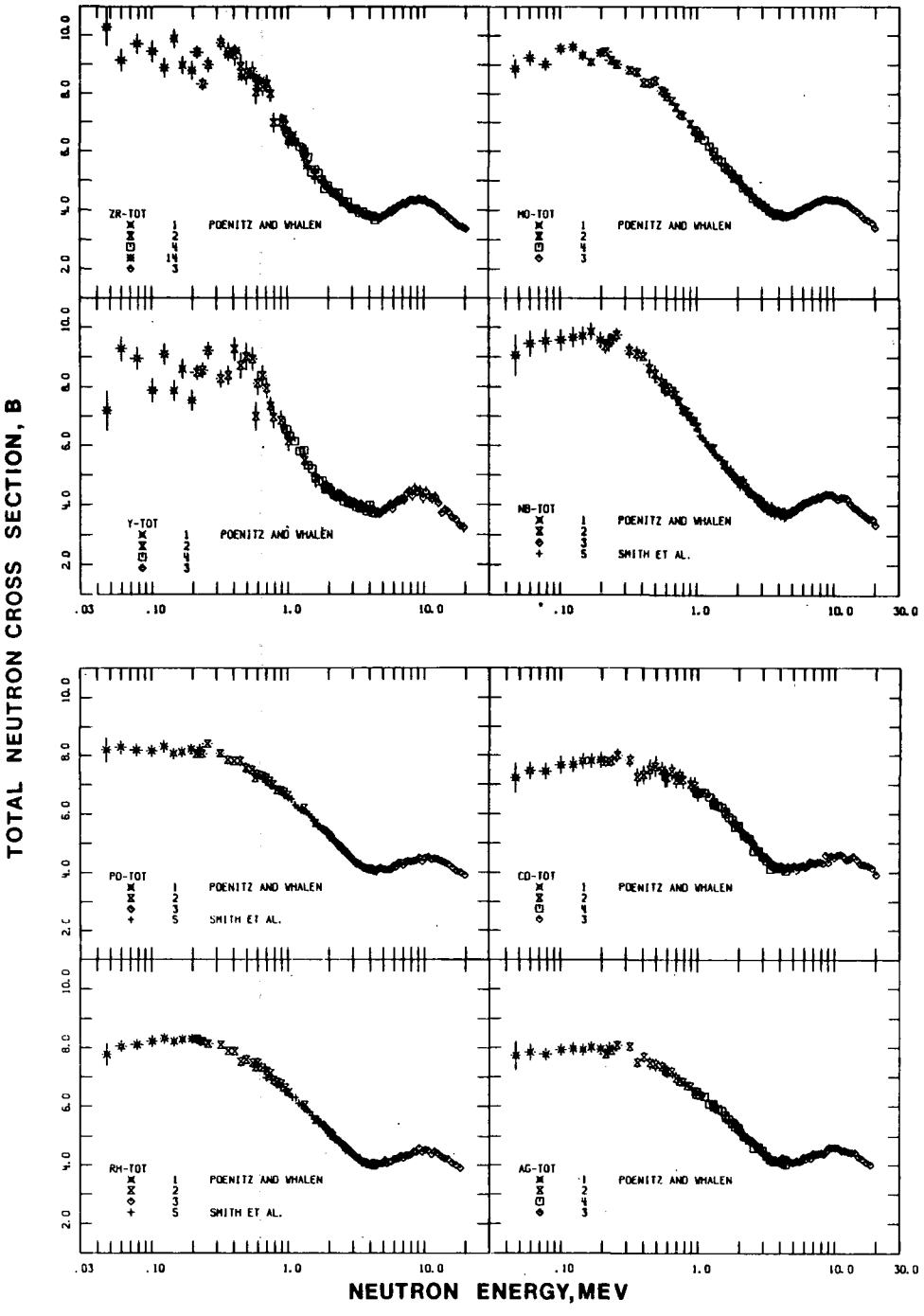

Fig. A-1. The present results for the neutron total cross sections of Yttrium, Zirconium, Niobium, Molybdenum, Rhodium, Palladium, Silver and Cadmium. Recent data by Smith et al. are shown for comparison.

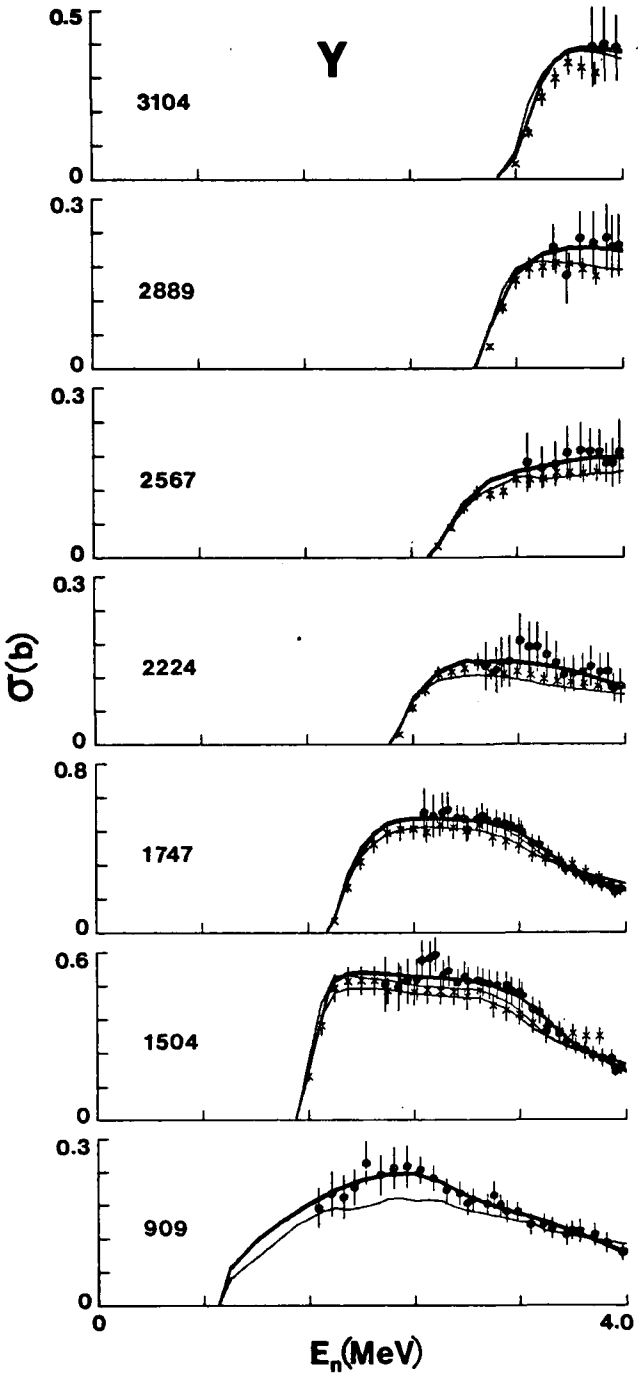

Fig. A-2. Inelastic-neutron-excitation cross sections of yttrium. Results of neutron time-of-flight measurements are noted by ● and those deduced from (n,n'γ) by X. Excitation energies are given in keV. Heavy curves are eyeguides, light curves the results of model calculations.

5. Cross Sections of the (n,n'γ) Reaction for ^{54}Fe, ^{63}Cu and ^{65}Cu in the Low-MeV Energy Range
(D. L. Smith and P. T. Guenther)

Work on this experiment was recently completed and papers are being prepared. They will present the combined results of total, elastic- and inelastic-scattering and gamma-production cross section measurements from this laboratory. Gamma-production cross sections have been obtained for transitions observed from ^{54}Fe at neutron energies below 4 MeV, and for ^{63}Cu and ^{65}Cu at neutron energies below 2 MeV. Gamma-production angular distributions were also measured at several energies. Experimental gamma-production cross sections for ^{54}Fe are shown in Fig. A-3(b); they correspond to transitions indicated in Fig. A-3(a). The gamma-ray results are useful for resolving inelastic scattering components which cannot be distinguished in neutron scattering studies alone. Furthermore, the sums of cross sections for certain individual transitions (e.g., the 1.408-, 2.950- and 3.166 -MeV gamma-rays from ^{54}Fe) are nearly equal to the total inelastic scattering cross sections, thereby allowing experimental total inelastic scattering cross sections to be deduced near threshold.

6. The Measurement and Evaluation of Niobium Neutron Data
(A. Smith, P. Guenther, J. Whalen and W. Poenitz)

A coordinated measurement and evaluation study of fast-neutron interaction with niobium is in progress. The neutron total-cross-section measurements and evaluation are completed to 20 MeV. Neutron scattering measurements are completed to 4 MeV and measurements to 10 MeV are nearing completion. Continuum neutron-emission spectra are being investigated. The development of a model suitable for interpolating and extrapolating the measured values is well along. The parameters of this optical model are of basic physical interest, particularly their energy dependencies. This effort is responsive to fusion-data needs.

7. The Fission Cross Sections of Some Th, U and Pu Isotopes Relative to ^{235}U
(J. W. Meadows)

The results from the earlier measurements of the fission cross sections of ^{230}Th, ^{232}Th, ^{233}U, ^{234}U, ^{236}U, ^{238}U, ^{239}Pu, ^{240}Pu and ^{242}Pu relative to ^{235}U were reviewed and revised to include changes in data processing procedures, alpha decay half-lives, and thermal fission cross sections. The question of errors was re-examined and put on a more consistent basis. Some new data were included. In particular, the shape measurement for ^{233}U was extended into energy regions that were not accessible at the time of the original measurement, and additional normalization measurements were made for ^{233}U, ^{239}Pu and ^{242}Pu. As a result of

this review, the energies of the older measurements were increased by amounts ranging from 1-2 keV near 0.2 MeV neutron energy to 50 keV near 10 MeV. Otherwise, there were few changes in the shape measurements. Corrections to the normalizations were generally small, but for four ratios the changes exceeded 1%. These were: $^{233}U/^{235}U$ -1.77%; $^{234}U/^{235}U$ -1.19%; $^{238}U/^{235}U$ -1.02%; $^{239}Pu/^{235}U$ +1.85%. The remaining ratios were < 0.5%. Details of this review and tables of the results are available in a report.[1]

---

[1] J. W. Meadows, ANL/NDM-83, Argonne National Laboratory (1983).

8. Cross Section Measurements for $^{51}V(n,p)^{51}Ti$ and $^{51}V(n,\alpha)^{48}Sc$ Below 10 MeV

(D. L. Smith, J. W. Meadows and I. Kanno[a])

Interest in neutron-induced hydrogen and helium production in vanadium stems from the anticipated role for this element in fusion-energy structures. Existing differential data for both of these reactions are sparse, and none exist for the important threshold regions. Data for both these reactions have been acquired at energies below ~ 10 MeV. The analysis is complete for $^{51}V(n,p)^{51}Ti$, and a report on this work is now in draft form (to be issued as an ANL/NDM report). Data processing for the $^{51}V(n,\alpha)^{48}Sc$ reaction is in progress.

---

[a] Visiting exchange associate, Kyoto University, Japan.

9. Neutron Activation Cross Section Measurements at 14 MeV

(D. L. Smith, J. W. Meadows and S. A. Cox)

Neutron activation cross section measurements have been performed in the vicinity of 14 MeV energy for a large number of reactions appearing in a recent compilation of nuclear data needs for fusion energy applications[1]. The objective of this experimental investigation is to provide a comprehensive and internally consistent data set which should cast new light on several long-standing cross-section discrepancies. These data are now in the process of being analyzed.

---

[1] E. T. Cheng, D. R. Mathews and K. R. Schultz, "Magnetic Fusion Energy Program Nuclear Data Needs," GA-A16886, GA Technologies, Inc., San Diego, California (1982).

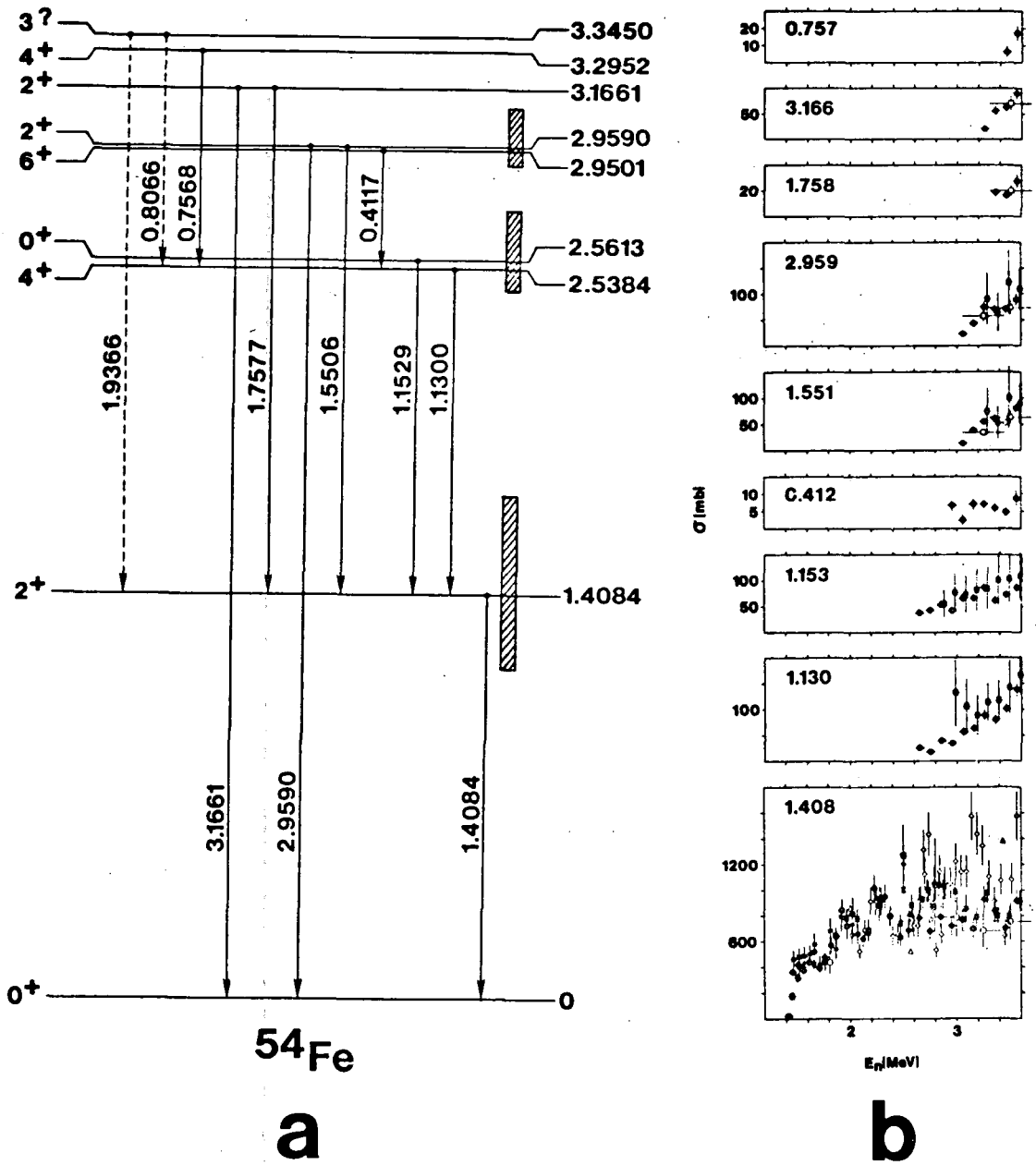

Fig. A-3. (a) Gamma-ray transitions observed in the present (n,n'γ) experiment.
(b) Measured gamma-ray production cross sections from the present experiment (filled circles). Other data from the literature are also shown for comparison.

10. Measurement of ^{27}Al and ^{54}Fe (n,2n) Reactions for Fusion Reactor Diagnostics and Waste Handling Assessments

(R. K. Smither and L. R. Greenwood)

Measurements of the ^{27}Al and ^{54}Fe (n,2n) cross sections were made recently in collaboration with the dosimetry group at the Princeton Plasma Physics Laboratory working on the new TFTR fusion reactor. The main interest in these reactions is their possible use in measuring the plasma ion temperature in d-t fusion reactors. Both reactions have threshold energies close to the centroid of the d-t neutron energy spectrum near 14 MeV. This feature makes their reaction yields a sensitive function of the width of the neutron energy spectrum which in turn is directly related to the ion temperature of the plasma. The ratio of the (n,2n) yield to the yield from other reactions, such as (n,p) or (n,α), in these nuclei is nearly linear with ion temperature, making the analysis particularly easy. Fig. A-4 shows some of the results for the Al(n,2n) reaction near threshold, compared to predicted fusion neutron energy distributions. The steep rise of the yields near threshold illustrates the high sensitivity of this technique for fusion reactors. Our data suggest that the Al reaction proceeds mainly to the 3+ state at 417 keV and to the 1+ state at 1057.8 keV rather than to the 5+ ground state and the 0+ isomeric state at 228.2 keV.

Measurements of the long-lived ($T_{1/2} = 7.3 \times 10^5$ y) ground state of ^{26}Al have been made since this reaction is of concern in the disposal of fusion waste materials. Measurements were made by the relatively new technique of accelerator mass spectrometry (AMS). In this method, a particle accelerator is used as a giant mass spectrometer, yielding sensitivities as low as one part in 10^{12}. These data are also shown in Fig. A-4. Our data indicate that the cross section is only about one fourth that predicted previously, making ^{26}Al of less concern in fusion waste handling. Further data are being obtained for this reaction by irradiating large samples at RTNS II so that we can directly measure the gamma activity. Other long-lived isotopes, such as ^{53}Mn from the ^{54}Fe(n,2n) reaction, will also be measured by the AMS technique. Stable isotopes can also be measured in some cases to determine transmutation rates.

11. Measurement of Al and Cu Spallation Cross Sections from 30-450 MeV

(L. R. Greenwood and R. K. Smither)

Neutron cross sections are poorly known at higher energies above 14 MeV; we are measuring data for spallation sources as well as for the Fusion Materials Irradiation Test Facility (FMIT) under development at Hanford Engineering Development Laboratory (HEDL). Spallation cross sections for Al and Cu are being measured at the IPNS at Argonne. Foils are placed directly in the proton beam, and the spallation products are measured by gamma spectroscopy. Over 20 different isotopes have been measured from Cu, and 3 from Al, in the energy range from 30 to 500 MeV, as illustrated in Fig. A-5.

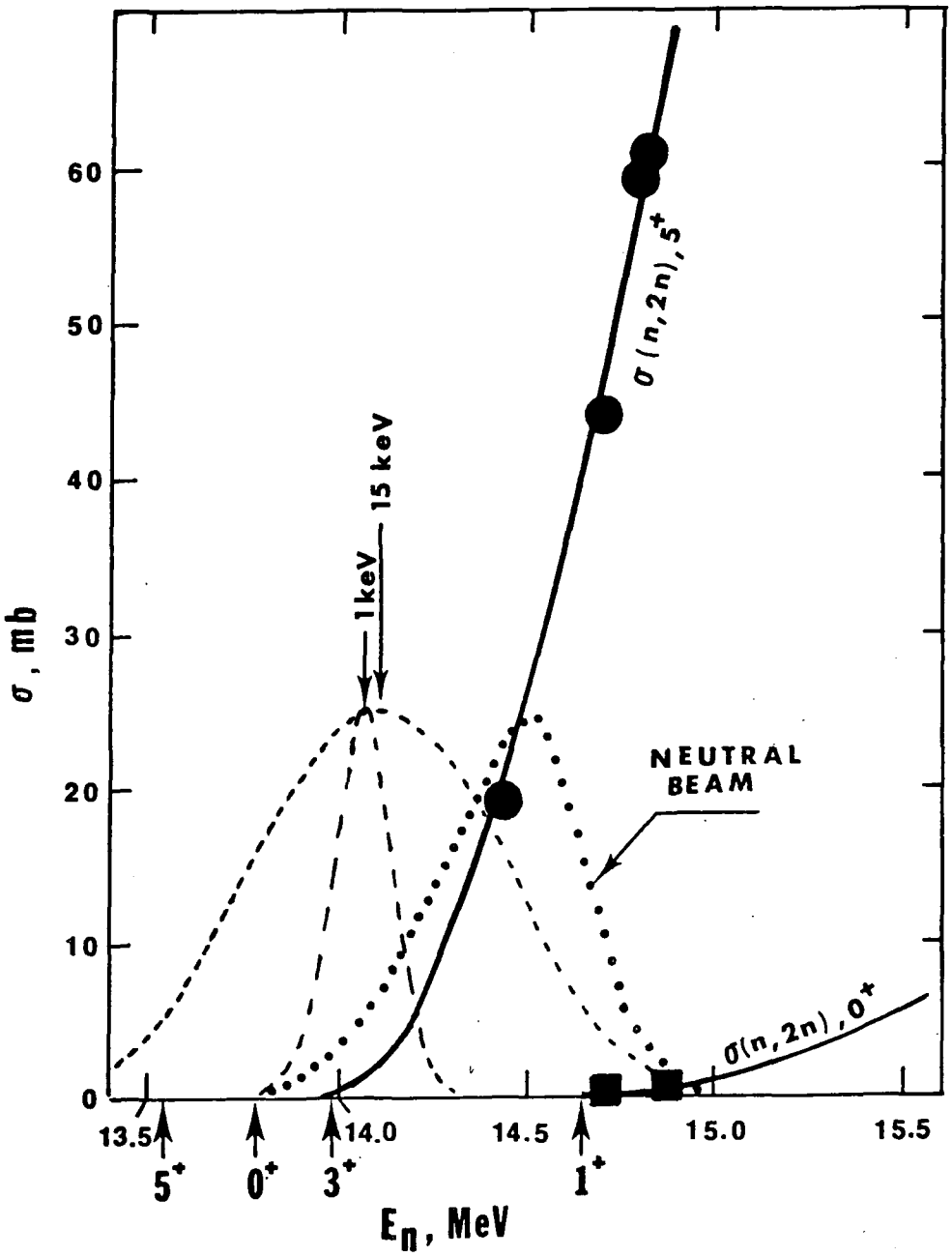

Fig. A-4. Comparison of the experimentally determined cross sections for the productions of the ^{26}Al ground state (730,000 y, filled circles) and the isomeric state (6 s, filled squares) with the predicted neutron energy spectra from a fusion reactor plasma at ion temperatures of 1 and 15 keV (dashed lines), and the addition of a 120 keV neutral beam injected into plasma (dotted line).

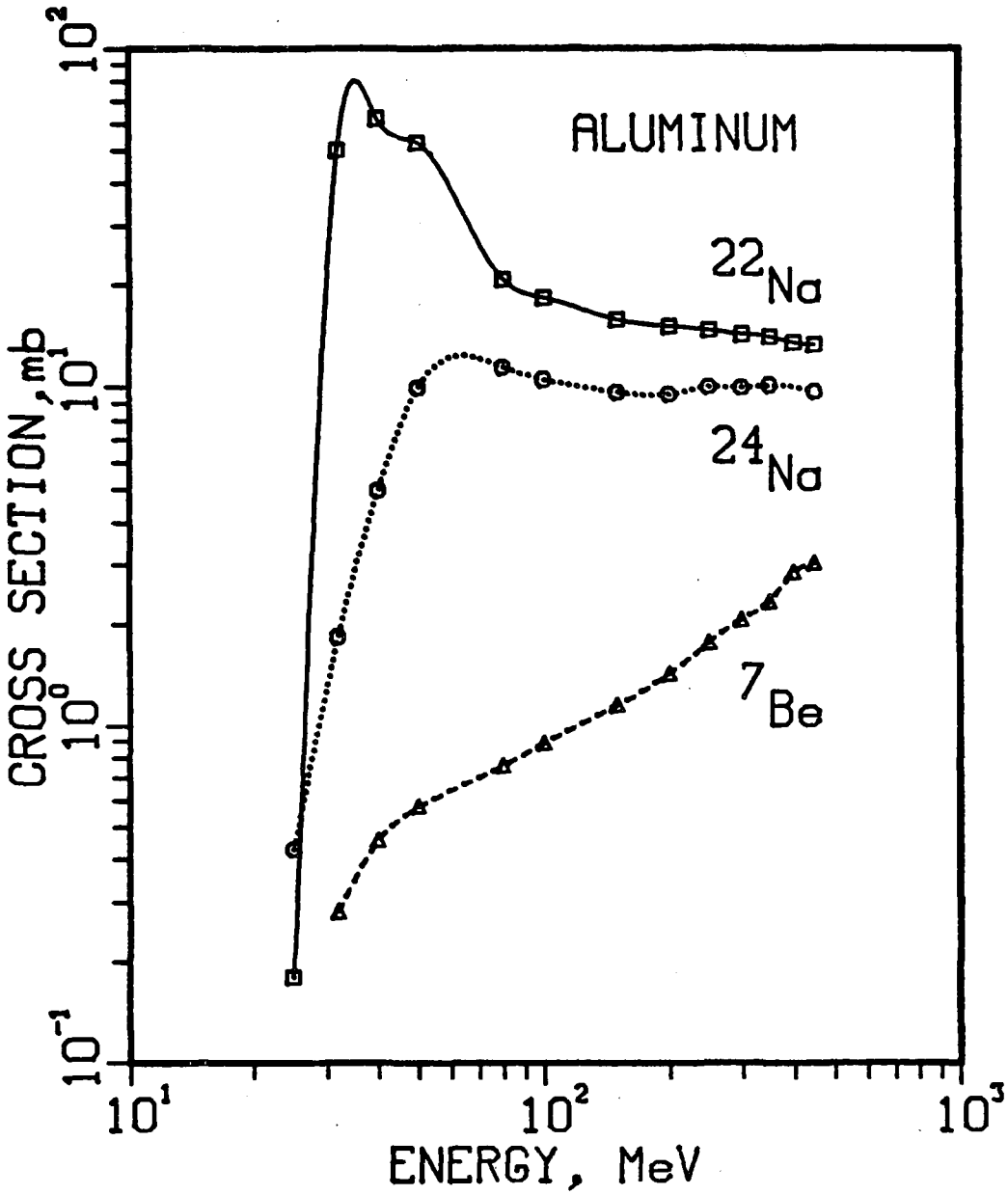

Fig. A-5. Spallation cross section measurements for aluminum are shown for the radioactive isotopes ^{22}Na, ^{24}Na, and ^{7}Be. The different energy dependence of each yield can be used in an integral flux measurement to unfold the flux energy spectrum.

Since the yield of each spallation product has a different energy dependence, the ratio of the products is quite sensitive to the neutron energy distribution. This technique will be used to extend our dosimetry measurements to 500 MeV, and may prove useful at the FMIT for the weak neutron flux between 30 and 55 MeV.

The experimental measurements are being compared with a semi-empirical model due to Rudstam, as updated by Silberberg and Tsao. The data show a systematic difference from the models, depending on the mass difference of the target and product. The data are being tested in integral measurements with the ultimate goal of neutron flux and spectral adjustments at these higher neutron energies.

12. Simultaneous Evaluation of Cross Sections for ENDF/B-VI (W. P. Poenitz)

The standards and some other cross sections of importance for reactor applications are linked by ratio measurements which make the available data base a twofold over-determined system[1]. It has been concluded that these data should be evaluated simultaneously[1,2].

The present effort is a major contribution toward this goal for ENDF/B-VI. The cross sections for $^{6}Li(n,\alpha)$, $^{6}Li(n,n)$ $^{10}B(n,\alpha_0)$, $^{10}B(n,\alpha)$, $^{10}B(n,n)$, $Au(n,\gamma)$, $^{238}U(n,\gamma)$, $^{238}U(n,f)$, $^{235}U(n,f)$ and $^{239}Pu(n,f)$ are being evaluated based on available absolute, shape, ratio and sum (e.g., total cross sections) data. Data sets with low uncertainties which might outweigh other data have been carefully scrutinized. Corrections for some of the data have been proposed, and uncertainties have been estimated where such information had not been given by the experimenters. Reported quantities have been converted to originally measured quantities, thus preserving experimental information free from ambiguities of reference cross sections. Correlations within each data set and correlations between data sets are being taken into account.

The result from a generalized least-squares fit will provide consistent values for the above cross sections, their variance-covariance matrices, and the cross covariances between these cross sections. The actual input for the ENDF/B-VI evaluation will be obtained from a somewhat reduced data base. Some of the data on ^{6}Li and ^{10}B, removed from the present data base, will be used together with angular distributions, inverse reaction data, etc., in an R-matrix analysis by G. Hale at LASL. The results from both analyses will be combined by R. Peelle, ORNL, to yield ENDF/B-VI.

---

[1] W. P. Poenitz, Proc. Conf. Nucl. Data Evaluation Methods and Procedures, BNL-NCS 51363, Vol 1, p. 249, Brookhaven 1981.

[2] Cross Section Evaluation Working Group (CSEWG), Evaluation Committee, Subcommittee for Standards, 1982 and 1983.

B. STANDARDS MEASUREMENTS

1. ^{235}U and ^{239}Pu Sample Mass Determinations and Intercomparison

(W. P. Poenitz and J. W. Meadows)

The neutron induced fission cross sections of ^{235}U and ^{239}Pu are of importance in reactor applications and are therefore required to be known with high accuracy ($\leq$ 1%). Consequently, the sample masses need to be known to even higher accuracy for measurements of these cross sections, or for reaction-rate-ratio measurements in reactor-test facilities. In order to establish the accuracy to which sample masses are presently known, fifteen ^{235}U samples were obtained from seven laboratories and four ^{239}Pu samples were obtained from two laboratories. The masses of these samples were determined by low-geometry alpha counting and were intercompared by relative fission counting. The fission intercomparison was done for 28 combinations between ^{235}U samples and for 6 combinations between ^{239}Pu samples. A back-to-back ionization chamber was used, and corrections were applied for transmission, neutron scattering, fission in minor isotopes, fission-fragment absorption, and losses below the electronic threshold.

Best values of the ^{235}U sample masses were obtained from a least-squares fit of the present mass determinations, the quoted masses, and the relative alpha and fission-ratio measurements. Figure B-1 shows the differences between the quoted sample masses and the best values. It can be concluded from this intercomparison that ^{235}U sample masses are known to within ± 0.3%, which is sufficiently accurate for cross-section and reaction-rate-ratio measurements.

^{239}Pu masses can be very well determined with low-geometry alpha counting, and good agreement between the present mass determinations and the quoted masses was obtained. However, the relative fission-ratio measurements resulted in disturbing inconsistencies of 1-3% which will be further investigated.

2. The Half-life of ^{234}U

(W. P. Poenitz and J. W. Meadows)

The fissile materials used in cross-section measurements or reaction-rate-ratio measurements usually contain about one percent ^{234}U. The alpha-decay rate of such materials is then dominated by the decay of ^{234}U, which provides a convenient technique for the mass assay of such samples. However, the half-life has to be known and some discrepancies exist between the available measured values and results from thermal parameter fits[1,2].

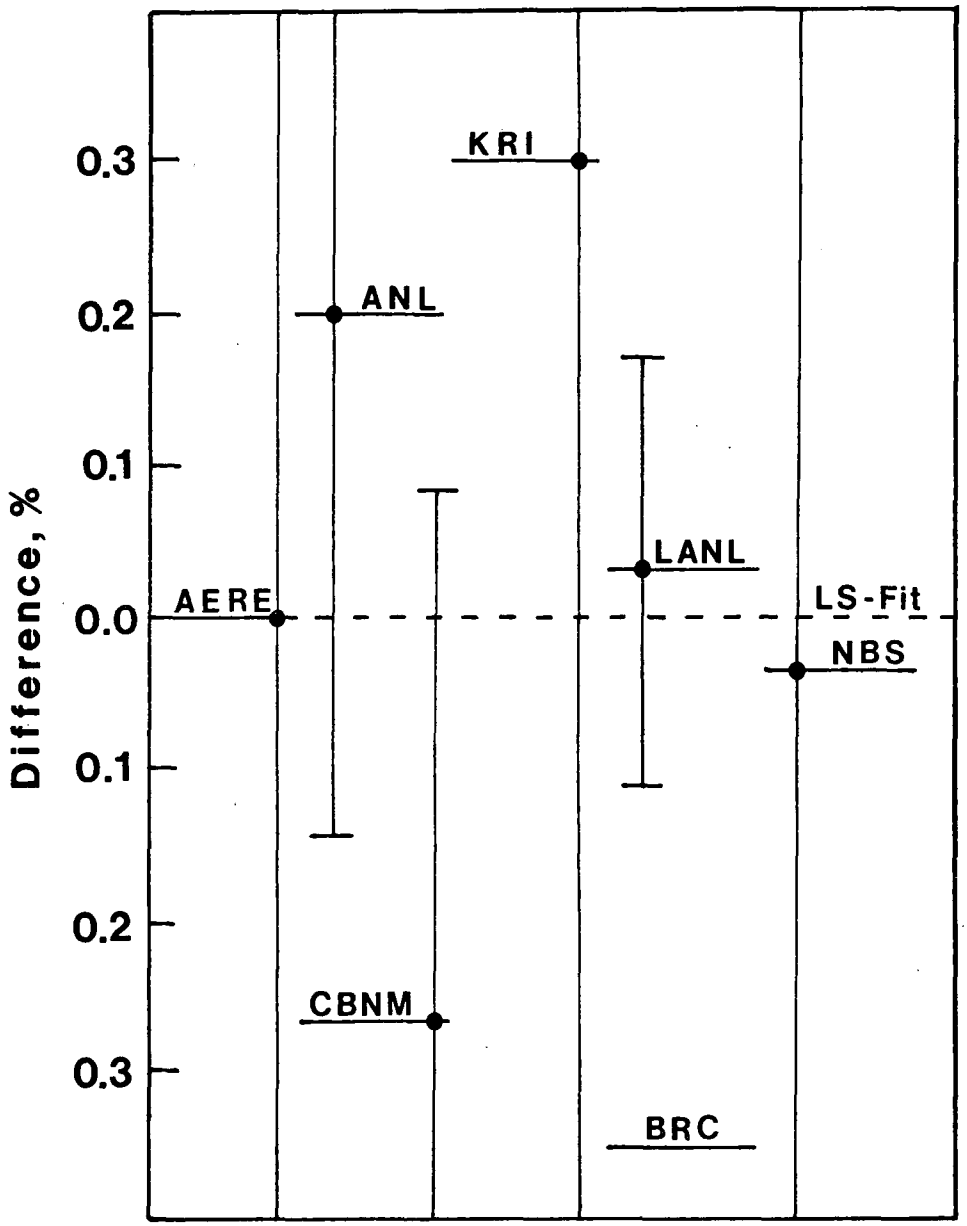

Fig. B-1. The differences between the quoted ^{235}U masses and their best values: AERE = Atomic Energy Research Establishment, Harwell, UK; ANL = Argonne National Laboratory, Argonne, Illinois, USA; BRC = Centre d'Etudes de Bruyeres-le-Chatel, Montrouge, Cedex, France; CBNM = Central Bureau for Nuclear Measurements, Geel, Belgium, EURATOM; KRI = Kloplin Radium Institute, Leningrad, USSR; LANL = Los Alamos National Laboratory, New Mexico, USA. NBS = National Bureau of Standards, Washington, D. C., USA.

The isotopic compositions of two of the fissile materials involved in the ^{235}U sample-mass intercomparison described above were extremely well known. On the other hand, the masses of several samples were well defined based upon the isotopic dilution technique. By removing all values based on the determination of sample masses from the isotopic composition and the half lives, a value for the half life of ^{234}U was obtained from a least-squares fit. This value of

$$(2.457 \pm 0.005) \cdot 10^5 \text{ y.}$$

is in good agreement with the latest measurement by Geidel'man et al.[3], as well as with an evaluated value by Holden[1]. Inclusion of the present value in the compilation of prior values by Holden results in a current best value of

$$(2.4566 \pm 0.0044) \cdot 10^5 \text{ y.}$$

---

[1] N. E. Holden "The Uranium Half-Lives: A Critical Review", Brookhaven National Laboratory Report BNL-NCS-51320 (1981).

[2] H. D. Lemmel, Proc. Conf. on Nuclear Cross Sections and Technology, NBS Spec. Publ. 425, 286 (1975).

[3] A. M. Geidel'man et al., Izv. Acad. Nauk. SSSR, Ser. Fiz. 44, 927 (1980).

C. TECHNIQUES AND METHODOLOGY

1. Project "Stonehenge"
(A. Smith and A. Engfer)

The multi-angle time-of-flight apparatus at the Fast Neutron Generator is being augmented with a massive new detector system, designated "Stonehenge". These modifications will provide for the use of ten detectors at flight paths of approximately 18 meters, all contained within a massive shield weighing approximately 300 tons. Large detector carts run on railroad tracks within the shielding to provide continuous coverage of the angular range 0-150° . The advantages of the improved system are: i) a factor of approximately three improvement in velocity resolution, ii) concurrent detection at ten angles, iii) wide angular coverage in a continuously variable manner, and iv) low backgrounds due to the massive shielding.

2. Reaction Differential Cross Sections from the Least-Squares Unfolding of Ratio Data Measured in Diverse Neutron Fields (D. L. Smith)

A previously-described procedure[1] for deriving threshold reaction differential cross sections from integral measurements in well-specified neutron fields by means of least-squares unfolding is extended to the analysis of the ratio data. The following information is required for the least-squares analysis of ratio data: i) shape specifications for the integral spectra and their uncertainties and correlations, ii) standard reaction group cross section values and their covariance matrix, iii) the ratio data and their covariance matrix, and iv) the a priori group cross sections and their covariance matrix. Knowledge of the absolute neutron fluence is not required. A special class of ratio measurements is investigated in detail, and numerical analysis is performed for a hypothetical simulated experiment in order to illustrate the method. A report on the results of this investigation is in draft form and will be issued as an ANL/NDM report.

---

[1] D. L. Smith, ANL/NDM-77 (1982).

D. NUCLEAR MODEL ANALYSES

1. The Optical Model of Few-MeV Neutron Elastic-Scattering from Z = 39 to 51 Targets (A. Smith, P. Guenther and J. Whalen)

A program of experimental study of neutron total and scattering cross sections of the light-mass fission products was completed. Neutron differential elastic-scattering cross sections of elemental Y, Zr, Nb, Mo, Rh, Pd, Ag, Cd, In, Sn and Sb were measured from $\approx$ 1.5 to 4.0 MeV at intervals of $\leq$ 100 keV, and at ten or more scattering angles distributed between 20 and 160°. Complimentary broad resolution neutron total cross sections were measured from $\approx$ 0.8 to 4.5 MeV at intervals of $\leq$ 50 keV. These experimental results have been interpreted within the framework of the optical-statistical model (OM). A "regional" OM parameter set, quantitatively describing the neutron-nucleus interaction in this mass-energy domain, has been deduced from the observed cross sections. These parameters display geometric, isospin and shell-dependent characteristics. They are particularly suitable for the calculation of the properties of the light-mass fission products. A paper describing this work has been accepted for journal publication.

2. Covariances for Neutron Cross Sections Calculated Using a Regional Model Based on Local-Model Fits to Experimental Data

(D. L. Smith and P. T. Guenther)

We suggest a procedure for estimating uncertainties in neutron cross sections calculated with a nuclear model descriptive of a specific mass region. It applies standard error propagation techniques, using a model-parameter covariance matrix. Generally, available codes do not generate covariance information in conjunction with their fitting algorithms. Therefore, we resort to estimating a relative covariance matrix a posteriori from a statistical examination of the scatter of elemental parameter values about the regional representation. We numerically demonstrate our method by considering an optical-statistical model analysis of a body of total and elastic scattering data for the light fission-fragment mass region. In this example, strong uncertainty correlations emerge and they conspire to reduce estimated errors to some 50% of those obtained from a naive uncorrelated summation in quadrature. The results of this investigation have been reported [1].

[1] D. L. Smith and P. T. Guenther, ANL/NDM-81 (1983).

The reactor-based neutron-nuclear physics research at BNL is composed of three categories: the study of nuclear structure with the (n,γ) reaction, the (n,γ) reaction mechanism and its application to pure and applied physics, and the spectroscopy of neutron-rich, fission product nuclides. These programs use the H-1 and H-2 beam ports of the HFBR. The tailored beam facility produces beams of thermal, 2- and 24-keV neutrons. A monochromator and chopper are used for resonance neutron studies. The TRISTAN on-line mass separator is used with a U-235 target to produce fission product nuclei. These facilities are operated in collaboration with a wide variety of collaborators from national laboratories and universities. In the following sections the complete program is outlined, and those sections of relevance to nuclear energy and other applications are described in detail.

A. NUCLEAR STRUCTURE WITH THE (n,γ) REACTION

The H-1 beam tube at the HFBR provides two beams used almost entirely for neutron capture γ-ray studies. These include the tailored beam facility, which provides beams of thermal, 2 and 24 keV neutrons, and the neutron monochromator, which provides thermal and energy-selected beams up to about 25 eV. These wide ranging beams provide a unique method of nuclear structure investigation due to the primarily nonselective character of the (n,γ) reaction. Indeed, in appropriate cases, all levels of a given spin-parity range in the final nucleus may be about equally populated without regard to the structure of the final state wave functions. This is primarily achieved with the use of the tailored beams, which provide resonance averaging of the primary transitions, and which are absolutely indispensable in the construction of level schemes. The primary transitions unambiguously disclose level positions, which can only be done indirectly from secondary transitions by the inferential application of the Ritz Combination Principle. The secondary transitions, however, are themselves of crucial importance for the information they provide on the electromagnetic matrix elements connecting low lying levels and, thereby, on the applicability of different nuclear models.

1. Studies of Deformed Even-even Nuclei: Tests of the IBA

In the last several years a major advance in nuclear structure studies has been the development and testing of the IBA. Briefly, the basic problem of nuclear structure in heavy nuclei is the practical intractability of the shell model in the face of large numbers of valence nucleons. The familiar geometrical models attempt to overcome this difficulty by the macroscopic strategem of assuming an overall nuclear shape. The IBA offers an alternate scheme, at once more abstract and more general: it assumes an enormous truncation of the possible shell model

configurations such that low lying excitations can be treated, in effect, in terms of bosons which represent pairs of fermions that are coupled to angular momentum 0 (s bosons) or 2 (d bosons). The complex Hamiltonian of the shell model is replaced by an extraordinarily simple one consisting of elementary interactions between bosons. A particularly attractive feature is that three natural limiting symmetries, denotedgroup theoretically as SU(5), SU(3), and O(6), arise when one or another term in this Hamiltonian dominates. These symmetries correspond crudely to the familiar vibrator, rotor, and asymmetric rotor of the geometrical models but contain features unique to the IBA which have been empirically verified. Since intermediate situations are easily handled by adjusting the relative sizes of the various terms in the Hamiltonian, the IBA offers the very attractive possibility of treating vastly different nuclei within a single scheme. Tests of the model to date have centered primarily on even-even nuclei, in particular near the O(6) and SU(3) (deformed) regions. Many tests have been carried out at BNL using the (n,γ) reaction which, due to its inherent nonselectivity and general applicability, is ideally suited to testing a model that itself attempts to generate complete sets of low-lying, collective excitations over broad regions of nuclei. As an outgrowth of our initial study of the deformed nucleus ^{168}Er, with the IBA, a number of other projects have ensued.

a. Axial Asymmetry and the IBA

It has been shown by many authors that the IBA-1 contains no triaxial solutions: that is, the corresponding classical potential always has a minimum at $\gamma=0°$. Nevertheless, it is also known that the O(6) limit corresponds to a γ-unstable nucleus and is similar in many respects to a triaxial one with $\gamma=30°$. Moreover, the K impurities that appear in IBA-1 wave functions when the SU(3) limit is broken correspond geometrically to at least a dynamic if not a static axial asymmetry. Therefore, in some sense, the IBA-1 does contain solutions that reflect an effective asymmetry γ: this is not a static asymmetry but results rather from zero point motion in a γ soft potential. In this study the predictions of the IBA, in the CQF framework, were compared with those of the Davydov asymmetric rotor model and a relation was established between χ and an effective asymmetry γ_{eff}: specifically, for the O(6) limit $\gamma_{eff}=30°$ whereas, for SU(3), γ_{eff} approaches values, near 10°, which are N dependent. The fact that $\gamma_{eff}\neq 0°$ in SU(3) is a finite boson number effect. In fact, for fixed χ, γ_{eff}(SU(3)) decreases with increasing N, and $\rightarrow 0$ only as $N\rightarrow\infty$. These results lead to an interesting parameter free prediction which is empirically verified, namely that γ_{eff} will increase as the deformation β decreases in a transition region from SU(3) to O(6). (BNL/Clark)

b. γ-softness vs. Static Asymmetry in the IBA

The effective dynamic asymmetry that appears in the IBA results from a softness in the corresponding geometrical potential as a function of γ. On the other hand, a static asymmetry (with $\gamma=30°$) may be introduced

with the IBA-1 by the addition of higher order terms of cubic type $[(d^+d^+d^+)^{(3)}\ (ddd)^{(3)}]$. An important question is whether or not the two origins of asymmetry may be distinguished empirically. In the usual IBA-1 model a large γ_{eff} requires and, indeed, arises from, a large γ softness. With a cubic term, the same γ_{eff} corresponds to a different softness. The combination of the two contributions to γ_{eff} leads to a flexibility in the mean γ--γ-softness relation. A series of calculations are being carried out to explore this flexibility. Initial results suggest that the γ band energy, most B(E2) values, and even quadrupole moments, depend mostly on the mean γ and are relatively insensitive to its dynamic fluctuations. However, the energy staggering within the γ band seems particularly sensitive to the softness and may provide the best empirical indicator of the relative importance of cubic terms. An existing Coulomb excitation study of ^{104}Ru provides some interesting data in this regard. More data in the same mass region would be useful and are currently being obtained in (n,γ) experiments (see next paragraph). (BNL/Gent/Stony Brook/Clark)

c. (n,γ) Study of ^{102}Ru

In an effort to study further the question of mean asymmetry vs γ-softness, a study of ^{102}Ru is being carried out using the ARC technique on a target of ^{101}Ru. This will complement an existing Coulomb excitation study of ^{104}Ru. By inspecting the energy staggering in the γ band, a measure of the γ softness should emerge (see above paragraph) and allow, at least in this mass region, an assessment of the relative importance of γ softness and static asymmetry in the origin of a net mean γ. It is anticipated to complement this experiment with a GAMS study of the low energy secondary γ rays at the ILL in Grenoble and also with γ-γ coincidence and angular correlation studies at BNL. (BNL/Stony Brook)

d. Studies of Transitional and O(6)-like Nuclei

Since the discovery of the O(6) limit in ^{196}Pt and of an O(6)→rotor transition in the Pt-Os region, a continuing program of studies in this mass region, and in others thought to exhibit similar structure, has been carried out.

i. ^{188}Os and the O(6)→Rotor Transition Region

A number of years ago a detailed (n,γ) study of γ-ray transitions in ^{188}Os was carried out at BNL. Some of the results from the level scheme, primarily concerning 0^+ states, were published; these analyses provided a principal part of the initial motivation to look at IBA predictions for these and neighboring nuclei. In turn, this resulted in the discovery of the O(6) limit in ^{196}Pt and, thereby, in a host of other studies. However, the full level scheme was never published due to some remaining questions and the need for electron conversion data. Such data have now been recorded at the ILL. These results are being used to

finalize the full ^{188}Os level scheme. Work on this project was halted during FY 1983 due to manpower limitations. It is expected to be completed in FY 1984. (BNL/ILL/Clark)

ii. The Nuclear Structure of ^{136}Ba

The nuclei in this region are similar to those in the Pt-Os region, in the sense that the underlying single particle structure consists of neutron holes and proton particles. In the IBA-2 framework, such a situation should give rise to an O(6)-like structure, and it is, therefore, of interest to look for the influence of such character in the structure of ^{136}Ba. The ^{135}Ba(n,γ)^{136}Ba reaction has been studied at the ILL, Grenoble using the spectrometers GAMS and BILL and at BNL via ARC measurements, and also measurements of low energy and primary γ rays following thermal neutron capture. During the past year this study has been extended by performing coincidence and angular correlation measurements on a thermal neutron beam at Grenoble. The results of all measurements have been combined to produce a detailed level scheme up to 2.3 MeV in excitation energy, and the interpretation of this scheme is currently in progress. (University of Manchester/BNL/ILL)

2. Other Studies of Even-even Nuclei

a. Intruder States in ^{114}Cd

The level structure of the even Cd nuclei has recently taken on new and greatly heightened interest due to the discovery that isotopes such as $^{112-116}$Cd are not good examples of vibrational nuclei but rather exhibit a quintuplet of levels at the energy expected for the two phonon triplet. To understand the structure of these "extra" states, very careful studies have been carried out at BNL and ILL as well as other laboratories in a multi-national collaboration. In the current study emphasis was placed on the study of E0 transitions and the interpretation of the level structure in terms of the coexistence of normal vibrational-like and deformed proton intruder states formed by exciting pairs of protons above the Z=50 shell gap. Calculations of the energies and mixing of these two level systems are able to account for the quintuplet structure, for the peculiar B(E2) values connecting these states and, qualitatively, for the abundance of E0 transitions observed. Further studies of intruder states in ^{118,120}Cd were also carried out in FY 83 and 84 at TRISTAN (see later paragraphs). (BNL/ILL/Munich/Gent)

b. Nuclear Structure near Z=64: Level Scheme of ^{148}Sm

The effects of the Z=64 subshell closure on the structure of the transitional rare earth nuclei near N=90 has been the subject of considerable current interest, and a comprehensive series of (n,γ) studies of ^{148}Sm have been made, including ARC, $\gamma\gamma$ coincidence, and singles measurements using the neutron monochromator facility at BNL to populate

the 3.4 eV resonance in ^{147}Sm. The data are currently being analyzed. (University of Manchester/BNL)

c. Level Structure of ^{184}W

Average resonance capture data at neutron energies of 2 and 24 keV have been taken and analyzed, and preliminary results have been published. Curved crystal (GAMS) data have also been taken, and the analysis of these, and subsequent construction of the level scheme, is in progress. It may well be that, contrary to common opinion, the W isotopes are perhaps the best examples of near SU(3) nuclei, in the heavy mass region. (BNL/Koln)

d. The ^{177}Hf(n,γ)^{178}Hf Reaction

A study of ^{178}Hf has been undertaken in collaboration with the University of Koln. Analysis of the 2 and 24 keV ARC spectra is still in progress at Koln as is data from the GAMS and BILL spectrometers of the ILL. (Koln/ILL/BNL)

e. The ^{97}Mo(n,γ)^{98}Mo Reaction

The nuclei near A=100 are of considerable interest because of the strikingly rapid onset of deformation which take place in this region. In addition, the presence of the Z=40 subshell gives rise to collective intruder bands at low excitation energy. Extensive Coulomb excitation studies of ^{98}Mo have been performed at the Daresbury and Oxford tandems, and an ARC measurement at BNL is planned for the near future. The results will be compared with recent calculations in an IBA-2 framework which attempts a description of Mo nuclei, by mixing configurations having different proton boson numbers, representing the "normal" and "intruder" states. Initial comparisons with the data have proved extremely encouraging, but it will be crucial to see if the theory correctly reproduces the complete set of low spin states which will be identified in the ARC measurement. (BNL/Manchester)

f. Levels in ^{244}Cm

Gamma rays and conversion electrons have been measured for the ^{244}Am beta decay isomers 10h ^{244g}Am and 26m ^{244m}Am using the GAMS and BILL spectrometers at the ILL, Grenoble. The activity was produced in an ^{243}Am target undergoing thermal neutron capture in the ILL reaction. New transitions accompanying the beta decay of 26m ^{244m}Am were observed. In particular, the observation of two E0 tansitions allowed the identification of the first low lying 0^+ band in ^{244}Cm. The associated X(E0) value for the bandhead has been compared with earlier calculations for actinide nuclei, made in the framework of BCS and RPA theory, and suggests that the 0^+ state in ^{244}Cm can be identified as a pairing isomer, built on the $1/2^+$[400] and $11/2^-$[505] proton orbits. (LLL/ILL/BNL)

3. Studies of Odd Nuclei

a. The IBA in Odd A Nuclei: Search for Possible Single and Multi-j Supersymmetries

The extension of the IBA formalism to include the fermion degree of freedom has suggested the intriguing possibility of symmetries in the boson-fermion system, similar to those already predicted and observed for the even mass systems. Indeed, there exists, in theory, the possibility of a supersymmetry (SUSY), which encompasses both the even and odd mass systems. Since a prerequisite for such a symmetry is that the even-even core of the odd mass system should itself exhibit one of the appropriate symmetries (SU(5), SU(3), or O(6)) the best region to search for such structures are those where the core exhibits such characteristics. An O(6)-like region is thus an ideal testing ground. Initially, theoretical predictions were worked out for a fermion in a j=3/2 orbit coupled to an O(6) core (U(6)4). Unfortunately, the shell model never provides an isolated j=3/2 orbit [there are always nearby $s_{1/2}$ (in a π=+ shell) or $p_{1/2}$ and $f_{5/2}$ (π=-) orbits]. Therefore, the group structure can describe only that subset of the empirical levels where the particle occupies a 3/2 orbit. In such a situation, the appropriate empirical probe is a particle transfer reaction that is sensitive to the shell model character of the 3/2 states observed. The earliest studies along these lines, utilizing, for example, results from (d,p), (t,p), and (p,t) studies, centered on the odd proton Ir and Au nuclei and revealed some resemblance between predicted and observed level sequences and selection rules, but also showed that a 3/2 x O(6) scheme had, at best, only approximate utility. Faced with this, recent group theoretical work has made substantial advances, and led to the prediction of a new supersymmetry U(6/12) corresponding to an O(6) core and a fermion that can occupy any of the j=1/2, 3/2, or 5/2 orbits. This situation is fortunate for it corresponds precisely to that occurring in the odd mass Pt isotopes and this SUSY scheme should account, therefore, for all low lying negative parity levels. The empirical probe of choice in this case must be a non-selective one, namely (n,γ), that can disclose all such states. During FY 1983, studies of ^{195,197,199}Pt were completed and compared with the SUSY predictions. Areas of both agreement and disagreement were identified. Two particular disagreements, in the energy of the second group (representation) of levels and of the energy scale within that group, have led to the proposal of alternate SUSY schemes. The paragraphs below describe work related to these developments.

i. Structure of Alternative SUSY Schemes in Nuclei

The interpretation of the (n,γ) data on ^{195,197,199}Pt disclosed points of agreement as well as disagreement with the original multi-j SUSY scheme (called Chain I). As regards the latter one discrepancy is that the second family of levels appears lower in energy than is possible theoretically. Faced with this, Sun and co-workers and,

independently, Bijker, have proposed an alternative SUSY scheme (called Chain II). The difference is technical but important. Both SUSY's are expressed as group chain decompositions of the parent supergroup U(6/12). However, whereas in Chain I, one link contains $O^B(6)xO^F(6)$, in Chain II, that is replaced by $U^{B+F}(6)$. As a result, a freedom in the relative energies of different representations (families of levels) is achieved which removes the above mentioned discrepancy while fully remaining within the context of a pure supersymmetry. Physically, the difference in the two schemes is that, in Chain I, an explicit O(6) core (boson) symmetry appears whereas it is absent in Chain II: that is, Chain II thus allows for the odd particle to polarize the core. To investigate the differences in the two chains a study was made of their respective wave functions. Those of Chain II were expanded in terms of Chain I states and both were written in terms of a physically transparent basis system of O(6) core states and an odd fermion with j = 1/2, 3/2 or 5/2. It was found that the wave functions for the lowest two representations were identical in both chains while higher ones differ. Specifically, Chain II states, which correspond to a stronger coupling picture, break the core O(6) symmetry, and contain amplitudes from more than one major (σ) family of O(6) states. Nevertheless, in both Chains, the wave functions, expanded in an O(6)xj basis are extremely simple, reflecting the appeal of symmetry schemes, and involve more than one orbit for the fermion, highlighting the importance of the multi-j aspect of the U(6/12) SUSY. (BNL/Drexel/Peking University)

ii. A New Supersymmetric Hamiltonian

Another discrepancy with the original SUSY disclosed by the Pt data was that the predicted levels of the second representation were compressed in energy compared to the data. To alleviate this, a new supersymmetric Hamiltonian was suggested, which involves higher order terms that the standard IBA one. Denoting the Hamiltonian of Chain II as $H_{U(6)}$ the new one is $H = (1+\alpha C_{2U(6)})H_{U(6)}$ where α is a parameter and $C_{2U(6)}$ is the quadratic U(6) Casimir operator. For $\alpha=0$ this reverts to the usual Hamiltonian. Fits to the Pt data give α values $\approx 10^{-2}$. The net effect of the α term is to provide a different energy scaling factor for each representation. For negative α values, it allows the second representation to be expanded without much affecting the lowest representation. Further study is required to determine if this new, but rather ad hoc, extension to the SUSY idea is physically reasonable and generally useful or if it is just a mock up of other effects. (BNL/Drexel/Peking University)

iii. Transitional Nuclei and the U(6/12) Scheme

The studies described above spotlight ^{185}W and ^{195}Pt as the best and only examples of odd mass nuclei well described by the SU(3) and O(6) limits of U(6/12). However, recent work has shown that it may be possible to describe the transition between these two limits in the IBFM framework in a manner analogous to the CQF developed for even-even nuclei. Specifically, the two limits can be generated from a common boson-fermion

Hamiltonian by choosing the appropriate values of the parameter χ of the quadrupole operator, so that a smooth transition between them can be produced by changing a single parameter. Such predictions could, in principle, verify the incredibly diverse properties of nuclei from ^{183}W to ^{199}Pt. It remains to be seen whether the predicted characteristics of this transition correspond to the empirical situation in this region and, to this end, a number of experimental investigations of odd A nuclei are planned or in progress as described in the following paragraphs. (BNL)

iv. (n,γ) Studies of ^{185}W and ^{187}W

A number of (n,γ) studies of ^{187}W have been undertaken, including ARC measurements (2 and 24 keV) at BNL and GAMS and BILL measurements at ILL. The data have been analyzed and a detailed level scheme has been constructed up to 1400 keV in excitation energy. In addition 2 and 24 keV ARC measurements of ^{185}W have recently been completed, and the data analysis is underway. These results should allow a more critical probe of the applicability of the SU(3) scheme of U(6/12) in this region, particularly as regards the higher lying excitations which correspond to coupling of the deformed single particle states to vibrational excitations of the core. (BNL/Manchester/ILL)

v. The $^{188}Os(n,\gamma)^{189}Os$ Reaction

The nucleus ^{189}Os has not yet been studied via the ARC technique, and so such studies are planned for FY 1984 in order to build up as complete a picture as possible of the odd A transitional region. Singles, coincidences and angular correlation data may also be taken using the thermal neutron beam of the monochromator facility. (BNL/Manchester)

vi. <u>$^{190}Os(n,\gamma)^{191}Os$ Reaction</u>

Earlier average capture data, as well as extensive Ge(Li) γ-γ coincidence studies at BNL, have been combined with data from the GAMS 1 spectrometer at the ILL. A partial level scheme has been constructed but its completion has been delayed due to several puzzling features. The most prominent of these is that five of the strongest transitions, which form a coincident cascade, cannot be incorporated into the existing level scheme. Work on this project was suspended during FY 1983 but will be renewed in the near future as part of a broad attack on the structure of all odd neutron nuclei from ^{183}W to ^{199}Pt. (BNL/ILL)

vii. (n,γ) Studies of $^{193,197}Pt$

Further investigations of the ^{197}Pt level scheme via secondary γ rays are in progress, including Ge singles measurements, γ-γ coincidences and angular correlation studies. It is hoped to initiate a similar series of measurements of the $^{192}Pt(n,\gamma)^{193}Pt$ reaction, if a suitable ^{192}Pt target can be obtained in the coming year. The rarity of this

isotope has previously precluded the use of the ARC technique in this case, but is hoped that, following the proposed upgrading of the three crystal pair spectrometer, such a measurement may become feasible. (BNL/ Manchester)

b. Other Related Studies

i. ARC Study of ^{199}Hg

ARC data at 2 and 24 keV leading to ^{199}Hg were recorded to test for a possible SU(5) multi-j SUSY in the heavy Hg isotopes. The data revealed no new low spin states beyond those already known. (BNL)

ii. Studies of ^{131,133}Ba

The odd mass Ba nuclei represent another region where the underlying core structure may be close to the O(6) limit, and hence a supersymmetry may also be evident in the odd mass system. The nuclei ^{131}Ba and ^{133}Ba have been studied at BNL, following thermal neutron capture on the neutron monochromator facility, and at ILL with the GAMS spectrometers. The data analysis and level scheme construction is still in progress. (BNL/ILL)

iii. Study of ^{135}Ba

This study is complementary to the above investigations of ^{131,133}Ba. ARC data at 2 and 24 keV were taken in order to identify the complete set of low spin states. The theoretical interpretation of the results will clearly be coupled to that for the two lighter mass Ba nuclei. Work on these two Ba projects has been tabled during FY 1983 due to manpower limitations and the press of other projects. It is hoped to return to it in the near future. (Yale/BNL)

iv. Study of ^{169}Er

Since the even-even core nucleus, ^{168}Er, is now so well characterized empirically, a study of ^{169}Er presents an ideal opportunity to carry out a thorough interpretation of an odd mass deformed nucleus. Therefore, as an initial step, ARC data at 2 and 24 keV have been recorded and analyzed during the year. At present there remain some difficulties in reconciling the results at the two energies. When this is achieved, the data should disclose the full set of low lying $1/2^-$ and $3/2^-$ states in ^{169}Er. Depending on the outcome, this may be followed up by bent crystal and electron conversion spectroscopy at the ILL. The nucleus ^{169}Er will provide an excellent test of the coupling of single particle and vibrational states in the Nilsson model as well as a test of the IBA for odd mass nuclei in a multi-j context. (BNL)

c. Other Studies of Odd Mass Nuclei

i. Level Structure of ^{239}U

ARC spectra at 2 and 24 keV leading to ^{239}U were recorded as well as the circular polarization of γ rays from the capture of polarized neutrons. As a result a number of new levels were discovered and assigned spin parity values. The level scheme was interpreted in a Nilsson scheme and includes the assignment of a large number of vibrational excitations built upon various Nilsson orbits. The results extend the systematics of these excitations in the actinide nuclei and help provide a firm basis for detailed calculations. Due to the high density of Nilsson orbits, collective vibrations are low lying in this mass region. This leads to the possibility, seldom realized in other deformed regions, of observing vibrations built on several different basis states. Their energies above these base states, their inertial parameters and decay characteristics, can provide crucial information on the microscopic structure of the vibrations themselves. (BNL/Petten)

ii. (n,γ) Studies of $^{161,163,165}Dy$

A series of extensive investigations of the odd mass Dy nuclei has been initiated. All three nuclei have been studied via the ARC technique at BNL, using both 2 and 24 keV neutron energies, while the spectra of secondary γ-ray and conversion electrons have been, or are scheduled to be, measured with the GAMS and BILL spectrometers at the ILL, Grenoble. In addition, (d,p) studies have been made using the magnetic spectrometer at the Technical University of Munich. These data, when fully analyzed and interpreted, should provide level schemes whose content and detail, as far as low spin intrinsic excitations are concerned, far exceeds what is currently available for deformed odd A nuclei. This in turn should offer an enhanced insight in the coupling of single particle and collective modes into such regions. (Munich/ILL/BNL)

4. Studies of Odd-odd Nuclei

a. Study of ^{176}Lu with ARC and the Modelling of Odd-odd Nuclei

The structure of odd-odd nuclei has long been a challenge for nuclear models. Generally, attempts to predict the levels of such nuclei, at least in heavy deformed regions, have been qualitatively based on the level schemes of the neighboring odd Z and odd N nuclei. Unfortunately, the extremely high level densities, even near the ground state, make theoretical predictions unreliable (since states are mixed) and experimental study difficult due to near degeneracies and finite instrumental resolving power. Recently, however, Hoff has developed a more sophisticated model that incorporates more fully the empirical results from neighboring odd A nuclei (including, for example, most of the effects of Coriolis mixing) as well as some of the effects of the neutron-proton interaction in

the odd-odd nucleus. The model yields level predictions up to well over one MeV. In order to test these ideas a very careful (n,γ) study of ^{176}Lu was carried out in the ARC mode with the 2 and 24 keV filtered beams at BNL. The ^{175}Lu target spin of $7/2^+$ should lead to the easy observation of all 2^--5^- levels in ^{176}Lu below about 1100 keV. However, special problems arise in an odd-odd deformed nucleus since the high level densities imply that some of the primary transitions may not be resolved. Therefore, a careful spectral analysis of multiplet structures and an interval calculation of the likelihood of missed levels must be carried out. The empirical results have now been obtained and are expressed in terms of histograms of the cumulative number of levels of different spins vs excitation energy. These histograms extend to 1124 keV, but above about 400 keV, they allow for possibly missed levels by displaying ranges for the minimum and maximum numbers of permitted levels. The results are being compared with the model calculations. Initial comparisons suggest excellent agreement. It is hoped that more careful comparisons may reveal fine structure in the level of agreement that may suggest improvements in the model. (BNL/LLL)

b. Study of Tm with ARC

As a complmentary study to the ^{176}Lu one discussed above, an ARC study of Tm will be carried out in FY 84. It should be pointed out that, aside from its interest as a model of the low energy structure of odd-odd nuclei, the Hoff model provides predictions at higher energies that can be of more general nuclear data interest, especially when applied to level density predictions in actinide nuclei. (BNL/LLL)

c. Study of ^{108}Ag

This empirical study, essentially completed in prior fiscal years, was submitted for publication in FY 83. In order to accommodate referee suggestions for revision, a more detailed treatment of the ARC results has been added to the paper in the form of a comparison of Monte Carlo calculations of the ARC process with observed intensities for several levels of known spins. (Imperial College/Munich/Julich/ILL/BNL/Leningrad/Hamburg/Boris Kidric, Belgrade)

d. Study of ^{134}Cs

As part of a collaborative multi-national study of ^{134}Cs, experiments were carried out at BNL and are being incorporated into an overall level scheme. (Boris Kidric, Belgrade/ILL/Leningrad/Julich/Munich/Vienna/BNL)

5. Other Studies

a. Reliability of ARC

The ARC studies of ^{168}Er and other deformed and O(6) nuclei have stimulated interest in more precise studies of the reliability of Average Resonance Capture to disclose all low lying levels of certain spins. Recently, this reliability was questioned as regards early studies at Argonne of ^{146}Nd. In order to assess the validity of these doubts, an analysis of BNL (n,γ) data on Nd was carried out. It was shown that the levels claimed to have been missed were in fact present in the data and that no levels of the spin and parity accessible in ARC were missed. The origin of the apparent problem seems to lie in poor statistics in the earlier work and to the use in that study of wrapped boron thermal neutron absorbers which led to a qualitatively different kind of averaging than that obtained with Sc and Fe filters at the BNL HFBR. The implications of this work are that ARC studies, carried out in cases where adequate averaging is obtained (i.e., away from closed shells), with adequate statistics (i.e., sufficient enriched target material), and careful analysis, are indeed capable of disclosing complete sets of low lying levels of appropriate spins and parities. (BNL/ORNL)

b. Use of Filtered Beams for Neutron Detector Calibration

Studies at TRISTAN utilizing proton recoil detectors and delayed neutron spectrometers require an energy dependent efficiency calibration in order to measure the intensity of particular neutron resonances at low energies. The thermal, 2, and 24 keV filtered beams at the HFBR provide appropriate standard neutron fluences that have been used for such calibrations by the Idaho group during the course of their TRISTAN experiments. (INEL)

B. NUCLEAR SPECTROSCOPY OF FISSION PRODUCT NUCLEI

The on-line isotope separator, TRISTAN, at the HFBR is a facility, unique in this country, for the study of neutron-rich nuclei far off stability, produced by thermal neutron induced fission of uranium. The reactor provides an intense external neutron beam, making excellent shielding possible. This combination of high beam intensity, long running time, and low background makes it possible to do experiments at TRISTAN which cannot be done elsewhere. As a user facility, most experiments are of a collaborative BNL/USER nature. The fruitful collaboration with a large group of outside users (including an expanding group of foreign scientists) permits a wide variety of approaches to nuclear structure studies. TRISTAN is also proving to be an excellent resource for training the next generation of nuclear chemists and physicists.

1. Nuclear Spectroscopy and Tests of Nuclear Models

a. Evolution of Intruder States in the Heavy Cd Isotopes

Even-even nuclei near closed shells are commonly described in terms of the vibrational phonon model. Although the Cd isotopes with Z=48 have been considered to be good examples of vibrational nuclei, their level schemes show significant deviations from such a description. Detailed studies of ^{112,114}Cd have shown the existence of a quintuplet of levels at ≈1 MeV instead of the predicted triplet. The members of the quintuplet were shown to be connected by enormously strong E2 transitions. This structure of states and the peculiar decay pattern present a critical challenge to theoretical interpretation. Recently, Heyde and collaborators have offered a quantitative explanation for ^{112,114}Cd in terms of mixtures of vibrational and intruder rotational states. Since the basic idea of the model is inherently simple it is possible to extend its predictions in a schematic calculation for the heavier Cd isotopes. The basic mechanism controlling the behavior of the normal and intruder states is the attractive quadrupole-quadrupole force within each system. The quadrupole term is long range and varies as n(n-1) where n is the number of valence particles. The intruder states are of 2p-4h character resulting from proton pair excitations into the next shell. Counting both particles and holes, these levels, therefore, experience a much stronger quadrupole interaction than the 2h normal states. They are therefore more rotational in character. Moreover, as the number of neutrons increases toward midshell, the total attractive quadrupole force, which varies roughly as $-N_\pi \cdot N_\nu$, increases rapidly and the intruder states drop in energy. At midneutron shell, near A=114, they are essentially degenerate with the normal states and strongly mix with them. However, with increasing A they must, in this simple model, rise in energy. Simple calculations also predict order of magnitude decreases in a certain B(E2) ratio. At TRISTAN, a study of ^{118}Cd was undertaken to test these ideas. From the singles, coincidence and angular correlation data a level scheme was developed, the key feature of which is the discovery of a 0^+ state at 1285 keV, and another at 1616 keV. The first is a vibrational two phonon level and the latter is most likely the intruder level. This result confirms, for the first time, the rise in intruder energies that must occur if the above model is valid. Moreover, the B(E2) ratio mentioned above drops by orders of magnitude confirming another key prediction of these simple calculations. This experiment is now being extended to ^{120}Cd where further evolution of the intruder states is expected. (BNL/Clark/Gent/Lafayette)

b. Parabolic Energy Dependence of Odd-odd p-n Multiplets

The study and interpretation of odd-odd nuclei has long been beset by difficulties. Experimentally, the high level densities render it difficult to establish reliable level schemes. Theoretically, the multiple possibilities for proton-neutron configurations enormously complicate the calculated spectra. Thus, little progress has been achieved in

understanding these nuclei in detail. Recently, though, the possibility of a significant breakthrough has emerged, following theoretical efforts by Schiffer, Molinari, and others. Under the principal and crucial assumption that configuration mixing is absent, the multiplets of levels formed by the angular momentum coupling of a neutron and proton behave very simply for any realistic force. Since the n-p force is attractive, it favors orbit orientations of the proton and neutron with large overlap. Thus the lowest states of the multiplet will be those with either maximum or minimum spin, and the mid-spin levels will be highest. If the proton and neutron are particle-hole in character, the opposite occurs with the mid-spin levels lowest. Under the more specific assumption of a quadrupole p-n interaction a simple parabolic dependence of the multiplet energies on I(I+1) results. The shape and orientation of the resulting bowl shape multiplets are sensitive to the specific orbits involved and their occupancy. Thus, data on such multiplets can be a probe of the filling of shell model orbits. Moreover, since the agreement of such simple theoretical considerations with the data depends essentially on the absence of configuration mixing, comparisons with theory can be a sensitive test of such interactions as one proceeds away from closed shells.

i. N=85 Nucleus ^{142}La

From data taken previously at TRISTAN for N=83 nuclides, the parabolic behavior of p-n multiplets near closed shells was described in terms of a quadrupole interaction (which leads to the parabolic shape) and a weaker dipole interaction (which shifts the vertex of the parabola). Extrapolating the results from the N=83 nucleus ^{140}La to N=85, it was possible to make qualitative predictions for ^{142}La. The parabolas were predicted to be more shallow for N=85 than for N=83 due primarily to changing quasi-particle blocking effects as the neutron occupancy increases. Low-lying multiplets in ^{142}La were found to be qualitatively described by the modified parabolas. (Maryland/BNL)

ii. N=85 Nucleus ^{140}Cs

The above treatment will also be applied to data recently obtained by studying the decay of ^{140}Xe. Analysis of the data is not yet at a stage to allow any conclusions concerning the applicability of the parabola treatment to this N=85 nucleus. (Maryland/BNL)

iii. Decay of ^{130}Sn to Levels in ^{130}Sb

Detailed angular correlation experiments have begun on this nuclide. The structure of odd-odd ^{130}Sb will be interpreted on the basis of the parabolic energy dependence of p-n multiplets as was done for N=83 and 85 nuclides. The previous success of the parabola technique was for systems with one neutron in excess of a closed shell. The Sb nuclei will be the first test of this interpretation for systems with one proton

in excess of a closed shell. Experiments on other odd-odd Sb nuclei will begin in FY 1984. (Maryland/BNL)

c. Rotational Structure and Nilsson Orbitals for Highly Deformed Odd-A Nuclei in the A≈100 Region: ^{99}Y, ^{101}Y, ^{99}Sr and ^{101}Zr

Six rotational bands have been found in ^{99}Y, ^{101}Y, ^{99}Sr and ^{101}Zr. All bands have small and very similar values of $h^2/2I$ that indicate deformations of $\beta \approx 0.3-0.4$ and imply that these nuclei are among the most deformed known, with $I \approx 0.8 I_{rigid}$. Previous to this study, only a single rotational band for an odd-A nucleus in the A≈100 region had been reported. This was for the decay of an 8.6-μs isomer of ^{99}Y that populates eight levels of a K=5/2 ground band. The level energies are well described by an odd-A rotor with negligible higher-order terms. Assuming that the bands observed in the present studies may also be described by a nearly rigid rotor, K values may be assigned to all the bands in the Y nuclei. These assignments may be made by deducing the deformation from $|(g_K - g_R/Q_0|$ obtained from branching ratios for intraband γ transitions under the assumption of pure K bands (i.e., Alaga rules), then noting which Nilsson state of the proper K value is near the Fermi surface for the deduced value of the deformation. For the two Y isotopes, the K=5/2 ground bands are well described by the 5/2[422] Nilsson state and the 590-keV K=5/2 band in ^{101}Y is most likely 5/2[303]. The present data for N=61 cannot determine which K=3/2 bands are 3/2[411] and which are 3/2[541]. The existence of the π5/2[422] and ν3/2[411] orbitals near the Fermi surface is consistent with the concept that the rapid onset of deformation in this region is strongly promoted by occupancy of neutron and proton spin orbit partner orbitals. With use of the high yields available from the thermal ion source, it may be possible to extend the study of this region to ^{103}Y and ^{103}Zr. (ISU/Oklahoma/BNL)

d. Decay of ^{124}Ag to Levels in ^{124}Cd

The decay of ^{124}Ag to ^{124}Cd was observed for the first time at TRISTAN. This new isotope was found to have a half life of 0.17±0.03s. A single γ ray was observed and postulated to depopulate a 2^+_1 level at 613 keV in ^{124}Cd. If the yield can be increased by ion source improvements, further experiments will be performed to learn more about levels in ^{124}Cd. Due to low fission yields, it will probably not be possible to obtain sufficiently detailed information to ascertain the location of the intruder 0^+ state in ^{124}Cd. (ISU/BNL/Clark)

e. Particle-hole Effects in Near Closed Shell Nuclei

Recent advances in ion source technology (specifically the FEBIAD, thermal and high temperature plasma ion sources) make it possible to produce a wealth of far from stability closed shell or near closed shell nuclei. These can provide sensitive tests, in a systematic fashion, of the effects of adding or removing protons or neutrons from the closed shell.

i. Decay of ^{130}In to Levels in ^{130}Sn

Preliminary experiments indicated that the activity from the first FEBIAD source was too low for the sort of detailed study required to fully understand this isotope. However, more recent improvements in the FEBIAD and especially the successful deployment of the thermal ion source will make it possible to do detailed angular correlations and g-factor measurements for levels in ^{130}Sn. During FY 1984 these experiments will begin as part of a program to study the heavier Sn isotopes, especially with the perturbed angular correlation technique using the superconducting magnet. (BNL/Georgia Tech)

ii. Decay of ^{135}Te to Levels in ^{135}I

Data from the decay of ^{135}Te to the N=82 isotope ^{135}I are being analyzed. The results will be compared to shell model calculations for 3 particles outside the ^{132}Sn core and attempts will be made to identify states corresponding to particle-hole excitations. (ISU)

iii. Decay of ^{83}Ge to Levels in ^{83}As

The level structure of the N=50 nucleus ^{83}As will be investigated by the decay of ^{83}Ge. Experiments began in early FY 1984 and ^{83}Ge was directly observed for the first time. A preliminary half life of 1.8 sec was measured and four γ rays were observed in a coincidence experiment. (ISU/BNL)

f. Perturbed Angular Correlation Studies

In the perturbed angular correlation (PAC) technique, a radioactive source is placed in a strong external magnetic field. Shifts in the normal angular distributions of coincident gamma rays are induced and measured. From these measurements, the magnetic moments of intermediate states can be extracted. For nuclei near closed shells, this moment is highly sensitive to the specific nucleon orbits involved in a given state, and small admixtures of certain configurations may considerably change its value. For deformed nuclei, the g-factors are close to the hydrodynamical value Z/A. An interesting region of nuclei is, therefore, at the onset of deformation. In these cases, the g-factors are also expected to exhibit a transition between shell-model values and the asymptotic Z/A value. Such an effect was observed for Nd isotopes near N=88-90. Moreover, in a recent TRISTAN study in this region it was found that deviations from a Z/A behavior of magnetic moments provides a particularly sensitive indicator of the active number of valence protons.

i. g-factor of the $7/2^+$ 1264.4 keV Level in ^{97}Zr

The time-dependent PAC technique was used for this measurement. This technique, useful for longer lived levels (>50 nsec),

gives more accurate results than the integral technique. The frequency of oscillations (Larmor frequency) of the decay of the level at a particular set of angles is determined by analysis of the time spectrum which results from coincidences in the pair of detectors determining the angles. A g-factor of +0.39±0.04 was determined. This value is consistent with that expected for a $g_{7/2}$ neutron and gives support to the postulate that ^{97}Zr has a simple shell model configuration consisting of a single neutron outside the ^{96}Zr core. This configuration is also indicated by the systematics of $2^+_1 \rightarrow 0^+_{g.s.}$ transitions in this region, transfer data, which show almost complete occupation of the $d_{5/2}$ neutron and $p_{1/2}$ proton subshells, and the $B(E2:7/2^+-3/2^+)$ value of 1.8 w.u. for ^{97}Zr. (BNL/ISU)

ii. g-factor of the 4^+_1 Levels in ^{138}Ba and ^{136}Xe

Data have been taken to measure the g-factors of the 4^+_1 states in the N=82 nuclei ^{138}Ba and ^{136}Xe. The activities were produced by the decay of ^{138}Cs and ^{136}I, respectively. The results will provide a probe of the proton orbital configurations for these nuclei with a closed neutron shell. The data are being analyzed and should be completed in FY 1984. (Negev, Israel/BNL/ISU)

g. Decay of ^{139}Xe to Levels in ^{139}Cs

Four-detector angular correlation data were taken for the decay of ^{139}Xe to levels in ^{139}Cs. After the data are analyzed, more extensive knowledge of the spin of excited states in ^{139}Cs will be available, making it possible to make more detailed comparisons to the closed shell N=82 nucleus ^{137}Cs and study the changes of odd mass Cs isotopes in the transition region from spherical to deformed shapes. (Maryland/BNL)

2. Precise Q-values for Neutron-rich Isotopes

a. Q-values for Neutron-rich Silver Isotopes

During FY 1983 the Q-value for the β decay of ^{118}Ag was measured to be 7200±50 keV by the technique of β singles and β-γ coincidence. In order to determine the Q-value, it was necessary to construct an accurate level scheme for ^{118}Cd so that it could be determined if the decay was to the ground state or to an excited state. During this phase of the analysis, the interesting behavior of the intruder 0^+ bands in Cd nuclei (discussed elsewhere in this report) was investigated. In FY 1984 it is anticipated that measurements of the Q value of ^{120}Ag (and if time permits ^{122}Ag) will begin. As before, a detailed level scheme will be constructed so that the β feeding pattern can be understood. (Clark/Lafayette/BNL)

b. ΔE-E β Spectrometer Studies

A ΔE-E detector telescope consisting of a 200 mm^2x300μmSi ΔE detector and a 500 mm^2x15mm hyperpure Ge detector was used to measure the β spectra from the decay of ^{99}Rb and ^{99}Sr. From this data, the endpoints were determined to be 11260±100 keV and 7830±150 keV, respectively. The advantage of this technique is that the spectra are free of any background by summing the ΔE and E detectors in coincidence. If the response function of the system is sufficiently determined, the β spectra can be unfolded to resolve the feeding to individual excited states. This information can be used to determine β strength functions which indicate the influence of the Ganow-Teller giant resonance on β decay. (McGill/BNL)

3. Delayed Neutron Emission

a. Half-lives and P_n Values of Isotopes Produced by the FEBIAD Ion Source

In order to survey neutron emitting isotopes and to deduce their gross properties (in particular, half lives and P_n values), it is advantageous to use an extremely high efficiency, low resolution neutron detector. Such a device, incorporating successive rings of neutron moderator and ^{3}He detectors, is being used at TRISTAN to measure these quantities for all the delayed neutron emitters produced by the FEBIAD ion source. Emphasis during FY 1983 was given to measuring half lives and P_n values for the delayed neutron precursors $^{121-124}$Ag and to relocating the neutron counting facilities to another beam line in order to obtain a lower background. P_n values and half lives were determined by simultaneously measuring neutron and β decay curves. The neutron and β activities at saturation were determined by decay curve analysis. The P_n value is then just the ratio (corrected for efficiency) of neutron to β activity. P_n values ranging from <0.003 for ^{120}Ag to >0.1 for ^{124}Ag were determined. Measurements of other delayed neutron precursors will continue in FY 1984. (PNW/BNL)

b. Delayed Neutron Spectroscopy Applied to Cross Sections and β-strength Functions of Nuclei Far from Stability

The neutron capture cross sections of nuclei far from stability are of great interest for the development of fast-fission reactors and fission-fusion hybrids, and are of particular importance in the study of nucleo-synthesis. The energy region just above the neutron binding energy is generally the most critical, since those states participate most strongly in the capture process. Since the cross sections for nuclei far from stability cannot be measured by capture techniques, the inverse mechanism (neutron emission following β decay) offers the only feasible means of investigating the quality of theoretical predictions of the cross sections. The essential quantities to be measured are the neutron level width (Γ_n) and the neutron energy (E_n) since these are difficult to

predict. Such measurements require high energy resolution at low neutron energy, a reasonable efficiency for neutron detection and a known energy response. Suitable neutron detectors are not commercially available and, therefore, a program to develop and test such detectors must be undertaken if these measurements are to be made.

Another application of delayed neutron spectroscopy is in the determination of complete β-strength functions. When the excitation energy of the β-decaying parent exceeds the neutron binding energy of the daughter, neutron spectroscopy becomes essential. In order to establish the relative β-feeding per energy interval, neutron γ-ray coincidence techniques are also necessary in order to unfold the singles neutron spectra into partial spectra for each final state. These studies can indicate the effects of small resonance-like structures in the Gamow-Teller giant resonance tail which may contribute strongly to β-decay properties. Detectors and techniques that are being developed to address these problems are described below.

i. Neutron Time-of-Flight

A time-of-flight (TOF) neutron spectrometer has been built and tested. This technique offers the best energy resolution at low energies (1-200 keV). However, because it is a coincidence technique, the efficiency tends to be low. Nevertheless, high resolution results have been obtained for the precursors ^{95,97}Rb. A preliminary value of 300±40 eV has been deduced for the natural line width of the 14-keV resonance in ^{95}Rb. This value is based on a system resolution that was calculated from system parameters. Ultimately, a measured resolution must be obtained. This may be possible by measuring the spectrum of delayed neutrons from ^{87}Br, where level widths have been measured by neutron capture techniques on stable ^{86}Kr. In FY 1984, the neutron background must be lowered in order to achieve a higher sensitivity. This will be accomplished by the construction of a boron-doped shielding wall around the counting system. (Cornell/BNL)

ii. Proton Recoil Spectrometer

Hydrogen gas-filled proportional counters offer an alternative to the low efficiency, high degree of difficulty of time-of-flight techniques. These detectors have relatively high efficiency, are insensitive to thermal neutrons and do not require detailed knowledge of the response function. However, the gamma background can obscure the lower energy portion of the spectrum and the data must be differentiated to obtain the desired energy spectrum. Significant progress has been made in the past year. Spectra from these detectors are now comparable to those obtained with other methods, in terms of both spectrum structure and intensity. Some inconsistencies still exist among the proton recoil detectors, time-of-flight measurements and ^{3}He ionization counters. These discrepancies may be resolved by careful analysis of neutron spectra from the decay

of ^{87}Br (produced by the FEBIAD and Negative Surface ionization source). (INEL/BNL)

C. RESEARCH AND DEVELOPMENT IN SUPPORT OF FACILITIES

1. TRISTAN Ion Source Development

Research and development in this crucial area was extremely fruitful this year with the successful operation of three new ion sources which expand manyfold the potential for future TRISTAN research capabilities.

a. The FEBIAD Source

The first operation of the FEBIAD source in late FY 1982 and early FY 1983 showed great promise. The source gave high yields and operated for a surprising 350 hours. During FY 1983, several modifications, both structural and operational, have led to higher yields and have made it possible to operate the source for a remarkable 1500 hours.

Four basic structural changes are responsible for the increased lifetime: 1) The target backing material was changed from graphite cloth to low density (high porosity) graphite less susceptible to deterioration, the gaseous products of which collect on insulators (which are at a somewhat lower temperature) and cause electrical shorts. 2) The construction material of the end cap and base plate were changed from graphite to molybdenum. 3) The diameter of the tungsten grid wires was increased from 0.005" to 0.025", allowing longer grid lifetimes. 4) The pumping holes in the cathode assembly tubes were increased in diameter allowing better pumping to the o-ring region and reducing the chance of forming a high pressure arc in the vacuum seal region.

In most applications of the FEBIAD ion source (generally heavy ion accelerators) the target consists of very thin metallic foils, allowing operations at relatively low pressures. At low pressures, the primary ionization mode is electron impact. The uranium targets used at a reactor based facility are by nature more volatile than thin foils and thus the ion source cannot easily achieve a low enough pressure to fully utilize the so-called "FEBIAD" (electron impact) mode of operation. In the TRISTAN FEBIAD source, electron impact generally competes with charge exchange and collisions with meta stable atoms (Penning ionization). By varing the operating conditions of the source, the best mode can be selected for optimum ion jet efficiency of a particular species. Yields for Ag were increased by nearly a factor of 20 by using this technique. During FY 1984 the operating parameters will be explored in order to understand the ionization mechanisms and systematize the conditions most likely to yield good results for specific elements. Further, the limitations of the source lifetime as a function of temperature will be investigated.

b. High Temperature Plasma Ion Source

In FY 1983 a new type of ion source was extensively tested on the off-line facility, ISTU. The high temperature plasma ion source represents a new concept in integrated ion source target design. The target is located inside the cathode, the anode consists of a grid which protrudes into the cathode and the end cap acts as a field penetration extractor by operating at negative potential. This allows the target to be larger than in a conventional design, containing approximately four times as much ^{235}U. The target can also be operated at a much higher temperature (maximum ≈2500°C) without compromising ionization efficiency. Furthermore, the design is much simpler than for the FEBIAD source and has many parts which are interchangeable with the thermal and negative ion sources, making "mass production" simpler and faster. The source appears to operate in two modes: electron impact and direct arc discharge. Both modes give stable operation, provided that the anode current is less than 1 amp for the direct discharge mode. The optics for the source are excellent, producing beams of less than 0.5 mm FWHM at the focal plane of the magnet.

This source has now been tested on-line at target temperatures of about 1800°C and has given yields that are at least four times higher than the best FEBIAD yields. For some isotopes, notably Sb, Zn and Ge, the yields appear to be at least ten times higher than the FEBIAD source. Further on-line tests will be conducted in FY 1984 which will involve higher temperatures. Consideration will be given to both the end product (nuclear) physics and to understanding the ion source physics. If the source can be operated for long periods of time (longer than one reactor cycle) it will eventually replace the FEBIAD source as the primary TRISTAN ion source. Already, it has been used in several experiments, near mass A=83 and A=130.

c. Thermal Ion Source

During FY 1983, a thermal ionization source was constructed and tested on-line. The source is similar to the surface ionization sources developed in previous years, but has heat shielding that allows higher temperature operation at lower power input (<2500°C at 1800 watts). The ionizer was redesigned to better conduct heat into the ionization region. Yields were determined for many elements and were generally (except for Rb and Cs) significantly higher than the surface ion sources. Various isotopes of Ga, As, Y, In, Sn, Ce, Pr, Pm, Sn, Eu, Gd, Tb, Dy and Ho were produced as primary ions from the source. Ge, Zr, Nb and Sb were observed as daughter products with good yields. The thermal ion source is especially suited to produce In and Ga. An ^{132}In spectrum disclosed all the known gamma rays in a few minutes. Since the spectrum is not contaminated by the ^{132}Cs spallation products observed at accelerator based ISOL facilities (like ISOLDE), TRISTAN users have a unique opportunity to do very detailed and complete studies of the structure of doubly-magic ^{132}Sn. During FY

1984, improvements will be made to extend the lifetime of the ion source to make long-term experiments more feasible.

d. Negative Surface Ion Source

Tests in early FY 1983 showed that the tantalum negative ion source could produce I and Br ions with yield $>10^4$ atoms/sec. These beams could not be focussed onto a tape collector because of the large beam divergence caused by excessive electron currents. The source has been redesigned to include an integral electron deflection magnet, heat shields for better thermal efficiency and a LaB_6 ionizer for higher efficiency and will be tested in FY 1984.

2. TRISTAN Beam Line and Facility Modifications

a. Beam Optics

Several scanners were purchased and installed in FY 1983 to aid in optimizing beam transmission and ion source output. The scanners have been helpful in obtaining the stringent requirements of the laser experiments and in general experiment setups. A surface barrier detector is being installed after the mass slit to monitor the activity level of the selected mass. By comparing this rate with the ratio in similar detectors, located at experimental facilities, the beam transmission through the switch magnet can be determined, thereby minimizing beam losses.

b. Delayed Neutron Facility Relocation

The delayed neutron counting facilities (Pn ring counters and time-of-flight spectrometer) were moved from the 0° to the 22-1/2° switch magnet port. The deposit position was moved to a location further from the switch magnet to allow sufficient room for detectors to be placed at adjacent facilities. An electrostatic quadrupole doublet and a set of steering plates were installed after the switch magnet to obtain the proper focal properties. After the move, better beam transmission and optics than were available at the 0° port were realized as well as a 50% reduction in the neutron and γ-ray background. During FY 1984, a shielding partition will be constructed to further reduce the background.

c. Superconducting Magnet for Perturbed Angular Correlations and Q_β Measurements

A superconducting magnet was ordered in late FY 1982. Its primary purpose will be for perturbed angular correlation experiments. It consists of two split coils and an angled opening that allows 4 Ge(Li) detectors to view the source spot with minimum absorption. The capability of inserting additional Fe pole pieces should provide a further 10% field increase. Although the cryostat is an integral part of the system, the design is modular and allows different bottom flanges, liquid nitrogen

casings, and moving tape through-tubes in order to accomodate a dual purpose. Specifically, by removing the optional Fe pole pieces, utilizing a through-tube with thin windows, and by inserting a hyperpure Ge detector in the central bore hole, it will be possible to carry out Q_β measurements with enormously increased efficiency and with low γ-ray background. The field will act to spiral the electrons from the source to the detector. This dual purpose facility will be a major addition to the array of experimental techniques available at TRISTAN. The system will be installed in mid FY 1984. An improved moving tape collector and a support/service stand have been constructed. A hyperpure Ge detector for Q_β experiments has been purchased and received. A new beam monitoring system is being installed. A solid state β detector (surface barrier) will be placed behind the tape at the point of deposit. This will have advantages over the NaI detector that was used previously, since it will view only the desired beam spot, making it easier to maximize the activity.

d. Solid-state Conversion Electron Detector

The Si(Li) conversion electron detector has been installed on the 0° switch magnet port that was vacated by the delayed neutron counters. The detector has been mounted in the cryostat and a vacuum chamber and moving tape collector system has been constructed. It is expected that the detector will be in operation in FY 1984. After adequate resolution electron spectra are obtained, the performance of the ion optics will be more thoroughly investigated and the appropriate lens system installed.

e. Parent Port Facility for Angular Correlation Measurements of Very Short-lived Nuclides

The present angular correlation facility is located downstream from the point of beam deposit (parent port) at a position referred to as the daughter port. This was necessary because of space restrictions and involved a tape move of >0.6 sec to obtain the desired activity in the measurement area. Thus, $\gamma\gamma(\theta)$ measurements were limited to nuclides with half lives > 1.0 sec. The tape collector/beam line configuration has been modified to allow $\gamma\gamma(\theta)$ measurements at the parent port, thereby removing the half life limitations. The facility was installed in early FY 1984 and used for study of the decay of heavy Ag isotopes and other short-lived species.

3. <u>(n,γ) Angular Correlation Facility</u>

The angular correlation facility has now been completed and initial test measurements made. Full scale routine operation for new experiments will be carried out in FY 1984.

4. Modifications to the Three-Crystal Pair Spectrometer ARC Facility

In considering the overall range of targets which can be studied with the ARC technique, the most crucial limitations are the level density at the binding energy, and the amount of target material available. While nothing can be done about the former, the latter limitation can be alleviated by improving the efficiency of the three-crystal pair spectrometer. The critical factors which determine this efficiency are the size and shape of the Ge crystal, the distance between it and the target, and the effective solid angle for 511 keV radiation detected by the NaI crystals. The current system employs NaI crystals which are far larger than necessary, with the result that the source-to-detector distance has been increased unnecessarily. A new design has therefore been developed, which employs a pair of NaI crystals of smaller diameter, and places the Ge crystal forward of center, in order to optimize these two conflicting factors. The expected increase in efficiency from this modification is a factor of ≈3.4. A further improvement of ≈2 could be obtained by obtaining a new Ge crystal. By or during FY 1985, the purchase and installation of the new pair spectrometer should be complete, making it possible to undertake a number of measurements which were hitherto considered impossible because of lack of sufficient target material. In many other cases, the quality of data should be considerably enhanced by the improved statistics obtainable.

D. NATIONAL NUCLEAR DATA CENTER

1. Cross Section Evaluation Working Group (CSEWG) Activities

The annual CSEWG meeting was held at BNL in May, 1983. At this meeting, it was decided to delay the schedule for ENDF/B-VI by approximately one year. The formats will be fixed at the May 1984 CSEWG meeting, and the "standards" evaluation will be completed by the end of 1984.

The release of ENDF/B-V Revision 2 has been completed. An update to ENDF-102, the formats manual, to cover changes to formats and procedures through Revision 2, has been distributed.

2. BNL-325 Volume 1 Part B

The evaluations of the thermal cross sections, resonance parameters, and average resonance properties for the isotopes in the mass range Z=61-100 has been completed. The introduction for this part deals with (1) the systematics of the s-, p- and d-wave strength functions, average radioactive widths, and potential scattering radii, (2) alpha widths of resonances, and (3) subthreshold fission.

It is expected that this work will be submitted to the Academic Press on March 1, 1984.

The production of the next edition of the neutron reaction data atlas has begun. Completion is scheduled for fall of 1985. Work has already been completed on the publication programs and an interactive "eyeguide" production program.

3. Nuclear Data Sheets

The NNDC has been producing the Nuclear Data Sheets at the rate of about an issue a month. Of these, nine issues a year are devoted to the nuclear structure evaluation and the remaining three to the publication of Recent References.

The U.S. is part of an international network of evaluators contributing recommended values of nuclear structure information to the Evaluated Nuclear Structure Data file (ENSDF). Publication of the Nuclear Data Sheets proceeds directly from this computerized file. In addition to the U.S., evaluations have been received or are anticipated from Germany, United Kingdom, USSR, France, Japan, Belgium, Kuwait, Sweden, the People's Republic of China and Canada. International meetings of the network evaluators are sponsored by the IAEA, and the next meeting will be held at Karlsruhe April 3-6, 1984.

It is planned to bring out a new edition of the Nuclear Wallet Cards (last published in 1979) incorporating the new Wapstra mass evaluation when it is available. Since this publication represents a subset of data extracted from the computerized ENSDF file, it is consistent and current with the Nuclear Data Sheets.

4. Data Request List

A small number of data requests especially for Fusion and FMIT will be considered in the mid-review period. This list will be reviewed by CSEWG and distributed by the NNDC in September, 1984. The data will be transmitted to Vienna for inclusion in the WRENDA publication planned for January, 1985.

CROCKER NUCLEAR LABORATORY
UNIVERSITY OF CALIFORNIA, DAVIS

A. ANGULAR DISTRIBUTION OF GIANT DIPOLE STRENGTH IN ^{6}Li AND ^{7}Li AS OBSERVED IN THE (n,p) REACTION AT 60 MeV (F.P. Brady, G.A. Needham, J.L. Romero, C.M. Castanda, T.D. Ford, J.L. Ullmann, and M.L. Webb)

The (n,p) reaction in ^{6}Li and ^{7}Li at 60 MeV reveals large structures at high excitations. The new structures exhibit giant dipole strength and are not seen in photoneutron data and exhaust a large fraction of the sum rule.[1]

Table A-1

^{6}Li				^{7}Li	
E_x = 15.5 MeV		E_x = 25 MeV		E_x = 20 MeV	
θ_{cm}°	$d\sigma/d\Omega$(mb/Str)	θ_{cm}°	$d\sigma/d\Omega$(mb/Str)	θ_{cm}°	$d\sigma/d\Omega$(mb/Str)
16.4	1.14	6.8	1.61	9.2	1.56
19.4	0.51	19.9	2.13	11.7	1.94
23.1	0.90	23.6	1.43	14.1	1.59
26.7	0.67	27.3	1.42	16.6	2.02
30.3	0.72	31.0	1.71	19.6	1.92
33.9	0.65	34.7	1.34	23.3	2.55
45.0	0.45	45.0	0.72	26.9	2.31
56.4	0.15	56.4	0.38	30.6	2.21
				34.2	1.93
				37.8	1.68
				48.6	0.90
				59.3	0.52

[1] F.P. Brady et al., Phys. Rev. Letters 51,1320 (1983).

B. ANGLE INTEGRATED AND Q-VALUE BIN ANGULAR DISTRIBUTIONS FROM THE $^{58-64}$Ni(n,px) REACTIONS (J.L. Ullmann, C.M. Castaneda, F.P. Brady, J.L. Romero, and N.S.P. King)

Data for the inclusive (n,px) reaction at 60 MeV on the nickel isotopes are presented. Angular distributions for Q-value Bins show a decrease of the forward peaking of the proton emission with increasing neutron excess. A marked dependence of the angle integrated spectra with (N-Z) is observed.[1]

Table B-1. Angle Integrated Cross Section For Nickel Isotopes in the (n,p) Reaction at 60 MeV

Ep (MeV)	(dσ/dE) mb/MeV*			
	^{58}Ni	^{60}Ni	^{62}Ni	^{64}Ni
10	12.9	6.1	3.8	3.1
15	7.9	5.2	4.1	4.0
20	6.7	4.8	3.9	3.7
25	6.5	4.4	3.8	3.4
30	6.2	4.3	3.7	3.4
40	4.2	3.1	2.5	2.6
50	2.8	1.8	1.4	0.9
52	2.2	1.2	0.8	0.3
55	1.7	0.5	0.06	0.04
57	1.09	0.03	-	-
60	1.12	-	-	-

* Experimental errors ∿10-20%

[1] C.M. Castaneda et al., Phys. Rev. C28,1493 (1983).

Table B-2 ^{58}Ni Q-value Bin Angular Distributions (mb/Str)

Q-value BINS (MeV) / θ_{CM} (degrees)	0→-5	-5→-10	-10→-15	-15→-20	-20→-25	-25→-30	-30→-35	-35→-40
6.1	119.56	138.14	107.98	160.44	156.29	155.52	157.02	137.30
10.1	38.48	59.65	94.83	94.20	96.45	105.53	101.09	98.72
16.2	29.40	44.38	76.49	78.60	79.20	88.49	87.36	70.88
20.3	36.02	55.15	84.57	89.86	102.81	102.87	106.60	97.50
25.4	24.18	44.68	67.92	71.11	76.67	78.44	78.66	79.09
33.0	14.87	37.34	62.44	61.24	67.75	74.87	68.42	72.67
40.6	8.50	22.69	35.11	40.19	51.87	61.08	60.28	67.43
48.2	8.35	15.75	25.02	34.97	39.75	51.77	60.47	68.76
55.8	3.20	11.76	19.33	21.56	29.97	33.46	38.85	46.33
63.6	0.44	5.72	11.73	16.86	21.10	30.02	33.35	40.47
70.9	0.85	3.29	4.99	7.44	10.20	13.91	18.46	23.21
78.4	0.43	3.23	4.63	6.56	12.26	14.19	20.73	30.60

Table B-3 ^{64}Ni Q-Value Bins Angular Distributions (mb/Str)

ϕ-value BINS (MeV) / θ_{CM} (degrees)	0→-5	-5→-10	-10→-15	-15→-20	-20→-25	-25→-30	-30→-35	-35→-40
6.1	2.43	12.92	29.18	37.75	45.36	54.43	56.74	45.47
10.1	1.53	8.66	32.58	36.87	40.13	52.24	45.31	45.20
16.2	0.25	8.68	35.12	41.97	48.46	56.69	52.70	47.93
20.3	-	7.57	30.02	35.37	38.42	51.84	54.83	44.12
25.4	0.43	6.59	26.79	29.59	33.66	36.43	35.86	34.84
33.0	0.34	3.70	19.19	24.55	31.03	30.88	36.30	31.20
40.6	-	3.39	12.14	20.06	22.43	27.26	30.27	30.87
48.2	-	2.80	7.68	13.48	16.26	20.28	22.12	23.63
55.8	-	1.31	6.31	7.84	11.22	15.20	16.33	19.75
63.6	-	2.19	3.99	7.35	11.21	13.13	16.85	19.14
70.9	-	0.57	3.89	5.22	7.49	13.27	12.41	15.72
78.4	-	-	-	-	-	-	-	-

A. NUCLEAR DATA EVALUATIONS

1. ENDF/B-VI Fission Product, Actinide, Fission Yields, Delayed Neutron, Activation and Dosimetry Evaluations (F. M. Mann, R. E. Schenter, F. Schmittroth, T. R. England* and C. W. Reich**)

A four-year plan has been developed to update, add and improve upon cross section, decay and yield data evaluations on ENDF/B-V for the above titled areas. Emphasis of these evaluations will be focused on breeder reactor application. This is part of the "LMFBR Nuclear Data Evaluation Task Force" effort which will produce ENDF/B-VI data files. Table A-1 outlines plans for the Fission Product and Higher Actinide Evaluations. Figure A-1 shows typical results of recent measurements and comparisons to calculations using the FERRET least squares approach for the important radioactive fission product nuclei I-129.

Table A-1. **Cross Section Evaluation Update Plans for ENDF/B-VI Fission Products and Higher Actinides**

- **Focus on 75 FP nuclides and 8 higher actinides (having Z greater than or equal to 94)**
- **To include new resolved resonance parameter data**
  - **a) Use computer code RESPARFM**
  - **b) Input primarily from BNL-325 (1982 Z=1-60, 1984 Z>60)**
  - **c) Obtain D_{obs} and Γ_γ from RESPARFM analyses**
- **Calculate nγ, nf, and nt cross sections using least squares code FERRET for selected nuclei**
  - **a) Use integral and differential data as input**
  - **b) Use elemental differential data as constraint on individual isotope cross sections**
  - **c) Use primarily latest CSIRS as source of differential data**
  - **d) Use CFRMF, STEK, EBR-II and FFTF as source of integral data**
- **Calculate nn', nγ, nf, nn, n2n, and γ production, etc for selected nuclei using HAUSER*6 code**
  - **a) Input levels from latest ENSDF files**
  - **b) Use optical model parameters obtained from expected HEDL study**
- **Include recent capture measurements of radioactive Nuclei(I-129, Pd-107, etc)—see example figure**
- **Evaluations to be completed May, 1986**

* Los Alamos National Laboratory

** Idaho National Engineering Laboratory

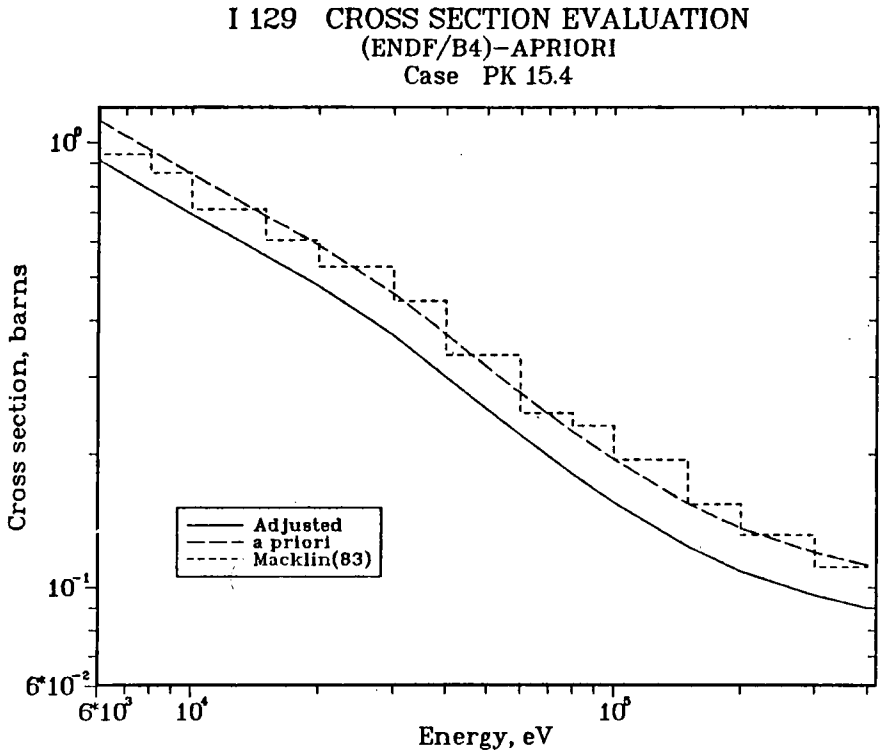

Figure A-1. I-129 Capture Cross Section Results. The "Adjusted" curve (ENDF/B-V, 1980) was made using integral results from STEK. The "a priori" curve (1973) was the result of a Hauser Feshbach calculation. The "Macklin (83)" (1983) result is from ORELA measurements.

2. Low Activation Cross Sections for Fusion Application (F. M. Mann)

Based upon the importance of long-term waste management for the fusion material programs, activation and transmutation evaluations of cross sections were generated and processed. Calculations for conceptual fusion designs show there are large gaps in the required cross section data if it is to be supplied by ENDF/B-V or even specialized activation libraries. Work on expanding the current HEDL library is planned as is the identification of important reactions for measurement and evaluation.

B. DELAYED NEUTRON DATA

1. Spectra Evaluations (F. M. Mann, R. E. Schenter, T. R. England* and W. B. Wilson*)

See LANL contribution B.6.

---

* Los Alamos National Laboratory

2. P_n Evaluation (F. M. Mann, M. Schreiber, R. E. Schenter and T. R. England*)

Delayed neutron precursor data are being compiled in preparation of a new ENDF/B evaluation of delayed neutron data. Precursor P_n values have been updated using ENDF/B-VM fission product yields, ENDF/B-V decay data, and recommended P_n values. Evaluations for 77 precursors were completed and a paper describing these results and their effects on fission yields, P_n systematics, and calculational models was submitted for publication.

C. FISSION YIELDS

1. ENDF/B Evaluations (T. R. England,* B. F. Rider* and R. E. Schenter)

Expanding and improving fission yield sets for the ENDF/B files using recent experimental results and refined nuclear model calculations is a continuing program. Currently we expect to update all data sets through 1985 (or later) for ENDF/B-VI and to modify the yield distribution parameters and decay-branching ratios. The most recent evluations now include 34 fissionable nuclides at one or more fission energies, including spontaneous fission, for a total of 50 yield sets. This is an expansion by a factor of 2½ over ENDF/B-V (11 fissionable nuclides and 20 yield sets). ENDF/B-IV, unlike ENDF/B-V and the current evaluations, contained only independent yields, no uncertainties, and it covered only six fissionable nuclides for ten yield sets. The recent evaluations include independent yields prior to delayed neutron emission and cumulative yields along each mass chain subsequent to delayed emission along with the uncorrelated uncertainties in each quantity. Table C-1 lists the fissionable nuclides and yield sets included in ENDF/B-IV, -V, and the preliminary evaluations for ENDF/B-VI. Table C-2 briefly summarizes the characteristics of each version.

D. FFTF EXPERIMENTS

1. FFTF Shield Measurements (W. L. Bunch, L. L. Carter and F. S. Moore)

A number of (n,γ) and (n,p) reaction rates were measured in accessible shield locations in the Fast Flux Test Facility (FFTF). Preliminary comparison of these reactions with calculated values using a 53-group cross section set derived from ENDF/B-V yielded satisfactory agreement considering the limitation of the model. Additional measurements and calculations are in progress to refine the model to incorporate more structural details and to include the effect of stored fuel.

Monte Carlo calculations were made to establish self-shielding factors for probes of various sizes, shapes and material composition. These factors are for use in interpreting the measured radioactivity of the probes that

---

* Los Alamos National Laboratory

Table C-1. ENDF/B Fission-Product Yield Sets[a]

Nuclide	Neutron Energy: Thermal	Fast	14 MeV	Spon.
^{227}Th	6			
^{229}Th	6			
^{232}Th		456	56	
^{231}Pa		6		
^{232}U		6		
^{233}U	456	56	56	
^{234}U		6	6	
^{235}U	456	456	456	
^{236}U		56	6	
^{237}U		6		
^{238}U		456	456	6
^{237}Np		56	6	
^{238}Np		6		
^{238}Pu		6		
^{239}Pu	456	456	56	
^{240}Pu		56	6	
^{241}Pu	456	56		

Nuclide	Neutron Energy: Thermal	Fast	14 MeV	Spon.
^{242}Pu		56		
^{241}Am	6	6	6	
^{242M}Am	6			
^{243}Am		6		
^{242}Cm		6		
^{244}Cm				6
^{245}Cm	6			
^{246}Cm				6
^{249}Cf	6			
^{250}Cf				6
^{251}Cf	6			
^{252}Cf				56
^{253}Es				6
^{254}Es	6			
^{254}Fm				6
^{255}Fm	6			
^{256}Fm				6

[a]The numbers 4, 5, and 6 refer to ENDF/B Versions IV, V, and preliminary VI. ENDF/B-IV contains only independent yields and does not include uncertainties.

Table C-2. Summary of ENDF Evaluations[a]

QUANTITY	ENDF/B-IV	ENDF/B-V	PRELIM. ENDF/B-VI
YEAR	1974	1978	1983
FISSIONABLE NUCS	6	11	34
NO. OF YIELD SETS	10	20	50
ISOMER RATIO EST.	50/50	YES	YES
PAIRING	NO	YES	YES
DELAYED NEUTRON	NO	YES	YES
CHARGE BALANCE	NO	YES	YES
TERNARY FISSION	NO	YES	YES
INDEP. YIELDS[b]	YES	YES	YES
CUMULATIVE YIELDS	NO	YES	YES
UNCERTAINTIES	NO	YES	YES
NO. OF REFERENCES	956	1119	1274
NO. OF YIELDS	11000	44000	110000

[a]ENDF/B yields through ENDF/B-V have been based on compilations by B. F. Rider at G.E. and modified at Los Alamos to extend the chains. G.E. compilations are NEDO-12154-1 (1974), -12154-2E (1978), -12154-3B (1980), and 12154-3C (1981). Current results are based on corrections and some added experimental data to the 1981 compilation.

[b]Beginning with ENDF/B-V, delayed neutron branching fractions have been incorporated into evaluations. Independent yields apply before delayed neutron emission and cumulative yields apply after emission.

were irradiated in the FFTF to establish the intensity and spectral distribution of the neutron flux.

2. Fission Yield Measurements (J. A. Rawlins, D. W. Wootan and F. Schmittroth)

Fast fission yield data have been determined from fission rate measurements in the FFTF (1,2). High purity fission foils of ^{239}Pu, ^{235}U, ^{237}Np and ^{238}U were loaded into dummy fission chambers along with solid state track recorders (SSTR) and were irradiated for two hours at approximately 100 kW reactor power. Multiple foils were loaded into the chambers. One foil of each set was counted eight times at HEDL; the remaining foils were counted by other laboratories for comparison. Thirty-two gamma rays from 13 fission products were analyzed. The gamma ray counting system was calibrated to approximately 1% with NBS absolute gamma ray standards. Evaluated gamma ray branching intensities, ENDF/B-V cumulative fission product yields and the experimental data were combined in the FERRET generalized least-squares data adjustment code (3) to obtain adjusted values for the branching intensities and cumulative fission product yields, as well as a bias factor for each foil at each location.

3. Noble Gas Cross Sections (R. E. Schenter, J. A. Rawlins and D. W. Wootan)

The Fast Flux Test Facility (FFTF) structural materials irradiation vehicle, MOTA, was designed to provide in-reactor creep rupture behavior results for structural materials (4). In order to identify precisely times when specimens rupture, "tag gases" of specific isotopic enrichments in Kr and Xe are put into the test capsules. Upon release of tag gas from a specimen rupture mass spectrometric measurements are made to determine precisely amounts of all the stable Kr and Xe isotopes. Significant changes occur in the concentration of several of these isotopes due to neutron capture providing a very good integral cross section measurement for fast neutrons (1 eV < E < 1 MeV).

---

[1]J. A. Rawlins, J. W. Daughtry and R. A. Bennett, "FFTF Reactor Characterization Program Review," Proceedings of the Fourth ASTM-EURATOM Symposium on Reactor Dosimetry, NUREG/CP-0029 (July 1982).

[2]D. W. Wootan, J. A. Rawlins, E. P. Lippincott, L. S. Kellogg, W. Y. Matsumoto and J. W. Daughtry, "Fission Rate Assessments in the FFTF Using Passive Techniques," Trans. Am. Nucl. Soc., 39, p. 901 (December 1981).

[3]F. Schmittroth, FERRET Data Analysis Code, HEDL-TME 79-40, Hanford Engineering Development Laboratory, Richland, WA (September 1979).

[4]R. J. Puigh and R. E. Schenter, "The In-Reactor Creep Rupture Experiment in MOTA," to be presented at the Twelfth International Symposium on Effects of Radiation on Materials," Williamsburg, VA (June 1984).

A. NUCLEAR DATA MEASUREMENT

1. Precise Gamma-Ray Emission-Probability Measurements for Selected Actinide Nuclides

As a part of our laboratory involvement in the work of an International Atomic Energy Agency Coordinated Research Program to measure and evaluate required nuclear decay data for selected transactinium nuclides, we are making precise (overall accuracy $\lesssim$1%) measurements of the emission probabilities (absolute intensities) of the prominent gamma-ray transitions from a number of such nuclides of particular importance for fission-reactor technology. Nuclides whose gamma-ray emission probabilities are being measured in this activity include: ^{238,239,240,241}Pu, ^{233,235}U, ^{232}U and members of its decay chain, ^{233}Pa and ^{229}Th. Thus far, papers describing our measurements for ^{240,239}Pu and ^{233}Pa have appeared in the literature, one for ^{238}Pu will appear soon, and papers on ^{233}U, ^{232}U and ^{235}U have been accepted for publication. Work on the ^{241}Pu decay has been completed (in collaboration with individuals from the University of Idaho) and work on ^{229}Th decay is in progress.

Briefly summarized below is the status of the measurement activity for those nuclides for which our data have not yet appeared in the literature.

^{238}Pu (R.G. Helmer, C.W. Reich)

To aid in the precise quantitative assay of ^{238}Pu by means of γ-ray spectrometry, we have remeasured the emission probabilities of the γ radiation associated with its decay. The decay-rate calibration was based on a measurement of the α-emission rate by the National Bureau of Standards. The γ-ray emission rates and energies were measured with calibrated Ge spectrometers. The energy values obtained for the three prominent γ rays are 43.498$\pm$0.001, 99.853$\pm$0.003 and 152.720$\pm$0.002 keV and the respective γ-ray emission probabilities are 38.2$\pm$0.8, 7.43$\pm$0.08 and 0.936$\pm$0.010 photons per 10^5 decays.

^{233}U (C.W. Reich, R.G. Helmer, J.D. Baker, R.J. Gehrke)

The following is the abstract of a paper that has been accepted for publication (in International Journal of Applied Radiation and Isotopes).

As an aid in the quantitative assay of ^{233}U by means of γ-ray spectrometry, we have measured the emission probabilities of thirteen prominent γ rays in the energy range from 29 to 320 keV. The decay-rate calibration of the source material was determined from the method of its original preparation and checked by comparison with an NBS-calibrated sample of ^{235}U using isotope-dilution mass spectrometry. The γ-emission rates and energies were measured with calibrated Ge spectrometers. The percentage uncertainties in the measured γ-emission probabilities range from 0.85% for most transitions above 120 keV to 2.2% at 29 keV.

<u>^{235}U</u> (R.G. Helmer, C.W. Reich

The abstract of a paper which has been accepted for publication in International Journal of Applied Radiation and Isotopes follows:

To aid in the precise quantitative assay of ^{235}U by means of γ-ray spectrometry, we have remeasured the emission probabilities of the radiation associated with its decay. The decay-rate calibration was based on the calibration of a standard solution by the National Bureau of Standards. The γ-ray emission rates and energies were measured with calibrated Ge spectrometers. The energy values obtained for six prominent γ rays are 25.509$\pm$0.009, 84.221$\pm$0.004, 143.768$\pm$0.003, 163.357$\pm$0.003, 185.722$\pm$0.004 and 205.318$\pm$0.004 keV and the γ-ray emission probabilities determined for the five lines above 50 keV are 6.84$\pm$0.10, 11.01$\pm$0.08, 5.12$\pm$0.04, 57.2$\pm$0.5 and 4.96$\pm$0.05 photons per 100 decays, respectively. The γ rays at 25 and 84 keV are produced in the decay of the 25-hr daughter ^{231}Th, while others are from the decay of ^{235}U.

<u>^{232}U and Members of its Decay Chain</u> (R.J. Gehrke, V.J. Novick, J.D. Baker)

A number of studies and evaluations have been performed on various members of the ^{232}U decay chain, including several which report γ-ray intensity measurements. However, a comprehensive study including all members of the ^{232}U chain to provide a consistent set of γ-ray emission probabilities has not been reported.

This study was undertaken to obtain a consistent and precise set of emission probabilities for a few γ rays throughout the entire ^{232}U decay chain.

For the ^{232}U γ rays at 57 and 129 keV, the respective emission-probability values were determined to be P_γ=0.200$\pm$0.004 and 0.0686$\pm$0.0007 γ rays per 100 decays of ^{232}U by 4π α-γ coincidence

techniques. The γ-ray emission probabilities of the daughter activities were determined from (1) the relative intensities from a ^{232}U source in equilibrium with its daughter activities and (2) grow-in of the daughter activities from an initially pure ^{232}U source. The former values were normalized to the absolute intensity of the 583-keV γ ray and the latter were normalized to the above P_γ values. The emission probability of the 2614-keV ^{208}Tl γ ray was calculated from a measured α-branch intensity and its internal conversion coefficient to be (35.86±0.06) γ rays per 100 decays of ^{228}Th and that of the 583-keV ^{208}Tl γ ray was determined from the decay scheme to be (30.52±0.17) γ rays per 100 decays of ^{228}Th. The adopted γ-ray emission probabilities per 100 decays of ^{228}Th, with γ-ray energies in parentheses, are: ^{228}Th, $P_\gamma(84)=1.246\pm0.029$; ^{224}Ra, $P'_\gamma(241)=4.16\pm0.04$; ^{220}Rn, $P'_\gamma(549)=0.130\pm0.003$; ^{212}Pb, $P'_\gamma(238)=43.2\pm0.4$; ^{212}Bi, $P'_\gamma(727)=6.57\pm0.05$ and $P'(39)=1.12\pm0.06$. P_γ is defined as the number of γ rays emitted per 100 decays of the parent (i.e., same) isotope; P'_γ is the number of γ rays emitted per 100 decays of the precursor, ^{228}Th, at equilibrium.

^{241}Pu, ^{237}U (R.G. Helmer, C.W. Reich)

Measurements of the emission probabilities of selected γ rays from the decay of ^{241}Pu and ^{237}U have been carried out as a part of a program to provide such data for a number of U and Pu isotopes important for fission-reactor technology (see discussions in previous sections). The decay-rate calibration of chemically purified source material was determined by comparison of the number of nuclei present with previously calibrated solutions of ^{239}Pu and ^{240}Pu using isotope dilution mass spectrometry. The results of these measurements are summarized in Table A-1.

Table A-1 Emission Probabilities of Selected Gamma-Ray Transitions from the Decay of ^{241}Pu and Its ^{237}U Daughter

Nominal γ-Ray Energy (keV)	Emission Probability ($\gamma/10^6$ Decays)
77.0	0.211 ±0.005
103.7	1.02 ±0.03
148.6	1.863 ±0.017
160.0	0.0654±0.0009
164.6	0.457 ±0.004
208.0	5.20 ±0.05
267.5	0.175 ±0.005

^{229}Th (R.G. Helmer, M.A. Lee, C.W. Reich, and I. Ahmad [ANL])

A measurement of the emission probabilities of the gamma radiation from the decay of ^{229}Th is being undertaken. The decay rate of a thin ^{229}Th source is determined by measuring the gross α-emission rate with a fixed-geometry counter. Since the source will contain the daughter activities, which also decay by α emission, the portion of the total α spectrum resulting from ^{229}Th decay alone will have to be determined. For the same source, the γ-emission rates will be measured on a calibrated Ge detector, and the emission probabilities calculated.

2. Efficiency Calibration of a Ge Detector for 30-2800 keV γ Rays (R.G. Helmer)

As a part of our effort to provide precise γ-ray emission-probability values from measurements with Ge detectors, we have carried out a precise efficiency calibration of an 8-cm^3 planar and an 114-cm^3 coaxial detector. The techniques utilized to carry out this calibration are discussed in some detail in a recently issued (November, 1983) laboratory report (EGG-PHYS-5735). The abstract of this report is as follows:

To meet the needs of some programmatic activities in precise radionuclide metrology and to support other EG&G Idaho, Inc. organizations at the Idaho National Engineering Laboratory, the Nuclear Physics Section of the Physical and Biological Sciences Division has for many years maintained a capability for precise γ-ray intensity measurements. Over the past three years a major emphasis of this work has involved the calibration of two Ge detectors for the measurements of emission rates of γ rays between 30 and 2800 keV. These calibrations involved over 20 sources, 20 nuclides and 60 γ rays with energies from 14 to 2754 keV. In this report, we give the magnitudes of the various corrections to the measured data, and the components of the uncertainty in the efficiency are discussed. As a result of this work the detector efficiency for point sources can be defined, at the calibration time, with uncertainty varying from 2% below 85 keV to 0.5% from 400 to 1400 keV. Corrections to these point-source efficiency functions for disk-source geometries are given. The efficiencies of both detectors have been observed to change with time in an energy-dependent manner.

3. Average Beta- and Gamma-Decay Energies of Fission-Product Nuclides (R.C. Greenwood)

The present status of average beta- and gamma-decay energy values for short-lived fission-product nuclides for the important region of half-lives, a few tens of seconds, in ENDF/B is poor. Either no measured data exist, in which case theoretically derived estimates are used in ENDF/B, or the measured data are (in most cases) derived from decay schemes studies, in which case they are likely to contain systematic biases. In any event, the average decay-energy values presently in ENDF/B (the Version-V Fission-Product File) give a rather poor description of the fission-product decay-heat source term for cooling times in this region.

We have recently initiated an effort to develop experimental systems to allow "direct" measurement of average beta- and gamma-decay energy values for short-lived fission-product nuclides using the Idaho ^{252}Cf-based on-line isotope-separator facility. This detector system will utilize a Ge semiconductor detector to monitor source purity, together with plastic and NaI(Tl) scintillation detectors, respectively, for measurement of total beta- and gamma-ray spectra. Each of these latter two detectors will be used in a ΔE-E counter-telescope arrangement. We expect that this technique will be an accurate and relatively rapid method of producing these important data.

4. Delayed-Neutron Spectral Measurements (R.C. Greenwood, A. J. Caffrey)

Measurements of delayed-neutron energy spectra are being carried out at the TRISTAN on-line mass separator facility at BNL. In order to obtain improved spectral data at energies below ~200 keV, the measurement effort, to date, has focussed on the use of gas-filled proton-recoil proportional counters. Pulse-shape discrimination circuitry is employed in our detector system in order to distinguish neutron pulses from background β/γ pulses, thereby allowing neutron spectral information to be obtained down to ~10 keV. A unique feature of these measurements is the use of the ^{56}Fe/Al and Sc filtered neutron beam facility, located adjacent to TRISTAN, for neutron energy calibrations and for characterization of the pulse-shape discrimination circuitry.

To date we have obtained from these measurements sets of high-quality delayed-neutron energy spectra from the precursor nuclides $^{93-97}$Rb and $^{143-145}$Cs covering an energy range from ~10 keV up to ~1300 keV. These data show good qualitative agreement

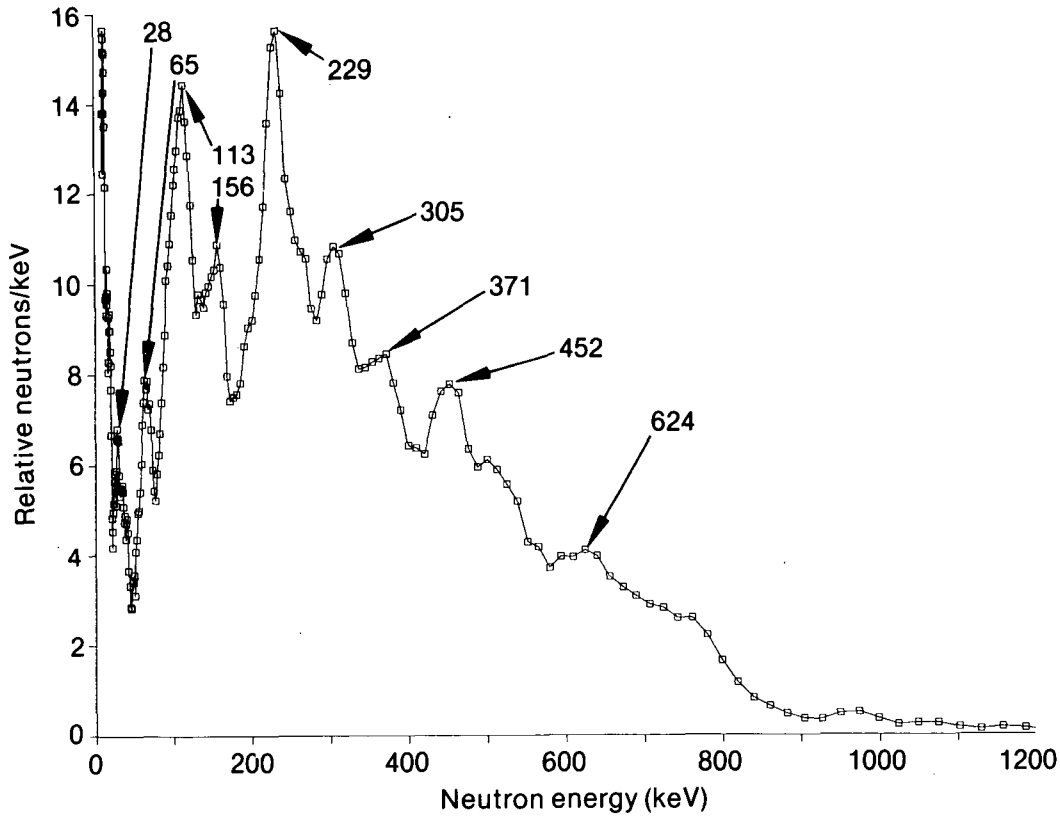

Fig. A-1. Delayed-neutron spectrum of ^{93}Rb obtained using 2.6 Atm., 2.5-cm diameter x 7.6-cm sensitive length H_2 and CH_4 gas-filled proportional counters.

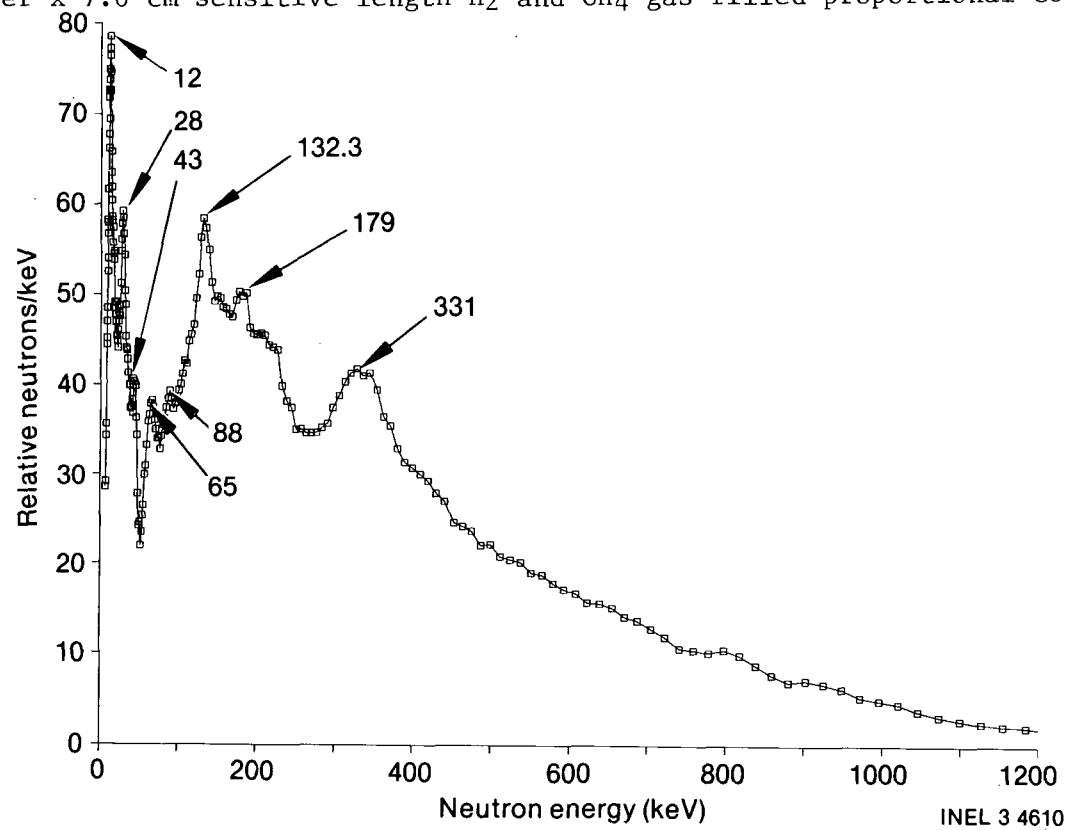

Fig. A-2. Delayed-neutron spectrum of ^{94}Rb obtained using 2.6 Atm., 2.5-cm diameter x 7.6-cm sensitive length, H_2 and CH_4 gas-filled proportional counters.

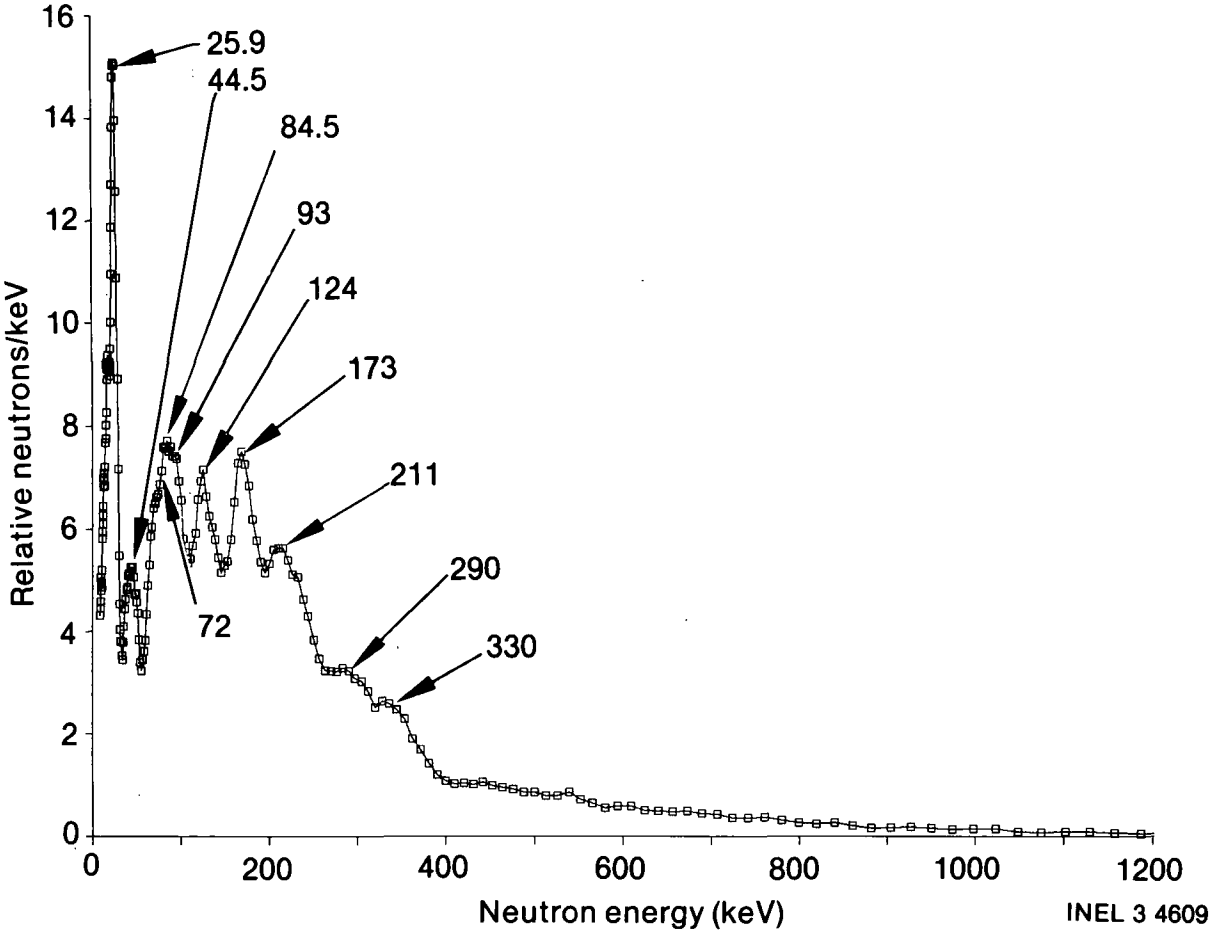

Fig. A-3. Delayed-neutron spectrum of ^{143}Cs obtained using 2.6 Atm., 2.5-cm diameter x 7.6-cm sensitive length, H_2 and CH_4 gas-filled proportional counters.

with the spectral shapes measured using the ^{3}He ionization chambers at energies $\geq$ 200 keV. In addition, they provide definitive spectral shape information in the energy region down to ~10 keV. In particular, we note our observation of fine structure in this lower energy region with energy resolution much better than that obtained using ^{3}He ionization chambers, i.e., the resolution varies from ~2 keV at 10 keV to ~8 keV at 100 keV and ~12 keV at 200 keV. Notable features of these data are that they confirm the existence of strong 14.2- and 26.5-keV lines in the ^{95}Rb spectrum, as well as a strong 25.9-keV line in the ^{143}Cs data. Fine structure in fact is observed in all of the delayed-neutron precursors studied to date at energies up to ~600 keV. The ^{93}Rb, ^{94}Rb and ^{143}Cs spectra are shown in Figs. A-1, A-2 and A-3, respectively, as examples of these data.

5. Measuring Delayed Neutron Spectra - A Comparison of Techniques (R.C. Greenwood, A. J. Caffrey)

The following is an abstract of a paper presented at the OECD/NEA Nuclear Data Committee Specialists Meeting on "Yields and Decay Data of Fission Product Nuclides" held Oct.24-27, 1983 at Brookhaven National Laboratory.

Currently, there are three quite different techniques that are in general use for measurement of delayed-neutron energy spectra from fission-product precursor isotopes. These three techniques use ^{3}He gas-filled gridded ionization chambers, proton-recoil proportional counters and neutron time-of-flight, respectively. Since there now exists a sufficient body of experimental data, especially for several of the Rb and Cs precursor isotopes, measured using each of these techniques, a meaningful intercomparison of the quality of data and range of applicability for each technique is now possible. Such an intercomparison is the subject of this paper.

B. NUCLEAR DATA EVALUATION

1. Mass-Chain Evaluation for the Nuclear Data Sheets (M.A. Lee, R.G. Helmer, C.W. Reich)

As a part of our involvement in the work of the International Nuclear Structure and Decay Data Evaluation Network, which carries out the evaluation of basic nuclear-physics data for publication in the Nuclear Data Sheets, we have the evaluation responsibility for the ten mass chains in the region $153 \leq A \leq 162$. Up to the present time, evaluations for the A=154, 159, 158 and 153 mass chains have been published in Nuclear Data Sheets, A=157 is scheduled

to appear soon in this journal, and A=161 is in the prepublication review process. Work on the A=160 and 162 mass chains is currently in progress and is scheduled to be completed in the Summer and Fall, respectively, of 1984. Work on the A=155 and 156 mass chains, the last two remaining within our area of responsibility, will begin later this year.

2. The ^{252}Cf Half-life Discrepancy (J.R. Smith)

Californium-252 is a standard for the neutron multiplicity factor $\bar{\nu}$ (average number of neutrons per fission) and for measurements of fission rates and neutron source strengths. Since ^{252}Cf decays at the rate of approximately 2% per month, the accuracy of any intercomparison depends upon how well the half-life and composition of the source are known.

At the time our investigations of the ^{252}Cf $\bar{\nu}$ problem were getting well under way, the half-life picture was essentially as summarized by Bozorgmanesh[1] in the thesis reporting his measurements of $\bar{\nu}$ for ^{252}Cf. His summary table included the first seven values (Refs. 2-8) listed in Table B-1. Bozorgmanesh used the weighted mean value 2.638±0.003 y in the analysis of his data. This weighted value is the same as Spiegel's published value,[8] and almost identical with a later

---

1 H. Bozorgmanesh, Thesis, U. Michigan, 1977

2 L. B. Magnusson et al., Phys. Rev. 96, 1576 (1954).

3 T. A. Eastwood et al., Phys. Rev. 107, 1635 (1957).

4 D. Metta et al., J. Inorg. Nucl. Chem. 27,33 (1965).

5 A. DeVolpi and K. G. Porges, Inorg. Nucl. Chem. Letters 5, 699 (1969).

6 V. T. Shchebolev et al., Soviet At. Energy 36, 507 (1974).

7 B.J. Mijnheer and E. Van den Hauten-Zuidema, Int. J. Appl. Rad. Isotopes 24, 185 (1973).

8 V. Spiegel, Nucl. Sci. Engr. 53, 326 (1974).

Table B-1. Summary of ^{252}Cf half-life values

Author and Date		T1/2 (y)
L. Magnusson[2]	(1954)	2.2 ±0.2
T. Eastwood[3]	(1957)	2.55 ±0.15
D. Metta[4]	(1965)	2.646±0.004
A. DeVolpi[5]	(1969)	2.621±0.006
V. Shchebolev[6]	(1973)	2.628±0.010
B. Mijnheer[7]	(1973)	2.659±0.010
V. Spiegel[8]	(1974)	2.638±0.007
V. Mozhaev[9]	(1976)	2.637±0.005
W. G. Alberts [10]	(1980)	2.648±0.002
V. Spiegel[10]	(1980)	2.653±0.001
J. R. Smith[11]	(1981)	2.651±0.003
F. Lagoutine[12]	(1981)	2.639±0.007

Table B-2.* Effect of ^{252}Cf Half-Life upon Neutron Source-Strength Comparison

Half-Life (y)	2.638	2.645	2.650	2.651
Difference between INEL and NPL (Percent)				
Source NZS-90	0.113	0.304	0.406	0.424
Standard Deviation of 7 measurement of itinerant source by 7 laboratories (Percent)	0.397	0.428	0.461	0.469
NBS measurement of itinerant source before and after (Percent)	0.132	0.200	0.434	0.481

*Prepared by E. J. Axton

measurement by Mozhaev[9]. We used the value of 2.638 y in the first analysis of our ^{252}Cf $\bar{\nu}$ data, and it appeared to agree with our data exceptionally well.

In November 1980, a workshop was held to discuss the status of $\bar{\nu}$ for ^{252}Cf. At this workshop Spiegel dropped the first of his two bombshells that have destroyed the serenity of the half-life picture. He revealed that he uncovered an error in his calculation of the time between two measurements of the ^{252}Cf source on which his half-life value was based. With the corrected time scale the half-life became 2.653±0.001 y. He had been in correspondence with Alberts on the subject. Alberts had from his own measurements derived the value 2.648±0.002 y. Spiegel and Alberts prepared a joint paper to announce their agreement on the higher half-life value.[10]

Since the fission-rate studies during our ^{252}Cf $\bar{\nu}$ measurement program had shown the neutron-fission coincidence technique to be essentially immune from distortions by self-transfer, as long as the whole angular correlation function is measured, it seemed appropriate to recalibrate one of the fission chambers and derive a half-life value consistent with the methodology of our ^{252}Cf $\bar{\nu}$ measurements. The resulting half-life was 2.651±0.003 y,[11] where the error represents the regression error of the fitting procedure.

The new value falls between the Alberts and revised Spiegel values. The ^{252}Cf half-life thus seemed well established. Then Spiegel dropped his second bombshell.[13] In reviewing the histories of other ^{252}Cf source measurements made at NBS, he found that he deduced different half-lives for different sources. His values were all within the range
encompassed by other measurements, but they were all obtained by the same experimenter, using the same method of measurement (comparison to the Ra-γ-Be source NBS-I in the NBS manganese bath) and the same method of allowing for the effects of other Cf isotopes.

---

9 V. K. Mozhaev, Sov. At. Energy 40, 200 (1976).

10 W. G. Alberts and V. Spiegel, unpublished.

11 J. R. Smith et al., EPRI report, to be published.

12 F. Lagoutine and J. Legrand, Int. J. Appl. Rad. Isot. 33, 771 (1972).

13 V. Spiegel, private communication, (March 1983).

Why should Speigel observe such a variety of half-lives when the techniques are the same, and the measurements overlap in time? The most obvious thing to question is the source composition. The possibility of substantial errors in the characterization of ^{252}Cf sources, whether in the isotopic analysis or in the presence of unidentified neutron emitters, should be investigated.

The uncertainty in the ^{252}Cf half-life is causing some problems in the comparison of neutron source strengths. For several years a ^{252}Cf source has circulated among laboratories of the world as a comparison source. Table B-2 shows a summary by Axton[14] of the effect of half-life upon the source comparison. The summary shows that the degree of agreement is dependent upon the ^{252}Cf half-life assumed in the analysis of the data. The agreement is somewhat enhanced by use of the shorter half-lives. From measurements made at NBS at the beginning and end of the tour of the source, it would appear that a half-life near 2.64 y should be favored.

There appears to be substantial support for ^{252}Cf half-life values near both 2.638 and 2.651 y. This difference contributes significant uncertainties to intercomparisons of neutron source-strength measurement techniques. The fault could lie in the inadequate characterization of the composition of ^{252}Cf sources. Further investigations should be pursued to identify the cause of this discrepancy. Pending resolution of the discrepancy, it would be well to adopt an intermediate value, with error bars covering the range of uncertainty. The value 2.645 ± 0.008 y is suggested as the interim value for the half-life of ^{252}Cf.

---

[14] E. J. Axton, report in progress.

DECAY STUDIES OF FISSION PRODUCTS WITH TRISTAN AT THE HFBR AT BNL

The TRISTAN on-line isotope separator facility at the High Flux Beam Reactor at Brookhaven National Laboratory is used to mass separate and study the decay of neutron-rich nuclides produced in the thermal neutron fission of ^{235}U. A number of different elements can be ionized and separated using a variety of surface ionization, FEBIAD, and high-temperature plasma ion sources. Measurements made with these ion sources are discussed below. Members of the Ames Laboratory group (Hill, Wohn, Berant, and Winger) have collaborated with other users from BNL, R. F. Petry (University of Oklahoma) and K. Sistemich (KFA Jülich). Experiments have involved decay scheme studies using γ-ray spectroscopy, γγ angular correlations, and perturbed angular correlations.

1. Decay of ^{83}Ge to Levels in the N=50 Isotone ^{83}As (J. A. Winger *et al.*)

The decay of ^{83}Ge was studied using sources produced by a high-temperature plasma ion source. No information is available on ^{83}Ge decay other than its half-life and no information exists on excited states in ^{83}As. This study is of interest since ^{83}As can be pictured as five protons outside of a doubly magic ^{78}Ni core. A strong γ ray at 306 keV which probably connects the $f_{5/2}$ and $P_{3/2}$ single quasi-particle states in ^{83}As was used to determine a half-life for ^{83}Ge of 1.8±0.1 s in good agreement with a value of 1.9 s obtained some years ago using milking techniques. Preliminary analysis of data from γ multiscale experiments reveal about 10 γ rays which can be attributed to ^{83}Ge decay. Data analysis is in progress.

2. Decay of ^{99}Rb and ^{99}Sr to the Deformed Nuclei ^{99}Sr and ^{99}Y (J. C. Hill *et al.*)

The decay of ^{99}Rb and ^{99}Sr were studied from activities produced by a surface ionization source. The half-lives were determined to be 52±5 and 266±5 ms respectively. In both cases γ singles, γγ coincidence, and γ multiscale measurements were made. Preliminary analysis of the ^{99}Rb decay data indicated 8 γ rays with energies ranging from 91 to 684 keV. The analysis of the ^{99}Sr decay data is more complete with 73 γ rays ranging in energy from 64 to 2279 keV. The preliminary data was used to establish ground-state rotational bands in ^{99}Sr and ^{99}Y with K=3/2 and 5/2 respectively.[1] Rotational bands based on the following Nilsson orbitals have been

[1] Wohn, Hill, Petry, Dejbakhsh, Berant, and Gill, Phys. Rev. Lett. 51, 873 (1983).

identified: 5/2[422] at 0 keV, 5/2[303] at 487 keV and 3/2[301] at 536 keV in ^{99}Y and 3/2[411] at 0 keV in ^{99}Sr.

3. Levels in ^{100}Zr Populated in the Decay of the Low-Spin Isomer of 100Y (F. K. Wohn *et al.*)

The decay chain $^{100}Sr \rightarrow {}^{100}Y \rightarrow {}^{100}Zr$ was studied with the primary purpose being $\gamma\gamma$ angular correlation measurements to establish spins and parities of levels in ^{100}Zr. From 2 γ multiscale measurements, half-lives of 193±7 and 735±7 ms were determined for ^{100}Sr and ^{100}Y respectively. This ^{100}Y half-life is assigned to the low-spin ^{100}Y isomer. (We found no evidence for ^{100}Y in the ion beam, as all observed ^{100}Y was produced from the decay of 0^+ ^{100}Sr.) A new 0^+ level at 830 keV was established via $\gamma\gamma(\theta)$ measurements on the $0^+(617)2^+(213)0^+$ cascade. The previously reported, anamously low-lying 0^+ level at 331 keV was confirmed to be 0^+ via $\gamma\gamma(\theta)$ measurements on the $0^+(118)2^+(213)0^+$ cascade. Several new γ rays were assigned to the low-spin ^{100}Y decay. A revised level scheme for ^{100}Zr is being constructed.

4. Decay of ^{101}Sr and ^{101}Y to the Deformed Nuclei ^{101}Y and ^{101}Zr (F. K. Wohn *et al.*)

Mass-separated A=101 fission products produced by a surface ionization source were studied by γ singles, $\gamma\gamma$ coincidence and γ multiscale measurements. Half-lives of 121±6 and 500±50 ms were obtained for ^{101}Sr and ^{101}Y, respectively. For the decay of ^{101}Sr, 39 γ rays with energies from 124 to 2694 keV were observed and have been placed in a level scheme with 16 levels. For the decay of ^{101}Y, 25 γ rays with energies between 98 and 1299 keV were observed and have been placed in a preliminary level scheme with 15 levels. Ground-state rotational bands in ^{101}Y and ^{101}Sr with K=5/2 and 3/2 respectively have been reported.[1] These bands are based on the Nilsson orbitals 5/2[422] and 3/2[411]. A second K=5/2 band in ^{101}Y and a second K=3/2 band in ^{101}Zr have been observed and are probably 5/2[303] and 3/2[541].

5. Decay of ^{124}Ag (J. C. Hill *et al.*)

Using the multi-element FEBIAD ion source a study was made of the decay of the new isotope ^{124}Ag to levels in ^{124}Cd. The half-life was measured to be 0.17±0.03 s using γ multiscaling techniques. Only one γ transition was observed of energy 613.2±0.2 keV depopulating the 2_1^+ state in ^{124}Cd. The systematics of 2_1^+ levels in neutron-rich Cd isotopes was

---

[1] Wohn, Hill, Petry, Dejbakhsh, Berant, and Gill, Phys. Rev. Lett. 51, 873 (1983).

interpreted in terms of a neutron subshell involving the $1g_{7/2}$, $2d_{3/2}$, and $1h_{11/2}$ orbitals. This material has been published.[2]

6. Decay of ^{135}Te to Levels in the N=82 Isotone ^{135}I (J. C. Hill *et al.*)

The decay of ^{135}Te to levels in ^{135}I was studied using the FEBIAD ion source. ^{135}I is of particular interest since it can be pictured as three protons outside of a doubly magic ^{132}Sn core. In addition to γ rays at 267, 604, and 871 keV known from previous studies, γ rays at 1184, 1711, 1726, 2028, 4464, and 4747 keV were observed. A preliminary half-life of 19 s for ^{135}Te is in good agreement with measurements of previous investigators. Analysis of γγ coincidence data is in progress.

7. "g" Factors for the 4_1^+ States in the N=82 Isotones ^{136}Xe and ^{138}Ba (Z. Berant *et al.*)

The magnetic dipole moments for the 4_1^+ states in ^{136}Xe and ^{138}Ba were measured using the technique of integral perturbed angular correlations. The levels were populated from the β^- decay of sources of ^{136}I and ^{138}Cs respectively. A magnetic field of about 25 kG was used to perturb the correlation. Counting was done with both field up and field down. A "g" factor of 0.77±0.27 was obtained for ^{138}Ba. A preliminary value for the corresponding "g" factor in ^{136}Xe is 0.79. The values agree well with shell-model calculations for the N=82 isotones. A new set of shell-model calculations to evaluate our results is being carried out by H. Kruse of Michigan State and B. H. Wildenthal of Drexel.

8. Decay of ^{146}La and Band Structure in ^{146}Ce (F. K. Wohn *et al.*)

The decays of the low-spin and high-spin isomers of ^{146}La to levels in even-even ^{146}Ce were studied by γ spectroscopy. More than 300 γ rays have been identified for this decay, which as a Q_β value of 6.4 MeV. A small direct production of ^{146}La from the TRISTAN ion source has been established at the ~1% level (i.e. ≈0.01 for the ratio of high-spin ^{146}La in the ion beam to low-spin ^{146}La from the decay of 0^+ ^{146}Ba in the ion beam. Half-lives of 6.45±0.05 and 9.55±0.28 s were determined for the low-spin and high-spin ^{146}La isomers respectively. Recent γγ(θ) measurements have been analyzed. The ^{146}Ce levels deduced include 0^+, 2^+, 4^+, 6^+ members of the ground state bands, 0^+_β, 2^+_β, 4^+_β, 2^+_γ, 3^+_γ, 4^+_γ and 1^-, 3^-, 5^- members of an octupole band. Deduction of separate decay scheme for the two ^{146}La isomers is in progress.

---

[2] Hill, Wohn, Berant, Gill, Chrien, Chung, and Aprahamian, Phys. Rev. C 29, 1078 (1984).

A. NUCLEAR STRUCTURE STUDIES

1. Shape Transitional Nuclei (Kleppinger, Khan, Yates)

The lowest excitations of heavy nuclei can usually be interpreted as collective motions of the quadrupole (or octupole) type, and multi-phonon quadrupole excitations have long been observed in nearly spherical nuclei. The evolution of these excitations in going from one region of deformation to another is not completely explained, but recent application of boson calculational techniques is promising and has provided new impetus for detailed studies of the properties of low-lying collective states which can provide tests of the model predictions. We have extensively utilized the unique capabilities of the $(n,n'\gamma)$ reaction to examine the properties of transitional nuclei in the osmium-platinum region.

a. Even-Even Nuclei

Our initial studies[1-6] of heavy transitional nuclei (^{190}Os, ^{192}Os, ^{194}Pt, ^{198}Pt, and ^{200}Hg) have focused on the structures of stable even-mass nuclei. While much of this work has been published[1-4] or is in press,[5] we briefly review here some of the important results of these studies.

The predictions of the IBA and BET were found to be generally successful in reproducing the observed level properties of transitional nuclei. A source of particular concern, however, is the characterization of low-lying 0^+ excitations. Such problems were first noted for the close-lying 0_3^+ and 0_4^+ states in ^{194}Pt (which could possibly be understood if supersymmetric two-fermion excitations are allowed) and later for the lowest 0^+ excitation in ^{198}Pt. We discounted[1] the applicability of the 0(6) limit for ^{198}Pt on the basis of this state, but one must also remain aware of

---

[1] Yates, Khan, Mirzaa, and McEllistrem, Phys. Rev. C 23, 1993 (1981).

[2] Filo, Yates, Coope, Weil, and McEllistrem, Phys. Rev. C 23, 1928 (1981).

[3] E.W. Kleppinger and S.W. Yates, Phys. Rev. C 27, 2608 (1983).

[4] Yates, Khan, Filo, Mirzaa, Weil, and McEllistrem, Nucl. Phys. A406, 519 (1983).

[5] A. Khan and S.W. Yates, Phys. Rev. C (in press).

[6] E.W. Kleppinger and S.W. Yates, Bull. Am. Phys. Soc. 28, 990 (1983).

the possibility of intruding spherical states.[4] Similar problems[3] arose with the decay of the 0_3^+ state of ^{192}Os. Moreover, a surprising lack of band structure built on the 0_3^+ and 3_1^- excitations intimates a seeming deterioration of rotational behavior at higher excitation in ^{192}Os which is not apparent in the lighter Os nuclei.

Our (n,n'γ) spectroscopic studies have permitted us to assess the limits of success of the nuclear models by comparisons of level energies and branching ratios. In our comparisons, as well as most previous ones, with the IBA and BET for example, transitions have been assumed to be of pure E2 multipolarity, thus ignoring possible M1 multipole admixtures. In very careful γ-ray angular distribution measurements on ^{196}Pt, considered the best example of an O(6) nucleus, we have determined that some transitions previously assumed to be E2's are of 60 to 70% M1 character.

Our initial investigation[5] of ^{200}Hg provided us with a useful evaluation of the capabilities of the (n,n'γ) reaction. The large difference of the excitation energies of the 3^- states in ^{198}Pt and ^{200}Hg supports the view that the lowest 3^- excitations in the Pt nuclei are not of octupole character, while those in the Hg and Pb nuclei are. We have recently begun a similar study of ^{204}Hg to examine the extent (i.e., how close to spherical) to which the boson models are applicable.

b. Odd-mass Nuclei and the Supersymmetry Schemes

For the case of an O(6) boson core coupled to a fermion with j = 3/2, a supersymmetry, applicable to both even- and odd-mass systems, emerges. The application of the supersymmetry scheme to the known low-lying positive-parity energy levels of ^{191}Ir was quite successful,[7] but one is forced to question whether the level properties of this nucleus are sufficiently well-known to merit detailed comparisons. We have initiated a systematic investigation of the level structures of ^{191}Ir and ^{193}Ir which has greatly extended our knowledge of these nuclei (15 new levels in ^{191}Ir and 33 new levels in ^{193}Ir). We might make note of the closeness of the newly-discovered $13/2^-$ and $15/2^-$ levels in ^{193}Ir which could be taken as a sign of γ = 30° triaxiality in this nucleus. Nevertheless, any comparisons of these data with the supersymmetry model (or other approaches such as the asymmetric rotor model) must await further analysis and the extraction of M1 and E2 components in the decay transitions.

Balantekin et al.[8] have introduced a more complex supersymmetry classification which considers the case in which the odd fermions can occupy single-particle orbits with j = 1/2, 3/2, and 5/2. Recent experimental

---

[7] F. Iachello, Phys. Rev. Lett. 44, 772 (1980).

[8] Balantekin, Bars, Bijker, and Iachello, Phys. Rev. C 27, 1761 (1983).

investigations of the heavy odd-mass Pt isotopes have shown that this proposed multi-j supersymmetry scheme may be a useful theoretical framework. As noted by Warner et al.[9], ^{195}Pt should be an excellent test case since the important low-lying single-neutron orbits available are $p_{1/2}$, $p_{3/2}$, and $f_{5/2}$.

Warner et al.[9] have recently studied ^{195}Pt by the ^{194}Pt(n,γ) reaction, and the resulting level structure was favorably compared with predictions of the multi-j supersymmetry, although some spin and parity ambiguities remained in the experimental spectrum. We initiated a study of ^{195}Pt by the (n,n'γ) reaction in an attempt to resolve these ambiguities and thus to evaluate better the degree of success of the multi-j supersymmetry picture. The results[10] of our work generally support arguments in favor of multi-j supersymmetry representation of the negative-parity states of ^{195}Pt, although a paucity of observed $J^{\pi} = 1/2^{-}$ states is apparent. Unfortunately, we were not able to assess the degree of multipole mixing in many of the critical transitions.

2. Deformed Nuclei (Kleppinger, Yates)

Following the latest detailed neutron capture spectroscopic study[11] of ^{168}Er, considerable controversy has arisen regarding the applicability of collective model descriptions for deformed nuclei. The observation and characterization of multiple-phonon excitations in these nuclei would, of course, provide valuable insights into a resolution of these problems. At present, the detail with which the ^{168}Er level scheme is known makes this nucleus an excellent case to search for two-phonon excitations.

Davidson et al.[11] constructed a level scheme for ^{168}Er which included 20 rotational bands below 2.2 MeV, and arguments have been advanced about the completeness of their level scheme. In an (n,n'γ) experiment[12] designed to search for low-spin excitations, we observed a previously unreported 2^{+} state at 1893 keV in ^{168}Er. We were, however, unable to find band structure associated with this new state; no new low-spin states below this level were observed and higher-lying candidates for $J^{\pi} = 3^{+}$ were seen neither in our work nor that of Davidson et al.[11] More recently, Davidson et al.[13] combined transfer reaction data and additional (n,γ) measurements with their earlier

---

[9] Warner, Casten, Stelts, Boerner, and Barreau, Phys. Rev. C 26, 1921 (1982).

[10] A.R. Ghatak-Roy and S.W. Yates, Phys. Rev. C 28, 2521 (1983).

[11] Davidson et al., J. Phys. G 7, 455, 843 (1981).

[12] E.W. Kleppinger and S.W. Yates, Phys. Rev. C 28, 943 (1983).

[13] Davidson, Dixon, Burke, and Cizewski, Phys. Lett. 130B, 161 (1983).

(n,γ) and (n,e^-) measurements and proposed a fourth $K^\pi = 0^+$ band based at 1834 keV in ^{168}Er. This 0_4^+ band included the 1893 keV 2^+ state as well as probable 4^+ and 6^+ levels at 2031 and 2245 keV, respectively.

In an effort to further characterize this 0_4^+ band, we initiated a very detailed series of $(n,n'\gamma)$ measurements on ^{168}Er. To enhance the observation of the 1754-keV transition, which Davidson et al.[13] attributed to the decay of the 0_4^+ state to the 2_g^+ level, we employed a very restrictive neutron-source to scattering-sample geometry; this distance was kept as small as possible yet consistent with detector shielding requirements. The remainder of the experiment was performed as reported previously,[12] except that each point on the excitation function and each angle in the angular distribution represented about one day of data accumulation. Coupling our new data with the measurements of Davidson et al.[13] it would seem that the 0^+ assignment of the 1834-keV state of ^{168}Er is quite firm. We have also re-examined the branching intensities of transitions from the 1893-keV level and some discrepancies are observed between our values and those reported.[13]

While the collectivity of the 0_4^+ band remains to be established, we can can make two observations. First, it seems unlikely that this band is the long-sought $\gamma\gamma$ two-phonon vibrational band. If anything, the decay pattern suggests a two-phonon component is more likely of $\beta\beta$ character, although the relative excitation energies suggests large anharmonicities. Secondly, the existence of this $K^\pi = 0_4^+$ band at this energy seemingly argues against the contention that the lowest $K^\pi = 0^+$ bands are of pure two-quasiparticle nature.

A comparison study of ^{170}Er by the $(n,n'\gamma)$ reactions is progressing well with several new rotational bands having already been established in this nucleus.

3. Spherical Nuclei.

a. $^{116}Sn(n,n'\gamma)$. (Gácsi, Shi, Zhou, Sa, Cao, Weil)

The excitation functions of γ-rays from this reaction have been measured in the bombarding energy range of $1.9 < E_n < 4.5$ MeV. Ninety-one previously unobserved γ-rays have been observed, and from the excitation functions 74 new excited states have been placed in the level scheme below $E_x = 4.4$ MeV. Since many of the decays are to well-separated, low-lying states, at least 60 of these new levels are uniquely assigned in energy, while the remainder have only a small uncertainty (~ 50-100 keV) in their excitation energy. A search for delayed γ-rays from long-lived states has also been made.

A preliminary measurement of the angular distributions of a dozen γ-rays has been made at $E_n = 3.05$ MeV, and although the analysis is still in progress, it is apparent that a number of new spin-parity assignments can be made. Angular distributions of γ-rays will be measured in the future at neutron energies of 3.7 and 4.5 MeV, leading to additional spin-parity assignments.

b. $^{120}Sn(n,n'\gamma)$. (Shi, Sa, Cao, Weil)

Excitation functions of γ-rays from this reaction have been measured over the incident neutron energy range of $2.1 \leq E_n \leq 4.5$ MeV. More than 95 previously undetected γ-rays from ^{120}Sn were observed in this experiment and excitation functions for individual γ-rays are being constructed. Angular distribution measurements will be made in the future.

c. $^{124}Sn(n,n'\gamma)$. (Weil, Sa, Gácsi)

Gamma-ray angular distributions have been measured at E_n=2.6 and 3.5 MeV. From an analysis of this angular distribution data, new spin-parity assignments have been made to 10 levels, and limitations on J^{π} have been established for 12 levels. Multipole mixing ratios have also been determined for many of the decays involving these levels. Based on these results we have been able to identify the vibrational two-phonon triplet levels at an excitation $\sim$ 2.1 MeV, and also 5 levels that appear to have a great deal of vibrational three-phonon character. Strong decays between the negative parity levels are observed, and it is expected that these data will lead to a firmer identification of those levels having $\nu(h_{11/2}, s_{1/2})$ and $\nu(h_{11/2}, d_{3/2})$ configurations. The identification of other collective and quasi-particle excitations in this nucleus is being pursued.

4. $^{54,56}Fe(n,n'\gamma)$ Reaction. (Gácsi, O'Brien, Sa, Weil).

Gamma-ray excitation functions were measured for $3.6 \leq E_n \leq 4.5$ MeV, and also an angular distribution at E_n = 4.3 MeV, to learn more about the character of a triplet of states at 3.60 MeV excitation. Two of the states decay by ground state transitions. By direct comparison to the spectrum of a ^{56}Co source, one of these states has been identified as the 3601.9-keV state seen in the beta decays of ^{56}Co and ^{56}Mn. Significant Doppler shifts as a function of emission angle were observed from many of the γ-rays. From the Doppler shift measurements new lifetime determinations have been made for the states at E_x = 3338, 3445, 3450, 4049, 4100 and 4119 keV excitation energy.

Measurements of excitation functions of $^{54}Fe(n,n'\gamma)$ for $2.6 \leq E_n \leq 4.2$ MeV and an angular distribution at E_n = 4.5 MeV revealed no new γ-rays nor level lifetimes beyond those already known.[14]

5. Investigation of the Effective Nucleon-nucleon Interaction in ^{96}Nb. (B.D. Kern)

The γ ray-spectra of the $^{96}Zr(p,n\gamma)^{96}Nb$ reaction have been measured with Ge(Li) detectors at several bombarding proton energies between 1.3 and 5.1 MeV. $\gamma\gamma$-coincidences were observed at E_p = 4.7 and 5.0 MeV. On the basis of experimental results a level scheme of ^{96}Nb was deduced, and

---

[14] Moss, Hendrie, Glashauser, and Thirion, Nucl. Phys. A194, 12 (1972).

γ-threshold energies and γ-branching ratios were determined. Computed Hauser-Feshbach (p,n') cross sections have been fitted to experimental data obtained from the γ-ray measurements, and spins and parities have been determined for some levels. The energies of ^{96}Nb levels were calculated on the basis of the parabolic rule derived from the cluster-vibration model,[15] and the experimental level scheme of ^{96}Nb was compared with the theoretical results. Thirty-four γ-rays have been assigned to the level scheme of ^{96}Nb. Five of the members of the $(\pi 1g_{9/2})(\nu 2d_{5/2})^{-1}$ multiplet were readily identified (the 7^+ was not sufficiently populated), as were also the previously-assigned members of the $(\pi 2p_{1/2})^{-1}(\nu 2d_{5/2})^{-1}$ doublet. However, the assignment of the 694.7-keV level as the 3^- member of this doublet has been questioned and it is now thought that the 867.9-keV level is the 3^- state. Other multiplets predicted by the parabolic rule are being sought.

B. NEUTRON SCATTERING - ELASTIC AND INELASTIC

1. $^{116-124}$Sn(n,n) and Neutron-Excess Effects. (Zhou, Harper, Weil)

The differential cross sections for elastic and inelastic neutron scattering from five even-A tin isotopes have been measured at 1.0, 1.6 and 4.0 MeV in order to investigate the effects of changing neutron excess in a sequence of isotopes with similar nuclear structure. A reanalysis of the 1.0 and 1.63 MeV differential cross sections with the spherical optical model (SOM) has removed an energy dependent discrepancy in the real well depth neutron-excess dependence; it is now found to agree well with the global value. We find an imaginary well depth neutron excess dependence that is 2-3 times larger than the 12-14 MeV value found in global fits. However, the inelastic scattering cross sections for the first excited state measured at E_n = 1.63 MeV are systematically lower than the calculated Hauser-Feshbach cross sections including level-width fluctuation corrections. Inclusion of a correction for channel-channel correlations would only make the discrepancy worse. This work is about to be submitted for publication. Coupled channel fits with recent β_2 values for the first excited states are under way, and are expected to give about the same result as the SOM for the real well, but a smaller neutron excess dependence for the imaginary well depth.

2. ^{190}Os, ^{192}Os(n,n'). (Hicks, McEllistrem, Weil).

Our differential cross section measurements for several states of these isotopes have been carefully analyzed and corrected for sample size effects, to ascertain with confidence that differences in cross sections for the two samples do not reflect the different sample sizes. We have now supplemented these differential cross sections with new measurements[16] of total cross sections for both isotopes over the incident energy range from 300

---

[15] V. Paar, Nucl. Phys. A331, 16 (1979).

[16] Hicks, Cao, Hanly and McEllistrem, Bull. Am. Phys. Soc. 28, 984 (1983).

keV to 3 MeV. We had found with coupled-channels analyses that these total cross sections would be sensitive at the 5 or 6% level to collective structure differences expected to obtain for these two isotopes. During the next six months we will be analyzing all of our cross sections to test for sensitivity to non-axial quadrupole collective effects on the total and differential scattering cross sections, both the elastic and inelastic scattering cross sections. The non-axial quadrupole excitations are the collective properties which are expected to show the most variations between the two nuclei.

Additional differential cross section measurements will be made at the Centre d'Etudes de Bruyeres-le-Chatel (BRC) in France (in collaboration with T.B. Clegg of North Carolina, G. Haouat and J. Lachkar of BRC). These measurements will be made at higher energies, where collective model interpretations of the inelastic scattering cross sections will be simpler than at the lower energies used in our laboratory, but where the sensitivity to collective effects in the elastic scattering cross sections will be much reduced. Subtle collective effects may be more difficult to discern at higher energy than those studied in this laboratory.

3. ^{204,206}Pb(n,n'γ) Structure Studies. (Hanly, Hicks, Yates, and McEllistrem)

Excitation functions for gamma rays from neutron inelastic scattering in ^{204}Pb and in ^{206}Pb have been measured from thresholds to about 4 MeV in both nuclei to ascertain the level and decay schemes. From the levels and relative transition rates we expect to ascertain the evolution of collective quadrupole character at low energies as we move away from doubly magic ^{208}Pb and toward the shape-transitional region near A = 190. Gamma-ray angular distributions will be measured at several incident neutron energies to fix spins of excited levels, and E2/M1 mixing ratios for decays of the levels. The multipole character of decays will help identify those levels which have vibrational collective character, and thus influence neutron scattering.

4. ^{204,206}Pb(n,n') and Vibrational Excitations. (Hanly, Hicks, McEllistrem, and Weil).

Early measurements at 7 MeV for ^{208}Pb had identified strong excitation of some levels at energies appropriate for two-phonon excitations. We now have taken some data for ^{206}Pb which still shows strong excitation of particular groups of levels, albeit substantially weaker excitations than those in ^{208}Pb. We propose to follow these excitations also into ^{204}Pb, and attempt to discern the diffusion of collective excitations into other excited levels as the number of valence nucleons is increased away from ^{208}Pb. Critical to the success of these measurements and the separation of neutron groups to highly excited levels is the dynamically biased neutron method developed here some years ago. These methods allow us to minimize backgrounds and optimize resolution for different energy neutron groups without sacrificing dynamic range.

5. Elastic and Inelastic Neutron Scattering at 2.5 MeV in ^{194}Pt. (Mirzaa, Delaroche, Hanly, Yates, Weil, and McEllistrem).

Measurements and analyses of differential elastic and inelastic neutron scattering have been completed. Coupled-channels methods have been used to show a marked dependence of the cross sections on the non-axial quadrupole excitations, and even some sensitivity to whether these were treated as rigid triaxial rotations or changes in shape away from axial symmetry when the nucleus was excited. Calculations have been done for different nuclear structure models assumed for ^{194}Pt, all of which have done a reasonably good job of characterizing the level and gamma-ray decay schemes. Some sensitivity to differences in these structural models is demonstrated. This study will shortly be submitted for publication, and efforts are continuing for higher incident neutron energies.

We plan also to make total cross section measurements for the incident neutron energy range from 300 keV to 4.5 MeV, to complement our differential cross section measurements at 2.5 MeV and 4.5 MeV. This is an important nucleus to include in our study of the influence of quadrupole collective effects on neutron scattering, because it is the nucleus whose quadrupole moment in the excited 2^+ level is closest to zero.

C. ENERGY DEPENDENCE OF THE PROTON-ABSORPTIVE POTENTIAL AT SUB-COULOMB ENERGIES.

1. $90 \leq A \leq 120$. (Flynn, Gabbard, Hershberger, Laird*).

During the past year, analytical work on proton strength functions at sub-Coulomb bombarding energies has continued. Using the programs GENOA (standard optical model), HELGA (Hauser-Feshbach model), CCHAN (Lane-model coupled channels), and ECIS (deformed-potential coupled channels), much work has been done to verify and gain a more detailed understanding of the anomalous, but systematic, variation of W, the imaginary part of the optical model (OM) potential, vs. A in the range $88 \leq A \leq 130$. This analysis has been based on (p,n), (p,p) and (p,γ) measurements done in this lab on eleven isotopes of Zr and Mo. An earlier analysis by Johnson *et al.*[17,18] which first demonstrated the anomaly was based almost entirely on (p,n) data alone. Measurements and their analysis at Kentucky have confirmed the existence of the W anomaly.[19,20]

---

* Eastern Kentucky University.

[17] Johnson, Galonsky and Kernell, Phys. Rev. Lett. 39, 1604 (1977).

[18] Johnson, Bair, Jones, Penny and Smith, Phys. Rev. C 15, 195 (1977).

[19] Flynn, Hershberger and Gabbard, Phys. Rev. C 26, 1744 (1982), and references contained therein.

[20] D.S. Flynn, Phys. Rev. C 27, 2381 (1983).

An analysis of the proton-induced reaction cross sections for the isotopes of zirconium and molydenum reveal strong energy dependences which vary from one nuclide to the next in such a manner that at 7 MeV proton energy W is approximately independent of mass-number, whereas at 2 MeV proton energy the absorptive potential varies strongly with mass in the manner suggested by Johnson et al.[17]. This variation is strongly correlated with the structure of the target nuclei.

The measured (p,p) and (p,n) strength functions for $^{92,94,96}Zr$ and $^{95,98,100}Mo$ were fitted on the energy range $2 < E_p < 7$ MeV using a standard optical model potential with an energy dependent proton absorptive potential. The volume integral of the proton absorptive potential shows strong A dependence at low proton energy and tends to a common value of 100 MeV-fm^3 for all isotopes studied as the proton bombarding energy is increased toward 15 MeV. This result is consistent with results from analysis at higher energies.

2. $50 \leq A \leq 90$. (Hershberger, Fisher and Gabbard)

Our study of the proton strength functions in the mass region $50 \leq A \leq 90$ has continued. Here the (p,n) contribution to the absorption cross section is not so dominant as in the mass-100 region. Below the (p,n) threshold (p,γ) is an important reaction; (p,p') and compound elastic scattering are important channels in the determination of the reaction cross section for protons.

The (p,p) and (p,n) cross sections have been measured for ^{51}V, ^{61}Ni, ^{65}Cu, ^{67}Zn, ^{68}Zn and ^{75}As targets. The (p,p) cross sections were measured at 135° and 165° for proton bombarding energies $1.5 \leq E_p \leq 6.6$ MeV. (p,n) strength functions have been determined and tabulated. Laboratory reaction rates assuming a Maxwellian distribution of proton energies at stellar temperatures have been computed and tabulated. Measurements of the (p,γ) reaction have been completed on ^{51}V, ^{67}Zr and ^{68}Zr. These will provide needed information for the analysis of the data and the understanding of systematic trends. The data will be analyzed using an Optical Model to study the variation of the potential parameters, particularly W, with atomic mass number, A.

D. NUCLEAR ASTROPHYSICS

1. Branching Ratios for EC Decay of ^7Be and ^{51}Cr. (Fisher, Hershberger)

Branching ratio for the EC decay of ^7Be to ^7Li has been measured by counting the total number of neutrons produced in the $^7Li(p,n)^7Be$ reaction and subsequently counting the yield of 478-keV γ rays from the activated targets. Six targets were measured with particular attention given to monitoring migration or loss of ^7Be during and after activation. The branching ratio for the EC decay of ^{51}Cr to ^{51}V (320 keV γ ray) was also measured using the same technique. The resulting branching ratios to the

first excited states in ^{7}Li and ^{51}V are (10.61±0.17)% and (10.30±0.19)% respectively. (Accepted by Nucl. Phys. A).

2. Studies on the $^{79,81}Br(p,n)$ Reactions. (Fisher, Hershberger, Gabbard)

The feasibility of using ^{81}Br as a detector of the solar neutrino flux has made the measurement of the $^{81}Br(p,n)$ strength function important. Preliminary measurements to determine the population of various levels in ^{81}Kr have been made using the TOF method and targets of natural NaBr on aluminum backings. Other compounds such as KBr are also being studied for use as targets. Further TOF measurements with separated isotopes will be made in the coming year.

3. Neutron Scattering from Os Isotopes at 60 keV and Re-Os Nucleochronology. (Hershberger, Macklin*, Balakrishnan, Hill*, and McEllistrem).

Neutron elastic and inelastic scattering cross sections have been measured for 60.5 keV neutrons incident on $^{187,188}Os$. For ^{187}Os the elastic scattering cross section is 11 barns and the inelastic scattering cross section to the 9.75 keV level is 1.13 barns. These and other scattering measurements allow prediction of neutron capture by Os isotopes, including capture from the 9.75 keV excited level of ^{187}Os. Also predicted are other neutron induced reaction rates. Capture rates thus provided and used in the Re-Os nucleochronology lead to a long galactic age, 18 to 20 Gyr. (Published in Phys. Rev. C28, 2249 (1983)).

4. Neutron Scattering from ^{189}Os. (Hershberger, Macklin*, Winters**, and McEllistrem).

Neutron elastic and inelastic scattering from the 36.2 keV excited level of ^{189}Os will be studied for several neutron energies in the range from 60 keV up to several hundred keV, to follow the energy dependence of inelastic scattering and measure the properties of scattering from the odd-A Os isotopes. The second excited 36.2 keV level of ^{189}Os and the ground level are the inverted doublet from the same pair of nucleon configurations in ^{187}Os. Thus our interpretation of neutron induced cross sections for neutrons incident on the excited state of ^{187}Os will be reinforced by the successful interpretation of scattering from both ^{187}Os and ^{189}Os in a single analysis framework. The first excited level of ^{189}Os at 30.8 keV is a high spin level which will not be appreciably excited, and thus will not interfere with the desired measurements.

---

* Oak Ridge National Laboratory.

** Denison University.

A. THE HALF-LIFE AND ABSOLUTE GAMMA RAY INTENSITIES OF ^{157}ER

(K.E. Gregorich, K.J. Moody, P. Juergens, D. Lee, and G.T. Seaborg)

A source of ^{157}Er was produced by the electron capture/positron decay of ^{157}Tm ($t_{1/2}$ = 3.3 m) made in the ^{141}Pr(^{20}Ne,4n) ^{157}Tm reaction at the 88-Inch Cyclotron. The target, which was made by a molecular plating procedure,[1] consists of a 0.55 mg/cm^2 layer of Pr as Pr_2O_3 on a 4.6 mg/cm^2 Be backing foil. The bombardment was carried out in the Actinide Recoil Target System[2] and the recoiling reaction products were caught in a 7 mg/cm^2 gold foil. After the bombardment, Er was chemically separated from Ho and other daughter products using an ammonium α-hydroxyisobutyrate cation column procedure.[3]

The gamma rays of the Er and its daughters were measured with a 40 cm^3 Ge(Li) detector coupled with a 4096 channel analyzer. This system had a full width at half maximum resolution of 2.0 keV for the 1332 keV ^{60}Co peak. The energy and efficiency calibration of the detector system were measured with a standard mixed gamma ray calibration source. Spectra were collected over a period of several days.

The decay curves for 15 of the most intense gamma rays of the ^{157}Ho daughter ($t_{1/2}$ = 12.6 m)[4] were given error-weighted least squares fits for growth and decay. From these fits, an approximate half-life for the ^{157}Er parent was found. From the ratio of parent to daughter activities in these fits, a time of chemical separation of Er from Ho was determined. Another round of least squares fits was carried out on the same Ho lines with the ^{157}Ho daughter activity fixed at 0 at the time of chemical separation. These fits were used to determine the half-life of the ^{157}Er parent to be 18.65±0.04 m. Taking other systematic errors into consideration, we have determined that a more reasonable value for this half-life is 18.65±0.10 m. This value is significantly different from the published value of 24^{+2}_{-4} m.[5]

Many gamma rays in the sample decayed with this half-life. The 18.65 m half-life for ^{157}Er is essentially identical to the half-life for ^{156}Er given as 19±1 m.[6] No gamma rays for ^{156}Er are known above 56 keV.[6] This prompted us to measure the excitation functions of these 18.65 m gamma rays to determine if they were due to the decay of ^{156}Er or ^{157}Er. The relative intensities of the 391.6 keV gamma ray[7] remained constant at three different bombarding energies, indicating that all the gamma rays were due to the decay of ^{157}Er.

The absolute intensity of the 326 keV gamma ray of the ^{157}Dy granddaughter of ^{157}Er is known to within 2%. The absolute intensities of the ^{157}Er gamma rays were therefore found by following the decay of the ^{157}Dy granddaughter to determine the number of mass 157 atoms in the sample at the time of chemical separation. The absolute intensity of the 391.6 keV gamma ray has been determined to be 14.2±1.0% and the relative intensities of the ^{157}Er gamma rays are given in Table I.

TABLE I

The relative intensities of the gamma rays accompanying the decay of ^{157}Er. The absolute intensity of the 391.6 keV line is 14.2±1.0%. The energy uncertainties are 0.2 kev for E < 1000 keV and 0.4 kev for E > 1000 keV.

ENERGY (keV)	REL. INT. (%)	UNCERTAINTY
66.8	–	–
121.0	56.	3.
179.6	8.0	0.4
303.8	9.8	0.5
347.8	11.3	0.6
391.6	100.	4.
431.1	5.8	0.3
503.2	9.8	0.5
527.5	5.4	0.3
549.4	19.9	0.9
574.1	3.4	0.2
584.2	5.9	0.4
611.4	5.0	0.3
641.0	2.0	0.2
652.5	3.2	0.2
673.2	3.3	0.3
722.2	3.8	0.4
747.5	3.5	0.3
786.0	2.6	0.3
792.0	3.6	0.3
807.5	2.4	0.3
1115.3	1.7	0.3
1242.6	3.9	0.3
1422.4	7.2	0.5

References

1. D.C. Aumann, G. Mullen, NIM **115**, 75-81 (1974); G. Mullen, D.G. Aumann, NIM **128**, 425-428 (1975).
2. R.M. McFarland: Ph.D. thesis, LBL 15027 (1982).
3. K.E. Gregorich, K.J. Moody, G.T. Seaborg, to be published.
4. J.P. Torres *et al.*, Nuc. Phys. A **185**, 574 (1972).
5. Zh. T. Zhelev *et al.*, Sov. J. Nuc. Phys. **2**, 956 (1965).
6. A.A. Aleksandrov *et al.*, Bull. Acad. Sci. USSR Phys. Ser. **39**, 1661 (1975).
7. V. Andrejchev *et al.*, INIS Microfiche 4388.

B. ISOTOPES PROJECT

(J.M. Dairiki, E. Browne, R.B. Firestone, C.M. Lederer, V.S. Shirley)

The Isotopes Project compiles and evaluates nuclear structure and decay data and disseminates these data to the scientific community. The group coordinates its evaluation efforts with those of other data centers via national and international nuclear data networks and is currently responsible for the evaluation of mass chains A = 167–194. All evaluated data are entered into the international Evaluated Nuclear Structure Data File (ENSDF) and are published in *Nuclear Data Sheets*. In addition to the evaluation effort, the Isotopes Project is responsible for production of the *Radioactivity Handbook*.

During the past year the evaluations of nuclear structure data for all nuclides with masses A = 169, 187 and 190 were published in *Nuclear Data Sheets*. Evaluations of A=192, A=174 and A=181 have been submitted for review; an updated evaluation of mass 171 is nearing completion.

Much of the group's effort has been directed toward production of the *Radioactivity Handbook*, a publication intended for applied users of nuclear data. The *Handbook* will provide a compilation of recommended decay data taken from the current version of ENSDF, with no further updating.

The mechanisms (computer codes) to facilitate the *Handbook* production are now largely in place. ENSDF data are restructured and pointers added to create a file (ENSDF database) that can be accessed with the commercially available DEC database management system DATATRIEVE. Data are subjected to both format and scientific checking programs; evaluator input is required to correct the deficiencies, inconsistencies, and errors detected. Another code, GAMUT, provides "best" values for γ-ray energies and intensities independent of the decay parent. Additional calculations are performed to provide recommended data on atomic radiations and conversion and Auger electrons.

Future efforts will focus on the tabular output formats and on the processing of mass-chain data from the ENSDF file. At the present time, 64 mass chains (A = 200–263) have been incorporated into the ENSDF database; the remaining mass chains will be entered by April 1984. Final tabular output will be produced using UNIX text formatting codes and a phototypesetter; skeleton scheme drawings will be produced manually. Plans call for submitting the completed manuscript to the publisher by the end of 1984.

The group has presented a proposal for production of a complementary volume - the *Nuclear Structure Handbook* - to the NAS/NRC Panel on Basic Nuclear Data Compilations which advises DOE. This handbook is intended to address the needs of the basic nuclear physics community for a compilation of nuclear structure data. Recommended data will be taken from the ENSDF file and the production mechanisms already developed for the *Radioactivity Handbook* can be used directly for the *Nuclear Structure Handbook*. Plans for this publication will be finalized in 1985.

Continued development and improvement of the ENSDF file and evaluation procedures are of critical importance in achieving a four-year evaluation cycle. Many of the codes and procedures developed for production of the *Radioactivity Handbook* can also be used as tools to increase the efficiency of the evaluation process. For example, the code SPINOZA is a valuable physics checking program; it is especially useful in deriving spin/parity assignments for complicated level schemes. The code GAMUT presents the network with a uniform, statistical process for deriving adopted γ-ray energies and intensities.

One of the goals of the U.S. Nuclear Data Network is to make ENSDF data available to remote users by on-line retrieval. A procedure has been implemented at LBL to allow access to the LBL Nuclear Structure Numerical Database which currently contains ENSDF data for mass chains A = 200–263. During 1984 ENSDF data for all other mass chains will be implemented in the database; these data can be accessed by telephone lines or via DECNET and MILNET.

In response to a request from the NAS Panel at its 1982 meeting, the Isotopes Project has designed a form to solicit author input for the preparation of nuclear-structure keyword abstracts. The check-list/matrix form style resulted from consideration of the prime criteria: author cooperation, completeness and uniformity of keywords, and efficiency of keyword preparation. A complete summary report was submitted to the Panel.

The seventh edition of the *Table of Isotopes* (published in 1978) continues to be the most up-to-date general reference source available for nuclear structure and decay data. Sales through April 1983 total 7844 copies (3708 clothbound and 4136 paperback). Nearly all 7000 copies of the *Nuclear Wallet Cards*, produced in 1979 by the Isotopes Project on behalf of the US. Nuclear Data Network, have been distributed to the user community.

Promoting the science of data evaluation and providing assistance to the user community are both important aspects of the Project's role. Project members organized the very successful First Annual Conference on Nuclear Structure Data Evaluation, held at Asilomar October 27–30, 1981. In addition to answering specific data requests, the Isotopes Project encourages general use of its extensive library, which contains comprehensive data files and major nuclear physics journals.

C. GAMUT, A COMPUTER CODE FOR STATISTICAL ANALYSIS OF γ-RAY DATA

(R.B. Firestone and E. Browne)

GAMUT was written to derive an adopted set of γ-ray energies and intensities from ENSDF decay and/or reaction datasets.[1] Adopted properties, independent of decay parent, are not yet contained uniformly in ENSDF but will be presented in the *Radioactivity Handbook*.

Input data to the computer code GAMUT can be supplied with three formats: via a DATATRIEVE (DEC database management system) procedure from the ENSDF database at LBL, with a special tabular input format, and in a modified ENSDF format. The latter two formats allow an evaluator to include multiple experimental values for each decay mode. GAMUT performs a least-squares fit of experimental γ-ray energies to the associated levels using the following relationship

$$E_{ki} = E_R - E_i + c$$

where E_{ki} is the γ-ray energy, and E_R and E_i are the energies of the initial and final levels, respectively. The parameter c adjusts the zero energy for each dataset. Adopted γ-ray energies are then calculated from the above equation using the fitted values of the parameters. Statistical uncertainties are corrected for the corresponding covariances. The uncertainty in the parameter c represents the systematic error consistent with the data. GAMUT adjusts the input data by an iterative chi-square analysis to obtain a new set of energies. First, the experimental uncertainties of the extreme outlying values are increased to improve the fit until a chi-square of 1.0 is achieved. Then the γ-ray energies are recalculated. The errors in the entire dataset are increased by the same factor if the new γ-ray energies still deviate significantly (chi-square > 1) from the input values. Otherwise, only those energies which lie outside a 99.5 percent confidence level are readjusted. This procedure continues until no more changes are required.

Gamma-ray intensities are averaged by a method similar to those described by Tepel[2] and Lederer[3]. For each level the γ-ray intensities are renormalized to a common scale by an iterative linear regression. Deviations from a weighted average intensity are minimized on each iteration until the process converges for all levels. These final weighted average values represent the best relative γ-ray branchings from each level. Relative intensities for each decay mode are obtained by converting the data to the original decay set scale. Statistical uncertainties are corrected for the covariances, and a chi-square analysis is performed to obtain the adopted values. The program may be run interactively and uncertainties in both γ-ray energies and intensities altered by the user during execution.

Footnotes and References

1. "Evaluated Nuclear Structure Data File", edited and maintained by the National Nuclear Data Center, Brookhaven National Laboratory, on behalf of the International Network for Nuclear Structure Data Evaluation.
2. J.W. Tepel in the summary report of the IAEA Advisory Group Meeting on Nuclear Structure and Decay Data, IAEA Report INDC(NDS)-115/NE (1980), p. 121.
3. C.M. Lederer, NDN Memorandum of 13 April, 1982.

D. BETA-DELAYED PROTON EMISSION OBSERVED IN NEW LANTHANIDE ISOTOPES

(J.M. Nitschke, W.-D. Zeitz,* P.A. Wilmarth, P.K. Lemmertz, J. A. Honkanen†)

We previously reported the discovery of several new beta-delayed proton emitters in the lanthanide region. The masses of these new isotopes were uniquely determined by the on-line isotope separator OASIS[1] and the Z-values were inferred from half-lives, mass-energy systematics and cross sections. A major addition to OASIS now allows us to obtain unique Z-identifications of new isotopes by observing characteristic x rays in coincidence with beta-delayed protons. The experimental procedure is as follows: the isotope under study is passed through a slit in the focal plane of the isotope separator and transported via ionoptical devices to a low background spectroscopy laboratory. Here the isotope is deposited on a fast-cycling tape and moved within 65 ms to an array of detectors which register protons, α- and β-particles, x rays and γ-rays. For neutron deficient isotopes two classes of events are of interest: (1) protons (or alphas) in coincidence with positrons, γ's, and x rays, and (2) positrons and x rays in coincidence with γ's.

This report covers only events of the first category. The second class of events yields information about members of the isobaric chain which are closer to the valley of beta stability and decay by positron emission, electron capture and γ-decay.

Mass chains A=139, 137, and 127 were investigated before the completion of the OASIS tape system. Only a dual proton telescope was used to measure half-lives and proton energy spectra. The reaction parameters and the principal results are shown in Table I. The Z-identification of the isotopes is based on a comparison between the observed and predicted values of three parameters: (1) the half-life calculated from the gross theory of β-decay with Q_{EC} values from the mass table by Liran and Zeldes, (2) the production cross section calculated with the code ALICE, and (3) the predicted ($Q_{EC} - S_p$) value as a function of Z for a known A. The motivation for selecting A=137 and 127 was the prediction[2] that $^{137}Tb_{65}$ and $^{127}Pm_{61}$ should be proton ground state emitters.

No ground state proton emission characterized by sharp proton lines was found, however. In the case of $^{137}Gd_{64}$ a significant discrepancy exists between the measured and the calculated half-life and the possibility that we are observing an isomeric state associated with the odd-A, N=73 configuration cannot be excluded. Cross bombardments with $^{92}Mo_{42} + {}^{54}Fe_{26}$ in the case of $^{139}Gd_{64}$ and $^{40}Ca_{20} + {}^{90}Zr_{40}$ in the case of $^{127}Nd_{60}$ were carried out to substantiate the respective Z-assignments.

For mass chain A=119 only the known beta-delayed proton precursor ^{119}Ba was observed with certainty. Its yield from the $^{58}Ni(^{64}Zn, 2pn)$ reaction was so overwhelming that a possible small proton branch from ^{119}La could not be detected.

Footnotes and References

*Present address: Hahn Meitner Institut für Kernforschung, Berlin, West Germany.
†Present address: Department of Physics, University of Jyväskylä, Finland.

1. J.M. Nitschke, Nucl. Inst. and Meth. **206**, 341 (1983).
2. J.M. Nitschke, M.D. Cable, and W.-D. Zeitz, Z. Phys. A **312**, 265 (1983).

E. DISCOVERY OF BETA-DELAYED TWO-PROTON RADIOACTIVITY: ^{22}AL*

(M.D. Cable, J. Honkanen,† R.F. Parry, S.H. Zhou,‡ Z.Y. Zhou,§ and J. Cerny)

Two-proton radioactivity has long been proposed (see the review by Gol'danskii[1]) as a potential mode of radioactive decay for some nuclei far from the valley of beta stability. More recently, Gol'danskii has also discussed beta-delayed two-proton radioactivity[2] and has suggested some potential candidates for this decay mode, among them light mass nuclides in the odd-odd, $T_z = -2$ series. The recent discovery[3] of the first known member of this series, ^{22}Al, and the subsequent observation of an additional member, ^{26}P, made these two nuclei prime candidates for a search for this new mode of decay. We would like to report here the discovery of beta-delayed two-proton emission from ^{22}Al. ^{22}Al is an ideal case for investigation since earlier work on its decay[3] by beta-delayed single-proton emission accurately located the T=2 analog state in its ^{22}Mg daughter (fed by the superallowed branch in ^{22}Al beta-decay), concomitantly showing that this state is unbound to two-proton emission by 6.118 MeV.

^{22}Al($t_{1/2}$ ~ 70 ms) was produced via the ^{24}Mg(^{3}He,p4n)^{22}Al reaction with 110 MeV $^3He^{+2}$ beams of 3–7 μA intensities from the 88-Inch Cyclotron. A helium jet system was used to transport the activity to a counting chamber with a high geometry, three element particle telescope (with detectors denoted "ΔE1", "ΔE2", and "E") capable of identifying and observing two protons simultaneously. The "ΔE1" (24 μm) and "ΔE2" (155 μm) detectors were fabricated such that the surface contact on one side was divided down the center, effectively producing two detectors on the same silicon wafer.

The two-dimensional, proton-proton coincidence spectrum obtained following a 690 mC bombardment is shown in Fig. 1(a); the summed proton energy spectrum appears in Fig. 1(b). Laboratory energies of the two-proton total energy peaks shown in Fig. 1(b) are 4.139±0.020 MeV and 5.636±0.020 MeV. Exact corresponding center-of-mass energies depend on the mechanism of two-proton emission; however, these peaks can be shown to correspond to transitions from the ^{22}Mg T = 2 analog state (fed by the superallowed beta decay of ^{22}Al) to the ground state and first excited state of ^{20}Ne (see Fig. 2).

Two possible decay mechanisms are A) single-step ^{2}He emission[1,2] (two protons coupled to a $^1S_0$ configuration) or B) a sequential two-step process proceeding through an intermediate state (or states) in ^{21}Na. Given the currently limited statistics, the proton-proton coincidence spectrum shown in Fig. 1(a) cannot conclusively distinguish the mechanism; the observed variation in yields and energies could result from either a ^{2}He type distribution or sequential decay through several states in ^{21}Na or both. Work is in progress to determine the two-proton decay mechanism(s) of ^{22}Al.

Footnotes and References

*Condensed from LBL-15453, Phys. Rev. Lett. **50**, 404 (1983).

†On leave from: Dept. of Physics, University of Jyväskylä, Finland.
‡On leave from: Institute of Atomic Energy, Beijing, China.
§On leave from: Dept. of Physics, Nanking University, China.

1. V.I. Gol'danskii, Usp. Fiz. Nauk **87**, 255 (1965); Sov. Phys. Uspekhi **8**, 770 (1966).
2. V.I. Gol'danskii, Pisma Zh. Eksp. Teor. Fiz **32**, 572 (1980); JETP Lett. **32**, 554 (1980).
3. M.D. Cable, J. Honkanen, R.F. Parry, H.M. Thierens, J.M. Wouters, Z.Y. Zhou, and J. Cerny, Phys. Rev. **C26**, 1778 (1982).

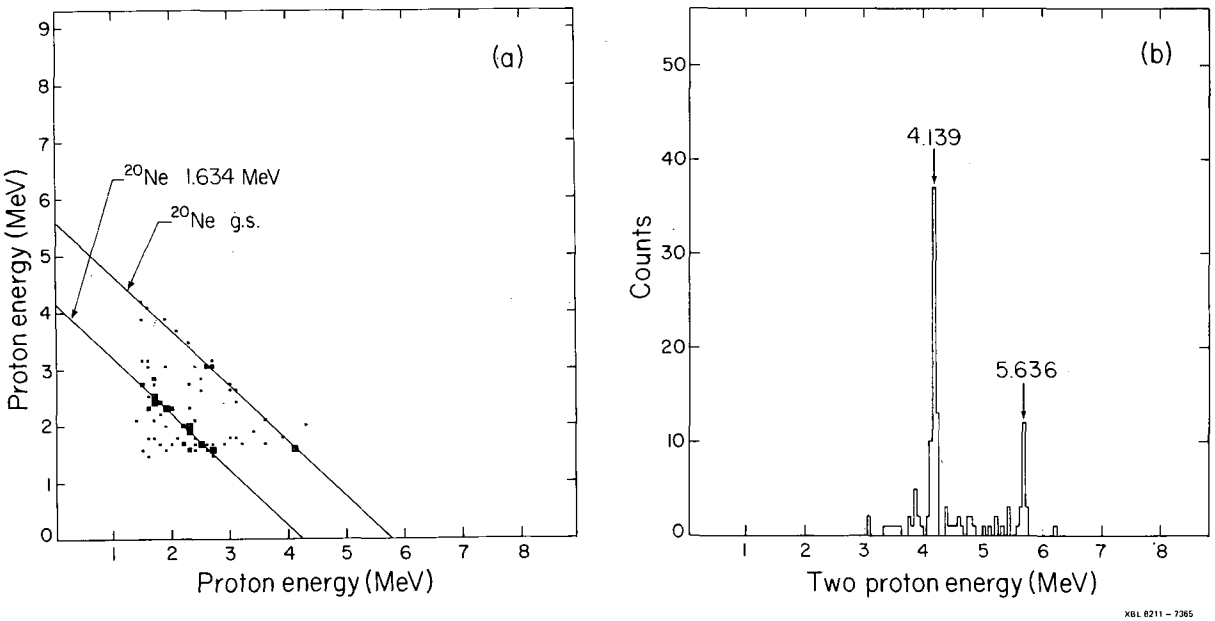

Fig. 1. (a): A proton-proton coincidence spectrum following the beta decay of ^{22}Al (E_p^L vs. E_p^R). Kinematic lines corresponding to decay to the ground state and to the first excited state of ^{20}Ne are shown. Increasing square size corresponds to increasing number of counts. (b): A summed energy spectrum for the two-proton coincidences in (a):($E_p^L + E_p^R$).

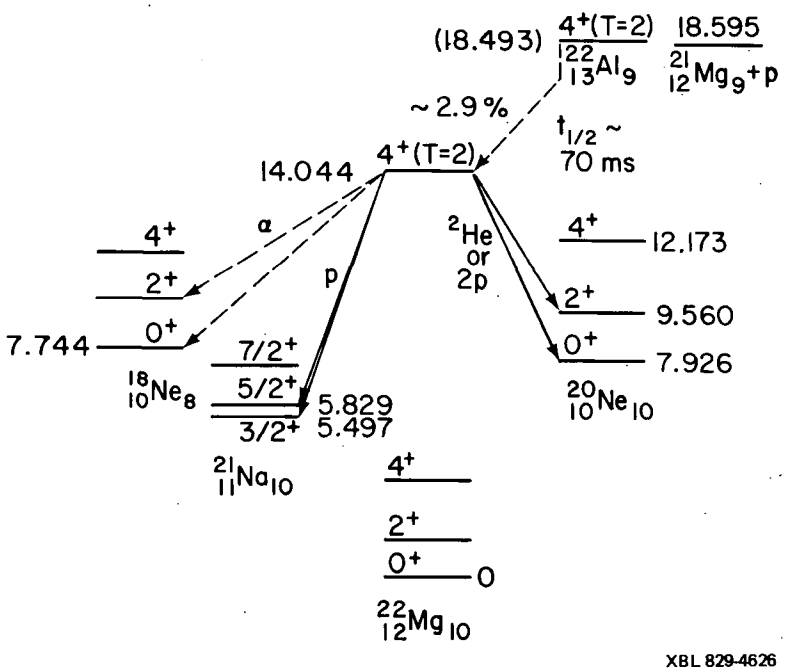

Fig. 2 Proposed partial decay scheme for ^{22}Al.

F. BETA-DELAYED TWO-PROTON DECAY OF ^{26}P*

(J. Honkanen,† M.D. Cable, R.F. Parry, S.H. Zhou,‡ Z.Y. Zhou,§ and J. Cerny)

Beta-delayed emission of two protons has recently been observed for the first time[1] in the decay of ^{22}Al. Observation[2] of beta-delayed single proton emission from another odd-odd $T_z = -2$ nucleus, ^{26}P, showed this nucleus to exist and, furthermore, indicated that the analog state in ^{26}Si is unbound to two-proton emission by 5291 keV. We would like to report here the observation of beta-delayed two-proton emission from ^{26}P. As opposed to the complex beta-delayed two-proton emission of ^{22}Al, the ^{26}P decay proceeds by a relatively simple mechanism and, as such, is well characterized by the experiments described below.

^{26}P ($t_{1/2} \sim 20$ ms) was produced via the ^{28}Si(^{3}He,p4n)^{26}P reaction by bombarding a natural silicon target with 110 MeV ^{3}He beams from the 88-Inch Cyclotron. A helium-jet system was used to transport the recoil atoms through a 70 cm long capillary into a measuring chamber where a specially constructed three element (14 μm ΔE1, 170 μm ΔE2, and 500 μm E) solid state particle telescope was used to observe beta-delayed protons. The ΔE detectors were fabricated such that the surface contact on one side was divided down the center, effectively providing two, two-element (ΔE1 and ΔE2) telescopes capable of detecting low-energy (1.0–4.5 MeV) protons in coincidence. The average angle between these telescopes was 40° with each side subtending 4.5% of 4π sr.

Fig. 1 is a summed energy spectrum of the coincident protons observed in the "left" and "right" low energy telescopes with a 20ns coincidence window. In addition to two-proton groups of ^{22}Al, which were also produced in this bombardment, a new group of 4.914 MeV was observed. This has been assigned to the decay from the ^{26}Si T = 2 analog state (fed by superallowed beta decay of ^{26}P) to the ground state of ^{24}Mg. An arrow at low energy indicates the expected location of the two-proton group corresponding to decay to the ^{24}Mg first excited state.

Possible decay mechanisms for the emission of the two protons can be categorized as sequential or simultaneous emission. Sequential emission is a two-step process in which a proton is emitted to a level in an intermediate nucleus, which is unbound to subsequent emission of a second proton; therefore, the individual proton spectra should show specific proton groups corresponding to these transitions. The individual proton spectra which comprise the 4.914 MeV two-proton group are relatively simple spectra with coincident groups at laboratory energies of 3699±15 keV and 1210±15 keV, indicating a sequential decay through a single intermediate state. Because the emission of the first proton causes a kinematic shift to the laboratory energy of the second proton (since the second proton is emitted from a recoiling nucleus), it is possible to determine the order of the decay by measuring the proton spectra at two different angles. Results of a second experiment performed with two separate telescopes (23 μm ΔE1, 270 μm ΔE2, 1000 μm E) mounted at 120° and each subtending 3.5% of 4π sr show a kinematic shift for the 1.2 MeV individual proton group, which indicates that this group corresponds to the second proton in the sequential process. Thus the intermediate state in ^{25}Al would lie at 3714±21 keV excitation and might correspond to the known $\frac{7}{2}-$ level at 3695.7±0.5 keV. The proposed decay scheme for ^{26}P two-proton emission is shown in Fig. 2.

Further experimentation is of interest to obtain information about the angular correlation of the two protons and to attempt to observe the decay to the ^{24}Mg first excited state. For this decay, ^{2}He emission is allowed and so might contribute. Comparison of the results of the relatively simple ^{26}P decay to the more complex spectra obtained from ^{22}Al decay is also proceeding.

Footnotes and References

*Condensed from LBL-16606, Phys. Lett. in press.
†On leave from: Dept. of Physics, University of Jyväskylä, Finland.
‡Present address: Institute of Atomic Energy, Beijing, China.
§On leave from: Dept. of Physics, Nanking University, China.

1. M.D. Cable, J. Honkanen, R.F. Parry, S.H. Zhou, Z.Y. Zhou and J. Cerny, Phys. Rev. Lett. **50**, 404 (1983).
2. M.D. Cable, J. Honkanen, R.F. Parry, S.H. Zhou. Z.Y. Zhou and J. Cerny, Phys. Lett. **123B**, 25 (1983).

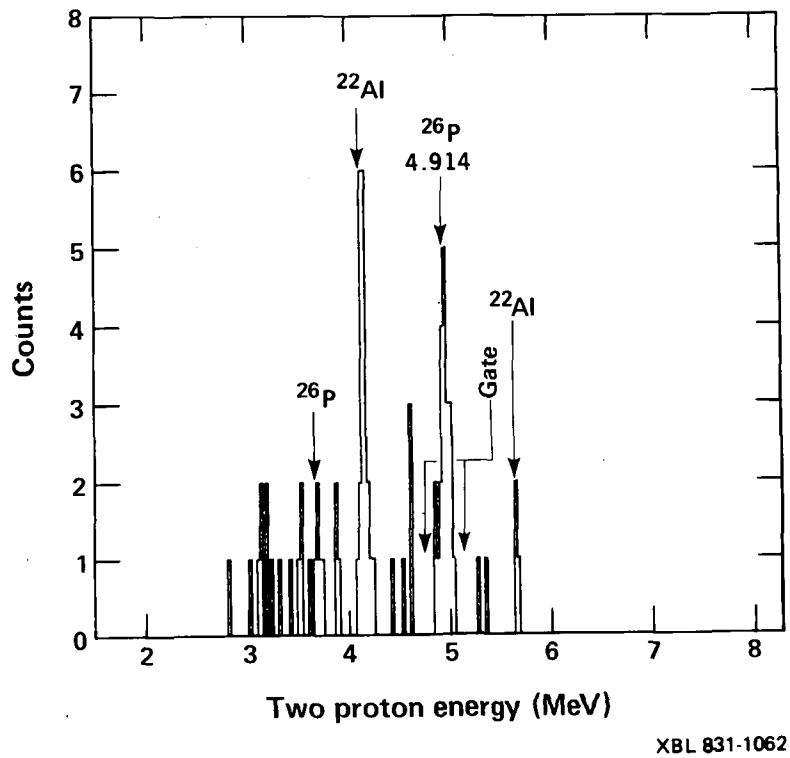

Fig. 1. A summed energy spectrum for two-proton coincidences arising from 110 MeV ^{3}He bombardment of ^{28}Si. The spectrum is measured with telescopes placed at an average separation angle of 40°.

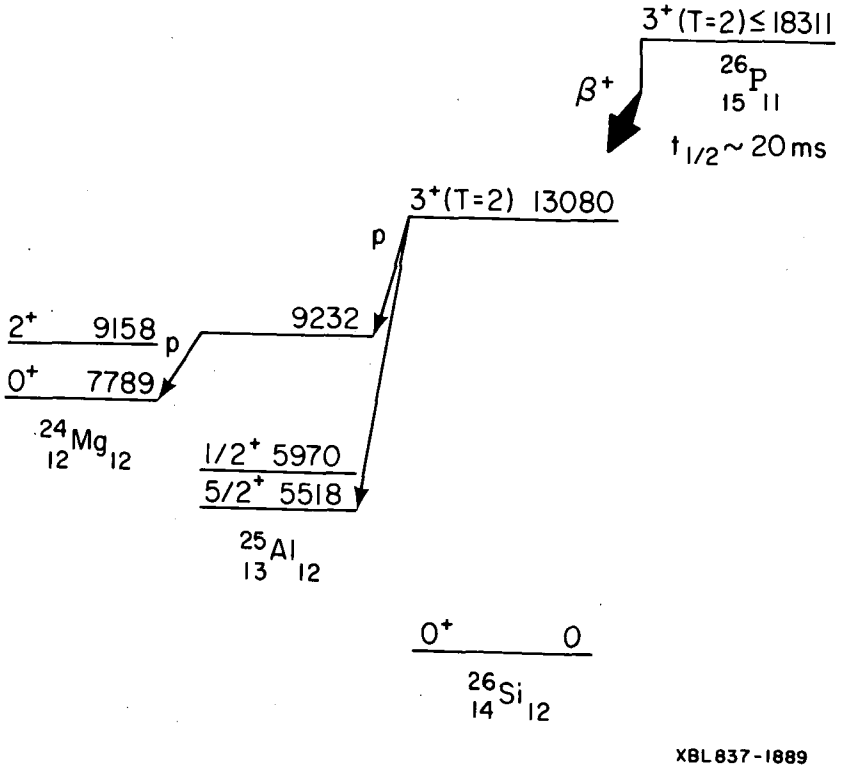

Fig. 2. Proposed decay scheme for the beta-delayed two-proton emission of ^{26}P.

A. NUCLEAR DATA APPLICATIONS-MEASUREMENTS

1. Measurement of the $^{6,7}Li(n,^4He)$ Cross Sections at E_n = 14 MeV (Goldberg, Haight, Kneff*)

Helium production by neutron bombardment of materials is of interest in the design of fusion reactors. Lithium, in various chemical forms, is proposed as a blanket material for nearly all fusion reactors based on the D-T fuel cycle. Further, the tritium breeding reactions on the lithium isotopes are major contributors to the total helium production. Investigation of the helium production may therefore shed light on the tritium production mechanism.

We have measured the helium produced when isotopic samples of lithium are bombarded with 15-MeV neutrons. The neutrons were produced with a rotating target neutron source (RTNS-I). After irradiation the ^4He was determined by isotopic dilution mass spectrometry. Preliminary values of the cross sections are 515 mb for the $^6Li(n,^4He)$ reaction and 334 mb for the $^7Li(n,^4He)$ reaction with uncertainties of about 5%.

2. Neutron Elastic and Inelastic Scattering from Carbon Near 14 MeV (Haight, Hansen, Wong, and Pohl)

Recent measurements[1,2] have suggested that the $^{12}C(n,n'3\alpha)$ reaction cross section and the kerma factor for carbon depend strongly on the incident neutron energy near 14 MeV. Because the total cross section does not vary strongly at these energies, significant variations should be observable in the elastic or the discrete inelastic scattering cross sections as functions of energy.

We have therefore measured the elastic and discrete inelastic cross sections for neutrons on carbon at five energies between 13.5 and 14.6 MeV. Both the angle-integrated cross sections and the shapes of the angular distributions are observed to change with incident neutron energy. Preliminary data indicate a rapid and irregular rise of the $^{12}C(n,n'3\alpha)$ cross section in this energy region.

---

* Rockwell International, Canoga Park, CA 91304.

1 R. C. Haight, S. M. Grimes, R. G. Johnson, and H. H. Barschall, Nuclear Science and Engineering (in press).

2 P. M. DeLuca, Jr., H. H. Barschall, R. C. Haight, and J. C. McDonald (to be published.).

3. Neutron Capture Cross Sections for ^{46}Ca and ^{48}Ca at Stellar Temperatures (Mathews, Käppeler*)

Stellar neutron capture cross sections have been measured for the heavy calcium isotopes by neutron activation using a spectrum of neutrons from the $^{7}Li(p,n)^{7}Be$ reaction which closely approximates a kT = 25 keV Maxwellian distribution. Corrections for geometry and sample scattering were checked by measuring with various sample thicknesses and extrapolating to zero thickness. The preliminary cross sections, normalized to the kT = 25 keV-averaged ENDF-B/V ^{197}Au capture cross section, are 6.4 ± 0.5 mb for ^{46}Ca and 1.9 ± 0.5 mb for ^{48}Ca. The measured cross sections indicate that it is not possible to account for the nucleosynthetic origin of ^{46}Ca and ^{48}Ca in a simple equilibrium neutron capture environment without subsequent selective depletion of ^{46}Ca.

4. Revised Neutron Capture Cross Sections for $^{142,143,144}Nd$ (Mathews, Käppeler*)

The neutron capture cross sections for Nd isotopes we reported in last year's report to the Nuclear Data Committee have been revised after it was discovered that hydrogenation of the samples introduced a significant background correction. The new kT = 30 keV cross sections (averaged over the energy region 6 to 200 keV) are 51 ± 4 mb for ^{142}Nd, 258 ± 11 mb for ^{143}Nd, and 123 ± 6 mb for ^{144}Nd. These cross sections have been fit with a power law to extrapolate to other energies and for applications at other temperatures:

$$\langle\sigma\rangle = 49(E/30)^{-0.664} \qquad ^{142}Nd$$

$$\langle\sigma\rangle = 259(E/30)^{-0.675} \qquad ^{143}Nd$$

$$\langle\sigma\rangle = 118(E/30)^{-0.694} \qquad ^{144}Nd$$

where $\langle\sigma\rangle$ is in mb and E in keV.

The new ^{142}Nd cross section is consistent with other s-process only isotopes, and indicates that there is no peculiarity in the s-process in this region as previously discussed.

5. Fragment Angular Distribution for Neutron Fission of ^{232}Th (Becker, Bauer)

The $^{232}Th(n,f)$ fission fragment angular distributions have been measured for incident energies from 0.7 to 10 MeV using the white source of neutrons produced at the 100-MeV LLNL Electron Linear Accelerator Facility

---

* Kernforschungszentrum Karlsruhe, Institut für Angewandte Kernphysik, Karlsruhe, Federal Republic of Germany.

and a recently developed multi-wire counter to detect the fission fragments. Time-of-flight techniques were used with a resolution of ≈90 ps/m. Thick thorium foils were mounted parallel to the multi-wire planes and at 30 degrees to the neutron beam direction. Fragments from thermal fission of ^{235}U were used as an isotropy reference. The ^{232}Th fragment angular distributions obtained with this arrangement were parameterized by the Legendre polynomial expansion $W(\theta) = 1 + A_2P_2(\cos\theta) + A_4P_4(\cos\theta)$. Resulting coefficients for 40-keV neutron energy bins within the incident neutron energy interval $0.72 \leq E_n(\text{MeV}) \leq 3.04$ are illustrated in Fig. A-1.

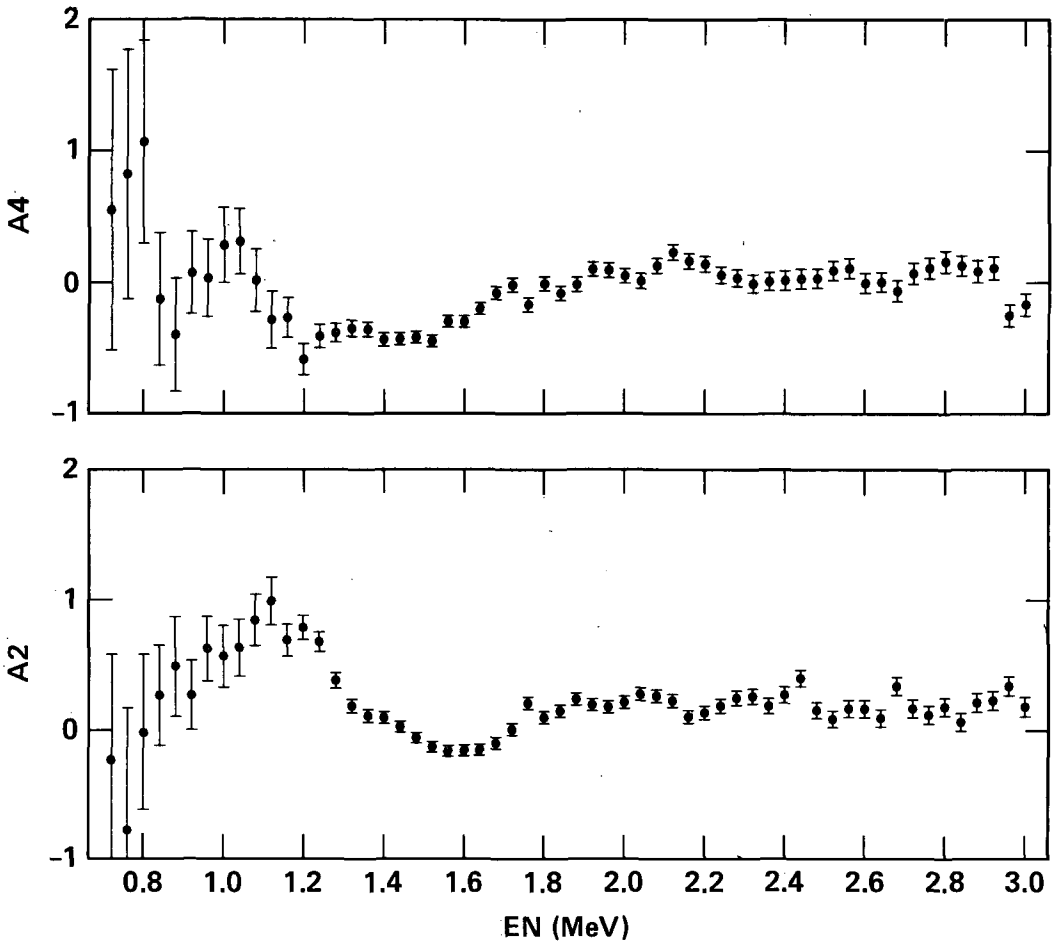

Fig. A-1. Legendre polynomial expansion coefficients for the fission fragment angular distribution produced in the $^{232}Th(n,f)$ reaction. The neutron energy bin width is 40 keV.

6. Neutron Differential Scattering Measurements in the Actinide Region (Hansen, Pohl, Wong, Haight)

Elastic and inelastic (unresolved) differential cross sections have been measured for neutrons scattered from ^{232}Th, ^{238}U and ^{239}Pu

at 14.1 MeV. The measurements cover the angular range from 9.2° to 159°. They are part of a program at LLNL to measure neutron scattering cross sections in the energy region from 14 to 30 MeV. These measurements are of interest to the fusion-fission reactor program and are intended to supply data in a region of the periodic table where differential scattering measurements at energies E > 10 MeV are scarce.

Since these nuclei are characterized by large and permanent quadrupole (β_2) and hexadecapole (β_4) nuclear deformations, the analysis of the data was done using the Tamura coupled-channel (CC) formalism. For ^{232}Th and ^{238}U, the ground state and the low-lying 2^+, 4^+, and 6^+ levels were included in the CC calculations. For ^{239}Pu, in addition to the g.s., the $3/2^+$, $5/2^+$ and $7/2^+$ levels were also included. Very good agreement with the measured angular distributions was obtained using the optical model parameters and deformation parameters β_2, β_4 of Klepatskij et al.[3] Their global set had been optimized for the actinide region in the energy interval 0.1-15 MeV, and in the present calculations no change in these parameters was required to fit the data. Since our measurements do not resolve the elastically scattered neutrons from those inelastically scattered from the low-lying excited levels (E_{ex} < 200 keV), the data were compared with the sum of the calculated differential cross sections for the g.s. and inelastic levels included in the CC calculations. It is interesting to note that although the sum of the integrated inelastic cross sections is less than 10% of the total elastic cross section, the calculated inelastic differential cross sections are comparable to the elastic differential cross sections beyond 80°. We find good agreement between the calculations and measurements for the elastic-plus-inelastic angular distributions.

7. Nuclear Structure of ^{244}Am Investigated with the (n,γ)Reaction (von Egidy,* Hoff, Lougheed, White, Börner,** Schreckenbach,** Warner,** Barreau,** and Hungerford*)

Secondary gamma rays and conversion electrons following the ^{243}Am(n,γ)^{244}Am reaction have been studied with crystal spectrometers and an electron spectrometer, respectively, at the Institut Laue-Langevin at Grenoble. Primary gamma rays following thermal neutron capture in ^{243}Am have also been measured. A level scheme for ^{244}Am has been constructed containing 67 excited levels. The levels are interpreted in terms of coupled proton and neutron Nilsson configurations. The results are found to be in good agreement with a semiempirical model in which excitation energies in odd-odd nuclei are calculated from those in adjacent nuclei (see Table A-1).

---

* Physik-Department, Technische Universität München, 8046 Garching, West Germany.

** Institut Laue-Langevin, 38042 Grenoble, France.

[3] A. B. Klepatskij, V. A. Kon'shin, and E. Sh. Sukhovitskij, INDC (CCP)-161/L, 9 (1981).

TABLE A-1. Comparison of experimental and predicted band head energies and rotational parameters for ^{244}Am.

Configuration	Band head energy (keV) E(model)	E(exp.)	Rotational parameter A (keV) A(model)	A(exp.)
$1^+\{5/2^+1642\uparrow\mid - 7/2^+1624\downarrow\mid\}$	60	85	3.0	3.4
$1^-\{5/2^-1523\downarrow\mid - 7/2^+1624\downarrow\mid\}$	161	173	5.4	5.3
$2^-\{3/2^-1521\uparrow\mid - 7/2^+1624\downarrow\mid\}$	235	259	5.8	5.8
$0^-\{5/2^-1523\downarrow\mid - 5/2^+1622\uparrow\mid\}$	319 (1^-)	286 (1^-)	5.4	5.3
$3^+\{1/2^+1400\uparrow\mid - 7/2^+1624\downarrow\mid\}$	(336)	345	(5.4)	5.2
$0^+\{7/2^+1633\uparrow\mid - 7/2^+1624\downarrow\mid\}$	362	374	6.9	(6.0)
$2^+\{5/2^+1642\uparrow\mid - 1/2^+1631\downarrow\mid\}$	451	(416)	3.1	(2.7)
$2^+\{5/2^-1523\downarrow\mid - 9/2^-1734\uparrow\mid\}$	426	417	4.2	4.1
$3^-\{5/2^-1523\downarrow\mid + 1/2^+1631\downarrow\mid\}$	442	418	5.7	5.6
$0^+\{5/2^+1642\uparrow\mid - 5/2^+1622\uparrow\mid\}$	463 (2^+)	(475) (2^+)	3.0	--
$2^-\{5/2^-1523\downarrow\mid - 1/2^+1631\downarrow\mid\}$	488	482	5.7	6.6
$2^-\{5/2^+1642\uparrow\mid - 9/2^-1734\uparrow\mid\}$	538	514	2.6	3.2
$2^+\{3/2^+1651\uparrow\mid - 7/2^+1624\downarrow\mid\}$	(395)	612	(6.2)	5.8
$1^+\{5/2^-1523\downarrow\mid - 7/2^-1743\uparrow\mid\}$	665	(668)		--
$1^-\{3/2^-1521\uparrow\mid - 5/2^+1622\uparrow\mid\}$	586		5.7	
	}	678	}	5.1
$1^-\{5/2^+1642\uparrow\mid - 7/2^-1743\uparrow\mid\}$	826		3.1	
Average deviations:	±19 (for 9 bands)		±7% (for 8 bands)	

8. Determination of the Conversion Coefficients of the M4 Transition in ^{193m}Ir (Gunnink, Lindner, Nagle, and Sisson)

An essentially massless source of ^{193m}Ir, free of radioactive contaminants except for a small amount of ^{192}Ir, was produced by thermal-neutron irradiation of ^{192}Os. The osmium was exhaustively removed and a carrier-free iridium fraction isolated. From this, sources were prepared for 4π β counting, for low-energy photon detection, and for conversion-electron energy and intensity determinations.

Absolute e^-/γ ratios were determined for the K-through-O shells. Because electron energies were determined with a windowless silicon diode, resolution could not equal that of a magnetic β spectrometer. We relied instead on the use of the GRPANL computer program[4] and the good statistics of the large number of accumulated events for the analysis of our data. The measured ratios, as well as those calculated by Rösel, et al.[5] are given in Table A-2.

TABLE A-2. ^{193m}Ir conversion coefficients.

Subshell	α(obs) x 10^{-2}	α(calc)[a] x 10^{-2}
K[b]	1.04 (-)[c]	1.03
L1	27.4 (3.0)	27.7
L2	5.5 (3.3)	4.9
L3	113.0 (3.0)	118.0
M1 (+ 1/2M2)	10.5 (3.3)	10.1
M3 (+1/2M2)	37.5 (3.1)	39.5
M4 + M5	3.1 (4.9)	3.4
N	13.4 (3.2)	14.0
O	1.9 (4.2)	2.2

a Interpolated from tables of Ref. 5.
b From K x-ray data only.
c Values in parentheses are estimated % standard deviations.

4 R. Gunnink and W. D. Ruhter, Lawrence Livermore National Laboratory, Livermore, CA, UCRL-52917 (1980).

5 F. Rösel, H. M. Fries, K. Alder, and H. C. Pauli, At. Dat. & Nucl. Data Tables, 21, Nos. 4 & 5, 292 (1978).

Most of the tabulated uncertainty resulted from the statistics of the measured 80.22 (± 0.02) keV unconverted γ transition. The discrepancy for the L2 coefficient appears to be real.

Because of the sample purity, we were able to follow the decay through many half-lives. We found a value of 10.53 ± 0.04d, in good agreement with the value reported by Bayhurst, et al.[6]

9. Study of the Gamma-Ray and Conversion-Electron Decay of the ^{238}U Shape Isomer (Kantele,* Stöffl, Ussery,** Decman, Henry, Estep, Hoff, Struble, and Mann)

We have measured both the gamma-ray and conversion-electron transitions that follow the decay of the 200-ns ^{238}U shape isomer, the only fissioning shape isomer known to decay by these modes. The reaction used to populate the shape isomer was the ^{238}U (d,pn) reaction at a deuteron energy of 18 MeV. We observed for the first time an EO conversion-electron transition following the decay of the isomeric state (see Fig. A-2). This EO transition established experimentally that the ^{238}U shape isomer has a spin and parity of 0^+. The production cross section of the 2512.7-keV E2 transition was determined to be 42 ± 12 μb. This cross section is less than half the only previous measurement of 90 ± 23 μb by Russo et al.[7] On the basis of the energy difference between the isomer energy, as determined by the E2 gamma ray into the 44.9-keV first-excited state and the EO conversion-electron energies, the binding energy of the K-electrons is found to be 115.2 ± 2.1 keV. The binding energy of K-electrons in U is 115.6 keV, giving further confidence to assigning the observed transitions to ^{238}U. The total production cross section of the shape isomer is approximately 120 μb obtained by summing the cross sections of all decay branches, including unobserved gamma rays. Percent decay branches are shown in Fig. A-2. Because the production cross section of the ^{238}U ground state by the (d,pn) reaction is 150 to 250 mb,[7] an isomer ratio of 2 to 12 x 10^{-4} is obtained.

---

* University of Jyväskylä, Finland.

** Florida State University, Tallahassee, FL 32306.

6 B. P. Bayhurst, J. S. Gilmore, R. J. Prestwood, J. B. Wilhelmy, N. Jarmie, B. H. Erkila, and R. A. Hardekopf, Phys. Rev., C 12, 451 (1975).

7 P. A. Russo, J. Pedersen, and R. Vanderbosch, Nucl. Phys. A240, 13 (1975).

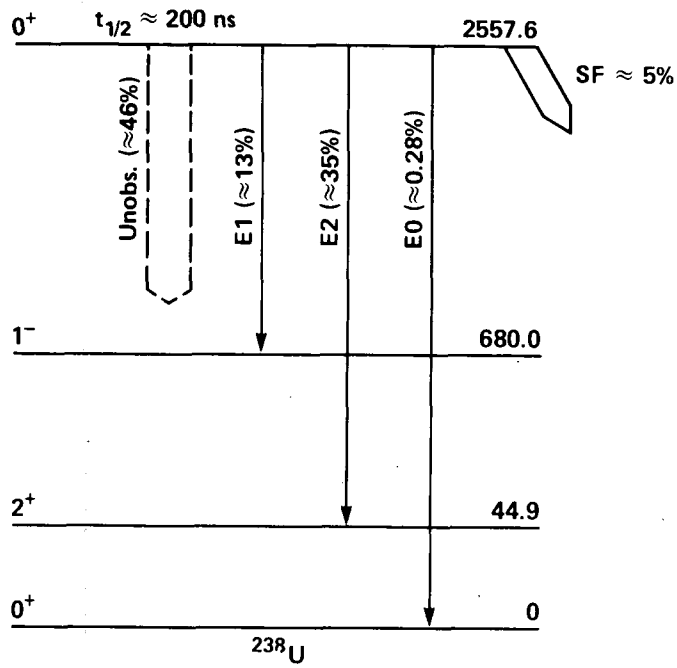

Fig. A-2. Decay scheme for ^{238}U-shape isomer.

10. Levels of ^{244}Cm Populated by the Beta Decay of 10-Hour ^{244g}Am and 26-Minute ^{244m}Am (Hoff, von Egidy, Lougheed, White, Börner,* Schreckenbach,* Barreau,* and Warner**)

Gamma rays and conversion electrons were measured for the ^{244}Am beta decay isomers in a ^{243}Am target undergoing neutron capture in a high-flux reactor. New transitions accompanying beta decay of 26-min ^{244m}Am were observed. These include 984.92-keV and 977.80-keV E0 transitions assigned to the de-excitation of a first-excited 0^+ band in ^{244}Cm with level energies of 984.91 (0^+) and 1020.76 (2^+) keV. (See Fig. A-3). The ratio of reduced transition probabilities B(E0)/B(E2) for this 0^+ level is 1.5 ± 0.2.

---

* Institut Laue-Langevin, 38042 Grenoble, France.

** Institut Laue-Langevin and Brookhaven National Laboratory, Upton, NY 11973.

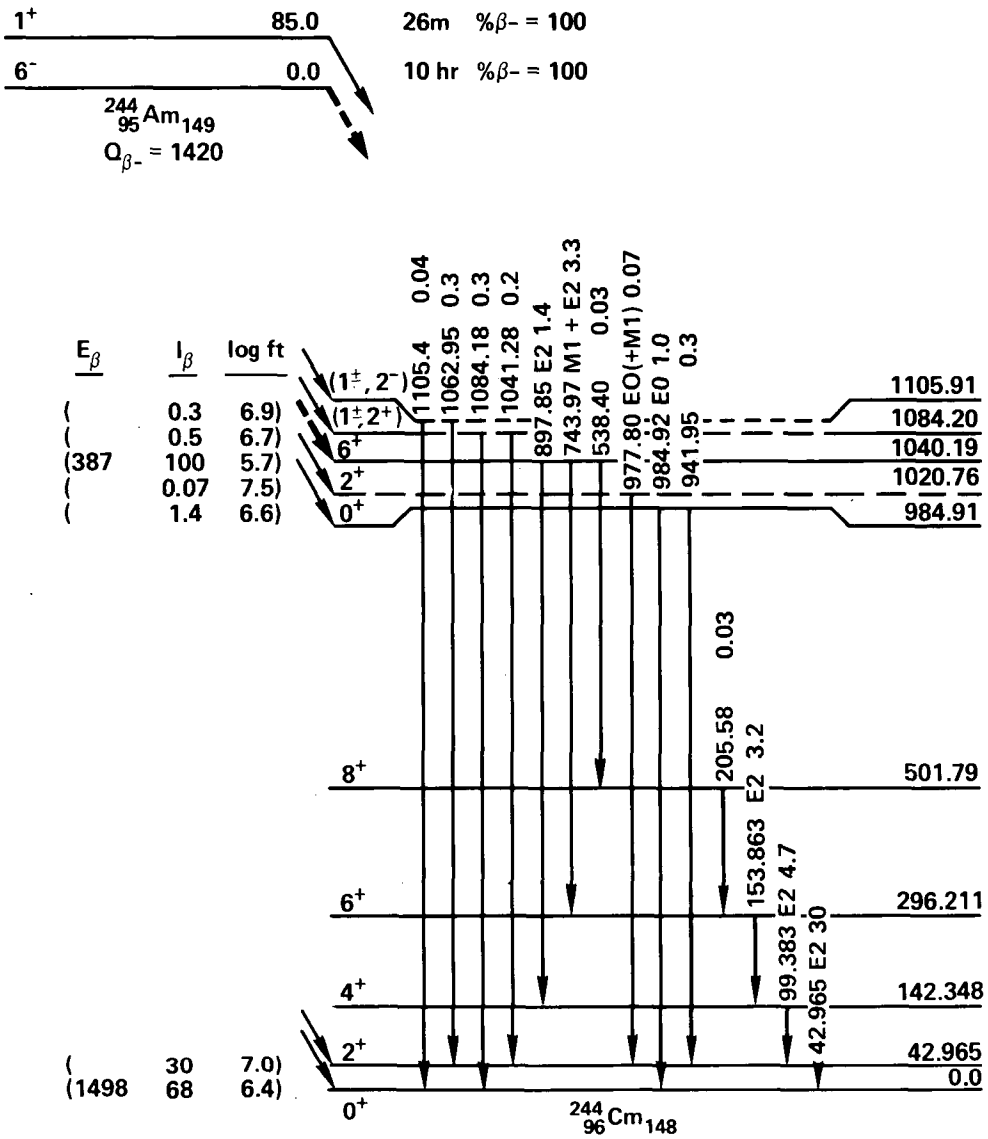

Fig. A-3. Levels of ^{244}Cm from gamma transitions accompanying beta decay of ^{244}Am isomers. Transition intensities ($I_\gamma + I_{ce}$) per 100 neutron captures are listed following gamma-ray energies and multipolarities.

B. NUCLEAR DATA APPLICATIONS-CALCULATIONS

1. Tests of Microscopic Optical Models for Neutron and Proton Scattering on Light Nuclei in the Range 14-45 MeV (Dietrich, Back, Hansen, Pohl, Poppe, Wong, Petrovich,* Finlay,** Petler,** Conzett,*** Eversheim,*** Rioux,*** and Larimer***)

As part of an effort to evaluate systematically the ability of microscopic optical models to predict elastic neutron scattering, we have begun a series of measurements and calculations of elastic scattering of both neutrons and protons on light nuclei. Previously reported[1,2,3] portions of this investigation have shown that calculations using microscopic optical potentials of both the Jeukenne-Lejeune-Mahaux (JLM)[4] and Brieva-Rook[5] form yield reasonable agreement with scattering data for medium and heavy nuclei if the real and imaginary parts of the optical potentials are normalized by factors that are smoothly varying with energy and target mass. These types of potentials are expected to be less reliable for the light nuclei, because of ambiguities in the application of the local density approximation, and because of exchange effects associated with nuclear recoil, which are not included in the simple folding-model treatment. Nevertheless, a study[3] of 14.6-MeV neutron scattering on targets for $A \geq 9$ has shown that the JLM potentials reproduce the angular distributions well for target masses as low as ^{12}C; the Brieva-Rook potentials are less successful in reproducing the shapes at back angles (>100 degrees).

To provide data for further tests of the microscopic models in light nuclei, we have measured polarized proton scattering from ^{6}Li and ^{14}C in the range 25-45 MeV at the LBL 88" cyclotron. Measurements with a polarized beam are useful because they are particularly sensitive to the recoil exchange effects. Elastic scattering angular distributions have also been measured for 24-MeV neutrons on ^{13}C at Ohio University, and are being

---

* Florida State University, Tallahassee, FL 32306.

** Ohio University, Athens, OH 45701.

*** Lawrence Berkeley Laboratory, Berkeley, CA 94720.

1 F. S. Dietrich et al., Phys. Rev. Lett. 51, 1629 (1983).

2 S. Mellema et al., Phys. Rev. C 28, 2267 (1983).

3 L. F. Hansen et al., LLNL report UCID-18987; to be submitted to Phys. Rev. C.

4 J. P. Jeukenne, A. Lejeune, and C. Mahaux, Phys. Rev. C 16, 80 (1977).

5 F. A. Brieva and J. R. Rook, Nucl. Phys. A 291, 299, 317 (1977).

analyzed together with data from the same laboratory on ^{12}C in the range 20-26 MeV.

Analysis completed up to the present time shows that the JLM potentials yield excellent reproduction of the ^{12}C and ^{13}C neutron scattering results. However, the same treatment yields very poor analyzing powers. The agreement for the analyzing powers is significantly improved by including a phenomenological ℓ-dependent term in the calculation, of a form suggested by calculations[6] that explicitly include exchange effects neglected in the simple folding model.

2. A New Dynamic Model for Fission (Mustafa and Kumar*)

We developed a dynamic deformation model (DDM) for fission that combines a dynamic deformation model for nuclear structure with an appropriate choice of nucleus-nucleus force acting between nascent fission fragments.[7] We used this dynamic model to calculate zero-point energy, inertial masses, fission barriers, and half-lives. The four main points of the model are outlined below:

1. The DDM has been successfully tested for the structure properties of spherical, transitional, and deformed nuclei from ^{12}C to ^{240}Pu [masses, E_{2^+}, B(E2), ...].[8] The DDM uses the microscopic-macroscopic method of calculating the potential energy of deformation and the Bohr Hamiltonian method of calculating the energy of zero-point motion. The Cranking-Generator Coordinate method is used to calculate inertial masses.

2. We emphasize the choice of the nucleus-nucleus force between nascent fragments. The force was chosen so as to reproduce spontaneous fission half-lives of ^{240}Pu and $^{260}104$, which vary by 20 orders of magnitude over a small mass region. The very sensitive nature of fission half-lives gives us a handle on the fragment interaction force.

3. The energy of zero-point motion is a very critical quantity, along with inertial masses and asymptotic fragment interaction, in calculating fission half-lives. We find that the zero-point energy is not a constant for different types of nuclei, but varies appreciably from ^{208}Pb to ^{240}Pu to superheavy nuclei.

---

* Tennessee Technological Univ., Cookeville, TN 38501.

6 D. J. Stubeda et al., Phys. Rev. C 17, 447 (1978).

7 K. Kumar and M. G. Mustafa, Lawrence Livermore National Laboratory, Livermore, CA, UCRL-89694 (1983), submitted to Phys. Letters.

8 K. Kumar, Collective Bands in Nuclei, D. H. Wilkinson, ed., Pergamon Press, London (1982).

4. The spontaneous fission half-lives were calculated by first minimizing the two-dimensional action integral for each charge/mass split and then adding the contributions from each split.

The known fission half-lives have provided a very sensitive test of the model, and this should add confidence to the predictions for unknown regions.

3. The Necessity of Discrete-Level Modeling in Isomer Ratio Calculations for Neutron-Induced Reactions on Deformed Nuclei (Gardner, Gardner, and Hoff)

The recent development of a technique for modeling level structure in deformed odd-odd nuclei[9] has enabled us to calculate isomer ratios in agreement with experiment for the reactions: $^{175}Lu(n,\gamma)^{176m,g}Lu$, $^{175}Lu(n,2n)^{174m,g}Lu$, $^{237}Np(n,2n)^{236m,g}Np$, $^{241}Am(n,\gamma)^{242m,g}Am$, and $^{243}Am(n,\gamma)^{244m,g}Am$. The calculations were of the Hauser-Feshbach type, with complete conservation of angular momentum and parity in the gamma-ray cascades. Below about 1500 keV in each product nucleus, we have replaced the conventional level density expression with a modeled discrete level set based on estimates of single-particle and rotational excitations. Among the discrete levels, the gamma-ray transitions were assumed to take place within a rotational band by M1 transitions, with no interband crossing except from the band head. The band heads de-excite by E1 and M1 transitions, using an E^3 energy dependence and the additional selection rule $\delta K = 0, \pm 1$. The M1 transitions are taken to be intrinsically faster than the E1 transitions by a factor of six.

The number of discrete levels used in each product nucleus was (in parenthesis): $^{174}Lu(433)$, $^{176}Lu(291)$, $^{236}Np(714)$, $^{242}Am(788)$, and $^{244}Am(769)$. Up to 30 gamma-ray branches were allowed from each band head. If a band head could not de-excite without violating the δK selection rule, it was identified as a potential isomeric state.

Figure B-1 illustrates our results for the reaction $^{175}Lu(n,\gamma)^{176m,g}Lu$. The lower curves give the best agreement with an m/g ratio derived from recent experimental work. Beer and Käppeler[10] measured the $^{175}Lu(n,\gamma)^{176m}Lu$ cross section to be 0.906 b at about 30 keV,

---

9 R. W. Hoff, J. Kern, R. Piepenbring, and J. P. Boisson, Nuclear Chemistry Division Annual Report FY83, Lawrence Livermore National Laboratory, Livermore, CA, UCAR-10062-83/1 (1983), pp. 218-223.

10 H. Beer and F. Käppeler, Phys. Rev. C 21, 534 (1980).

while Allen et al.[11] measured it to be 0.958 b. The total $^{175}Lu(n,\gamma)$ cross section at 30 keV ranges from about 1.2 b[12,13] to 1.4 b,[14] leading to an experimental m/g ratio between 1.8 and 4.0.

For the ^{236}Np isomer ratio calculation, our level scheme assigns the long-lived ^{236}Np isomer (1.2×10^5y) to be the ground 6^- level and the 22.5h ^{236}Np to be the 1^+ isomer. Our preliminary calculation of the ratio of the long-lived to short-lived isomer is in good agreement with the measured value of 0.35 reported by Myers et al.[15] Further details of this work may be found in Ref. 16.

---

11 B. J. Allen, G. C. Lowenthal, J. W. Boldeman, and J. R. deLoeter, Proc. 4th Intern. Symp. on Neutron-Capture Gamma-Ray Spectroscopy and Related Topics (the Institute of Physics, Bristol and London, 1982), Conf. Series No. 62, p. 573.

12 H. Beer, F. Käppeler, and K. Wisshak, Proc. Intern. Conf. on Nuclear Cross Sections for Technology, Knoxville, TN, 1979, NBS Special Publication 594, p. 340.

13 R. L. Macklin, D. M. Drake and J. J. Malanify, LANL Report La-7024-MS (1977)

14 R. L. Macklin and J. H. Gibbons, Phys. Rev. 159, 1007 (1967).

15 W. A. Myers, M. Lindner, and R. S. Newbury, J. Inorg. Nucl. Chem. 37, 637 (1975).

16 D. G. Gardner, M. A. Gardner, and R. W. Hoff, Nuclear Chemistry Division Annual Report FY83, Lawrence Livermore National Laboratory, Livermore, CA, UCAR-10062-83/1 (1983), pp. 51-55.

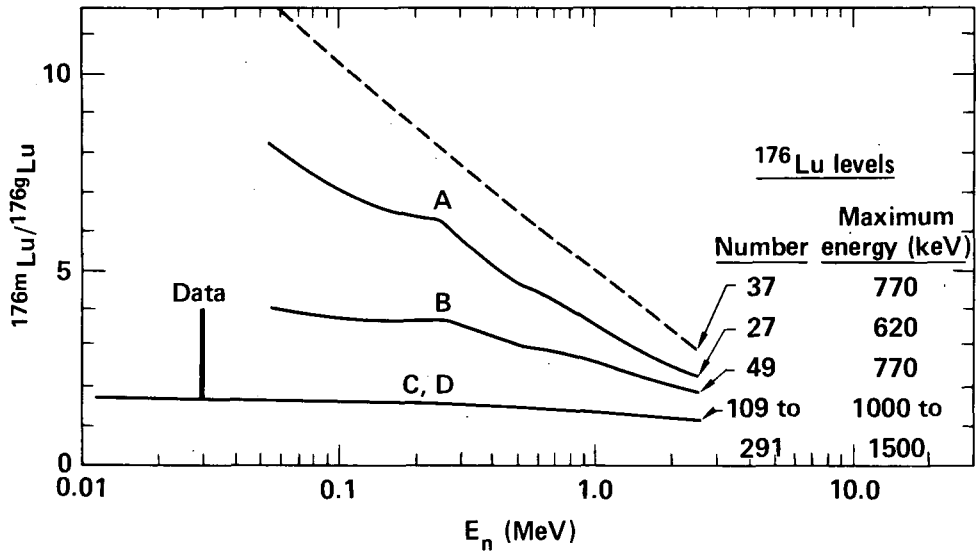

Fig. B-1. ^{175}Lu(n,γ)^{176}Lu isomer ratio as a function of incident neutron energy. Solid curves show results obtained when the full set of 291 levels for ^{176}Lu was truncated; essentially no difference was obtained for calculations C and D, with 109 and 291 levels, respectively. The dashed curve shows an earlier calculation, with an older set of ^{176}Lu levels. The data are derived from Refs. 10-14.

C. NUCLEAR DATA APPLICATIONS-EVALUATIONS

1. A Reevaluation for ENDL of σ(n,f) and $\bar{\nu}_p$ for ^{235}U and ^{239}Pu from 100 keV to 20 MeV[1] (Howerton and White)

Reevaluations of the neutron-induced fission cross sections from 100 keV to 20 MeV and $\bar{\nu}_p(E)$ from thermal to 20 MeV for ^{235}U and ^{239}Pu have been completed and entered into the Livermore Evaluated Nuclear Data Library (ENDL). For ^{235}U(n,f) the recent evaluation of W. P. Poenitz[2] of Argonne National Laboratory has been adopted as the ^{235}U(n,f) ENDL standard. The ^{239}Pu/^{235}U fission cross section ratio measurements of Carlson and Behrens,[3]

---

1 R. J. Howerton and R. M. White, Lawrence Livermore National Laboratory report UCID-19973 (1984).

2 W. P. Poenitz, "Evaluation of ^{235}U(n,f) Between 100 keV and 20 MeV," Argonne National Laboratory, ANL/NDM-45 (1979).

3 G. W. Carlson and J. W. Behrens, Nucl. Sci. Eng. 66, 205 (1978).

Kari,[4] Weston and Todd,[5] and Meadows,[6] have been used as the basis for the new $^{239}Pu(n,f)$ ENDL evaluation.

For $\bar{\nu}_p(E)$ ratio values of Soleihac, et al.[7] were renormalized to the currently accepted value for ^{252}Cf $\bar{\nu}_{sf}$ and used as the basis for the present ENDL evaluation. Results of criticality calculations using the new evaluated cross sections and $\bar{\nu}_p(E)$ have been compared for various critical mass assemblies. Also, Monte Carlo calculations using these new evaluations have been compared with experimental data from the LLNL 14-MeV pulsed sphere measurements.[8]

---

4 K. Kari, "Messung der Spaltquerschnitte von ^{239}Pu an ^{240}Pu Relative zum Spaltquerschnitt von ^{235}U and Streuquerschnitte H(n,p) in dem Neutronenenergiebereich Zwischen 0,5-20 MeV," Kernforschungszentrum Karlsruhe, KfK2673 (1978).

5 L. W. Weston and J. H. Todd, Nucl. Sci. Eng. 84, 248 (1983).

6 J. W. Meadows, "The Fission Cross Sections of Some Thorium, Uranium, Neptunium and Plutonium Isotopes Relative to ^{235}U," Argonne National Laboratory, ANL/NDM-83 (1983).

7 M. Soleihac, J. Frehaut, J. Garian, M. Labat, and J. Percheran, J. Nuclear Energy, 23, 257 (1969). Revised by authors in 1976 (ECSIL Reference 211).

8 L. F. Hansen, Nucl. Sci. Eng. 72, 35 (1979).

A. NUCLEAR DATA MEASUREMENTS

1. Low-Energy Fusion Cross Sections (N. Jarmie, R. E. Brown)

The goal of this project is to measure cross sections for interactions between hydrogen isotopes in the bombarding energy range 10-120 keV. Such cross sections are fundamental to the operation of future controlled fusion systems.

In addition to the measurements of the reaction D(t,α)n reported on last year, new measurements have been made at the lowest energies to clarify the possibility of a resonance in that energy region. No evidence for a resonance was seen. This augmented final data set has again been used to calculate Maxwellian reactivities for plasma temperatures up to 20 keV. In addition, the data have been expressed in a type of power series useful for computation. A final report has been submitted for publication.

We have now completed our measurements for the D+D reactions. We have measured angular distributions for D(d,p)T and D(d,n)^{3}He for a bombarding energy range of 20-117 keV. Most of the angular distributions have relative errors on the order of 1%; and the integrated cross sections have absolute errors of about 1.5%. The angular distributions are quite anisotropic, the n + ^{3}He channel the most. Astrophysical S functions have been extracted from the data and also from a least squares fit of a + b cos^2 to the data. The cross sections agree with previous less accurate experiments but the angular asymmetries do not. An attempt to fit the data with R-Matrix theory did not give good results.

We are now making a major effort to study the T(t,α)2n reaction which not only has a much smaller cross section than the D(t,α)n reaction, as do the D+D reactions, but also has a three-body final state. It also requires that we flow tritium in our windowless gas target, forcing considerable modification of our apparatus.

We have also begun an attempt to measure thin-target cross sections for the D(t,γ)^{5}He reaction (E_γ=16.6 MeV) which may be important as a plasma diagnostic. The possibility of studying other fusion reactions producing high energy gamma rays and studying the ^{3}He(d,p)^{4}He reaction is being considered.

2. Measurement of the T(d,γ)/T(d,n) Branching Ratio
(G. L. Morgan, P. W. Lisowski, S. A. Wender, R. E. Brown, N. Jarmie, J. F. Wilkerson, and D. M. Drake)

Measurements have been made of the ratio between the reactions T(d,γ) and T(d,n). Pulsed deuteron beams from the LANL Van De Graaff were used to bombard thick tritium gas targets. Neutrons were detected at 0° using a calibrated NE-213 scintillator with n-γ discrimination. Gamma rays were detected at 90° with a 3"x3" bismuth germanate detector especially developed for good time resolution.[1] Time-of-flight techniques were used to discriminate against neutron induced backgrounds in the BGO detector. The figure shows a typical pulse height spectrum due to the 16.7 MeV gamma-ray from the T(d,γ) reaction. Measurements were made for a number of incident energies and target thicknesses. These provide data for the following ranges of deuteron energies in the target: 0-275 keV, 0-715 keV, 194-715 keV, and 534-715 keV. Values of the gamma ray to neutron branching ratio for these energy ranges are $6.2\pm.6\times10^{-5}$, $8.4\pm.9\times10^{-5}$, $8.6\pm.9\times10^{-5}$, and $11.7\pm1.2\times10^{-5}$ respectively.

[1] S. A. Wender, G. F. Auchampaugh, and N. W. Hill, Nucl. Instr. and Meth. 197 (1982) 591.

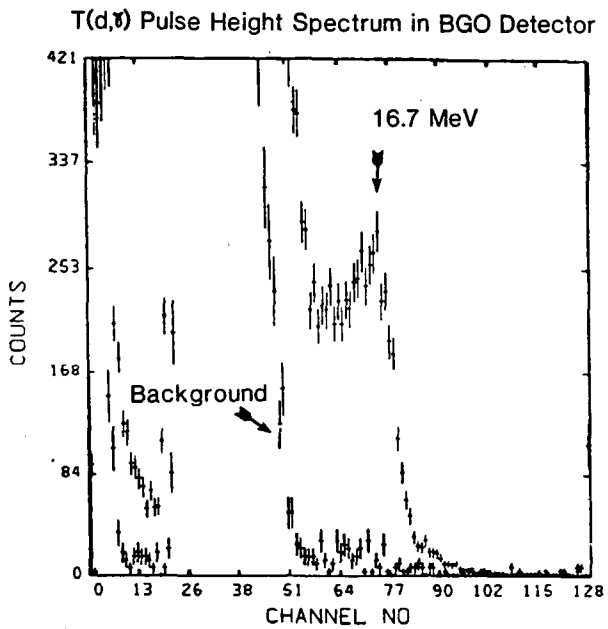

Fig. A-1. A typical pulse height spectrum for 16.7 MeV gamma rays from the T(d,γ) reaction. A background spectrum measured by shadowing the detector with 5.1 cm of lead is also shown.

3. Cross Sections for Neutron Production by ^6Li + t reactions (P. W. Lisowski, R. E. Brown, J. C. Gursky, S. D. Howe, N. Jarmie, and G. L. Morgan)

Neutrons produced in a fusion reactor will interact in the lithium blanket giving secondary deuterons and tritons. As these particles recoil they in turn will react with the lithium to produce neutrons and a wide variety of charged particles. Such reactions will affect both the tritium breeding ratio as well as the reactor neutron spectrum. Calculations[1] presently indicate that such effects will be small, but the cross sections for (t,n) reactions on the lithium isotopes were measured at low energies over two decades ago with techniques that are likely to have yielded incorrect results.

In this experiment we have measured neutron spectra for triton reactions with ^6Li using a pulsed beam and time of flight techniques. A low-mass chamber was used to hold the lithium target and to permit us to continuously monitor the thickness by detecting charged particles from other tritium induced reactions. We have obtained angular distributions for $\sigma(E_n,\theta)$ in 15° steps from θ=0° to 150° at five triton energies from 2 to 4.5 MeV. The spectra show neutron groups corresponding to energy levels in ^8Be at 0.0, 2.94, 16.63, and 16.92 MeV. We are in the process of extracting absolute differential and integrated cross section values.

---

[1] S. D. Howe, private communication.

4. Neutron Induced γ-Ray Production at WNR (S. A. Wender and G. F. Auchampaugh)

During the past year we have completed development of a unique system to study high-energy gamma rays produced by neutron-induced reactions. This system consists of five bismuth germanate (BGO) scintillators used in conjunction with a pulsed spallation neutron source (WNR). The simultaneous acquisition of gamma-ray excitation functions and angular distributions for incident neutrons in the energy range from 1 to 200 MeV is possible with this system. Fig. 2A shows the diagram of the apparatus.

The physics program presently consists of studying two broad areas: (1) inelastic neutron excitation of γ-rays from bound states using the (n,n'γ) reaction, and (2) fast neutron capture reactions into the giant resonance region of nuclei. In addition to these two programs we are also investigating the properties of the BGO detectors to optimize their characteristics.

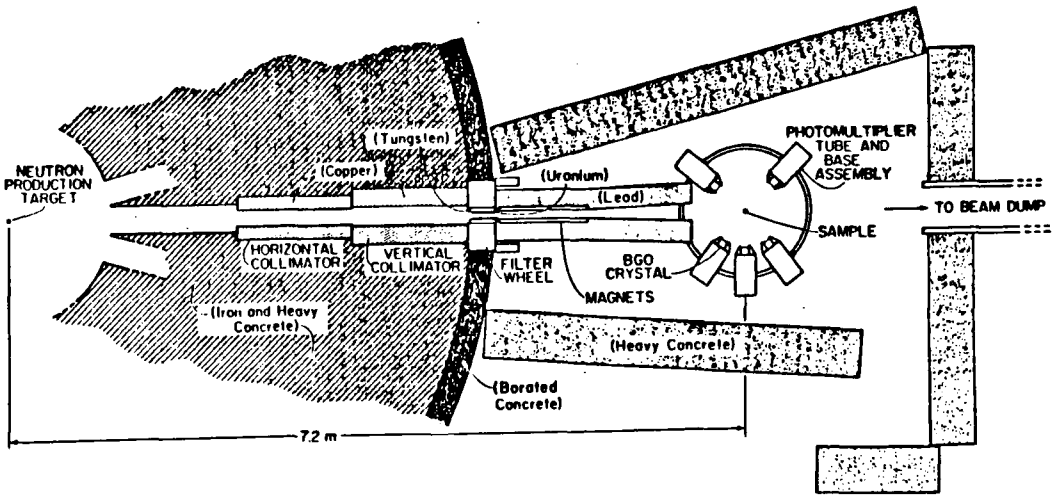

Fig. 2A. Experimental setup showing neutron collimators, shielding, and detector assembly.

5. Proton Induced Reactions on Sr Isotopes (D. W. Barr, S. A. Beatty, K. Eskola, M. M. Fowler, J. S. Gilmore, R. J. Prestwood, E. N. Treher, and J. B. Wilhelmy)

We have measured absolute excitation functions for (p,n) and (p,2n) reactions from threshold to 17 MeV on three strontium isotopes, ^{86,87,88}Sr. We have determined the following cross sections in addition: for ^{86}Sr, (p,γ) between 3.5 and 8 MeV, (p,α) between 14.7 and 17 MeV, and (p,pn) between 15.5 and 17 MeV; for ^{87}Sr, (p,p$'$)^{87m}Sr between 7 and 17 MeV; and for ^{88}Sr, (p,pn)^{87m}Sr between 14.7 and 17 MeV. The ratio of the yield of ^{86m}Y to that of ^{86g}Y has been measured as a function of proton energy from both the ^{86}Sr(p,n) and ^{87}Sr(p,2n) reactions, while the ratio of ^{87m}Y to ^{87g}Y has been measured from the ^{86}Sr(p,γ), ^{87}Sr(p,n) and ^{88}Sr(p,2n) reactions. Advanced nuclear-model interpretation of this data is in progress.

Approximately 100 μg/cm^2 targets of enriched strontium isotopes were irradiated in a scattering chamber at the Los Alamos Tandem Van de Graaff Accelerator. Target thicknesses were measured from Rutherford scattering and the yields of the yttrium nuclides were determined from their decay properties using Ge(Li) spectrometry.

6. Cross Sections for Radionuclide Production by Spallation Neutrons (R. C. Reedy, P. Englert*)

Several packages of elemental targets were irradiated near the main beam stop of the LAMPF accelerator. Reactions with known cross sections for neutrons, such as (n,p) and (n,np) with Ti and ^{58}Ni or (n,xn) with Y and Au, are being used to determine the neutron fluxes and spectra at low energies. A number of high-energy products from iron (such as ^{48}V and ^{46}Sc), whose production systematics by high-energy secondary particles in extra-terrestrial matter is known, are being used to ascertain the fluxes as a function of energy for the high-energy particles incident on the various packages. Activities of radionuclides with unknown cross sections for their production by neutrons are being compared with the production rates calculated with the unfolded fluxes and with measured proton-induced cross sections. The observed activities of ^{22}Na and ^{7}Be from Al seem much lower than those calculated with proton cross sections. The preliminary measured-to-calculated ratio for ^{54}Mn from ^{56}Fe is about 1.4, similar to this ratio determined for ^{53}Mn from iron in meteorites and lunar samples. Neutron-induced cross sections for these and additional radionuclides, such as ^{26}Al and ^{10}Be, are being or will be investigated for a variety of targets.

---

*Univ. Koeln, FRG

7. (p,n) Cross Sections for Nuclear Data Needs (M. M. Meier, G. J. Russell, H. Robinson, R. Whitaker, G. L. Morgan D. Holtkamp, W. Amian, and N. Paul)

Neutron yields from proton bombardment of C, Al, Ni, W, Pb and depleted U have been obtained at bombarding energies of 800 and 318 MeV. Additionally, at 318 MeV, data were obtained for Be and Ta. The data were obtained at angles/flight-paths of 7deg/30m, 15deg/30m and 30deg/40m and were collected in two-parameter histograms of time-of-flight and pulse-height. Pulse-height information was obtained in order to facilitate the analysis by providing the possibility for post-experiment selection of bias and to permit comparison of calculated and experimental pulse height spectra in the calculation of detector efficiency. The experiment was designed to provide energy resolution better than 1% and statistical accuracy of 5% or better for any 1% energy bin. The data are being reduced to cross-sections for comparison to calculations.

Additional measurements on Be, Li, Fe, Cu, Ta, and Th are planned at 800 MeV.

B. NUCLEAR DATA EVALUATION

1. Polarized d+d Fusion (G. M. Hale and G. D. Doolen)

Since the properties of polarized d+t fusion are well described by the single resonance S-wave transition, we have concentrated our study on the more complex d+d reactions. Magnetic fusion interest in polarizing these reactions comes primarily from the prospect of suppressing them in the spin-parallel configuration, and thereby reducing secondary production of neutrons and tritons in the d-^{3}He fuel cycle.

We have calculated Maxwellian averaged reaction rates for the polarized d+d reactions,[1] using cross sections obtained from the latest Los Alamos four-nucleon R-matrix analysis.[2] New low-energy polarization data for the d+d reactions were included in this most recent analysis to give increased reliability of the polarized cross-section predictions.

The angular distributions of reaction products for the polarized reaction rates exhibit strongly non-isotropic shapes that are characteristic of the projections (m,n) of the deuteron spins on the axis of quantization. This is shown in Fig. B-1, which gives reaction-rate angular distributions for D(d,p) and D(d,n) at kT = 2 and 10 keV for the four independent combinations of spin projections (m,n) = (1,1), (1,0), (1,1), and (0,0).

RELATIVE ANGULAR DISTRIBUTIONS

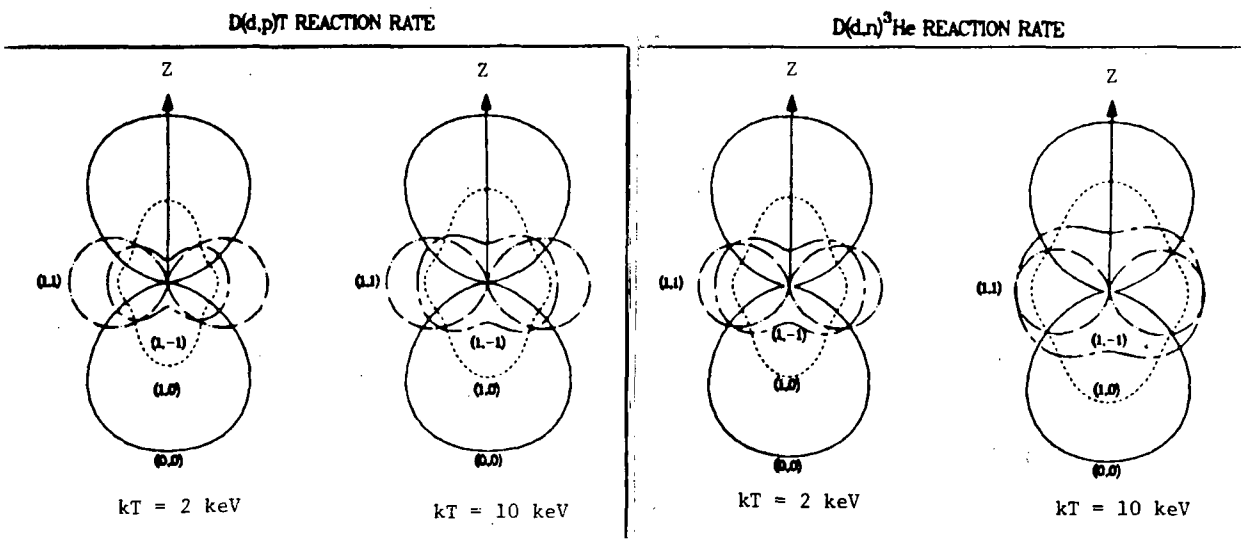

Fig. B-1. Relative shapes of the four independent reaction rates $\langle\sigma_{m,n} v\rangle(\hat{v}')$ for the D(d,p) [left] and D(d,n) [right] reactions, at temperatures kT = 2 and 10 keV.

Integrated reaction rates for the d+d reactions are listed for the four independent (m,n) combinations as a function of temperature in Table B-1. One can see that little or no suppression of the spin-parallel (1,1) configuration occurs at temperatures below 10 keV. This results from the fact that the quintet S-wave transitions in our R-matrix analysis are not negligible, in contrast with earlier theoretical work.

TABLE B-1. Polarized Reaction Rates for the d-d Reactions.

A. $D(d,p)T^a$

kT (keV)	$\langle\sigma_0 v\rangle$ (cm^3/sec)	$\frac{\langle\sigma_{1,1} v\rangle}{\langle\sigma_0 v\rangle}$	$\frac{\langle\sigma_{1,0} v\rangle}{\langle\sigma_0 v\rangle}$	$\frac{\langle\sigma_{1,-1} v\rangle}{\langle\sigma_0 v\rangle}$	$\frac{\langle\sigma_{0,0} v\rangle}{\langle\sigma_0 v\rangle}$
2	3.239×10^{-21}	1.223	0.875	0.902	1.251
4	4.550×10^{-20}	1.181	0.898	0.921	1.203
6	1.585×10^{-19}	1.146	0.918	0.936	1.165
8	3.432×10^{-19}	1.115	0.935	0.950	1.131
10	5.905×10^{-19}	1.088	0.950	0.962	1.100

B. $D(d,n)^3He^a$

kT (keV)	$\langle\sigma_0 v\rangle$ (cm^3/sec)	$\frac{\langle\sigma_{1,1} v\rangle}{\langle\sigma_0 v\rangle}$	$\frac{\langle\sigma_{1,0} v\rangle}{\langle\sigma_0 v\rangle}$	$\frac{\langle\sigma_{1,-1} v\rangle}{\langle\sigma_0 v\rangle}$	$\frac{\langle\sigma_{0,0} v\rangle}{\langle\sigma_0 v\rangle}$
2	2.950×10^{-21}	1.038	0.923	1.039	1.154
4	4.224×10^{-20}	0.984	0.955	1.061	1.089
6	1.494×10^{-19}	0.941	0.981	1.078	1.038
8	3.280×10^{-19}	0.904	1.003	1.093	0.994
10	5.711×10^{-19}	0.872	1.022	1.106	0.955

[a]The reaction rates satisfy

$$(2\langle\sigma_{1,1}\rangle + 4\langle\sigma_{1,0} v\rangle + 2\langle\sigma_{1,-1} v\rangle + \langle\sigma_{0,0} v\rangle)/9 = \langle\sigma_0 v\rangle$$

Therefore, the prospect of using polarization to suppress the d+d reactions does not look promising. However, the characteristic angular distributions of the reaction rates could provide a useful diagnostic for learning about depolarization mechanisms in an initially polarized deuterium plasma.

[1] G. M. Hale and G. D. Doolen, "Cross Sections and Maxwellian Reaction Rates for Polarized d+d Reactions," Los Alamos National Laboratory report LA-9971-MS (1984).

[2] G. M. Hale and D. C. Dodder," A=4 Level Sructure from an R-Matrix Analysis of the Four-Nucleon System," Proc. 10th Int. Conf. on Few Body Problems in Physics, Karlsruhe, W. Germany, 1983, B. Zeitnitz, Ed., p. 207 (1983).

2. Calculation of Proton Emission Spectra from $^{87}Sr(p,pn+p,np)$ and $^{91}Zr(p,pn+p,np)$ Reactions (E. D. Arthur)

Cross sections measured with incident charged particles can be used to provide or optimize nuclear model parameters necessary for the calculation of neutron-induced reaction data. Such a class of experiments[1] has recently been completed involving measurements of ^{87}Sr and ^{91}Zr (p,np + p,pn) spectra in which emitted neutrons and protons were detected in coincidence. The ^{87}Y and ^{91}Nb compound nuclei reached in these experiments exhibit large "proton windows" where only proton emission is allowed energetically. These measurements can then provide information regarding sub-Coulomb barrier proton optical models as well as the magnitude of gamma-ray strength functions.

Our analysis of these data employed the multistep Hauser-Feshbach statistical model code GNASH[2] and used parameters determined from previous calculations[3] in this mass region. We have not yet attempted the introduction of isospin effects into the statistical model calculations because significant isospin effects were not readily apparent in the experimental data examined thus far. Our main effort has been directed towards verification of input parameters through use of corroborating independent data sources. For example, sub-Coulomb barrier proton optical model parameters were determined through fits to low-energy $^{89}Y(p,n)$ data,[4] neutron optical parameters were adjusted to reproduce total and elastic cross sections as well as resonance information, and gamma-ray strength functions were determined from fits to neutron capture data available for a variety of nuclei in this mass region.

The experimental proton emission spectrum detected in coincidence with neutrons can be correlated directly to production of levels in the residual ^{86}Sr or ^{90}Zr nuclei reached in $^{87}Sr(p,pn + p,np)$ and $^{91}Zr(p,pn + p,np)$ reactions. Comparison to such data places stringent constraints on the theoretical models and parameters employed since fixed states with known spins and parities are populated. Figure B-2 shows the results of such a comparison between experimental values for levels of ^{90}Zr produced by 16-MeV protons on ^{91}Zr and the theoretically calculated values. The calculations are in good agreement with these measured results, which provides confirmation of the sub-Coulomb proton optical parameters and the gamma-ray strength functions employed in this analysis.

---

[1] J. C. Dousse, D. M. Drake, J. Gursky, J. D. Moses, N. Stein, J. W. Sunier, and E. D. Arthur, "Coincident Neutron-Proton Emission from Proton Bombardment of ^{87}Sr and ^{91}Zr," to be submitted to Phys. Rev. C.

[2] P. G. Young and E. D. Arthur, "GNASH: A Preequilibrium Statistical Nuclear Model Code," Los Alamos Scientific Laboratory report LA-6947 (1977).

[3] E. D. Arthur, "Calculation of Neutron Cross Sections on Isotopes of Yttrium and Zirconium," Los Alamos Scientific Laboratory report LA-7789-MS (1979).

[4] C.H. Johnson, R.L. Kernell, and S. Ramavataram, Nucl. Phys. A107, 21 (1968).

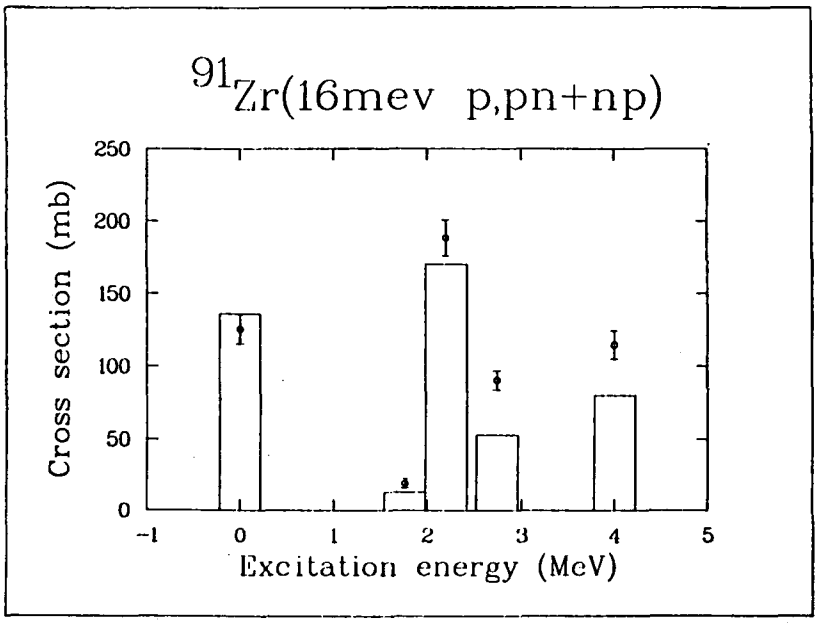

Fig. B-2. Comparison of calculated (histogram) and experimental values for production of ^{90}Zr levels resulting from 16-MeV $^{91}Zr(p,pn + p,np)$ reactions.

3. Analysis of n+^{197}Au Cross Sections for E_n = 0.01-30 MeV (P. G. Young and E. D. Arthur)

We have completed an analysis of neutron reactions with ^{197}Au for neutron energies between 0.01 and 30 MeV. The analysis combines a deformed optical model potential with Hauser-Feshbach statistical theory to produce satisfactory agreement with experimental data for all major reaction types. Because the current ENDF/B-V evaluation does not contain gamma-ray production data, particular emphasis was placed on obtaining gamma-ray strength functions that describe gamma-ray measurements between E_n = 0.1 and 20 MeV.

Using neutron transmission coefficients calculated from the deformed optical model potential of Delaroche[1] and a giant-dipole-resonance form for the M1 strength function (relative strength $\Gamma_{M1}/\Gamma_{E1} \sim 0.13$),[2] an E1 strength function shape was obtained by fitting Morgan and Newman's measurement[3] at E_n = 0.4-0.8 MeV. Overall normalization of the E1 strength function came from resonance analyses[4] of average gamma-ray widths and mean level spacings for s-wave neutrons. The inferred strength function is compared to other results in Fig. B-3.

Good agreement with the remainder of Morgan and Newman's (n,γ) data was obtained using the solid curve in Fig. B-3. To adequately reproduce their measurements at higher energies, however, a second slightly modified strength function was required, shown by the curve labelled (n,n'γ) in Fig. B-3. With this E1 strength function, it was possible to satisfactorily represent the measurements up to E_n = 20 MeV, including (n,n'γ), (n,2nγ), and (n,3nγ) reactions.

The results of this analysis have been combined with ENDF/B-V at lower energies to provide evaluated neutron and gamma-ray data over the complete energy range of 10^{-5} eV to 30 MeV.

---

[1] J. P. Delaroche, "Potential Optique Nucleon- ^{197}Au Entre 10 keV et 57 MeV," Int. Conf. Neutron Physics and Nuclear Data for Reactors and Other Applied Purposes, Harwell, England (1978), p. 366.

[2] G. L. Morgan and E. Newman, "The Au(n,xγ) Reaction Cross Section for Incident Neutron Energies between 0.2 and 20.0 MeV," Oak Ridge National Laboratory report ORNL-TM-4973 (1975).

[3] M. A. Lone, "Photon Strength Functions," Proc. Third Int. Symp. Neutron Capture Gamma-Ray Spectroscopy and Related Topics, Brookhaven, New York, September 18-22, 1978 (Plenum Press, New York, 1979), p. 161.

[4] S. F. Mughabghab and D. I. Garber, "Neutron Cross Sections, Volume 1, Resonance Parameters," Brookhaven National Laboratory report BNL-325, 3rd Ed., Vol. 1 (1973).

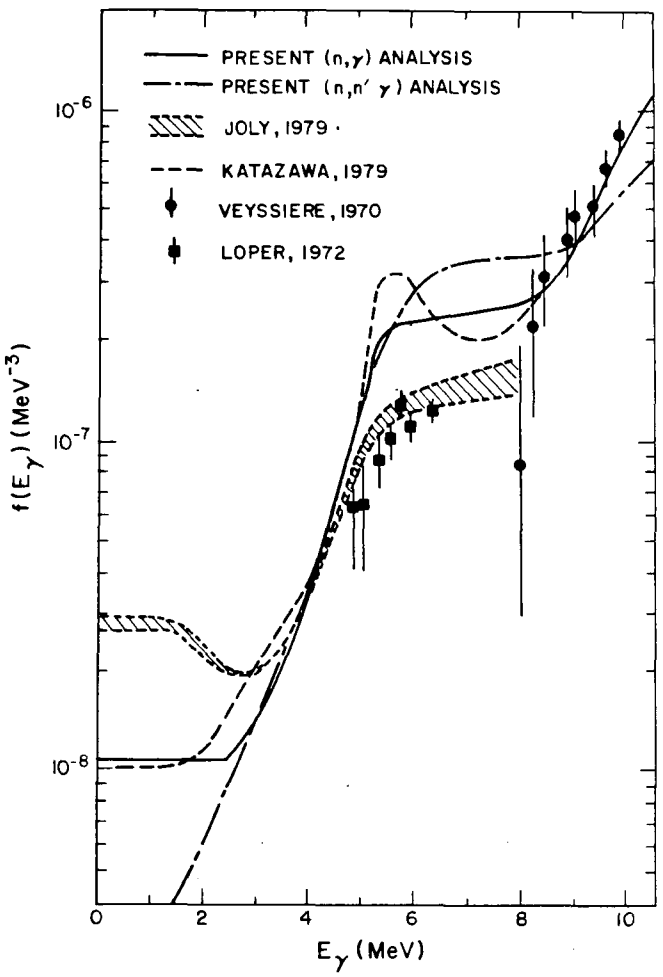

Fig. B-3. E1 gamma-ray strength functions inferred from n+^{197}Au measurements. All results were obtained from analysis of (n,γ) measurements except the curve labeled (n,n'γ).

4. Prompt Fission Neutron Spectrum and Average Prompt Neutron Multiplicity for the ^{252}Cf(sf) Standard Reaction (D. G. Madland and J. R. Nix)

Our most recent calculation[1] of the prompt fission neutron spectrum for the ^{252}Cf(sf) standard reaction is shown in Fig. B-4 compared with a new experiment[2] and with the best-fit Maxwellian spectrum. We used our exact expression[3] for the spectrum and obtained the value of the average nuclear level-density parameter by a least squares adjustment to the experiment. Our value of χ^2_{min} is a factor ~ 2.2 better than that of the best-fit Maxwellian spectrum. We obtain an average energy <E> = 2.134 whereas the value <E> = 2.144 MeV is obtained for the best-fit Maxwellian spectrum. Our corresponding calculation of the average prompt neutron multiplicity gives a value $\bar{\nu}_p$ = 3.810.

---

[1] D. G. Madland and J. R. Nix, invited paper to the Specialists' Meeting on Yields and Decay Data of Fission Product Nuclides, Brookhaven National Laboratory, Upton, New York, October 24-27, 1983 (proc. to be published).

[2] W. P. Poenitz and T. Tamura, Proc. International Conference on Nuclear Data for Science and Technology, Antwerp, Belgium, 1982, Reidel, Dordrecht (1983) p. 465, and W. P. Poenitz, private communication (April 1983).

[3] D. G. Madland and J. R. Nix, Nucl. Sci. Eng. 81, 213 (1982).

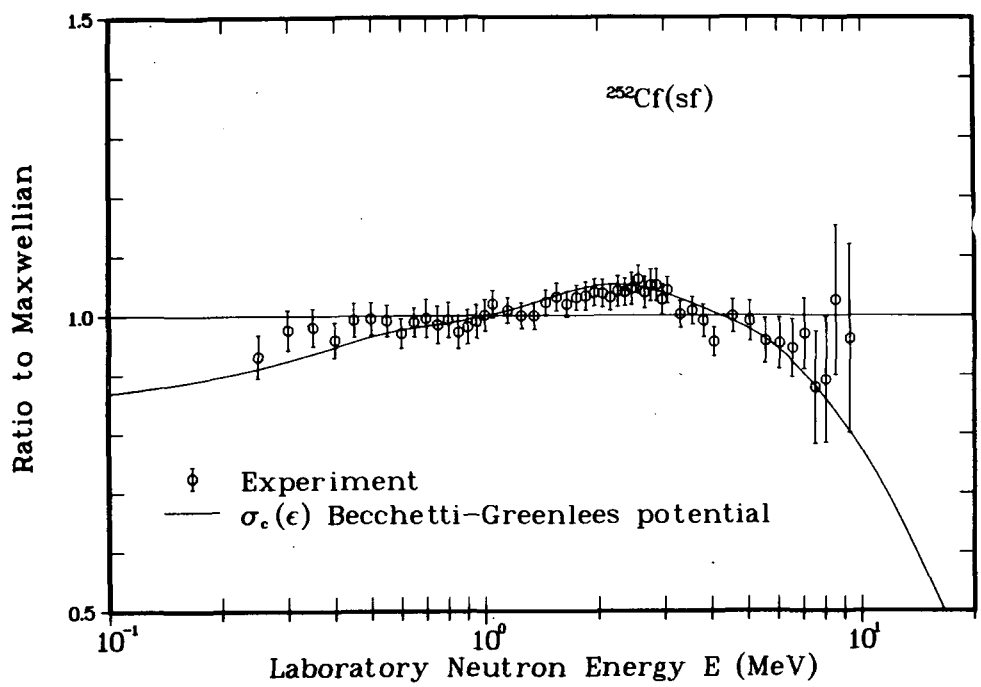

Fig. B-4. Ratio of the exact energy-dependent cross-section spectrum[1] and the experimental spectrum[2] to the best-fit Maxwellian spectrum.[1]

5. Development of the DKPOWR Code and Data Library for the Calculation of Aggregate Fission-Product Decay Power, Energy, Curies, and Multigroup β and γ Spectra (W. B. Wilson, T. R. England, R. J. LaBauve, and D. C. George)

DKPOWR calculates aggregate fission-product decay power at specified elapsed cooling (shutdown) times using an input fission history for each of the fissionable nuclides and the decay power pulse functions of the 1979 ANSI/ANS 5.1 Standard for Decay Heat Power in Light Water Reactors.[1] Pulse functions f(t), used to describe aggregate fission-product decay properties t seconds following a single fission "pulse," may be combined with any fission history to describe the cumulative contributions at any time from all previous fissions. The standard includes fission-product decay power pulse functions for ^{235}U thermal neutron fission (tf), ^{238}U fast neutron fission (ff), and ^{239}Pu tf in the absence of fission-product neutron absorption. The code also uses the Standard and/or extensions to it to calculate fission-product decay power uncertainty and upper-bound neutron absorption correction, limited actinide decay power, and the integrated shutdown decay energy contributions of fission products and limited actinides.

CINDER-10 summation calculations with ENDF/B-V data of fission-product decay power, activity (curies) and β and γ spectra have been made for ^{232}Th ff, ^{233}U tf, ^{235}U tf, ^{238}U ff, ^{239}Pu tf, and ^{241}Pu tf. The results of these calculations have recently been fit with accurate pulse functions describing the aggregate decay power, activity, 18-group β spectra, and 19-group γ spectra of fission products generated in the six fission systems. These pulse functions are incorporated in the DKPOWR code data library for the calculation of associated properties.

Documentation of the code and library is now in preparation for distribution by the Electric Power Research Institute.

---

[1] "American National Standards Institute/American Nuclear Society Standard, Decay Heat Power in Light Water Reactors," ANSI/ANS 5.1 (1979).

6. Development of the SOURCES Code and Data Library for the Calculation of β^-,n Delayed Neutron, (α,n) and Spontaneous Fission Decay Neutron Sources and Spectra (W. B. Wilson, R. T. Perry*, J. E. Stewart, T. R. England, E. D. Arthur, and D. G. Madland)

SOURCES calculates neutron sources for an input inventory of radionuclides and specified material elemental composition. Delayed neutron sources are calculated with the inventory of β^-,n precursors and the measured and/or calculated β^-,n branching-fraction (Pn) values and normalized 10-keV-binned neutron spectra for 105 precursors of England et al.[1]

Neutron sources due to (α,n) reactions are calculated by combining α-emitter inventories and α-spectra data with (α,n) reaction probabilities calculated with measured and/or GNASH[2]-modeled (α,n) cross sections and functional fits to the α stopping cross-section data of Ziegler.[3] The (α,n) neutron spectra are calculated using the simplifying assumption of isotropic neutron emission in the center-of-mass system.[4] These calculations require α-energy-dependent branchings for the compound nucleus decay to product nuclide energy levels; these branching have been evaluated for a number of (α,n) reactions from available measured partial (α,n_i) cross-section data, reciprocal (n,α_0) data, and/or GNASH nuclear model code calculations. Cross-section data is now present in the library for the target nuclides ^{7}Li, ^{9}Be, $^{10,11}{}^{NAT}B$, ^{13}C, $^{17,18}O$, ^{19}F, ^{23}Na, ^{NAT}Mg, ^{27}Al, $^{29,30}Si$, and ^{37}Cl. Level branching data is present for the target nuclides ^{7}Li, $^{10,11}B$, ^{13}C, $^{17,18}O$, and ^{19}F. α spectra are present for 89 actinides.

Spontaneous fission (SF) neutron source calculations combine SF-nuclide inventories, SF decay branchings, and SF $\bar{\nu}$ data. SF neutron spectra are calculated with Watt spectrum parameters obtained for 15 principal SF actinides from fits to more precise spectral descriptions or using parameters for additional SF actinides obtained from fits based on the 15 nuclides. SF branching, $\bar{\nu}$, and Watt spectrum parameters are present in the library for 43 actinides.

SOURCES calculations have been made for various source nuclides in ThO_2, UO_2, PuO_2, UF_6, PuF_4, $Pu(C_2O_4)_2 \cdot 6H_2O$, PuC, UO_2F_2, and various Pu process solutions. Documentation of the code and library, now in preparation includes an extensive bibliography of neutron source data.

---

* Texas A & M University

1 T. R. England, W. B. Wilson, R. E. Schenter, and F. M. Mann, "Aggregate Delayed Neutrons and Spectra Using Augmented ENDF/B-V precursor Data," Nucl. Sci. Eng 85, 139 (1983).

2 P. G. Young and E. D. Arthur, "GNASH: A Preequilibirum-Statistical Nuclear Model Code for Calculations of Cross Sections and Emission Spectra," Los Alamos Scientific Laboratory report LA-6947 (November 1977).

3 J. F. Ziegler, Helium Stopping Powers and Ranges in All Elemental Matter, Vol. 4 of The Stopping and Ranges of Ions in Matter, (Pergamon Press, New York, N. Y., 1977).

4 B. G. Whitmore and W. B. Baker, "The Energy Spectrum of Neutrons from a Po-Be Source," Phys. Rev. 78, 799 (1950).

7. Fission Product Yield Evaluations (T. R. England and B. F. Rider)

The status and summary information for the fission product yields of 34 nuclides at one or more incident neutron energies, including spontaneous fission, was completed and presented in Ref. (1). The fissionable nuclides are listed in Table B-2. Each yield set contains evaluated independent and cumulative yields and uncertainties for ~ 1100 products.

TABLE B-2. ENDF/B Fission-Product Yield Sets*

	Neutron Energy					Neutron Energy			
Nuclide	Thermal	Fast	14 MeV	Spon.	Nuclide	Thermal	Fast	14 MeV	Spon.
^{227}Th	6				^{242}Pu		56		
^{229}Th	6				^{241}Am	6	6	6	
^{232}Th		456	56		^{242m}Am	6			
^{231}Pa		6			^{243}Am		6		
^{232}U		6			^{242}Cm		6		
^{233}U	456	56	56		^{244}Cm				6
^{234}U		6	6		^{245}Cm	6			
^{235}U	456	456	456		^{248}Cm				6
^{236}U		56	6		^{249}Cf	6			
^{237}U		6			^{250}Cf				6
^{238}U		456	456	6	^{251}Cf	6			
^{237}Np		56	6		^{252}Cf				56
^{238}Np		6			^{253}Es				6
^{238}Pu		6			^{254}Es	6			
^{239}Pu	456	456	56		^{254}Fm				6
^{240}Pu		56	6		^{255}Fm	6			
^{241}Pu	456	56			^{256}Fm				6

* The numbers 4, 5, and 6 refer to ENDF/B Versions IV, V, and preliminary VI. ENDF/B-IV contains only independent yields and does not include uncertainties.

[1] T. R. England and B. F. Rider, "Status of Fission Yield Evaluations," to be published in the Proc. of the Specialists' Meeting on "Yields and Decay Data for Fission Product Nuclides," October 24-27, 1983 (sponsored by the OECD/NEA Nuclear Data Committee).

UNIVERSITY OF LOWELL

A. NEUTRON SCATTERING CROSS SECTIONS IN THE ACTINIDES

(L.E. Beghian, G.H.R. Kegel, J.J. Egan, A. Mittler, J.Q. Shao, G.C. Goswami and C.A. Ciarcia*)

1. Ground State Rotational Bands of Th-232 and U-238

Differential neutron elastic and inelastic scattering cross sections have been measured at 125° for the ground and first two excited states of Th-232 and U-238 (Th-232, E_x = 0, 49, 162 keV; U-238, E_x = 0, 45, 148 keV) using the time-of-flight technique. The U-238 measurements completed in the past year cover the incident neutron energy range 500-900 keV in 40-keV steps thus spanning the region between our 200 to 500-keV data referred to in our 1983 Report and our earlier 900 to 3100-keV measurements.[1]

The Th-232 measurements were also made at 40-keV intervals up to 900-keV completing the work which as of the last report extended from 200 to 500 keV. In addition we have carried out measurements on these same three states in Th-232 in 100-keV steps from 900 to 2500 keV paralleling our higher energy U-238 work. Figure A-1 shows a typical time-of-flight spectrum demonstrating the resolution of our spectrometer. The flight path for this spectrum was 3m and the data acquisition time was 14 hours.

We have also measured angular distributions for these first three states in Th-232 and U-238 at 520-keV incident neutron energy.

2. States in Th-232 and U-238 Above 650 keV

These measurements which were undertaken in three phases have now been completed. The three phases corresponded to optimization of the spectrometer for detection of scattered neutrons in three energy regions. (i.) This phase, corresponding to 200 to 400-keV scattered neutron energies, was completed in 1982 and included in last year's report. (ii.) This phase, where we made measurements for scattered neutrons in the 400-800 keV range for states up to 1550 keV in excitation in Th-232 and U-238 at bombarding energies up to 2.0 MeV in 50-keV steps was completed in 1983. Last year's report included measurements in 100-keV steps and we have since filled in the intermediate points.

---

*Present address: Dept. of Physics, Rochester Institute of Technology, Rochester, NY 14623

[1]L.E. Beghian, G.H.R. Kegel, T.V. Marcella, B.K. Barnes, G.P. Couchell, J.J. Egan, A. Mittler, D.J. Pullen and W.A. Schier, Nucl. Sci. and Eng. 69, 191 (1979).

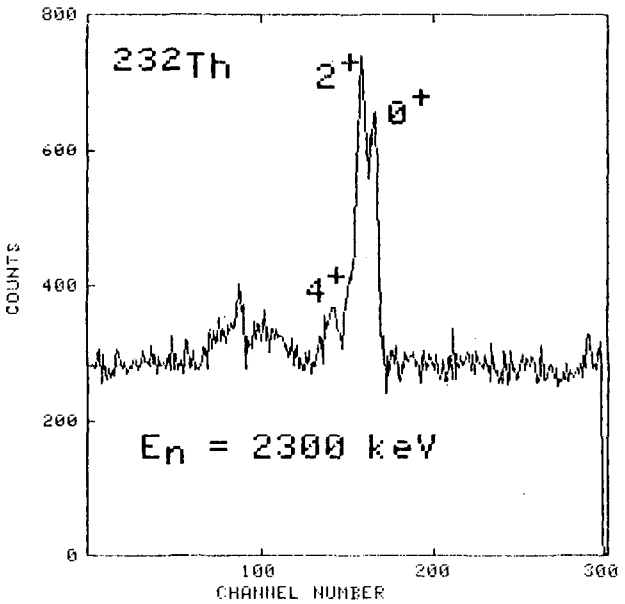

Fig.A-1. Time-of-flight spectrum for Th-232 showing neutron groups for the ground and first two excited states at 49 and 162 keV.

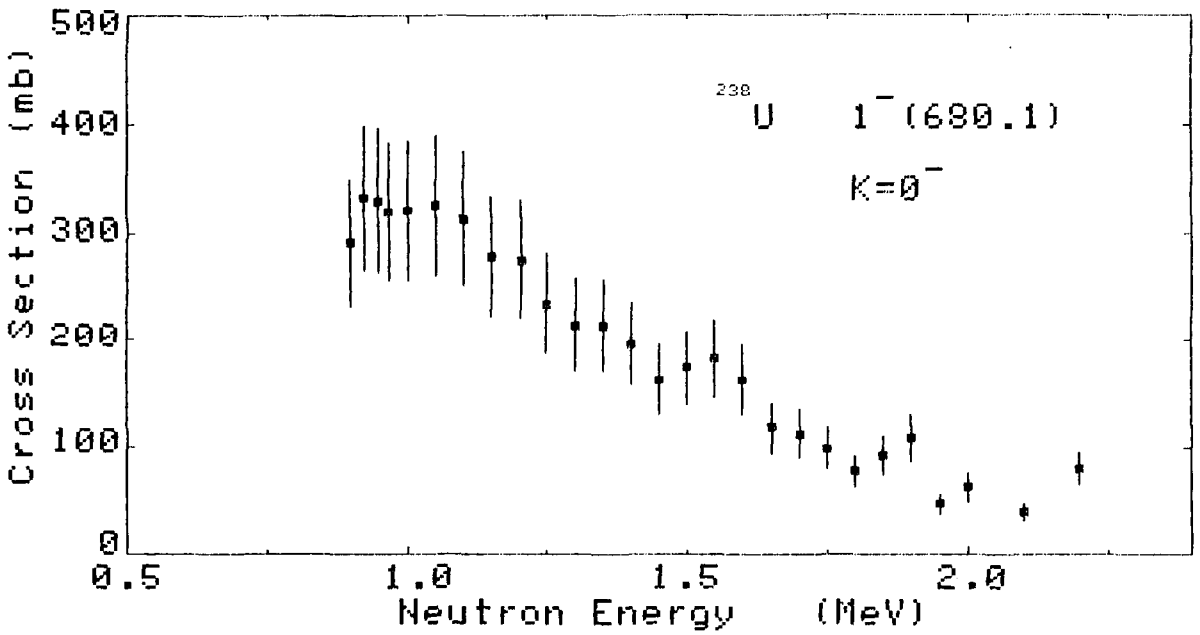

Fig.A-2. Neutron inelastic scattering cross section for the 1^- state at 680 keV in ^{238}U.

(iii.) These data were taken for 800 to 1500-keV scattered neutron energies for incident energies in the range 1.7 to 2.2 MeV yielding cross sections for states in the 700 to 1200-keV excitation energy range.

Figure A-2 shows our results for the 680 keV, 1^- state in U-238, where we have combined data from all three phases of the experiment. The integrated cross section was obtained from the 125° differential data

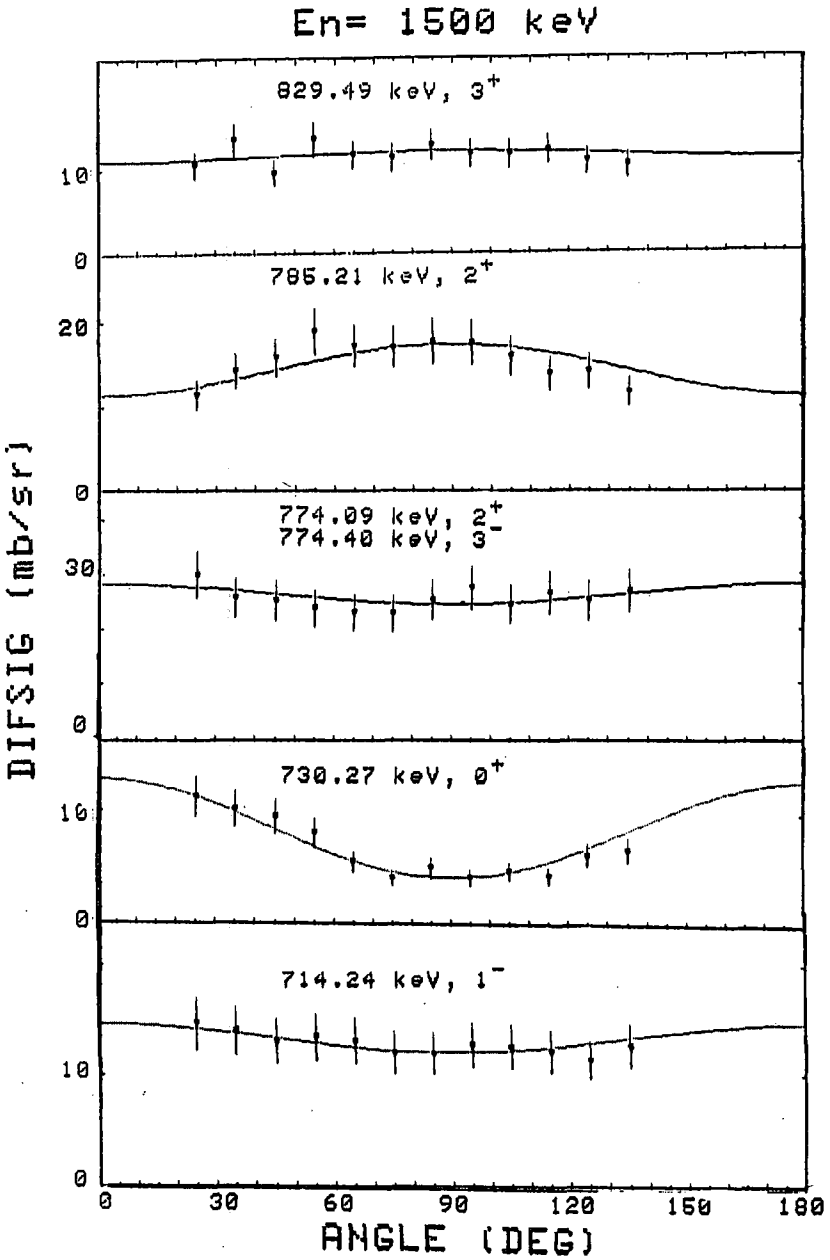

Fig.A-3. Th-232 angular distribution at 1.5 MeV.

by multiplying the latter by 4π. This procedure appears to be justified based on Legendre polynomial fits to angular distribution data where only terms of $\ell = 0$ or 2 are needed at all but the highest energies (i.e. above 2 MeV) where an asymmetry becomes perceptible for some states.

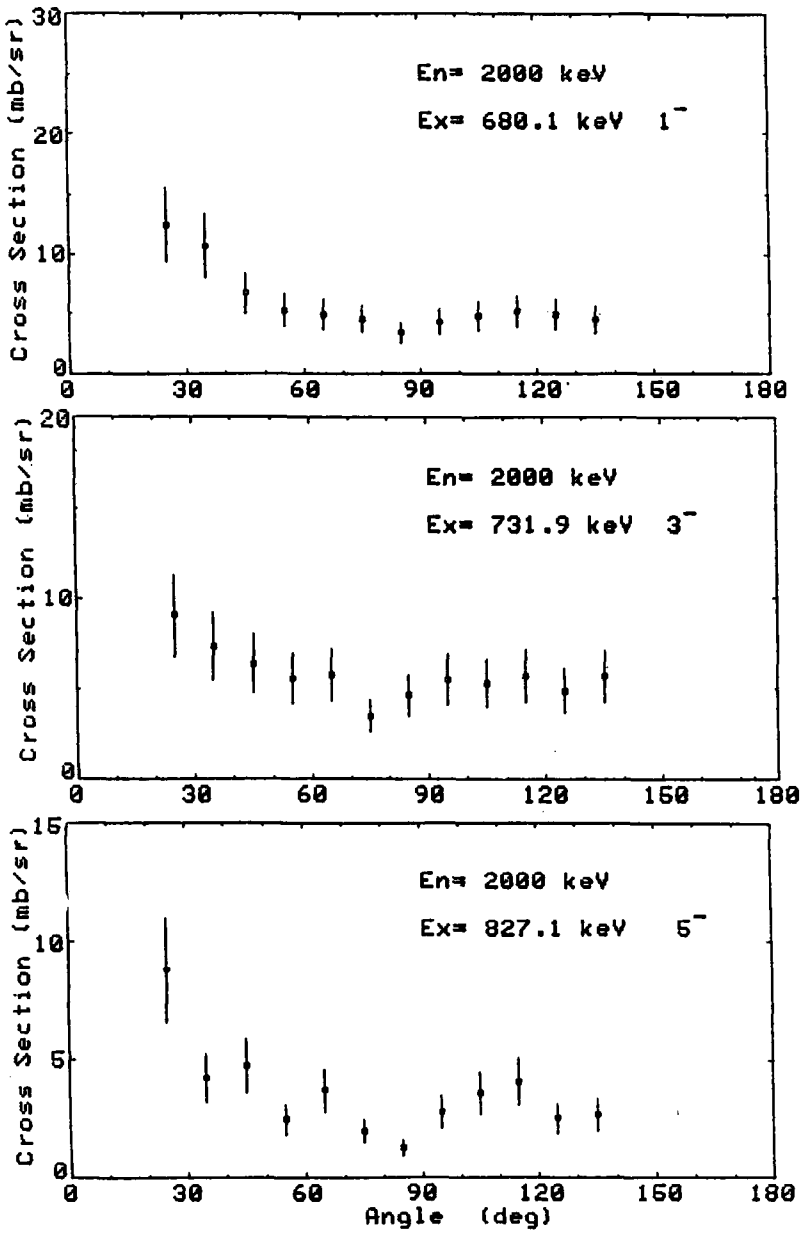

Fig.A-4. U-238 angular distribution at 2.0 MeV.

We have measured neutron inelastic scattering angular distributions at 1.2, 1.5 and 2.0 MeV for five states in Th-232: 714, 730, 774, 785 and 829 keV; and at 1.5 and 2.0 MeV for nine states in U-238: 680, 732, 827, 928+931, 950, 966, 993, 1037 and 1060 keV. Fig.A-3 shows the Th-232 angular distributions at 1.5 MeV where the curves through the data are Legendre polynomial fits including only $\ell=0$ and $\ell=2$ terms. Fig.A-4 shows our results at 2.0 MeV for three states in U-238.

3. U-235 Measurements

We have initiated, in February 1984, a series of measurements of the U-235 elastic and inelastic cross sections starting at an incident neutron energy of 200 keV, using a disk-shaped metallic scatterer similar to the U-238 and Th-232 samples. We plan to investigate cross sections for states below 1 MeV in excitation in the coming year.

THEORETICAL CALCULATIONS OF LEVEL CROSS SECTIONS FOR INELASTIC NEUTRON SCATTERING ON THE PRINCIPAL EVEN-MASS ACTINIDE NUCLEI (TH-232, U-238, PU-240 AND PU-242). (E. Sheldon)

As foreshadowed in the previous (1983) Report to the DOE Nuclear Data Committee, the primary emphasis in the computation of level cross sections for inelastic neutron scattering to individual collective (rotational or vibrational, quadrupole or octupole) levels of the even-A actinide nuclei Th-232, U-238, Pu-240 and Pu-242 has progressed from the evaluation of angle-integrated cross sections and the generation of level excitation functions to the calculation of differential cross sections for the determination of level angular distributions, as a basis for the analysis of experimental data measured by the Lowell group. The previous Report outlined the sequence of developments in this theoretical effort, contrasting the findings from the "standard" (CN + DI) approach with those derived from the statistical S-matrix formalism of Tepel, Hofmann, Weidenmuller, et al.[1]

Meanwhile, in an invited paper[2] prepared for presentation at the Sixth Soviet National Conference on Neutron Physics (Kiev, USSR, October

---

[1]J.W. Tepel, H.M. Hofmann and H.A. Weidenmuller, Phys. Letters 49B, 1 (1974); H.M. Hofmann, J. Richert, J.W. Tepel and H.A. Weidenmuller, Ann. Phys. (NY) 90, 391 & 403 (1975); H.M. Hofmann, T. Mertelmeier, M. Herman and J.W. Tepel, Z. Phys. A 297, 153 (1980).

[2]E. Sheldon, "Fast Neutron Inelastic Scattering Cross Sections for Actinide Nuclei", prepared for publication in the Proceedings of the Sixth Soviet National Conference on Neutron Physics, Kiev, USSR, October 10-17, 1983.

10-17, 1983) the excitation-function and angular-distribution theoretical data, derived from both formalisms and corrected for the effects of level-width fluctuations as well as for fission and radiative capture competition, were contrasted against the experimental values determined by the Lowell group for Th-232 and U-238. The comparison indicated generally good to excellent agreement. However, international circumstances at that time in the wake of the Korean airliner incident precluded participation in the meeting and terminated contact with its organizers. Consequently, these results together with those for all four above nuclei presented at the 1982 Cambridge International Conference on The Neutron and its Applications and subsequent unpublished data were recompiled into a comprehensive survey designed to be published as a single paper in the Journal of Physics. During this recompilation, an error in the DI computer program "KARJUP" became evident, however, necessitating the re-evaluation of the entire batch of "standard" (CN + DI) data, and this has occupied the recent past months. It is now almost completed, and work has begun on assembling this body of information into tabulations and figures that will be transmitted to neutron data banks and built into a set of three review papers[3-5] that will replace the previously submitted material. It will include all of the past analyses, together with some new angular distribution data for Th-232 and U-238 that supplement the recent reports by Haouat et al.[6] (Bruyeres-le-Chatel), and Hodgson and Kobos[7] (Oxford).

The latest findings are also intended for presentation at international meetings later this year (e.g., the 1984 Europhysics Study Conference on Nuclear Reactions, Crete, June 24-30, and the XVI. Polish Summer School in Nuclear Physics, Mikolajki, August 27 - September 8) and will be amplified in preparation for the 1985 International Nuclear Data meeting (Santa Fe). As additional experimental data become available, the theoretical calculations will be extended to cover new findings. A dynamical approach to the underlying formalism is also being studied.

---

[3]E. Sheldon, "Fast Neutron Inelastic Scattering Cross Sections for Actinide Nuclei: I. ^{232}Th(n,n')", in preparation for submission to J. Phys. G - Nucl. Phys.
[4]ibid. : II. ^{238}U(n,n').
[5]ibid. : III. $^{240\ 242}$Pu(n,n').
[6]G. Haouat, J. Lachkar, Ch. Lagrange, J. Jary, J. Sigaud and Y. Patin, Nucl. Sci. Eng. 81, 491 (1982).
[7]P.E. Hodgson, "The Inelastic Scattering of Neutrons by Uranium-238", Nuclear Physics Laboratory Report 65/82 (October, 1982), University of Oxford (unpublished); P.E. Hodgson and A.M. Kobos, submitted to Nucl. Sci. Eng. (1984).

C. DELAYED-NEUTRON MEASUREMENTS

(G.P. Couchell, W.A. Schier, D.J. Pullen, M.N. Haghighi, N.M. Sampas, Q. Sharfuddin and R.S. Tanczyn)

Delayed neutron spectra were measured on the University of Lowell 1-Mw swimming-pool reactor with ^{235}U fission induced by thermal neutrons. Fission fragments were transferred to a low background environment using a helium jet fast transfer system. Delayed neutrons were detected by 4 4-1/2" diameter Pilot U plastic scintillators. The neutron time-of-flight (TOF) technique employing beta-neutron correlations was used to suppress random background and to measure the energies of delayed neutrons over the range 0.1 - 2.0 MeV. Spectral measurements were taken over eight successive delay time intervals ranging from 0.17 to 85 seconds. Details of this work will appear in three papers which will be published in the Proceedings of the International Symposium on the Use and Development of Low and Medium Flux Research Reactors, M.I.T., Cambridge, MA, Oct. 16-19, 1983.

The spectra measured for the two shortest delay time intervals, 0.17-0.37 s and 0.41-0.85 s, represent the only composite delayed-neutron measurements to date that provide information on the energy spectra of the two shortest lived groups having half-lives of 0.2 and 0.6 s. For measurements involving short delay times, it is important that the time response function of the helium jet transfer system be accurately known. The University of Lowell 5.5 MV Van de Graaff accelerator was used for these measurements. A thick ^{7}Li target was bombarded with protons and neutrons generated by the $^{7}Li(p,n)$ reaction irradiated the ^{235}U foil lining the fission chamber. Timing information was provided by interrupting the proton beam with a mechanical beam chopper, which consisted of a rotating tantalum cylinder having two opposite-facing rectangular apertures. Thus, pulses of fission fragments were created by each neutron pulse generated by the chopped beam. These fragments were then transferred to a beta detector by the helium jet and tape transport systems.

The time distribution of the transferred fission-product beta activity was measured using a multi-channel analyzer in multiscaling mode, with sweep triggering provided by a beam current pick-up signal from the target. The neutron-burst time profile was also similarly measured using a BF_3 proportional counter positioned near the fission detector to monitor the neutrons.

The helium jet time response function has been determined for the 14-m capillary length used for all the longer delay time intervals and for the 4.6-m capillary used for the two shortest delay times. These are shown in Fig.C-1. The response function (Fig.C-1b) had a mean transfer time of 0.83 s with a time spread of 0.43 s with the 14-m capillary. To optimize measurements for the shorter lived groups, the shorter 4.6-m

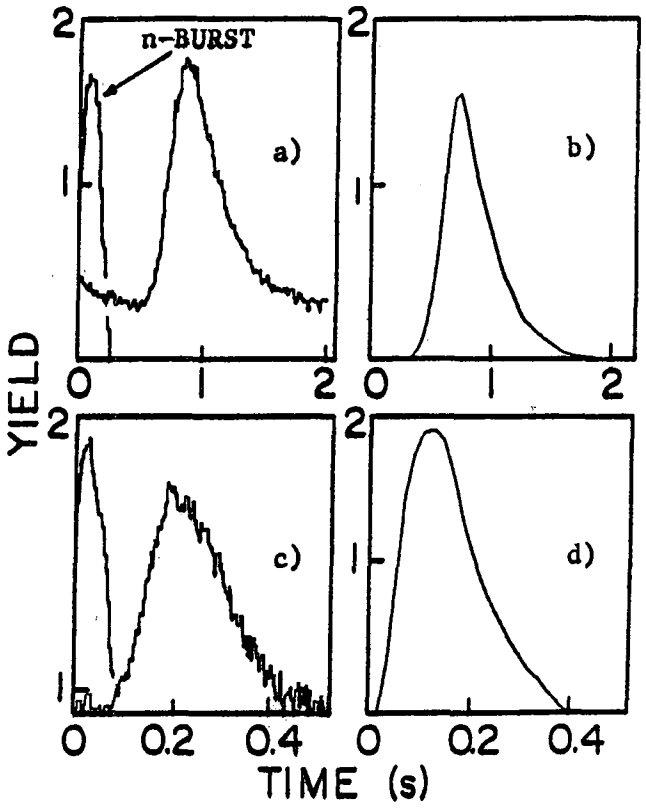

Figure C-1. Time distribution of transferred beta activity and corresponding transfer system response function for 14-m capillary (a and b, respectively) and 4.6-m capillary (c and d, respectively).

long two-stage capillary was employed. In this case (see Fig.C-1d) the mean transfer time was just 0.16 s with a time spread of only 0.15 s.

The delayed-neutron energy spectra derived from the Pilot U measurements have been compared with spectra constructed from the recent Studsvik[1] compilation. The latter is based on spectra determined for individual precursors. There is generally good agreement in the gross shape of the spectrum for each of the eight delay time intervals studied; furthermore, there is similarity in much of the detail structure. One noteworthy difference in the two data sets is the consistently larger fraction of high energy neutrons ($E_n > 0.8$ MeV) determined from our TOF studies than reported in the Studsvik spectra based on ^{3}He spectrometer measurements.

---

1. G. Rudstam, Nucl. Sci. Eng. 80, 238 (1982).

During the last few months we have investigated a possible source of this discrepancy. A typical time-of-flight spectrum has the delayed neutrons superimposed on a random, nearly isotropic background with an intense gamma peak from β-γ coincidences to the right of the neutrons. Knowing the precise shape of this gamma peak is important, particularly on the delayed-neutron side because a tail on the gamma peak could be mistaken for high-energy neutrons. A very small percentage of the coincidences may arise from "delayed" gammas if an isomeric state is populated in a beta decay. This would give rise to a tail on the gamma peak which could extend beneath the delayed neutrons.

To obtain the gamma-peak shape in the Pilot U measurements, we placed 15 cm of paraffin at the beta detectors and in the neutron flight path. All other conditions remain the same; namely, the fission fragments are once again transferred to the tape and the tape speed is set to give the same delay-time intervals after fission. When this gamma peak is normalized and superimposed on our delayed neutron spectrum, the shape of the peak with its Compton back-scattering shoulder is well reproduced.

We have now reanalyzed the spectrum determined for the delay time interval 2.1-3.9 seconds, using the above procedure for subtracting the contribution of the β-γ coincidences from the TOF spectrum. The delayed-neutron energy spectrum is plotted in Fig. C-2 as a solid curve. This revised spectrum has fewer high energy neutrons, particularly above 1.5 MeV. Even though this spectrum has more neutrons above 1 MeV than the Studsvik data, much better agreement has been achieved in this region, with the present discrepancy falling within the experimental uncertainties of the two measurements. A similar gamma-ray tail subtraction procedure will be applied to the spectrum for each of the eight delay times previously reported. A similar reduction in the spectra above E_n = 1.0 MeV is quite likely.

We are now extending these measurements to lower neutron energies by introducing Li-6 loaded glass scintillators as neutron detectors in our TOF spectrometer. Because of their lower detection efficiency for neutrons, they are positioned only 15 cm from the transport tape bearing delayed-neutron precursors, whereas a 50-cm flight path was used with the Pilot U detectors. At this distance the system is sensitive to neutrons with energies as low as 10 keV, thus affording a ten-fold reduction in the low energy threshold of our delayed-neutron spectrometer.

The delayed-neutron energy spectrum derived from the Li-6 glass TOF spectrum is shown as a dotted curve in Fig.C-2. The excellent energy resolution of the system for low energy neutrons is indicated by the sharp structure observed in the region below 100 keV. It is satisfying to observe the agreement between the two measurements in the region 100-500 keV where both Li-6 glass and Pilot U have good neutron

sensitivity. In particular the position and shape of most of the detailed structure match very well. The agreement is rather remarkable considering the vastly different flight paths used in the two measurements; the resulting difference in flight-path dispersion does introduce additional broadening of some of the structure in the Li-6 glass spectrum above 100 keV. The Li-6 glass measurements which are now underway will enable us to determine the shapes of composite delayed-neutron spectra to energies as low as 10 keV with greater reliability and better energy resolution than has hitherto been possible.

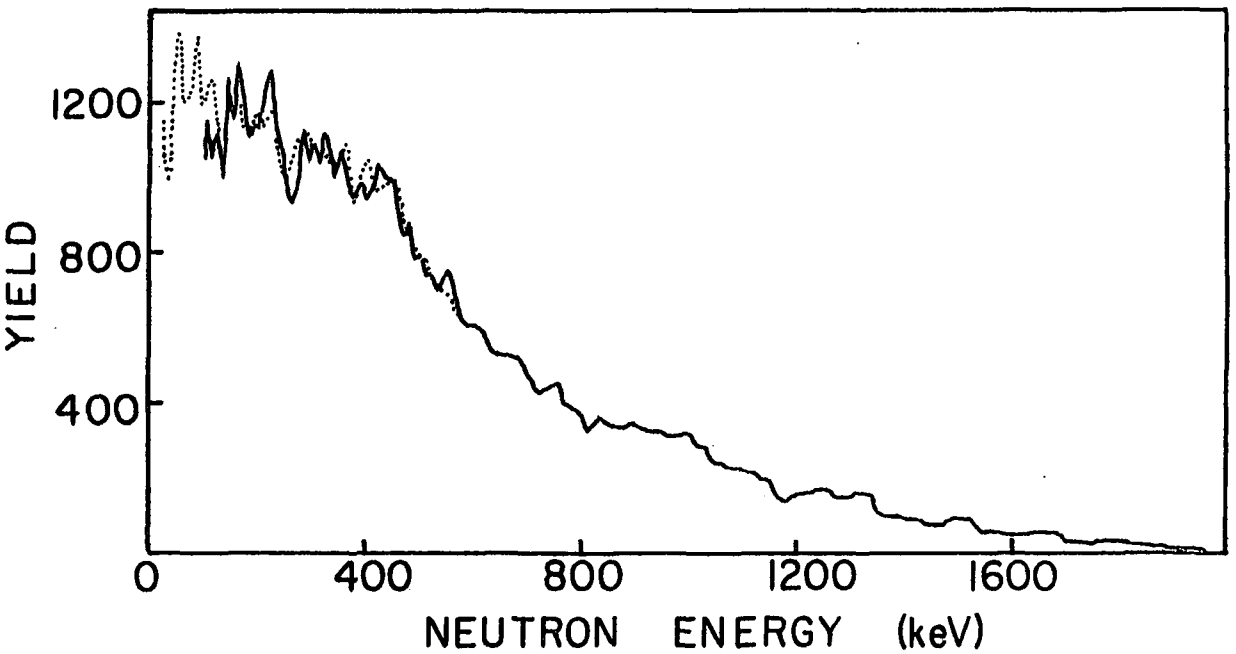

Fig.C-2 A delayed neutron energy spectrum from the fission of ^{235}U in the delay-time interval 2.1 to 3.9s. The solid curve is derived from a TOF measurement with Pilot U scintillators at a 50 cm flight path. The dotted curve is from a TOF measurement with ^{6}Li-glass scintillators at a 15 cm flight path.

THE UNIVERSITY OF MICHIGAN
Department of Nuclear Engineering

A. INTRODUCTION

The cross section project at The University of Michigan is continuing activities in two major experimental areas. The first is oriented around the extensive facilities developed over the past decade for the irradiation, handling, and calibration of a series of photoneutron sources ranging in energy from 23 to 964 keV. These activities are housed in the Phoenix Memorial Laboratory, adjacent to the Ford Nuclear Reactor, and make use of a one-meter diameter manganese bath and a low-albedo neutron irradiation laboratory. The second area centers about our newly established laboratory for cross section measurements using a 14 MeV neutron generator. These facilities are located in the Neutron Experimental Bay, formerly the site of the University of Michigan 83-inch cyclotron. This location provides a near-ideal environment in which the neutron source can be operated in a shielded laboratory of large dimensions to minimize the experimental complications from room-scattered neutrons. Extensive counting facilities have also been developed in conjunction with both laboratories.

B. CAPTURE CROSS SECTIONS OF Th-232 AND U-238 (S. Wilderman, E. Quang, G. Knoll)

The photoneutron facilities are now being employed to extend our previous measurement[1] of the thorium capture cross section at 23 keV to the remaining energies (up to 964 keV) provided by our available sources. The experimental procedures followed in our work involve a unique radiochemical separation of the induced Pa-233 activity from the much larger natural activity of the thorium target. The availability of an accurately assayed Np-237 foil from our previous fission work provides a convenient and precise reference source of its Pa-233 daughter product. This reference source obviates the need for an efficiency determination for the gamma ray detectors used in the activity measurements. The separation yield is monitored through the use of a small amount of accelerator-produced Pa-232 as a tracer. The entire activity determination can thus be reduced to a small number of ratio measurements that can be carried out to high precision. Because the remaining photoneutron sources are much weaker than the Sb-Be source employed in the earlier work, we are developing counting techniques of much higher sensitivity than the germanium spectrometer used previously. Our scoping calculations indicate that the thorium measurements can be expected to have an estimated error

---

1. G. Baldwin and G. Knoll, Proc. of the NEANDC/NEACRP Specialists' Meeting on Fast Neutron Cross Sections, ANL-83-4, pp. 302-311 (1983).

of about 3 to 4% at each of the three photoneutron source energies (265, 770, and 964 keV from Na-D, La-Be, and Na-Be).

Because of the large remaining uncertainties in the U-238 capture cross section in the keV region, we are also beginning preliminary experiments aimed at extending the experimental techniques developed for thorium target to U-238. Preliminary plans are to expose targets of hundreds of grams of U-238 to the photoneutron flux, followed by subsequent radiochemical separation of the induced Np-239 activity with its 2.35-day half life. High-resolution gamma ray spectroscopy will be used to determine the purity of the separated sample, but low-resolution counting will be used to enhance the counting efficiency. As in the thorium measurements, a tracer technique (possibly using Np-237) will be needed to accurately quantify the separation yield.

C. FISSION CROSS SECTIONS AT 14 MEV (H. Agrawal, K. Zasadny, G. Knoll)

We have previously reported[2] on measurements of the U-235 and Pu-239 fission cross sections at 14 MeV. We have now extended these measurements to include U-233 and Np-237 using existing target foils which have been previously documented as part of our photoneutron cross section work. In addition, a U-238 target has also been obtained from ORNL and applied in these measurements. As in the past, all of these fission measurements have used the track etch recording technique to quantitatively determine the fission fragment yields in a restricted solid angle geometry. The number of tracks in small subdivisions of each film are then manually counted and recorded. While other less tedious counting techniques are feasible, we have retained these methods because of our extensive past experience with the approach and our confidence in the high level of precision attainable in low-geometry track registration. Each film is manually counted by two independent scanners who keep a detailed map of the counts per unit area. These data are then intercompared and any discrepancies resolved by subsequent recounting of the subsection in question.

Because of our use of restricted solid angle counting, an absolute determination of fission yield requires information on the angular distribution of fission fragments. We have also undertaken a series of these angular distribution measurements at 14 MeV using the track-etch recording technique to register the angular yield from each of our fission targets. Results have been presented[3] for U-235 and Pu-239, and data are being processed for U-233, Np-237, and U-238.

---

2. Mahdavi, Knoll, and Robertson, Proc. of Int. Conf. on Nuclear Data of Science and Technology, Antwerp, pp.58-61 (1983).

3. Mahdavi, Knoll, and Robertson, Trans. Am. Nucl. Soc. 44, 532 (1983).

D. NEUTRON CAPTURE AND CHARGED PARTICLE PRODUCTION REACTIONS AT 14 MeV

(H. Agrawal, K. Zasadny, Y. Lai, G. Knoll)

The extensive facilities developed for 14 MeV neutron measurements are being turned from our previous fission emphasis to the determination of neutron-induced capture and charged particle production reactions. We have selected a series of such reactions of greatest interest as standards or because of their importance in fusion reactor design, fast neutron dosimetry, or other technological applications. Work is now underway on the first three such reactions chosen for our initial effort:

^{59}Co(n,alpha)^{56}Mn

^{64}Zn(n,2n)^{63}Zn

^{52}Cr(n,p)^{52}V

Our initial measurements are being carried out by measuring the neutron flux relative to the Fe-56(n,p) cross section. However, we plan to supplement this approach by using a proton recoil telescope of unique design now under development. In this design, the effect of uncertainties in the n-p scattering angular distribution at 14 MeV are minimized through a geometric design similar to that employed in our previous measurement[4] of the Li-6(n,alpha) cross section.

Activity determinations are carried out using the 4-pi beta-gamma coincidence system described in our previous measurements[5] on In-115. In some instances, we will also be employing high-resolution germanium gamma ray spectroscopy and/or other counting techniques to provide independent verification of induced activities.

Because we are employing thick tritium targets, there is some uncertainty in the median neutron energy under different experimental conditions. We are therefore conducting regular measurements of the effective neutron energy using a technique[6] that is based on irradiation of a thick fully-depleted silicon detector. The shift in the apparent position of the neutron-induced peaks in the spectrum recorded from this detector during neutron irradiation at 0° and 90° is used to deduce the neutron energy at the irradiation position.

---

4. Engdahl, Knoll, and Robertson, Nucl. Sci. and Eng. 78, 44-52 (1981).

5. Grady, Knoll, and Robertson, Proc. of the NEANDC/NEACRP Specialists' Meeting on Fast Neutron Cross Sections, ANL-83-4, 179-185 (1983).

6. T. B. Ryves and K. J. Zieba, Nucl. Instr. and Meth. 167, 449-453 (1979).

A. NEUTRON DATA MEASUREMENTS AND DETECTORS

1. Determination of the Area of the Collimator Used in Absolute Flux Measurements (A. D. Carlson, R. G. Johnson)

Three recent neutron data measurements at NBS depend on the area of the collimator located at the 200 m flight path of the NBS linac facility. Considerable effort was applied to obtain an accurate area of this collimator (~ 1/2 inch diameter) which defines the size of the neutron beam striking the neutron flux detector. It was found that conventional optical techniques for collimator alignment over the great distance involved are not reliable even when the alignment is done at night (with the beam tube windows removed) when apparent thermal equilibrium has been obtained. The collimator was made by a company which produces gun barrels which are "straight" to 0.002 cm in 30 cm. It was determined that the collimator did not meet these specifications. The effective area of the collimator as it was positioned for the neutron flux measurements was accurately determined by taking x-ray radiographs with the film carefully positioned near the collimator. The x-ray source for these exposures was the bremsstrahlung obtained by using the same target and electron beam from the linac as was used for the cross section measurements. By making the radiographs in this manner, the measured effective area includes small penumbra corrections which must be used for the neutron flux determination. Radiographs were made with no filters and with 1/8 inch of uranium in the beam. The results from these two types of measurements are in agreement.

For each film the optical density (which was converted to intensity) was determined as a function of position with analog and digitizing scanning microdensitometers. Both the length and optical density scales were calibrated for each of the systems used. Good agreement was obtained for each of the densitometers. The overall accuracy of the effective area determination is ~ 0.2%.

2. Absolute Measurements of the $^{235}U(n,f)$ Cross Section for Neutron Energies from 0.3 to 3.0 MeV (A. D. Carlson, J. W. Behrens)

The analysis of the data from this experiment is now nearing completion. The measurement was performed at the NBS Neutron Time-of-Flight facility. The neutron flux was measured at the 200 m experimental station with a black detector in conjunction with the collimator described previously in this report. The fission chamber reaction rate measurements were made on the same beam line at 69 m from the neutron target. Comparisons are now being made of the measured black detector pulse height distributions as a function of neutron energy versus those calculated with a Monte Carlo technique. The individual data sets obtained in this experiment are now being compared and will be combined to yield the final fission cross section results.

3. An Absolute Measurement of the ^{235}U Fission Cross Section for Neutron Energies from 2 to 6 MeV (M. S. Dias,* R. G. Johnson, A. D. Carlson, O. A. Wasson)

The dual thin scintillator (DTS) neutron detector[1] has been developed as a neutron flux monitor for neutrons in the 1-20 MeV range. As an application of this detector, it was used as the flux monitor for a measurement of the ^{235}U fission cross section over the 2 to 6 MeV range. The measurement used the same physical and electronic setup as used in the experiment described in Section 2. Analysis of the data obtained in this measurement is nearly complete. Since this measurement and that described in Section 2 share much in common, many of the corrections required are the same and are being determined concurrently [see especially Section 1].

4. ^{252}Cf Fission-Spectrum-Averaged ^{235}U Fission Cross Section (I. G. Schröder, Li Linpei,** C. M. Eisenhauer, D. M. Gilliam, E. D. McGarry)

A new measurement of the ^{252}Cf fission-spectrum-averaged ^{235}U fission cross section has been completed together with an extensive study of neutron room return.[2] This new measurement yields a value of 1218 mb. Error components such as those involved in the determination of the fissionable deposit masses, the absorption of fission fragments in the deposits and the separation between the deposits have been evaluated in terms of improvements associated with this new measurement. Furthermore, the influence of neutron scattering in the source capsule, support structures, the fission chamber and in the deposit backing have been thoroughly analyzed. A preliminary estimate of the total error for the new determination is ± 2% at the one standard deviation level. It is expected that the final error will be about one third less.

---

* Ph.D. student from the Instituto de Pesquisas Energéticas e Nucleares - São Paulo - Brazil.

** Visiting scientist from the National Institute of Metrology, Beijing, Peoples Republic of China.

[1] Dias, Johnson, Wasson, Nucl. Instr. and Meth., to be published.

[2] Li Linpei, Radiation Protection Dosimetry, to be published.

5. Measurement of the Efficiency of the Black Neutron Detector at 2.3 MeV (K. C. Duvall, A. D. Carlson, W. E. Slater, O. A. Wasson)

A measurement of the black neutron detector efficiency at 2.3 MeV is being carried out with the use of the associated particle method and the D(d,n)^{3}He source reaction. The black detector is operated in coincidence with associated particles detected at 45° in a silicon surface barrier detector. The utilization of a more forward associated particle detection angle allows the more kinematically energetic ^{3}He particles to be readily distinguished from scattered deuterons using foil absorption. The calculated efficiency for the black detector is determined with a Monte Carlo code and has been compared to values obtained from associated particle measurements below 900 keV. The measurement of the black detector efficiency at 2.3 MeV will be used to verify the usefulness of the Monte Carlo calculation at the higher neutron energies. The black detector is being utilized as the primary neutron flux monitor in the absolute measurement of the ^{235}U(n,f) cross section from 0.3 to 3.0 MeV.

6. International Intercomparison of Neutron Flux Measurement Capability (A. D. Carlson, R. G. Johnson, K. C. Duvall, O. A. Wasson)

The NBS has participated in a new international intercomparison of neutron flux measurement capability sponsored by the International Bureau of Weights and Measures (BIPM). The intercomparison which will include eight international laboratories is by means of a large ^{235}U fission ionization chamber which was supplied by the Harwell laboratory. This chamber design allows both linac and Van de Graaff neutron facilities to participate whereas only Van de Graaffs participated in previous tests. NBS was the first laboratory to complete the measurements which were done at a neutron energy of 500 keV on both the linac and Van de Graaff using the Black Detector flux monitor. The good agreement in detector efficiency measured at the two facilities will further refine the analysis of the systematic errors involved in neutron standards measurements at NBS. A useful by-product of this intercomparison will be a new international measurement of the ^{235}U(n,f) cross section with a common ^{235}U deposit.

7. Development of a ^{3}He Gas Scintillation Detector (J. W. Behrens, R. G. Johnson, A. D. Carlson)

A prototype detector was developed to establish the ^{3}He(n,p)T reaction as a useful standard cross section in the keV and MeV neutron energy regions. The gas scintillation detector consists of a 2 atmosphere He-Xe gas mixture in a 11 cm diameter by 25 cm length cylindrical volume. The light is viewed through glass windows by two photomultiplier tubes positioned at opposite ends of the cylinder. Using the facilities at Duke University a diphenylstilbene wavelength shifter was evaporated onto the inside of the windows to convert the ultraviolet light emitted by the scintillating gas into the visible region to which the photomultiplier

tubes are sensitive. The response of the detector was measured with thermal neutron beams from the NBS reactor and higher energy neutrons from the linac facility. The light output increased a factor of two as the Xe gas fraction was increased from 5% to 32% in order to reduce the range of the product particles. The spectral resolution, which was nearly constant throughout the central 10 cm, was governed by the statistics of the number of summed photoelectrons from the two tubes (25 keV per photoelectron). The encouraging results obtained from these preliminary studies indicate the potential usefulness of this reaction as a neutron standard.

8. Detector Development for eV Neutron Scattering Studies (R. G. Johnson)

One of the techniques being used to exploit the extension of neutron scattering to the eV energy region is to define the energy of the scattered neutron by a low energy nuclear resonance. To fully exploit this technique requires detectors with high efficiency and good background rejection. Two promising candidates for such detectors are BGO (bismuth germanate) scintillators and HPGe (high-purity germanium) detectors. Simple tests using examples of these detectors were performed at the NBS Neutron Time-of-Flight facility. Recoil scattering from an aluminum sample was detected for two resonances (the 4.905-eV resonance in gold and the 1.457-eV resonance in indium) using both detectors. The BGO scintillator is 5-cm in diameter and 5-cm thick while the planar HPGe detector has an active area of 300 mm^2 and is 5-mm thick. The efficiency at the peak of a resonance was measured to be over 20% for the BGO detector. Although the efficiency of the HPGe detector was less, most of the difference can be ascribed to its smaller area. The HPGe detector had a peak to background ratio of 6.4, in the best case, which was four times better than that for the BGO detector. It appears that a large area planar HPGe detector is the best choice for this application.

9. ^{235}U Foil Mass Measurements (I. G. Schröder, D. M. Gilliam)

Measurements are being performed to determine the mass of two ^{235}U foils made available by the IAEA via Argonne National Laboratory (W. P. Poenitz). These foils have been used at the Khlopin Radium Institute in Leningrad and at the Technical University of Dresden for precise measurements of the 14-MeV-neutron fission cross section of ^{235}U.[3] Alpha decay rates of the samples have been measured by means of low-geometry surface-barrier detector alpha counting. Geometry factors have been determined using standard ^{241}Am (provided by the NBS Radioactivity Section) and ^{237}Np sources previously used in the mass assay of NBS fission foils. The alpha counting will be followed by fission counting and area density uniformity measurements. Finally, a check will be made by a second alpha-decay rate determination.

---

[3] R. Arlt et al. Kernenergie 24, 48 (1979).

10. U-235 Measurement in Waste Material by Resonance Neutron Radiography (R. A. Schrack)

A direct application of nuclear cross section data has been developed at NBS. Resonance neutron radiography has been utilized to determine the amount of U-235 in waste material as a calibration technique for field measurement systems. A matrix of vermiculite simulating in density and atomic weight incinerator ash was inoculated with U-235 in concentrations ranging from 4.8×10^{-4} to 4.6×10^{-3} g/cm^3. Containers ranging in size from two liters to 55 gallons were scanned in a neutron total cross section measurement. The content of U-235 in the sample was determined by measuring the absorption of neutrons by the 8.78 eV uranium-235 resonance line. Figure A-1 shows a typical absorption spectrum. The smooth curve is the best fit to the resonance line at channel 230. The fit is obtained using a Doppler broadened spectrum using ENDF/B-V cross section data for uranium-235. The results obtained for different containers and concentrations are shown in Table A-1. Note that the technique depends only on the knowledge of the neutron total cross section and is not calibrated or normalized. The absolute error of the technique could be considerably reduced by utilizing a calibration technique to reduce the systematic errors.

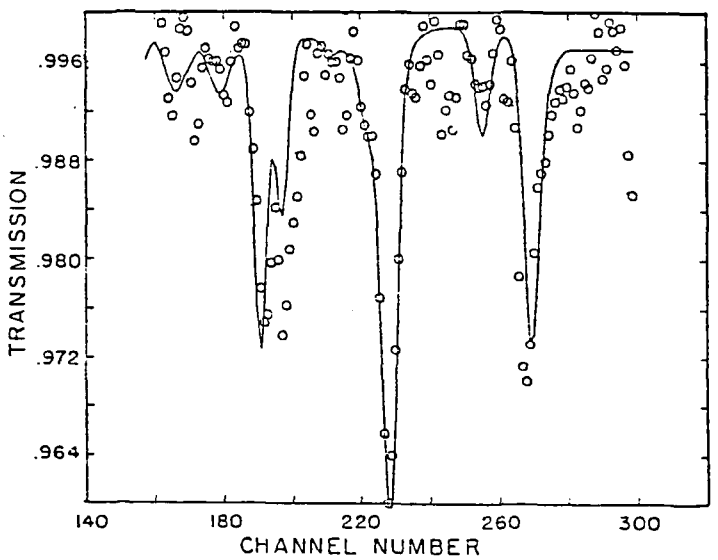

Fig. A-1. Experimental Data and Best Fit for Neutron Absorption in Waste Sample. The smooth curve is the best fit obtained by ENDF/B-V neutron total cross section data for U-235. The amount of U-235 in the sample was determined using the resonance at channel 230.

Table A-1. Summary of Measurements

Container	Total wt U-235 g	Effective Concentration grams/cm^3	Effective Areal Density grams/cm^2	Atoms/barn	Predicted Uncertainty	Observed Uncertainty	Absolute error
2 liter	0.958	4.8×10^{-4}	8.7×10^{-3}	2.2×10^{-5}	10%	16%	9.9%
2 liter	2.901	1.5×10^{-3}	2.6×10^{-2}	6.7×10^{-5}	4.3%	7.2%	6.3%
2 liter	9.219	4.6×10^{-3}	8.4×10^{-2}	2.1×10^{-4}	1.8%	2.5%	2.3%
5-gallon	9.219	8.0×10^{-4}	1.6×10^{-2}	4.1×10^{-5}	4.2%	9.6%	16%
55-gallon	9.219	3.2×10^{-4}	6.2×10^{-3}	1.6×10^{-5}	32%	12%	16%

11. Microchannel Plate Neutron Detector (R. A. Schrack)

A study of the resolution characteristics of the microchannel plate neutron detector was carried out. A Monte Carlo model of the optical performance of the system was developed. Experiments were carried out and measurements of resolution made under four different conditions that were very model-sensitive. These different conditions are described in Table A-2.

Table A-2. Experimental Results

Case	Scintillator Back Surface	Scintillator Thickness (mm)
1	black	0.5
2	white	0.5
3	black	1.0
4	white	1.0

The edge response function of the system was measured with low energy neutrons so that backscattering effects would be minimized. From these measurements the effective line response function and normalized mean displacement $\bar{x}$ were determined as well as the number of photoelectrons detected for each incident neutron. Table A-3 shows the results obtained experimentally as well as the Monte Carlo results for photoelectron number.

Table A-3. Comparison of Photoelectron Numbers for Experimental Data and Adjusted Monte Carlo Results.

Case	Experiment	Monte Carlo
1	96 ± 10	103 ± 1
2	192 ± 19	209 ± 1
3	117 ± 12	103 ± 1
4	207 ± 21	209 ± 1

Table A-4 shows the comparison for $\overline{X}$. The agreement between the Monte Carlo results and the experimental results is acceptable indicating that the model is adequate to describe the system under a wide variety of parameter changes.

Table A-4. Comparison of Resolutions $\overline{X}$ for Experimental Data and Adjusted Monte Carlo Results.

Case	Experiment	Monte Carlo
1	.46 ± .05	.51 ± .01
2	.52 ± .05	.45 ± .01
3	.34 ± .03	.27 ± .01
4	.39 ± .04	.37 ± .01

Figure A-2 shows the edge response function obtained experimentally with a 0.5 mm thick scintillator and white scintillator backing together with the Monte Carlo results shown as a smooth line. The results indicate that the major source of resolution broadening in the system is the fiber optics faceplate. The fiber optic system was designed to work from an air interface. Coupling the faceplate to the lithium glass scintillator with a refractive index of 2.55 produces an optical system that only traps about 25% of the scintillator light. The remaining 75% of the light is then free to scatter in the face plate and produce a large scattered light cone at the photocathode. This analysis indicates that the resolution of the microchannel plate neutron detector could be improved by a factor of 2 if extra-mural absorbers were incorporated in the faceplate to eliminate the 75% scattered photons. A more elegant solution that would preserve all the photons would be to use the lithium glass scintillator in the vacuum system and evaporate the photocathode directly onto the scintillator and remove the necessity of a fiber optic faceplate entirely.

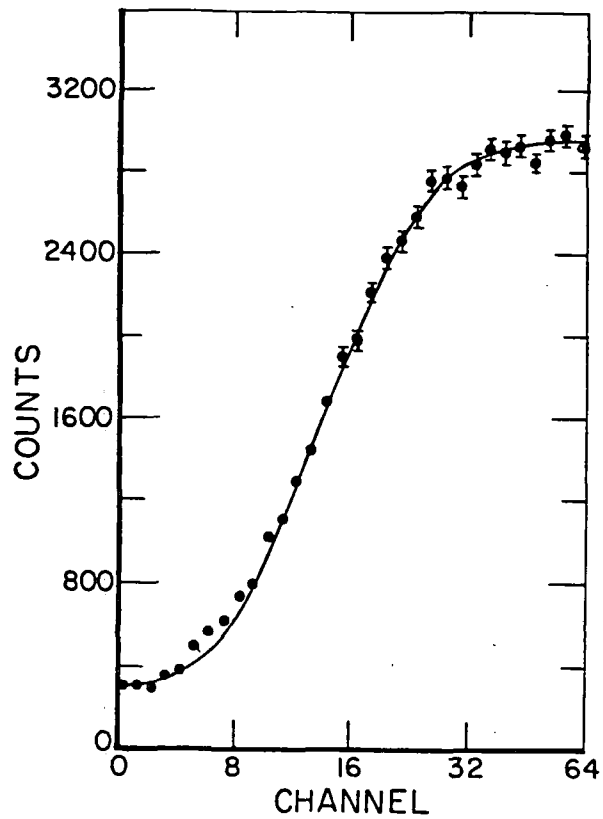

Fig. A-2. Edge response function obtained with a 0.5 mm thick scintillator.

12. Standard Cross Section Data (A. D. Carlson)

A review paper on "Standard Cross Section Data" was completed during this year. This document will be published in a special issue of Progress in Nuclear Eneergy devoted to Cross Section Data for Nuclear Reactor Analyses.[4] The standards paper contains information on the need for standards, properties of standards, applications and measurement techniques for the standards, comparisons of experimental data, comparisons of evaluations, and the status of standards. Light element, capture, and fission standards are considered. Significant effort has gone into graphical plots of recent experimental data and evaluations. A comprehensive bibliography is included.

[4] A. D. Carlson, Progress in Nuclear Energy, to be published.

13. Fission Cross Section Systematics (J. W. Behrens*)

During the past decade considerable effort has been spent in measuring the neutron induced fission cross sections of the actinides in the MeV range. Measured cross sections now exist for over 24 nuclides. However, the half-lives of other important nuclides are too short to allow cross section measurements. Significant progress has been made in inferring these cross sections in the MeV region from the systematics of the neighboring nuclei. It is planned to continue these studies this year. Also, measurements of the cold fission fragments from fission of U-236 will be undertaken.

B. DATA COMPILATION

Photon and Charged Particle Data Center (M. J. Berger, E. G. Fuller, H. Gerstenberg, J. H. Hubbell, S. M. Seltzer)

A program for providing critically-evaluated radiation data in computer-readable form has been initiated by the Photon and Charged Particle Data Center of the Center for Radiation Research. Two such data files, stored on magnetic tape, have recently been prepared. Data file XGAM contains data pertaining to the interaction of x- and gamma rays with atoms and electrons (scattering, photo-electric absorption and pair production cross sections, attenuation coefficients) in the energy region 1 keV to 100 GeV, for all elements with atomic numbers Z=1 to 100. Data file ESTAR contains stopping powers for electrons in 285 materials, and for positrons in 29 materials of dosimetric interest. The information on the tape includes collision, radiative, and total stopping powers, density-effect corrections, ranges, and bremsstrahlung yields.

The first three volumes of the Photonuclear Data-Abstract Sheets,[5] including nuclei up through carbon, have been published. These abstract sheets cover most classes of experimental photonuclear data leading to information of the electromagnetic matrix element between the ground and excited states of a given nucleus. This fifteen volume work contains nearly 7200 abstract sheets and covers 89 chemical elements from hydrogen through americium. It represents a twenty-seven year history of the study of electromagnetic interactions. The sheets are ordered by target element, target isotope, and by an assigned bibliographic reference code. Information is given on the type of measurement, excitation energies studied, source type and energies, detector type, and angular ranges covered in the measurement. For a given reference, the relevant figures and tables are mounted on a separate sheet for each nuclide studied.

---

* Visiting scientist at Bruyeres le Châtel, Jan. to Sept. 1984.

[5] E. G. Fuller and H. Gerstenberg, Photonuclear Data-Abstract Sheets, 1955-1982, Vol. 1 (Hydrogen-Helium), Vol. 2 (Lithium-Boron) Vol. 3 (Carbon); NBSIR 83-2742 (1983).

Tables of relativistic Hartree-Fock-Slater modified atomic form factors have been published.[6] Tabulations are presented of relativistic Hartree-Fock-Slater modified atomic form factors from x = 0 to 100 $Å^{-1}$ for all elements from Z = 1 to Z = 100. These modified form factors represent the atomic Rayleigh scattering amplitudes with good accuracy at energies well above the K-shell binding energies and small momentum transfers and therefore should be used instead of the normal relativistic atomic form factors in the MeV energy range.

---

[6] Schaupp, Schumacher, Smend, Ralhusen, and Hubbell, Small-Angle Rayleigh Scattering of Photons at High Energies: Tabulations of Relativistic HFS Modified Atomic Form Factors, J. Phys. Chem. Ref. Data, Vol. 12, No. 3, 1983.

A. CROSS SECTION MEASUREMENTS

1. Capture and Total Cross Sections

a. Determination of Unbound States of ^{35}S from Neutron Total and Capture Cross Section Measurements on ^{34}S* (R. F. Carlton,** W. M. Good, J. A. Harvey, R. L. Macklin, and B. Castel)

The high neutron resolution capability of the Oak Ridge Electron Linear Accelerator has been used to investigate the unbound region of ^{35}S via neutron resonance spectroscopy studies of the ^{34}S+n system. The total cross section of ^{34}S was measured over the neutron energy range from 90 to 1500 keV, and the capture cross section was measured over the range from 30 to 1100 keV. Analysis of the data yielded spectroscopic factors for the s-states in the unbound region for excitation energies from 7 to 8 MeV. Continuum shell model calculations of the s- and d-states were also performed for both the bound and the unbound regions of ^{35}S. In general, the measured and calculated neutron strengths for s-waves in the unbound region are in reasonable agreement, although the fragmentation of single-particle strength seen experimentally is somewhat higher than that predicted. Core-particle calculations for the p-states in the unbound region of ^{35}S were also performed, and, on the basis of all these results, plus those of others, we have summarized our understanding of the distributions of single-particle neutron strengths in the s-, p-, and d-states of ^{35}S for excitation energies up to 8.5 MeV.

b. Neutron Resonances in ^{70}Zn+n† (J. G. Garg,‡ V. K. Tikku,‡ and J. A. Harvey)

Parameters (E_0, $g\Gamma_n$, J^π, etc.) of the resonances observed in the neutron induced reaction on $^{70}_{30}Zn$ have been determined from 10 keV to about 400 keV using pulsed neutron time-of-flight spectroscopy at ORELA with a neutron burst width of 5 ns and a nominal resolution of 0.07 ns/m at the highest energy. From these results we have obtained the values of average parameters such as $S_0 = (1.51 \pm 0.28)$ and $S_1 = (0.90 \pm 0.10)$ in units of 10^{-4}, $D_0 = (6.82 \pm 0.53)$ and $D_1 = (2.42 \pm 0.23)$ in keV. The experimental data are in excellent agreement with the Wigner distribution of nearest neighbor level spacings and the Porter-Thomas distribution of neutron reduced widths. Good agreement has been also obtained with the $\Delta 3$ statistic of Dyson and Mehta.

---

*Submitted to Physical Review C.
**Middle Tennessee State University, Murfreesboro, Tennessee 37132
†To be submitted to Physical Review C.
‡State University of New York, Albany, New York 12222

c. Solid State Effects on Thermal Neutron Cross Sections and on Low Energy Resonances* (J. A. Harvey, H. A. Mook, N. W. Hill, and O. Shahal)

The neutron total cross sections of several single crystals (Si, Cu, sapphire), several polycrystalline samples (Cu, Fe, Be, C, Bi, Ta), and a fine powder copper sample have been measured from 0.002 to 5 eV. The Cu powder and polycrystalline Fe, Be and C data exhibit the expected abrupt changes in cross section. The cross section of the single crystal of Si is smooth with only small broad fluctuations. The data on two "single" Cu crystals, the sapphire crystal, cast Bi, and rolled samples of Ta and Cu have many narrow peaks $\sim 10^{-3}$ eV wide. High resolution (0.3%) transmission measurements were made on the 1.057-eV resonance in ^{240}Pu and the 0.433-eV resonance in ^{180}Ta, both at room and low temperatures to study the effects of crystal binding. Although the changes in Doppler broadening with temperature were apparent, no asymmetries due to a recoilless contribution were observed.

d. Neutron Spectroscopy as a High Resolution Probe: Identification of the $1/2^+$ state in ^{31}Si** (J. A. Harvey, W. M. Good, R. F. Carlton,† B. Castel,‡ J. B. McGrory, and S. F. Mughabghab¶)

e. Measurements of the Neutron Transmission and Capture Cross Sections in ^{204}Pb,§ (D. J. Horen, R. L. Macklin, J. A. Harvey, and N. W. Hill)

High resolution neutron transmission measurements have been performed on ^{204}Pb in the energy interval E = 0.4-105 keV. The transmission data were analyzed using a multilevel R-matrix code to deduce resonance parameters. Previously obtained neutron capture data were re-analyzed in the interval 2.6-86 keV. Values of $g\Gamma_n\Gamma_\gamma/\Gamma$ were determined from the capture data. For those resonances where Γ_n could be determined from the transmission data, the capture data were analyzed to extract Γ_γ. Our results yield an average capture for a stellar temperature kT = 30 keV of 89.5 ± 4.5 mb. The s-wave density for ^{205}Pb corresponding to the neutron energy range investigated (i.e., E $\sim$ 105 keV) relative to that for ^{207}Pb (which has about the same neutron separation energy) is greater by about a factor of ten. The average s-wave strength function in this energy region is determined as $S_0 = 0.93 \times 10^{-4}$. This is an order of magnitude greater than that for a similar energy region in ^{206}Pb+n where a doorway is observed at E $\sim$ 500 keV. However, the strength function in the initial E = 0-100 keV in ^{204}Pb+n is almost identical to the average value of that for ^{206}Pb+n when the averaging

*Proc. of Int. Conf. on Nucl. Data for Sci. and Tech., Antwerp, Belgium, Sept. 6-10, 1982, p. 961 (1983).
**Phys. Rev. C. 28, 24 (1983).
†Middle Tennessee State University, Murfreesboro, Tennessee 37132.
‡Queen's University, Kingston, Ontario, Canada.
¶Brookhaven National Laboratory, Upton, New York 11973.
§To be submitted to Physical Review C.

interval for the latter is taken as $E_n \approx$ 0-1000 keV (i.e., over the doorway state). This suggests that the s-wave doorway state observed in the higher mass lead isotopes is completely mixed with "background" states in ^{205}Pb, and most likely no intermediate structure will be observed in the s-wave strength function for the ^{204}Pb+n reaction.

f. ^{187}Os + n Resonance Parameters in the Interval 27-500 eV Neutron Energies,* (R. R. Winters,** R. F. Carlton,† J. A. Harvey, and N. W. Hill)

The neutron total cross section for ^{187}Os, in the energy range, 27 eV to 500 eV, has been measured at the ORELA facility by the neutron time-of-flight technique, utilizing a 2.0 gm Osmium sample (n = 0.008401 Os-nuclei/barn) enriched to 70.38% ^{187}Os. Measurements were performed at a 80 m flight station with an energy resolution, $\Delta E/E$, of 0.1% using a ^{6}Li glass scintillator. Resolved resonances have been analyzed by a Reich-Moore multilevel code (SAMMY) to obtain parameters for 85 resonances up to 500 eV. Preliminary determinations of the level spacing (5 eV) and s-wave strength function (3.9×10^{-4}) for ^{187}Os are in agreement with recent analyses of the Osmium isotopes, made in connection with the use of the Re/Os chronometer for estimating the duration of stellar nucleosynthesis.

g. Neutron Capture Cross Sections and Resonances of Iodine-127 and Iodine-129,‡ (R. L. Macklin)

h. Resonance Neutron Capture by ^{35,37}Chlorine,¶ (R. L. Macklin)

Neutron capture by enriched ^{37}Cl and by natural Cl was measured at the Oak Ridge Electron Linear Accelerator (ORELA) as a function of neutron time-of-flight over a 40 meter path. Resonance peaks were fitted by least squares to Breit-Wigner parameters. The energy range covered was 4 to 225 keV for 54 ^{35}Cl resonances and 8 to 151 keV for 12 ^{37}Cl resonances. Corresponding average capture in stellar environments at kT = 30 keV is calculated as (10.0 ± 0.3) mb for ^{35}Cl and (2.15 ± 0.08) mb for ^{37}Cl.

i. Neutron Capture Cross Sections of ^{182}W, ^{183}W, ^{184}W, and ^{186}W from 2.6 to 2000 keV§ (R. L. Macklin, D. M. Drake,△ and E. D. Arthur▲)

---

*Proc. of Int. Conf. on Nucl. Data for Sci. and Tech., Antwerp, Belgium, Sept. 6-10, 1982, p. 943 (1983).
**Denison University, Granville, Ohio 43023.
†Middle Tennessee State University, Murfreesboro, Tennessee 37130
‡Nucl. Sci. Eng. 85, 350-361 (1983).
¶Submitted to Physical Review C.
§Nucl. Sci. Eng. 84, 98-119 (1983).
△Los Alamos National Laboratory, Los Alamos, New Mexico 87545
▲Los Alamos National Laboratory, Los Alamos, New Mexico 87545

j. Neutron Capture Cross Sections of Tantalum from 2.6 to 1900 keV* (R. L. Macklin)

Neutron capture by a tantalum sample was measured at the Oak Ridge Electron Linear Accelerator pulsed neutron time-of-flight facility on a 40-m flight path. Average cross sections for $^{181}Ta(n,\gamma)$ in the energy range from 2.6 to 1900 keV were derived. The partially resolved region from 2620 to 4000 eV was fitted in terms of resonance parameters by least-squares adjustment.

k. Resonance parameters of $^{60}Ni+n$ from measurements of transmission and capture yields from 1 to 450 keV** (C. M. Perey, J. A. Harvey, R. L. Macklin, F. G. Perey, and R. R. Winters†)

l. Overlapping β decay and resonance neutron spectroscopy of levels in ^{87}Kr‡ (S. Raman, B. Fogelberg, J. A. Harvey, R. L. Macklin, P. H. Stelson, A. Schröder¶ and K.-L. Kratz¶)

m. Neutron Capture in s-wave Resonances of ^{64}Ni§ (K. Wisshak,△ F. Käppeler,△ R. L. Macklin, G. Reffo,▲ and F. Fabbri▲)

The neutron capture widths of the s-wave resonances at 13.9 and 33.8 keV in ^{64}Ni have been determined using a setup with extremely low neutron sensitivity completely different from all previous experiments on this isotope. This feature is important because these resonances exhibit a very large scattering to capture ratio. A pulsed 3-MV Van de Graaff accelerator and a kinematically collimated neutron beam, produced via the $^{7}Li(p,n)$ reaction, was used in the experiments. Capture gamma-rays were observed by three Moxon-Rae detectors with graphite-, bismuth-graphite-, and bismuth-converter, respectively. The samples were positioned at a neutron flight path of only 6-8 cm. Thus events due to capture of resonance scattered neutrons in the detectors or in surrounding materials are completely discriminated by their additional time of flight. The short flight path and the high neutron flux at the sample position allowed for a signal to background ratio of ∿1 even for the broad resonance at 33.8 keV. The data obtained with the individual detectors were corrected for the efficiency of the different converter materials. For that purpose, detailed theoretical calculations of the capture gamma-ray spectra of the measured isotope and of gold, which was used as a standard, were performed. The final radiative widths are Γ_γ (13.9 keV) = 1.01 ± 0.07 eV and Γ_γ (33.8 keV) = 1.16 ± 0.08 eV, considerably smaller than the rough estimates obtained in previous work.

*Nucl. Sci. Eng. (in press).
**Phys. Rev. C. 27, 2556 (1983).
†Denison University, Granville, Ohio 43203
‡Phys. Rev. C. 28, 602 (1983).
¶Institut fur Kernchemie, Universitat Mainz, D-65 Mainz, Federal Republic of Germany.
§KFK 3582 (1983); also Nucl. Sci. Eng. (in press).
△Kernforschungszentrum Karlsruhe, Institut fur Kernphysik.
▲E.N.E.A., Bologna.

n. The Neutron Capture Cross Sections of ^{178,179,180}Hf and the Origin of Nature's Rarest Stable Isotope ^{180}Ta* (H. Beer** and R. L. Macklin)

The neutron capture cross sections of ^{178,179,180}Hf were measured in the energy range 2.6 keV to 2 MeV. The average capture cross sections were derived and fitted in terms of strength functions. Resonance parameters for the observed resonances below 10 keV were determined by shape analysis. Maxwellian averaged capture cross sections were computed for thermal energies with kT between 5 and 100 keV. The cross sections for kT = 30 keV were used to determine the population probability of the 8^- isomeric level in ^{180}Hf by neutron capture as (1.24 ± 0.06)% and the r-process abundance of ^{180}Hf as 0.0290 (Si ≡ 10^6). These quantities served to analyze s- and r-process nucleosynthesis of ^{180}Ta, nature's rarest stable isotope.

o. The ^{56}Fe 1.15 keV Resonance Parameters from Transmission Measurements at ORELA (F. G. Perey, J. A. Harvey, and N. W. Hill)

Transmission measurements with 80-m flight paths were made on samples of natural iron of 0.01319 a/b and 0.2179 a/b at room temperature and on a sample of 0.01754 a/b cooled to liquid nitrogen temperature. All of the data were analyzed with the code SAMMY and the parameters of the 1.15-keV resonance determined to be E = 1151.03 ± 0.04 eV, Γ_γ = 0.574 ± 0.040 eV and Γ_n = 0.0617 ± 0.0009 eV. These values of the resonance parameters are consistent with all previous determinations from transmission measurements but have much smaller uncertainties. The value of Γ_n for this resonance from the ORELA transmission measurements is in disagreement with its recent determination from capture measurements at ORELA and at GELINA.

p. Accurate Determination of the Parameters of the 292.4-eV Resonance of ^{91}Zr and the 301.3-eV Resonance of ^{96}Zr (M. M. Salah,† J. A. Harvey, N. W. Hill, F. G. Perey, and A. Z. Hussein‡)

High resolution transmission measurements of zirconium metal samples have been carried out at ORELA using the 80-meter flight-path station and an improved ^{6}Li-glass scintillation neutron detector. The main concern and interest of the present work are the parameters of the 292.4-eV s-wave resonance of ^{91}Zr and the 301.3-eV p-wave resonance of ^{96}Zr. Four different thicknesses of the natural zirconium metal and one sample of zircalloy were used in four separate experiments. The transmission data for these samples were measured at room temperature, and one of them was cooled with liquid

---

*Proc. of Int. Conf. on Nucl. Data for Sci. and Tech., Antwerp, Belgium, Sept. 6-10, 1982, p. 945 (1983).

**Kernforschungszentrum Karlsruhe GmbH, Institut fur Angewandte Kernphysik, Karlsruhe, Federal Republic of Germany.

†Minia University, El-Minia, Egypt.

‡Nuclear Research Center, Atomic Energy Establishment, Cairo, Egypt.

nitrogen to a cold temperature. These data were analyzed using the multilevel R-matrix computer code SAMMY. Different modes of analysis using SAMMY were used to derive the most out of the data available. The resonance parameter (and statistical uncertainties) obtained for this s-wave resonance of ^{91}Zr obtained are: $J^{\pi}=3^{+}$, E_o = 292.40 ± 0.10 eV, Γ_n = 662 ± 3 meV and Γ_γ = 131 ± 7 meV. In addition, the p-wave resonance of ^{96}Zr at 301.3 eV with J=1/2 has been also analyzed and the parameters (and statistical uncertainties) obtained are: E_o = 301.14 ± 0.10 eV, Γ_n = 221 ± 7 meV, and Γ_γ = 283 ± 23 meV. A careful investigation of the systematic uncertainties is in progress.

q. Neutron, Radiation and Alpha Widths of Resonances in ^{33}S+n (G. Coddens,* M. Salah,** J. A. Harvey and N. W. Hill)

High resolution transmission measurements on a 0.97-gm sample enriched to 88.2% ^{33}S were made by the time-of-flight technique using an NE-110 scintillation detector at the Oak Ridge Electron Linear Accelerator. Transmission data on this nuclide is of special interest since the alpha widths of the resonances are large and the (n,α) cross section has been measured recently at GEEL. New resonances not seen in an earlier transmission measurement with a thinner sample were observed. The multilevel R-matrix formalism was used in analyzing the data by a computer code SAMMY based on Bayes' Theorem. The external R-function was used to allow for the contribution of resonances outside the region of analysis. Two neutron entrance channels were required for specific resonances. Three exit channels (Γ_n, Γ_γ and Γ_α) were taken into account in the analysis. A good fit to the data were obtained covering the energy range from 10-400 keV. The J^{π}, Γ_n and either Γ_γ or Γ_α were obtained for most of the resonances. The neutron strength functions for s- and p-wave neutrons and the level spacings were obtained.

2. Scattering and Reactions

a. Neutron Scattering from Os Isotopes at 60 keV and Re/Os Nucleochronology† (R. L. Hershberger,‡ R. L. Macklin, N. W. Hill, M. Balakrishnan,‡ and M. T. McEllistrem‡)

b. ^{187}Os(n,n') Inelastic Cross Section at 34 keV ¶ (R. L. Macklin, R. R. Winters,§ N. W. Hill, and J. A. Harvey)

c. Neutron-Induced Gamma-Ray Production in Fe-57 for Incident-Neutron Energies Between 0.16 and 21 MeV △ (Z. W. Bell, J. K. Dickens, D. C. Larson, and J. H. Todd)

*NEA Data Bank, Saclay, France.
**Minia University, El-Minia, Egypt.
†Phys. Rev. C 28, 2249 (1983).
‡Physics and Astronomy, University of Kentucky, Lexington, KY 40506.
¶Astrophysical Journal 274, 408 (1983).
§Denison University, Granville, Ohio 43203.
△Nucl. Sci. Eng. 84, 12 (1983).

d. Neutron Flux Measurements at the 22-Meter Station of the Oak Ridge Linear Accelerator Flight Path No. 8* (Z. W. Bell, J. K. Dickens, J. H. Todd, and D. C. Larson)

The measurement of the ORELA flux at neutron energies from 0.16 MeV to 31 MeV is described. The techniques of fitting calculated responses to measured responses and the method of calculating the covariance matrix are detailed. The measured neutron flux is presented.

e. Gamma Ray Production Due to Neutron Interactions with Copper for Neutron Energies Between 0.7 and 10.5 MeV** (G. G. Slaughter and J. K. Dickens)

f. Gamma-Ray Decay of Levels in ^{63}Cu and ^{65}Cu† (J. K. Dickens)

g. Gamma-Ray Transitions Among Levels of ^{206}Pb‡ (J. K. Dickens)

h. Cross Sections for the Mo(n,xn) Reactions Between 3 and 21 MeV¶ (Z. W. Bell)

Differential cross sections for Mo(n,xn) reactions have been measured for incident neutron energies between 3 and 21 MeV and for secondary neutron energies between 2 and 21 MeV. The data are compared with current ENDF/B evaluated data and with experimental data of two recent measurements. Discrepancies with evaluation for E_n between 5 and 9 MeV are discussed but not resolved. The present data agree reasonably well with evaluation for $E_n > 10$ MeV and with previous experimental data for $E_n = 4$ MeV.

i. High Resolution (n,xγ) Measurements for $0.2 \leqslant E_n \leqslant 40$ MeV (D. C. Larson and J. K. Dickens)

Gamma-ray production measurements have been made at the 20-m flight-path on samples of ^{7}Li, ^{56}Fe, ^{nat}Ni, ^{58}Ni, ^{nat}Cr, and ^{53}Cr using a 100-cc Ge(Li) detector and the ORELA neutron source. Gamma rays are observed from the (n,nα), (n,2n), (n,np) and (n,3n) reactions. The data are currently being analyzed and converted to cross sections. A new large volume intrinsic Ge detector has been received and calibrated and will be used for planned (n,xγ) measurements on ^{10,11}B and ^{59}Co.

---

*Abstract of ORNL/TM-8514 (May 1983).
**Nucl. Sci. Eng. 84, 395 (1983).
†Nucl. Phys. A401, 189 (1983).
‡Phys. Rev. C 28, 916 (1983).
¶Abstract of ORNL/TM-8863 (October 1983).

3. Actinides

a. Nature of the Coupling in Subthreshold Fission of ^{238}Np* (G. F. Auchampaugh,** M. S. Moore,** J. D. Moses,** R. O. Nelson,** R. C. Extermann,**, C. E. Olsen,** N. W. Hill, and J. A. Harvey).

b. The Neutron Total Cross Sections of ^{249}Bk and ^{249}Cf Below 100 eV† (R. W. Benjamin,‡ J. A. Harvey, N. W. Hill, M. S. Pandey,¶ and R. F. Carlton§)

c. Measurement of the ^{242m}Am Neutron Fission Cross Section△ (J. W. T. Dabbs, C. E. Bemis, Jr., S. Raman, R. J. Dougan▲ and R. W. Hoff▲)

d. Fission Cross Section Measurements of ^{244}Cm, ^{246}Cm, and ^{248}Cm▽ C. R. S. Stopa,▼ H. T. Maguire, Jr.▼ D. R. Harris,▼ R. C. Block,▼ R. E. Slovacek,□ J. W. T. Dabbs, Richard Hoff,◘ and Ronald Lougheed■

e. Neutron Fission Cross Sections of Pu-239 and Pu-240 Relative to U-235○ (L. W. Weston and J. H. Todd)

f. Comparison of Measured and Calculated ^{238}U Capture Self-Indication Ratios from 4 to 10 keV● (R. B. Perez, G. de Saussure, J. T. Yang,☆ J. L. Munoz-Cobos,★ and J. H. Todd)

From 4 to 149 keV, the ^{238}U cross sections are represented in ENDF/B-V by unresolved-resonance parameters (URPs). The purpose of this

---

*Phys. Rev. c 29, 174 (1984).
**Los Alamos National Laboratory, Los Alamos, New Mexico 87545.
†Nucl. Sci. Eng. 85, 261 (1983).
‡E. I. du Pont de Nemours and Company, Savannah River Laboratory, Aiken, S. C. 29808.
¶Present address: 73 Winston Drive, Somerset, New Jersey 08873.
§Middle Tennessee State University, Murfreesboro, Tennessee 37130.
△Nucl. Sci. Eng. 84, 1 (1983).
▲Lawrence Livermore National Laboratory, Livermore, CA 94550.
▽Proc. Top. Meeting on Advances in Reactor Physics and Core Thermal Hydraulics, Vol. II, p. 1090, (Kiamesha Lake, N.Y., Sept. 1982), NUREG/CP0034 (1983).
▼Gaerttner Linac Laboratory, Rensselaer Polytechnic Institute, Troy, N.Y.
□Knolls Atomic Power Laboratory, Niskayuna, New York.
◘Lawrence Livermore National Laboratory, Livermore, CA 94550.
○Nucl. Sci. Eng. 84, 248 (1983).
●Trans. Am. Nucl. Soc. 44, 537-38 (1983).
☆Inst. Nuclear Research, Taiwan.
★Universidad Politecnica de Valencia, Spain.

representation is to enable the calculation of resonance self-protection as a function of temperature and dilution. Since the URPs are not defined unambiguously by the cross-section data, it is important that the unresolved representation be tested with appropriate experiments, such as capture self-indication ratio (SIR) measurements. In this paper, we compare ^{238}U capture SIR measurements in the 4- to 10-keV energy range with calculations done with ENDF/B-V and with recently published resolved-resonance parameters.

g. Measurements of the 232-Th(n,f) Subthreshold and Near-Subthreshold Cross Section* (R. B. Perez, G. de Saussure, J. H. Todd, T. J. Yang, and G. F. Auchampaugh)

h. Measurement of Neutron Energy Dependence of the Average Number of Prompt Neutrons Emitted in Fission $\nu_p(E)$, of U-233, U-235, Pu-239, and Pu-241 Relative to ν_p for Spontaneous Fission of Cf-252** (R. Gwin)

A series of experiments have been performed to measure the dependence on the incident neutron energy of the average number of prompt neutrons emitted per fission from ^{233}U, ^{235}U, ^{239}Pu, and ^{241}Pu relative to the average number of prompt neutrons emitted in spontaneous fission of ^{252}Cf. The incident neutron energy range was 0.005 to 10 eV. A white neutron source was generated by the Oak Ridge Electron Linear Accelerator and the energies of the neutrons incident on the fissile samples were determined by time-of-flight techniques. In each experiment the samples, including the ^{252}Cf standard, were contained in different sections of a fission chamber that was surrounded by a large volume (0.91 m^3) of liquid scintillator loaded with gadolinium. The fission chamber detected fission events, and the scintillator detected the accompanying prompt neutrons. The resulting data were analyzed to yield: $\overline{R}_p(E) = \overline{\nu}_p(E)[\text{fissile}]/\overline{\nu}_p[^{252}Cf]$. Only for ^{239}Pu was any neutron energy dependence definitely confirmed, with $\overline{R}_p(E)$ for ^{239}Pu being lower by 0.7% in the resonance at 0.3 eV than it was near 0.025 eV. For incident energies of 0.02 to 0.05 eV, values of $\overline{R}_p(E)$ were 0.6597 ± 0.0018 for ^{233}U, 0.6443 ± 0.0014 for ^{235}U, 0.7655 ± 0.0014 for ^{239}Pu, and 0.7820 ± 0.0018 for ^{241}Pu.

i. Neutron Fission Cross Sections of Pu-239 and U-235 Relative to $^{10}B(n,\alpha)$† (R. Gwin, R. R. Spencer, R. W. Ingle, J. H. Todd, and S. W. Scoles)

Measurements have been made of the energy dependence of the ^{235}U neutron fission cross section over the energy range from 0.01 eV to 30 keV and of the ^{239}Pu fission cross section over the range from 0.01 to 60 eV.

---

*Phys. Rev. C 28, 1635 (1983).
**Submitted to Nucl. Sci. & Eng., 1983.
†Submitted to Nucl. Sci. & Eng., 1983.

The energy integral of the fission cross section for ^{235}U was normalized to 19.26 b·eV in the 0.0206- to 0.0639-eV interval; this yielded a value of 248 ± 1.7 b·eV for the 7.8- to 11-eV interval, which is in good agreement with other measurements normalized in the same manner. The energy integral for ^{239}Pu was normalized to 25.15 b·eV in the 0.02001- to 0.06001-eV interval; the resulting value of 504 b·eV in the 9- to 12.6-eV interval was also in good agreement with other data. For the energy ranges covered, the energy dependence of both the ^{235}U fission cross section and the ^{239}Pu fission cross section are consistent with ENDF/B-V data except for a few energy intervals in which the ^{235}U cross section differs by as much as 4%.

j. Subthreshold Fission Cross Section of Pu-240 and the Fission Cross Sections of U-235 and Pu-239* (L. W. Weston and J. H. Todd)

The subthreshold fission cross section of ^{240}Pu was measured relative to the $^{10}B(n,\alpha)$ or the $^{6}Li(n,\alpha)$ cross sections from 20 eV to 100 keV. Resonance parameter fits to the data were derived from 20 to 5700 eV. Many more resonances and more resonance structure were observed than in previous measurements. During the course of this measurement, the fission cross sections of ^{235}U and ^{239}Pu were also measured and are compared to the ENDF/B-V evaluation. The ^{235}U experiment is in good agreement with ENDF/B-V, however, the ^{239}Pu measurement is lower than ENDF/B-V and many of the previous measurements, particularly above 25 keV.

k. Fission-Product Yields for Thermal-Neutron Fission of ^{243}Cm Using a High-Resolution, Low-Energy Germanium Gamma-Ray Detector** (L. Douglas Merriman)

Cumulative fission-product yields have been determined for 13 gamma rays emitted during the decay of 12 fission products created by thermal-neutron fission of ^{243}Cm. Using a high-resolution, low-energy germanium detector, pulse-height spectra of gamma rays emitted from a 77-ng sample of ^{243}Cm after thermal-neutron irradiation were acquired and analyzed. Reduction of the spectra resulted in the identification and matching of gamma-ray energies and half-lives to individual radioisotopes. From these results, 12 cumulative fission product yields were deduced for radionuclides with half-lives between 4.2 min and 84.2 min.

l. ORELA Contribution to Thorium Cycle Nuclear Data† (D. K. Olsen)

The measurements of direct importance to the $^{232}Th/^{233}U$ fuel cycle using neutrons from the Oak Ridge Linear Accelerator facility are gathered together and discussed. These measurements were done in response to specific data discrepancies, as part of generic programs, and for basic

---

*Submitted to Nucl. Sci. & Eng.
**Abstract of ORNL/TM-9049 (in preparation).
†U.S.-Japan Joint Seminar on the Thorium Fuel Cycle at Nara, Japan, October 18-22, 1982.

fission physics studies. In particular, completed transmission and capture work on ^{232}Th has yielded the most accurate parameters for the first four s-wave resonances; the largest average capture width, 25.2 meV; and the largest s-wave strength function of recent measurements. These results allow improved agreement between differential and integral capture rates. Moreover, the ORNL ^{252}Cf $\bar{\nu}$ measurement of unprecedented accuracy and ^{233}U $\bar{\nu}$ ratio measurement give a ^{233}U (prompt $\bar{\nu}$ (thermal) of 2.490 ± 0.009 neutron/fission. This result allows a much more satisfactory understanding of the ^{233}U 2200 m/s constants. In addition, a ^{232}Th gamma-ray production measurement provides needed cross sections for shielding, and important data for both application and fission physics were obtained from ^{232}Th fission and both ^{231}Pa and ^{234}U fission and total cross section measurements. Data requirements and discrepancies suggested from this work are discussed.

m. High Resolution Measurements and R-Matrix Analysis of the Total and Fission Cross Sections of ^{237}Np + n from 1 to 600 eV* (G. F. Auchampaugh,** M. S. Moore,**, J. D. Moses,** R. O. Nelson,** C. E. Olsen,** R. C. Extermann,** N. W. Hill, and J. A. Harvey)

High-resolution measurements of the total and fission cross sections of ^{237}Np + n have been made using the pulsed-neutron facilities at the Oak Ridge Electron Linear Accelerator and at the Los Alamos Meson Physics Facility. The samples were cooled to liquid-nitrogen temperature. This report presents the total and fission cross sections from 1 to 600 eV as well as the parameters obtained from an R-matrix fit of these data.

4. Experimental Techniques

a. Calculation of the ORELA Neutron Moderator Spectrum and Resolution Function† (C. R. Coceva,‡ R. Simonini,‡ and D. K. Olsen)

b. Neutron Filters for Producing Monoenergetic Neutron Beams¶ (J. A. Harvey, N. W. Hill, and J. R. Harvey§)

Neutron transmission measurements have been made on high-purity, highly-enriched samples of ^{58}Ni (99.9%), ^{60}Ni (99.7%), ^{64}Zn (97.9%) and ^{184}W (94.5%) to measure their neutron "windows" and to assess their potential usefulness for producing monoenergetic beams of intermediate energies from a reactor. Transmission measurements on the Los Alamos Sc filter (44.26 cm Sc and 1.0 cm Ti) have been made to determine the characteristics of the

*Los Alamos National Laboratory Report LA-9756 (May 1983).
**Los Alamos National Laboratory, Los Alamos, New Mexico.
†Nucl. Instrum. Methods 211, 459 (1983).
‡ENEA Bologna, Italy
¶Proc. of Int. Conf. on Nucl. Data for Sci. and Tech., Antwerp, Belgium, Sept. 6-10, 1982, p. 856 (1983).
§CEGB Berkeley Nuclear Laboratories, Berkeley, England.

transmitted neutron beam and to measure the total cross section of Sc at the 2.0 keV minimum. When corrected for the Ti and impurities, a value of 0.35 ± 0.03 b was obtained for this minimum.

c. Determination of the Energy Dependence of the Effective Length, Experimental Energies and Energy Resolution Function, and Their Uncertainties for Flight Path 1 at ORELA* (D. C. Larson, N. M. Larson, and J. A. Harvey)

Flight path 1 at ORELA is nominally 200 m in length and has been extensively used for neutron transmission and scattering measurements. Due to moderation effects in the neutron producing target and to the finite thickness of the neutron detector, the effective flight-path length is a function of neutron energy. In this report, we determine the effective length as a function of energy, its uncertainty, and time-of-flight energies and their uncertainties. Finally, we determine the resolution function and its uncertainty and compare this resolution function with an experimental determination of this quantity.

d. A Parallel Plate ^{10}B Neutron Detector** (J. H. Todd, L. W. Weston, and G. J. Dixon)

Parallel plate ionization chambers with vacuum deposited ^{10}B electrodes have been constructed and tested. Plating thicknesses of ^{10}B from 24 $\mu g/cm^2$ to 61 $\mu g/cm^2$ were used. Pulse height resolutions of the alpha particle and of the ^{7}Li fragment from the $^{10}B(n,\alpha)$ reaction were measured using low energy neutrons. The pulse height resolutions of the chambers were found to be better than a theoretical analysis would indicate.

e. Measurement of the 200, 80, and 18-m Flight Path Lengths and Determination of Their Uncertainties† (D. C. Larson, N. M. Larson, J. A. Harvey, and F. G. Perey)

A Hewlett-Packard Model 3820A laser electronic distance meter was used to measure portions of the lengths of the 18, 80, and 200-m flight paths at ORELA. Measurements were not able to be made to the neutron-producing target itself; distances from the target to nearby benchmarks were taken from existing drawings, and checked where possible. An offset correction was determined for the laser device, which reduced the final measurement uncertainties. Bayes' equations were utilized to combine statistical uncertainties and systematic errors to produce the final average values and uncertainties.

---

*Abstract from ORNL/TM-8880 (March 1984).
**Nucl. Instru. and Methods, 1983 (in press).
†Abstract from ORNL/TM-9097 (in preparation)

f. Counting Anticoincidences to Reduce Statistical Uncertainty in the Calibration of a Multiplicity Detector* (R. W. Peelle and R. R. Spencer)

g. A Digital Pulse-Pair Detecting Circuit** (Z. W. Bell, J. W. McConnell, and E. D. Carroll)

5. Integral Measurements

a. The ORNL Integral Experiment to Provide Data for Evaluating Magnetic-Fusion-Energy Shielding Concepts. Part IV: Second Streaming Measurements† (G. T. Chapman)

Integral experiments to measure the energy spectra of neutrons and gamma rays due to the streaming of approximately 14-MeV $T(d,n)^4He$ neutrons through a duct designed to simulate those required in MFE reactor-shield designs have been performed at the Oak Ridge National Laboratory. An NE-213 detector and conventional pulse-shape-circuitry were used to record the pulse-height distributions from which the energy spectra were derived. Tables and curves showing the results of these measurements are given in this report.

b. The ORNL Integral Experiment to Provide Data for Evaluating Magnetic-Fusion-Energy Shielding Concepts. Part II: Streaming Measurements‡ (G. T. Chapman and J. W. McConnell)

Integral experiments to measure the energy spectra of neutrons and gamma rays due to the streaming of approximately 14-MeV $T(d,n)^4He$ neutrons through a duct designed to simulate those required at the Oak Ridge National Laboratory. An NE-213 detector and conventional pulse-shape-circuitry were used to record the pulse-height distributions from which the energy spectra were derived. Tables and curves showing the results of these measurements are given in this report.

c. Integral Measurements of Neutron and Gamma-Ray Leakage Fluxes from the Little Boy Replica¶ (F. J. Muckenthaler)

This report presents integral measurements of neutron and gamma-ray leakage fluxes from a critical mockup of the Hiroshima bomb Little Boy at Los Alamos National Laboratory with detector systems developed by Oak Ridge National Laboratory. Bonner ball detectors were used to map the neutron fluxes in the horizontal midplane at various distances from the mockup and for selected polar angles keeping the source-detector separation constant.

*Nucl. Instrum. Methods 211, 167 (1983).
**Nucl. Instrum. Methods 211, 551 (1983).
†Abstract from ORNL/TM-9027 (1984).
‡Abstract from ORNL/TM-9021 (1984).
¶Abstract from ORNL/TM-9005 (1984).

Gamma-ray energy deposition measurements were made with thermoluminescent detectors at several locations on the iron shell of the source mockup. The measurements were performed as part of a larger program to provide benchmark data for testing the methods used to calculate the radiation released from the Little Boy bomb over Hiroshima.

d. Phase I Measurements for the HTGR Reflector and Support Block Neutron Streaming Experiment* (F. J. Muckenthaler, J. L. Hull, L. B. Holland, and J. J. Manning)

This report presents measurements made for the initial phase of the High-Temperature Gas-Cooled Reactor Lower Reflector and Core Support Neutron Streaming experiment conducted at the Tower Shielding Facility during FY83. In this phase, neutron measurements were made behind the first four of eight segments that comprise the full experimental mockup. The last four segments will be studied in FY84. Measurements include both neutron energy spectra and integral neutron responses.

e. Streaming of 14-MeV Neutrons Through an Iron Duct - Comparison of Measured Neutron and Gamma-Ray Energy Spectra with Results Calculated Using the Monte Carlo MCNP Code** (R. T. Santoro, J. M. Barnes, R. G. Alsmiller, Jr., and P. D. Soran†)

f. Comparison of Measured and Calculated Neutron and Gamma Ray Energy Spectra Behind an In-Line Shielded Duct‡ (R. T. Santoro, R. G. Alsmiller, Jr., J. M. Barnes, G. T. Chapman, and J. S. Tang)

B. DATA ANALYSES

1. Theoretical Calculations

a. High Resolution s- and p-wave Neutrons on ^{30}Si and ^{34}S. Part I. Spherical Optical Model Analysis¶ (R. F. Carlton,§ J. A. Harvey, and C. H. Johnson)

The s- and p-wave neutron scattering functions obtained previously by R-matrix analyses of high resolution transmission data for 0 to 1.4-MeV neutrons on ^{30}Si and ^{34}S have been averaged by means of a simple analytic approximation to obtain experimental optical model scattering functions. To describe these with a spherical optical model potential requires the real well

*Abstract from ORNL/TM-8977 (1984).
**Nucl. Sci. Eng. 84, 260-70 (1983).
†Los Alamos National Laboratory, Los Alamos, N. M.
‡Journal of Fusion Energy 2(6), 403-12 (1983).
¶To be submitted to Phys. Rev. C.
§Middle Tennessee State University, Murfreesboro, Tennessee 37132.

depth be about 20% deeper for p-waves than for s-waves. This result agrees with an earlier analysis for ^{32}S and suggests that deformation effects must be included for all three nuclei.

b. Implementation of an Advanced Pairing Correction for Particle-Hole State Densities in Precompound Nuclear Reaction Theory* (C. Y. Fu)

An advanced pairing correction for an existing formula of particle-hole state densities, needed in calculations of cross sections with the precompound nuclear reaction theory, is examined. The Pauli correction is derived to be consistent with this pairing correction. The accuracy of the pairing correction plus the Pauli correction is shown to be sufficient for applied calculations. Numerical solutions of the pairing equations, needed for generating the corrections, have been carried out. The relevant numerical results are presented as simple functions of the excitation energy and the exciton number. A relationship between the pairing correction for particle-hole state densities and the pairing correction for the total state densities in the closed-form formulation is developed. Utilization of the existing level-density parameters and data for deducing parameters for the particle-hole state densities are shown.

c. Pairing Correction for Particle-Hole State Densities** (C. Y. Fu)

The pairing correction proposed by Ignatyuk and Sokolov for particle-hole state densities has been examined. It has been found that the accuracy of the correction is sufficient for practical applications only if the system is in its normal state ($\Delta = 0$). In the superfluid state ($\Delta \neq 0$), a consistent pairing-Pauli correction is developed here for improved accuracy. Practical implementations of the pairing correction are given and further developments are outlined.

d. Application of Group Theory to Data Reduction† (F. G. Perey)

The analysis within the framework of a theory of what was observed in experiments is essential to the testing of theories and is fundamental to physics. It is shown in this report how group theory can be used to provide a general method of data reduction whereby only the laws of a particular theory are used in the analysis of observations. This application of group theory involves introducing a group of transformations of the physical system upon which the observations were made. This group of transformations leaves invariant the entities of the theory corresponding to the observations made but transforms the entities that were not observed from what they are presumed to be in this theory into what they are not, called possibilities for what they are. This group of transformations is called the

*Accepted by Nucl. Sci. Eng.

**IAEA Advisory Group Meeting on Basic and Applied Problems of Nuclear Level Densities, Upton, N.Y., April 11-15, 1983, BNL-NCS-51694 (June 1983), p.379.

†Abstract from ORNL-5908 (September 1982).

possibilities-generating group for the entities for which the observations are being reduced. Since possibilities for entitites of theories so obtained are functionals of a known group of transformations, the subsequent use of these possibilities in the theories must be made consistent with the theory of representations of groups. There is a well-known invariant associated with functionals of group elements which is invariant with respect to the parametrization of this group. It is the normalized volume measure in the group manifold of the possibilities-generating group. In this report this invariant measure is called the physical probability of the possibilities since it is a probability measure which has a Borel algebra. The above proposed method of data reduction allows us to deal unambiguously with the uncertainties in entities of physical theories obtained from all of the observations made in experiments and the distinction between systematic and statistical uncertainties disappears. Concrete realizations of possibilities-generating groups are given and explanations in group theoretical terms are offered for several important intuitive notions related to probabilities.

e. Parity Dependence of the Level Densities of ^{53}Cr and ^{55}Cr at High Excitation* (H. M. Agrawal,** J. B. Garg,** and J. A. Harvey)

The neutron total cross sections of ^{52}Cr and ^{54}Cr have been measured in the energy range from a few tens of keV to about 900 keV using the neutron time-of-flight technique and the pulsed Oak Ridge Electron Linear Accelerator. The nominal resolution of the measurements was about 0.06 ns/m. The total cross section data have been analyzed using an R-matrix multilevel multichannel code to determine values of resonance parameters (E_0, J^π, $g\Gamma_n$). From these analyses we obtain the following values for the average properties of the resonance parameters for s-wave resonances up to about 900 keV and for p-wave resonances up to 600 kev: D_0 = (45 ± 6) keV, S_0 (x 10^4) = (3.0 ± 1.0), D_1 = (8.5 ± 0.6) keV, S_1 (x 10^4) = (0.70 ± 0.12) for ^{52}Cr; and D_0 = (60 ± 9) keV, S_0 (x 10^4) = (2.6 ± 0.9), D_1 = (9.2 ± 0.5) keV, S_1 (x 10^4) = (0.67 ± 0.11) for ^{54}Cr. The distributions of neutron-reduced widths for s- and p-wave resonances show good agreement with the Porter-Thomas distribution for each isotope. The value of Δ_3 statistic for the long-range correlation of s-wave energy levels for ^{52}Cr, as well as ^{54}Cr, is found to be in reasonable agreement with the theoretical prediction of Dyson and Mehta. For both nuclides, the value for the mean p-wave level density is larger than that expected from the (2J + 1) law, indicative of a parity dependence of the level densities at high excitation.

f. Average Scattering Matrix Elements from High Resolution Neutron Total Cross Sections for ^{32}S† (C. H. Johnson and R. R. Winters‡)

*To be submitted to Phys. Rev. C.
**State University of New York, Albany, New York 12222.
† Phys. Rev. C 27, 416 (1983).
‡Denison University, Granville, Ohio 43023.

g. Calculation of the Energy-Averaged Scattering Function from High Resolution Low-Energy Neutron Scattering Data* (C. H. Johnson, N. M. Larson, C. Mahaux,** and R. R. Winters†)

h. Sensitivity Analysis for a Specific Fusion Reactor Shielding Experiment‡ (R. G. Alsmiller, Jr., R. T. Santoro, R. L. Childs, J. M. Barnes, and J. L. Lucius)

i. Monte Carlo Calculations of Neutron and Gamma-Ray Energy Spectra for Fusion Reactor Shield Design: Comparison with Experiment¶ (R. T. Santoro and J. M. Barnes)

Neutron and gamma-ray energy spectra resulting from the interactions of ∿14 MeV neutrons in laminated slabs of stainless steel type-304 and borated polyethylene have been calculated using the Monte Carlo code MCNP. The calculated spectra are compared with measured data as a function of slab thickness and material composition and as a function of detector location behind the slabs. Comparisons of the differential energy spectra are made for neutrons with energies above 850 keV and for gamma rays with energies above 750 keV. The measured neutron spectra and those calculated using Monte Carlo methods agree within 5% to 50% depending on the slab thickness and composition and neutron energy. The agreement between the measured and calculated gamma-ray energy spectra are also within this range. The MCNP data are also in favorable agreement with attenuated data calculated previously by discrete ordinates transport methods and the Monte Carlo code SAM-CE.

j. User's Guide for ALEX: Uncertainty Propagation from Raw Data to Final Results for ORELA Transmission Measurements§ (Nancy M. Larson)

This report describes a computer code (ALEX) designed to assist in AnaLysis of EXperimental data at the Oak Ridge Electron Linear Accelerator (ORELA). Reduction of data from raw numbers (counts per channel) to physically meaningful quantities (such as cross sections) is in itself a complicated procedure; propagation of experimental uncertainties through that reduction procedure has in the past been viewed as even more difficult - if not impossible. The purpose of the code ALEX is to correctly propagate all experimental uncertainties through the entire reduction procedure, yielding the complete covariance matrix for the reduced data, while requiring little additional input from the experimentalist beyond that which is required for

*Phys. Rev. C 27, 1913 (1983).
**Institut de Physique, Universite de Liege, 4000 Liege, Belgium.
†Denison University, Granville, Ohio 43023.
‡Nucl. Sci. Eng. 83, 389 (1983).
¶Abstract from ORNL/TM-8707 (August 1983).
§Abstract from ORNL/TM-8676 (February 1984).

the data reduction itself. This report describes ALEX in detail, with special attention given to the case of transmission measurements (the code itself is applicable, with few changes, to any type of data). Application to the natural iron measurement of D. C. Larson et al. is described in some detail.

k. Report to the U-238 Discrepancy Task Force on SIOB Fits to the ORNL, CBNM, and JAERI Transmission Data* (D. K. Olsen)

Least-squares simultaneous-sample shape fits to the recent ORNL, CBNM, and JAERI ^{238}U transmission data have been completed using the computer code SIOB. These fits over the energy regions 1460 to 1820 eV, 2470 to 2740 eV, and 3820 to 4000 eV indicate that much of the systematic discrepancy in the published neutron widths from these data arose in the data analysis procedure. Except for the 3820 to 4000-eV JAERI data, the systematic differences in the resulting neutron widths from the present analyses of the three measurements with no background corrections is less than 2 to 4%. The neutron widths are larger than those contained in any existing evaluation. These fits were performed as part of the work for NEANDC ad hoc U-238 Discrepancy Task Force.

2. ENDF/B Related Evaluations

a. An Annotated Bibliography Covering Generation and Use of Evaluated Cross Section Uncertainty Files** (R. W. Peelle and T. W. Burrows†)

Literature references related to evaluated cross section uncertainty (variance-covariance) files are listed with comments intended primarily to guide the reader toward materials of immediate interest. Papers are included that cover covariance information from individual experiments and that relate to production and use of multigroup covariance matrices. Titles are divided among several major categories. The comments by the compilers may not reflect the views of the authors of the papers cited.

b. Major Questions About Derivation of Variance-Covariance Information for Nuclear Data Evaluations‡ (R. W. Peelle)

---

*Abstract from ORNL/TM-9023 (February 1984).

**Abstract from BNL-NCS-51684, ENDF-331, March 1983, Information Analysis Center Report, National Nuclear Data Center, Brookhaven National Laboratory Report.

†Brookhaven National Laboratory, Upton, New York.

‡International Conference on Nuclear Data for Science and Technology, Antwerp, Belgium, Sept. 6-10, 1982, "Nuclear Data for Science and Technology, K. H. Bockhoff, ed., pp. 694-697, 1983.

c. Impact of Uncertainties in ^{238}U Resonance Parameters on Performance Parameters of Thermal Lattices* (R. Q. Wright, G. de Saussure, and R. B. Perez)

The calculated and measured values of integral parameters may be considered discrepant if their differences are significantly greater than the combined uncertainties assigned to the integral experiment, the calculational methods, and the evaluated differential data. This paper presents an assessment of the uncertainties in the calculated values of performance parameters of selected uranium metal and uranium oxide lattices due to uncertainties in ENDF/B-V data, particularly the ^{238}U resolved resonance parameters.

d. The Nuclear Data of the Major Actinide Fuel Materials** (W. P. Poenitz† and G. de Saussure)

This is Chapter III of an eight chapter special issue of Progress in Nuclear Energy entitled "Cross Section Data for Nuclear Reactor Analyses" and edited by S. Pearlstein. In Chapter III the authors review the status of the nuclear data for the major actinides (Th-232, U-233, U-235, U-238, Pu-239, Pu-240, Pu-241, and Pu-242), with regard to application for the optimization of fuel cycles and core designs for thermal and fast breeder reactors. The most important measurements are reviewed and the consistency and completeness of contemporary evaluations (ENDF-V, JENDL-2, KEDAK, SOKRATOR, etc.) are compared. The impact of uncertainties or discrepancies in the data on neutronic calculations is assessed.

e. Uncertainties in the ^{238}U Resolved Resonance Parameters and Their Impact on Calculated Group Constants‡ (G. de Saussure, R. Q. Wright, and R. B. Perez)

In assessing the contribution of the uncertainties in a data set to the uncertainty in a computed performance parameter (such as capture to fission ratio in a benchmark, or Doppler coefficient of reactivity), it is required to assess the uncertainty in the pertinent group constants due to uncertainty in the basic data. In this presentation we will review the data base for the ENDF/B-V evaluation of the ^{238}U resolved resonance parameters and show how the analysis of the data base leads to the estimated systematic uncertainties in the evaluated parameters. We will then show how these systematic uncertainties propagate to uncertainties in Bondarenko-type group constants as a function of dilution and temperature. The impact on benchmarks is discussed in the presentation of R. Q. Wright. We will also compare

*Trans. Am. Nucl. Soc. 45, 701 (1983)

**Chapter in "Cross Section Data for Nuclear Reactor Analysis," to be published.

†Argonne National Laboratory, Argonne, Illinois.

‡Proc. Second Jackson Hole Colloquium on Fast Reactor Physics: The Doppler Effect in LMFBRs, Teton Village, Wyoming, June 27-29, 1983, Session III, No. 3 (1983).

the ENDF/B-V ^{238}U resolved resonance parameters with those of two recent independent evaluation (JENDL-2 and Moxon and Sowerby 1982). The comparison shows that the very different approaches used in the three evaluations lead to very consistent average data.

f. Impact of Uncertainties in ^{238}U Resonance Capture Cross Sections on Benchmark Performance Parameters* (R. Q. Wright, G. de Saussure, and R. B. Perez)

Calculated uncertainties in CSEWG fast reactor benchmarks using uranium and plutonium evaluations from ENDF/B-V are a major concern to the fast reactor community. As an introduction to this presentation the performance parameters for the plutonium oxide fueled ZPR-6/7 and the uranium oxide fueled ZPR-6/6A benchmarks will be reviewed. In a companion presentation, de Saussure et al. will describe uncertainties in the ^{238}U Bondarenko-type group constants, as a function of dilution and temperature, prepared from the ENDF/B-V ^{238}U evaluation. Sensitivity calculations were used to investigate the effect of changes in the group constants on the benchmark performance parameters. In this presentation, the impact of the uncertainties in the ^{238}U capture cross sections on ZPR-6/7 and ZPR-6/6A eigenvalues and central reaction rate ratios will be discussed. Of special interest are performance parameter uncertainties resulting from uncertainties in resolved resonance Γ_n and Γ_γ and in the unresolved resonance range. The impact of uncertainties in ^{238}U capture will be compared to the impact due to uncertainties in ^{239}Pu fission for the ZPR-6/7 eigenvalue and ^{238}U capture/^{239}Pu fission reaction ratio at the center of the one-dimensional spherical model of the assembly. Revision 2 to the ENDF/B-V ^{239}Pu has been proposed. The impact of the proposed evaluation on performance parameters of Pu-fueled benchmark assemblies will be discussed.

---

*Proc. Second Jackson Hole Colloquium on Fast Reactor Physics: The Doppler Effect in LMFBRs, Teton Village, Wyoming, June 27-29, 1983, Session IV, No. 5 (1983).

A. MEASUREMENTS

1. Elastic and Inelastic Scattering of 20, 22 and 26 MeV Neutrons from ^{16}O.† (M.S. Islam, R.W. Finlay, A.S. Meigooni, J.S. Petler, S. Mellema, C.E. Brient and J.R.M. Annand)

Differential cross sections for scattering of 22 MeV neutrons from ^{16}O were measured using the Ohio University beam swinger time-of-flight spectrometer. Similar experiments at 20 and 26 MeV are underway. A 99.8% pure solid cylindrical Al_2O_3 sample of mass 57.1 gm was our target. A pure aluminium cylinder of the same mass as the amount of aluminium in Al_2O_3 was used as sample out. The states 3^- (6.13 MeV), 2^+ (6.92 MeV) and 2^- (8.872 MeV) were observed at each energy. Data are being analyzed in terms of an energy dependent optical model potential, DWBA and coupled-channel calculations.

2. Differential Elastic and Inelastic Neutron Scattering from ^{18}O.†† (P.E. Koehler, D.A. Resler, H.D. Knox, R.O. Lane and G.F. Auchampaugh†††)

Differential cross sections have been measured at 42 energies between 5 and 7.5 MeV for the $^{18}O(n,n)^{18}O$ and $^{18}O(n,n')^{18}O^*$ (1.98 MeV) reactions at 9 to 12 angles from 20° and 160°. The data have been corrected for finite geometry and multiple scattering effects. The Legendre polynomial expansion coefficients for the elastic cross section reveal that angular momentum channels up to and including f-waves are resonant over at least part of the region studied. This fact suggests the possibility that we may be seeing the effects of states involving the major strength of the $f_{7/2}$ shell in ^{19}O. No previous differential elastic neutron scattering measurements for ^{18}O have been reported at these energies. There have been no previous reports of differential inelastic neutron scattering from ^{18}O besides our measurements.

---

† Supported by PHS Grant Number 5-R01-CA-25193 awarded by the National Cancer Institute, DHHS.

†† Work supported by the U.S. Department of Energy.

††† Present address: Los Alamos National Laboratory, Los Alamos, NM.

3. Study of the Level Scheme of ^{28}Si.† (H. Satyanarayana, M. Ahmad, C.E. Brient, P.M. Egun, S.L. Graham and S.M. Grimes)

The $^{27}Al(d,n)^{28}Si$ reaction has been studied at bombarding energies between 2.5 and 6.5 MeV in .5 MeV steps. A 28 m flight path was used and energy resolution as good as 15 keV was obtained for low outgoing neutron energies. Because the spacing of some levels was too small relative to our resolution to allow them to be resolved, some levels were seen as doublets. Our spectra show evidence for all levels listed in Endt and van der Leun[1] with only three exceptions. We also find evidence for most of the new levels proposed by Mass and Sherman,[2] which are not listed in Endt and van der Leun. Although the spectra appear to have large contributions from stripping reactions forward of 75°, the back angle spectra show smaller variations in intensity from peak to peak and are consistent with a compound nuclear reaction mechanism. We are planning to repeat the measurements at higher bombarding energies and with better energy resolution to look for levels beyond the maximum energy currently tabulated in Endt and van der Leun.

4. Scattering of 21.7 MeV Neutrons from ^{34}S and ^{40}Ca.†† (R. Alarcon, D. Wang, J.R.M. Annand and J. Rapaport)

Using the Ohio University time-of-flight facility, elastic and inelastic neutron data at 21.7 MeV from ^{34}S and ^{40}Ca have been obtained. An enriched (93.6%) cylindrical scattering sample of 18.02 gms of ^{34}S (powder) and a metal cylinder of 22.9 gms of natural calcium for ^{40}Ca were used. An energy resolution of about 400 keV was achieved. The scattering neutrons were observed at 39 angles between 13° and 160°.

Data analysis in ^{34}S, using the coupled-channels formalism, for the elastic transition, 2_1^+ (E_x = 2.13 MeV), 2_2^+ (E_x = 3.30 MeV), 2_3^+ (E_x = 4.11 MeV), 3_1^- (E_x = 4.69 MeV) and 5_1^- (E_x = 5.69 MeV) has been completed. In ^{40}Ca, microscopic optical model potential analysis for the elastic transition and collective model analysis for the states 3_1^- (E_x = 3.73 MeV) and 5_1^-(E_x = 4.49 MeV) have been carried out.

---

† Work supported by U.S. Department of Energy.

†† Supported in part by National Science Foundation Grant PHY-810456.

1 P.M. Endt and C. van der Leun, Nucl. Phys. A310, 1 (1978).

2 C.E. Mass and J.D. Sherman, Nucl. Phys. A259, 413 (1976).

5. Fast Neutron Inelastic Scattering from $^{54,56}Fe$.† (S. Mellema and R.W. Finlay)

Inelastic differential cross section data for neutron scattering to numerous states in $^{54,56}Fe$ at bombarding energies of 11 and 26 MeV have been taken using the high-resolution beam swinger time-of-flight spectrometer at Ohio University. Analysis using a collective model and DWBA calculations, as well as coupled channels calculations, have been performed. Comparisons to proton inelastic scattering data, where such data exist, have been made in order to investigate the isospin composition of the excitations involved.

6. Inelastic Neutron Scattering from ^{182}W and ^{184}W.†† (J.R.M. Annand and R.W. Finlay)

Previous elastic and inelastic cross section measurements[1,2] for the isotopes of tungsten have been confined to energies less than 4 MeV, where substantial compound nucleus contributions can mask direct excitation effects. Using the Ohio University beam swinger facility, elastic and inelastic cross sections for the isotopes ^{182}W and ^{184}W were measured at 5 and 6 MeV incident energy, where compound effects are small. With an energy resolution of about 1%, all of the ground state band up to 6^+ state and some β and γ band excitations were separable. An initial coupled channels analysis has used the rotational model of Delaroche coupling 0^+, 2^+, 4^+ and 6^+ states. Experimental evidence is presented for direct excitation of the 6^+ state.

7. Neutron Scattering from ^{208}Pb and ^{209}Bi at Energies 4 to 6 MeV.†† (J.R.M. Annand and R.W. Finlay)

Differential elastic and inelastic cross sections have been measured at energies 4.0, 4.5, 5.0, 5.5 and 6.0 MeV for the nuclei ^{208}Pb and ^{209}Bi in the angular range 10° - 160° using the Ohio University Beam

---

† Work supported in part by the National Science Foundation.

†† Partially funded by National Science Foundation Grant PHY-8108456.

1 J. Delaroche et al., Phys. Rev. C23, 136 (1981).

2 P.T. Geunther et al., Phys. Rev. C26, 2433 (1982).

Swinger Time of Flight facility.[1] Forward of 35° the elastic cross sections are very similar in both isotopes, while in ^{208}Pb at larger scattering angles the cross section is consistently larger. While this is not unexpected at the lower energies where the ^{208}Pb compound elastic cross section should be larger, the effect persists up to 6 MeV where compound nucleus effects in both isotopes ought to be negligible. Cross sections have also been measured for the 2.61 MeV 3^- state of ^{208}Pb and the 0.90 $7/2^-$ and 1.16 $13/2^+$ states of ^{209}Bi. The ^{209}Bi $7/2^-$ and $13/2^+$ excitations appear to be essentially compound in nature with negligible strength about 5.5 MeV.

B. MODEL CALCULATIONS AND ANALYSES

1. Development of a New General Purpose Shell Model Code--CRUNCHER.† (D.A. Resler, S.M. Grimes and R.O. Lane)

We are currently writing a code to do shell model calculations. It uses the Lanzcos method in an uncoupled basis and is patterned after the code VLADIMIR[2] which is currently being used regularly at LLNL and LANL. Preliminary results show that our new code CRUNCHER will be faster than VLADIMIR and also it will allow larger dimension spaces for a given size computer. The code is being developed on an IBM 4341 and will soon be tried on an LLNL CRAY.

2. Shell Model Calculations for Normal and Non-Normal Parity States of ^{6}Li, ^{7}Li and ^{8}Li.† (D.A. Resler, H.D. Knox, R.O. Lane and S.M. Grimes)

Using our newly developed shell model code CRUNCHER,[3] we are undertaking a program of shell model calculations for the light nuclei. To begin this program we have started with the lithium isotopes ^{6}Li, ^{7}Li and ^{8}Li. Both normal and non-normal parity states are calculated using the same single-particle energies, two-body interactions and shell model space. The problem of spurious states has been studied by diagonalizing first with the Center-of-Mass Hamiltonian. Results of our calculations are being compared with our current R-matrix studies, with other known experimental results and with other theory calculations.

---

† Work supported by the U.S. Department of Energy.

1 R.W. Finlay et al., Nucl. Instr. and Meth. 198, 197 (1982).

2 R.F. Hausman, Jr., LLNL Report No. UCRL-52178, Ph.D. Thesis (1976).

3 D.A. Resler, S.M. Grimes and R.O. Lane, Bull. Amer. Phys. Soc. 28, 971 (1983).

3. Structure of ^{7}Li and ^{6}Li+n Reaction Cross Sections for $E_n \lesssim 6$ MeV.† (H.D. Knox and R.O. Lane)

An earlier R-matrix study[1] of the ^{7}Li system has been extended to higher energies in ^{7}Li. In this new study excitation energies and reduced widths for states in ^{7}Li included in the analysis were obtained from existing model calculations.[2,3] Six particle channels are included in this study: ^{6}Li(n,n)^{6}Li, ^{6}Li(n,n′)^{6}Li* (2.18), ^{6}Li(n,n′)^{6}Li* (4.31), ^{6}Li(n,d)^{5}He, ^{6}Li(n,d′)^{5}He* and ^{6}Li(n,t)α. The structure observed in recent ^{6}Li(n,t)α differential cross section measurements[4] for 2 MeV $\leq E_n \leq$ 4 MeV and the mechanism of the large ^{6}Li(n,d) cross section have been investigated in terms of the level structure of the ^{7}Li system.

4. Structure of ^{8}Li for an R-Matrix Analysis of ^{7}Li+n Scattering and Reactions.† (H.D. Knox and R.O. Lane)

An earlier R-matrix analysis[5] of ^{7}Li+n scattering and reactions has been revised for the region of incident neutron energies below 4 MeV. In this new study spectroscopic factors and excitation energies for states in ^{8}Li obtained directly from model calculations[2,3] were used as initial values of the R-matrix parameters in the fitting process. The final parameter set provides good fits to all existing experimental ^{7}Li+n data in this energy region. Comparison of the model calculation predictions with the R-matrix analysis results are being made.

---

† Work supported by the U.S. Department of Energy.

1 H.D. Knox and R.O. Lane, Nucl. Phys. A403, 205 (1983).

2 N. Kumar, Nucl. Phys. A225, 221 (1974).

3 A. Aswad, H.R. Kissener, H.U. Jager and R.A. Eramzhian, Nucl. Phys. A208, 61 (1973).

4 H.D. Knox, G. Randers-Pehrson, P. Koehler, D. Resler, R.O. Lane and B. Rodricks, Bull. Amer. Phys. Soc. 27, 732 (1983); and H. Conde, private communication.

5 H.D. Knox and R.O. Lane, Nucl. Phys. A359, 131 (1981).

5. Coupled Channel Analysis of Neutron Scattering from the 0^+, 2^+, 0_2^+, 3^-, 1^-, 4^+ States of ^{12}C in the Energy Range 20-26 MeV.†
(A.S. Meigooni, J.S. Petler, R.W. Finlay and J.P. Delaroche††)

The analysis of neutron elastic and inelastic scattering from highly deformed nuclei such as ^{12}C requires a deformed optical model potential and coupling between the different states. The 0^+ (g.s.), 2^+ (4.4), 4^+ (14.08) can be described by a rotational model; however, the suggested octupole vibration does not adequately fit the 3^- (9.6) data nor does a β-vibration predict the measured 0_2^+ (7.6) cross section. In order to fully describe the differential cross sections for all these states, form factors must be introduced into ECIS79 externally.

6. Microscopic Optical Model Analyses of Nucleon Elastic Scattering from $^{12,13}C$.††† (J.S. Petler, R.W. Finlay, A.S. Meigooni, S.H. Mellema and F.S. Dietrich +)

Differential neutron and proton elastic scattering from $^{12,13}C$ in the energy region 20-60 MeV has been analyzed using two different microscopic optical models.[1,2] The nuclear matter approach of Jeukenne et al. provides a consistent representation of the differential, total and reaction cross sections if the imaginary potential is reduced by $\sim$ 15%. The Brieva-Rook folding model systematically overpredicts the elastic scattering cross section. RMS radii and volume integrals per nucleon are compared with the results of phenomenological S.O.M. and coupled-channels calculations.

---

† Work supported by Grant Number CA25193 awarded by the National Cancer Institute, DHHS.

†† Present address: Centre d'Etudes de Bruyeres-Le-Chatel, France.

††† Support by PHS Grant Number CA25193 awarded by the National Cancer Institute, DHHS and National Science Foundation Grant Number PHY-8108456.

+ Present address: Lawrence Livermore National Laboratory, Livermore, CA.

1 J.-P. Jeukenne, A. Lejeune and C. Mahaux, Phys. Rev. C16, 80 (1977).

2 F.A. Brieva and J.R. Rook, Nucl. Phys. A291, 299 (1977).

7. States in ^{19}O from Measurement and R-Matrix Analysis of $\sigma(\theta)$ for $^{18}O(n,n)^{18}O$ and $^{18}O(n,n')^{18}O^*$ (1.98 MeV).† (P.E. Koehler, D.A. Resler, H.D. Knox, R.O. Lane and G.F. Auchampaugh††)

New differential elastic and inelastic cross section data[1] at 42 energies for $5 \lesssim E_n \lesssim 7.5$ MeV ($8.7 \lesssim E_n \lesssim 11$ MeV) have been analyzed using a multilevel multichannel R-matrix program to determine J, π, E_λ, and $\gamma_{\lambda c}$ for states in ^{19}O. Previous to the present analysis virtually nothing was known about the energy levels of ^{19}O in this excitation region. Even though the structure evident in the cross sections is very complicated at these energies, the R-matrix calculations fit the data well and several new J^π assignments have been made. Prominent among these are four $7/2^-$ levels at E_x = 9.6, 9.8, 10.2 and 10.7 MeV. The implications of these new assignments on the structure of ^{19}O are being investigated.

8. Microscopic DWBA Analysis of Fast Neutron Inelastic Scattering from ^{54}Fe and ^{56}Fe.††† (S. Mellema, R.W. Finlay and F.S. Dietrich+)

Inelastic differential cross section data for neutron scattering on ^{56}Fe at 11 and 26 MeV and on ^{54}Fe at 11, 20, 22 and 26 MeV have been taken using the new, high resolution beam-swinger time-of-flight spectrometer at Ohio University. DWBA analysis of low lying quadrupole and octupole states has been carried out using form factors generated microscopically from a density dependent effective interaction as well as entrance and exit channel wave functions calculated consistently from the same effective interaction and a local density approximation. Analysis has been extended to proton inelastic scattering data in the same energy region in order to examine the isovector nature of the various transitions.

---

† Work supported by the U.S. Department of Energy.

†† Present address: Los Alamos National Laboratory, Los Alamos, NM.

††† Work supported by the National Science Foundation and by the Department of Energy, W-7405-Eng-48.

+ Present address: Lawrence Livermore National Laboratory, Livermore, CA.

1 P. Koehler, D. Resler, H. Knox, R. Lane and G. Auchampaugh, Bull. Amer. Phys. Soc. 28, 984 (1983).

9. Inelastic Nucleon Scattering from Nuclei with Two Open Shells.† (R.W. Finlay, R.G. Kurup††, J. Rapaport and J.P. Delaroche†††)

Differential cross sections for elastic and inelastic scattering of 8 and 10 MeV neutrons from ^{76,80}Se have been measured and analyzed in a coupled-channel framework. Several collective models for the levels of the Se nuclei were tested. Deformation parameters were extracted for the first 2^+ and 3^- state in each nucleus and compared with similar quantities obtained from (p,p′) and Coulomb excitation measurements. A similar study of 11 MeV neutron scattering from ^{92,96,98,100}Mo has been carried out. Systematic trends in the values of the deformation parameters and isovector potential strengths have been studied.

10. An Optical Model Analysis of Neutron Scattering from ^{208}Pb and ^{209}Bi for $E_n < 7.0$ MeV.+ (J.R.M. Annand, R.W. Finlay and F.S. Dietrich++)

A phenomenological optical model analysis is made of neutron elastic and inelastic scattering data, for the nuclei ^{208}Pb and ^{209}Bi, taken at the Ohio University beam swinger facility, in the energy range 4-7 MeV. At these energies, compound nucleus effects are significant and are calculated using Hauser-Feshbach theory with width fluctuation correction. Various methods of calculating the latter are compared. The potential geometry produced differs significantly from that produced in higher energy analyses. Reduction of the energy dependence of the geometrical parameters by introduction of an energy dependent, real, surface peaked, potential well, predicted in optical potential dispersion relation calculations, is tested. In addition to the phenomenological analysis, calculations are made using microscopic folding models to investigate their applicability at low energy.

---

† Work supported by the National Science Foundation Grant PHY-8108456.

†† Present address: M.D. Anderson Hospital and Tumor Institute, Texas Medical Center, Houston, TX.

††† Present address: Centre d'Etudes de Bruyeres-Le-Chatel, France.

+ Funded by National Science Foundation Grant PHY-8108456 and Department of Energy Contract W-7405-Eng-48.

++ Present address: Lawrence Livermore National Laboratory, Livermore, CA.

11. An Optical Model Analysis of n+^{208}Pb Elastic Scattering at Energies 7-50 MeV.† (R.W. Finlay, J.R.M. Annand, T.S. Cheema††, J. Rapaport and F.S. Dietrich†††)

A phenomenological optical model analysis of neutron elastic scattering from ^{208}Pb at incident energies 7-50 MeV has been studied. The analysis is based on differential cross sections, analyzing powers and total cross sections. Using a conventional parameterization of the scattering potential, with a combination of volume and surface absorption above 11 MeV and surface only below 11 MeV, a good overall description of the data is achieved. Apart from the spin-orbit component, which is assumed real and energy independent, potential well depths are taken to be linear with energy and a geometry independent of energy is assumed. Possible improvement resulting from inclusion of a real surface peaked component or an imaginary spin-orbit component in the potential has been examined.

C. INSTRUMENTS AND METHODS

1. A Facility for Studying Neutron-Induced Charged Particle Reactions.+ (D. Wang, R. Alarcon, J. Annand and J. Rapaport)

A pulsed neutron facility used in the study of neutron induced charged particle reactions has been implemented. Monoenergetic neutrons in the energy range 20-26 MeV are produced via the T(d,n)^{4}He reaction with a subnanosecond pulse width. An evacuated neutron collimator cavity is embedded in a 80 cm concrete wall along the direction of the neutron beam. The measured neutron beam profile at the target location has been measured. The telescope detector system is mounted in a specially designed scattering chamber and can be rotated between 0° and 90°. The ΔE and E detector are fast plastic scintillators, 1 mm and 4 mm respectively. Proton and deuteron spectra at E_n = 25 MeV from (n,p) and (n,d) reaction on ^{6}Li, ^{27}Al and CH_2 have been obtained.

---

† Funded by National Science Foundation Grant PHY-8108456 and Department of Energy Contract W-7405-Eng-48.

†† Present address: Punjab University, Chandiagarh, India.

††† Present address: Lawrence Livermore National Laboratory, Livermore, CA.

+ Supported by the National Science Foundation.

2. Development of a Spectrometer for (n,z) Reaction Studies.† (M. Ahmad, S.L. Graham, S.M. Grimes and H. Narayan)

We have developed a new spectrometer for the study of (n,z) reactions. It consists of a 17 cm diameter plastic scintillator (E detector) at the end of a 2 m flight path. A proportional counter near the target serves as the ΔE counter. The background in the spectrometer is reduced by using a pulsed beam and demanding that the time-of-flight of the particle be consistent with the energy inferred from the E counter.

3. Time Resolved Microdosimetry at $E_n > 20$ MeV with a Graphite Proportional Counter.†† (J.S. Petler, R.W. Finlay, G. Randers-Pehrson†††, and J.F. Dicello+)

The radiation quality of neutron radiotherapy beams is often determined by measuring event-size spectra with tissue equivalent proportional counters. One of the major uncertainties when comparing theoretical calculations with experimental spectra is the neutron-carbon interaction. Also, at energies above 21.5 MeV there is not source of truly monoenergetic neutrons. We have designed and built a graphite-walled proportional counter with excellent timing characteristics (2.5 nsec FWHM) which will enable us to use time-of-flight techniques to separate neutron groups of different energies and hence store only those events induced by neutrons with a specific energy.

4. Neutron Multiple Scattering Corrections Including Extensive Realistic Simulations of Inherent Experimental Conditions.† (P.E. Koehler)

An improved and more realistic method for the correction of neutron time-of-flight measurements for the effects of multiple scattering and finite geometry has been developed. Several important inherent experimental conditions which are often neglected or treated very approximately in previous techniques are more rigorously included in the present calculation. In particular, in the study of elastic and inelastic scattering of neutrons from samples of light nuclei in the form of chemical compounds, the energy spectrum of the neutron source, the time spreads of the source and detector, and finite sizes of the source and detector often lead to sizable corrections.

---

† Supported by the U.S. Department of Energy.

†† This investigation was supported by Grant Number CA25193, awarded by the National Cancer Institute, DHHS.

††† Present address: Columbia University Nevis Lab, Irvington, NY.

+ Present address: Clarkson College of Technology, Potsdam, NY.

For each detector position the computer program calculates time-of-flight spectra which agree well with those measured during the experiment. The calculated "measured" differential cross sections are also compared to the actual measured ones in a straightforward manner. Several examples demonstrating the importance of the above effects on the calculated time-of-flight spectra and differential cross sections are given.

The proper simulation of all the important experimental parameters make possible the confident measurement of new differential cross sections for cases such as deep inelastic scattering where the cross sections are usually small and the multiple scattering corrections related to the above effects are relatively large. Without such a method, certain important measurements might well not be performed because of the uncertainty regarding proper corrections caused by these added effects.

PACIFIC NORTHWEST LABORATORY

A. DELAYED NEUTRON STUDIES

1. Half-Lives and Emission Probabilities of Ga, Sr, Y, Ba and La Precursors (P. L. Reeder and R. A. Warner)

We have recently published measurements of half-lives and emission probabilities (P_n) for Sr and Y precursors at masses 97-99 and Ba and La precursors at masses 147-148.[1] These measurements are continuing at the TRISTAN on-line isotope separator facility at Brookhaven. The same techniques have been extended to mass chains 81, 100,101 and 149. Preliminary values for half-lives and P_n values are given in Table A-1.

TABLE A-1. Half-lives and P_n Values of Ga, Sr, Y, Ba, and La Precursors. Preliminary Results

Precursor	Half-life (s)	P_n (%)
^{81}Ga	1.23 ± 0.02[a]	32 ± 15
^{100}Sr	0.198 ± 0.004[b]	1.1 ± 0.1
^{101}Sr	0.13 ± 0.02[c]	3.1 ± 0.4
^{100}Y	0.71 ± 0.02[c]	1.3 ± 0.1
^{101}Y	0.5 ± 0.1[c]	2.0 ± 0.3
^{149}Ba	0.7 ± 0.3[c]	0.7 ± 0.2
^{149}La	1.2[d]	1.0 ± 0.3

[a] Measured from neutron decay.
[b] Measured from beta decay.
[c] Weighted average from neutron and beta decay.
[d] From Chart of the Nuclides.

2. Survey of Delayed Neutron Emission Probabilities (P. L. Reeder)

An invited talk with the above title was presented at the OECD/NEA Specialists' Meeting on "Yield and Decay Data of Fission Product Nuclides" held at Brookhaven National Laboratory on 24-27 October 1983. This paper will be published in the proceedings of this meeting.

[1] P. L. Reeder and R. A. Warner, Phys. Rev. C 28, 1740 (1983).

3. Distribution of Delayed Neutron Yields Versus Z, N, and A: Application to Proton Pairing in Fission Yields. (P. L. Reeder and R. A. Warner)

We have obtained the ENDF/B-V fission-yield data sets for 20 fissioning systems. We have also created a computer file of P_n values containing 74 measured values and 174 estimated values. With this total of 248 P_n values, we have mapped out the delayed neutron yield distribution for all the fissioning systems. These calculations show which precursors with unmeasured P_n values should have highest priority in future measurements. The six precursors with the highest estimated yields are ^{88}As, $^{100-103}$Y, and ^{137}Sb. Plots of delayed neutron yields versus proton, neutron, or mass number show effects due to nucleon pairing. By comparing calculated and total delayed neutron yields, we can estimate the proton pairing factor (even Z enhancement) to be used in fission yield models if we assume that the other parameters are well known. A paper on this work has been accepted for publication in Nuclear Science and Engineering.

4. Beta-Delayed Two-Neutron Emission (P. L. Reeder and R. A. Warner)

The radioactive decay process of beta-delayed two-neutron emission occurs for nuclides which are very neutron-rich. We have previously observed this decay mode in the fission product ^{98}Rb and are currently searching for other examples.[2]

The emission of two-neutrons may be a unique way to study neutron-neutron interactions on the outgoing neutrons. The "di-neutron" is not bound, but there may be correlations which alter the isotropic distributions expected if the two neutrons are emitted sequentially and independent of each other. We are presently measuring a coarse angular distribution for two-neutron emission by dividing our high-efficiency polyethylene moderated neutron counter into 4 quadrants and measuring in which quadrants the two-neutron events are located.

Preliminary data have been obtained on the average energy of the neutrons from the two-neutron process in ^{98}Rb decay. By use of a ring ratio technique, we measure an average energy of 100 ± 80 keV which is considerably smaller than the average energy of 480 ± 100 keV measured for the single neutron emission process.

B. INDEPENDENT ISOMER YIELD RATIO FOR ^{90}RB AND ^{138}CS (P. L. Reeder and R. A. Warner)

At the SOLAR on-line mass spectrometer facility which we operate at Washington State University, we are measuring isomer yield ratios for fission of ^{235}U with thermal neutrons. The mass spectrometer is tuned to the desired

---

2 P. L. Reeder, R. A. Warner, T. R. Yeh, R. E. Chrien, R. L. Gill, M. Shmid, H. I. Liou, and M. L. Stelts, Phys. Rev. Lett. 47, 483 (1981).

mass number. Fissions are induced by a burst of neutrons from the TRIGA reactor. Fission product ions are collected for a time interval very short compared to the decay half-life of the parent nuclide. For ^{90}Rb and ^{138}Cs, the half-lives of the isomers are long enough so that beta counting can be performed off-line in a low background environment. For these two cases, the yields from a single TRIGA pulse are sufficient to resolve the isomeric components in the beta decay curve. The ratio of initial activities of the ^{90}Rb isomers has been measured for ion collection times of 3 s down to 0.3 s. These short collection times are necessary because of the large contribution from decay of 32 s ^{90}Kr in the target/ion source. Preliminary analysis of our data gives an independent isomer yield ratio for ^{90}Rb which is more than twice the estimated value from Madlund and England's prescription.[3] Similar data have been obtained for ^{138}Cs. In this case, the isomeric transition is strong and the uncertainty in the isomeric transition branching ratio is an important factor. Analysis of these data is still in progress.

[3] D. Madlund and T. England, Nucl. Sci. Eng. 64, 859 (1977).

A = 5 - 10

This review has been published as Nuclear Physics A413 (1984) pp. 1-214.

A = 11, A = 12

Preprints of these two reviews have been sent out to 120 colleagues as PPP 3-83 (August 1983) and PPP 1-84 (February 1984). We plan to submit A = 11 - 12 to Nuclear Physics in July 1984 and to begin at that time the review of A = 13 - 15.

"Nuclear Spectroscopy"

Published in Physics Today (November 1983) pp. 26-32 by F. Ajzenberg-Selove and E. K. Warburton.

F. Ajzenberg-Selove and G. C. Marshall

A. NEUTRON PHYSICS

1. Helium Generation Cross Sections for 14.8-MeV Neutrons

(D. W. Kneff, B. M. Oliver, R. P. Skowronski, and Harry Farrar IV)

Neutron-induced helium generation is a major consideration in the development of materials for fusion reactor components. Rockwell International is engaged in two programs to measure total helium generation cross sections for fast neutrons. The Department of Energy's Office of Basic Energy Sciences (OBES) is sponsoring the measurement of the cross sections of a large range of separated isotopes and their associated pure elements for fast (8-15 MeV) monoenergetic neutrons. The Office of Fusion Energy is supporting cross section measurements of other fusion-related materials for ~14.8-MeV T(d,n) neutrons, plus helium generation cross section measurements in broad high-energy neutron spectra used for fusion materials irradiation testing.

The OBES cross section measurements are made by irradiating small (~10-50 mg) samples of a wide range of pure elements and separated isotopes in a nearly monoenergetic neutron spectrum. The amount of helium generated in each sample is subsequently measured by high-sensitivity gas mass spectrometry. The neutron fluence distribution for the irradiation volume is mapped using a comprehensive set of radiometric plus helium accumulation neutron dosimeters, and then combined with the helium generation measurements for multiple samples of each material to deduce cross sections. Absolute fluence normalization is based on the $^{93}Nb(n,2n)^{92m}Nb$ cross section; the fluence mapping is the dominant source of uncertainty (~5-8%) in the cross section measurements. Helium measurement uncertainties are typically ~1-3%.

Irradiations performed to date have utilized the ~14.8-MeV neutron spectra from the T(d,n) Rotating Target Neutron Sources-I and -II (RTNS-I,II) at the Lawrence Livermore National Laboratory (LLNL). Rockwell's previous 14.8-MeV cross section measurements have been summarized in part in earlier Reports to the DOE Nuclear Data Committee.[1-4] A detailed paper covering our 14.8-MeV measurements (26 elements and 22 isotopes), and providing a comprehensive survey of the helium-related cross section data

---

[1] Kneff, Oliver, Nakata, and Farrar, BNL-NCS-27800, p. 181 (1980)

[2] Kneff, Oliver, Nakata, and Farrar, BNL-NCS-29426, p. 155 (1981)

[3] Kneff, Oliver, Nakata, and Farrar, BNL-NCS-31052, p. 144 (1982)

[4] Kneff, Oliver, Skowronski, and Farrar, BNL-NCS-32614, p. 172 (1983)

available in the literature, has been completed and will be submitted shortly for publication in Nuclear Science and Engineering.

Since the last report, cross section measurements have been completed for ^{9}Be, O, Cr, ^{55}Mn, and Ag from RTNS-II, and for samples of ^{6}LiF, ^{7}LiF, ^{10}B, and ^{11}B previously irradiated in RTNS-I. The oxygen cross section was derived from multiple samples of Nb_2O_5 and PbO. The stoichiometries of these oxides (Nb_2O_5 and $PbO_{1.134}$) were determined from an independent series of Rockwell analyses comparing the helium generation in four oxide powders in a fast reactor neutron environment. Cross sections for ^{6}Li and ^{7}Li were derived from the ^{6}LiF and ^{7}LiF samples, which were selected for irradiation because of their well-known stoichiometries. The fluorine cross section was previously derived from irradiated samples of PbF_2; the stoichiometry of this compound has now been verified to be within 1% of the nominal value, based on DC plasma emission spectrometry and specific ion electrode analysis tests. The RTNS-I Li and B cross section results are consistent with our RTNS-II measurements.

The results of these cross section measurements are summarized in Table A-1. The reported values are weighted averages (based on the uncorrelated uncertainties) of the measurement results from RTNS-I and RTNS-II. Also included in this table are results from last year's work which have not been previously tabulated in the Reports to the DOE Nuclear Data Committee.

The LiF-derived ^{6}Li(n,total helium) cross section is significantly higher than current ENDF/B-V and ENDL evaluations. A new joint Rockwell-LLNL RTNS-I experiment was performed to resolve this discrepancy and to obtain a more precise value for the ^{7}Li(n,total helium) cross section. This experiment used lead-encapsulated ^{6}Li and ^{7}Li metal samples, developed with LLNL for another program. Preliminary results support the current ENDL evaluation for the ^{6}Li cross section, and indicate a significant (~10%) (n,2nd)α contribution to the ^{7}Li helium production cross section. Monte Carlo analyses of that experimental geometry (by E. Goldberg, LLNL) indicate the presence of a degraded neutron fluence component from inelastic scattering in the RTNS source and sample assemblies, in an energy region not readily covered by activation dosimetry (~1 keV-2 MeV). An estimated systematic uncertainty of 5% was correspondingly added to the ^{6}Li and ^{10}B measurements summarized in Table A-1, to reflect the possible contribution from the scattered neutrons in those experiments.

Initial construction of the new high-sensitivity constant-temperature sample furnace was completed since the last report, and was followed by a series of furnace tests using various materials with well-characterized helium concentrations. This furnace incorporates a liquid nickel bath for helium release by sample dissolution. Its purpose is to provide a more constant helium measurement background than can be achieved by sample vaporization, and to allow the analysis of larger samples with lower helium concentrations. The initial furnace tests indicated a need to modify the remote sample entry path; these changes are nearly complete.

Future work will utilize this furnace to analyze RTNS-irradiated materials with small (~1 mb) helium generation cross sections, and to extend our helium production measurements to new neutron energies.

TABLE A-1

Total Helium Generation Cross Sections
for ~14.8-MeV Neutrons

Material	Cross Section (mb)	Material	Cross Section (mb)
Li	407 ± 62 [a]	F	501 ± 36
^{6}Li	616 ± 105 [a]	Al	143 ± 7
^{7}Li	363 ± 55	Ti	38 ± 2
Be	1018 ± 83	Cr	34 ± 3
B	390 ± 32 [a]	Mn	28 ± 2
^{10}B	693 ± 84 [a]	Y	9.3 ± 0.7
^{11}B	306 ± 21	Ag	7.6 ± 0.6
C	894 ± 60	Ta	1.10 ± 0.09
O	401 ± 32		

[a] Includes estimated systematic uncertainty for degraded neutrons; see text.

TRIANGLE UNIVERSITIES NUCLEAR LABORATORY

A. NEUTRON CROSS SECTION EXPERIMENTS

1. Brief Overview (R. C. Byrd, J. Dave, C. E. Floyd, C. R. Gould, P. P. Guss, G. Honore, C. Howell, K. Murphy, H. Pfutzner, R. Pedroni, S. Singkarat,* L. W. Seagondollar, J. Templon, R. L. Walter, S. Whisnant, J. P. Delaroche**)

The neutron program at TUNL has been devised to provide elastic and inelastic scattering data in the 8-17 MeV energy range, a range of importance to the magnetic fusion energy program and a good range in which to test the energy dependence of direct interaction model parameters. During the past year data for many nuclei have been obtained, some improvements to the measuring system have been implemented, and a post-acceleration chopper for the pulsed ion beams is being developed. The first set of cross-section data taken with this new device was obtained at a neutron energy of 17 MeV.

An extension of the global models for the 1p-shell nuclei will be made as our new data for ^{14}N is put into final form. New TUNL data at 17 MeV for ^{9}Be will also be incorporated. A phase shift analysis for $^{12}C(n,n)$ from 9 to 12 MeV has been undertaken in cooperation with W. Tornow at Tübingen. Data for Aluminum were obtained from 10-17 MeV to provide a basis for an Al(n,n) optical model; this model will eventually incorporate a spin-spin interaction, the nature of which will depend on the size of the effects observed in the TUNL experiments involving the polarized Aluminum target and polarized neutrons. The interpretation of our earlier Silicon data has been enhanced by our new 17-MeV cross-section data; a parallel project for Sulfur is also underway. The new measurements for ^{40}Ca at 14 and 17 MeV will permit extended coupled-channels tests.

The status of the cross-section results for heavier nuclei is the following: Data sets for $^{54,56}Fe$ and $^{63,65}Cu$ for 8 to 14 MeV have been transmitted to the National Nuclear Data Center, and similar results for $^{58,60}Ni$, $^{116,120}Sn$ and ^{208}Pb will be mailed shortly. Experiments for ^{89}Y and ^{93}Nb have been completed from 8-17 MeV. Data for ^{58}Ni and ^{54}Fe at 17 MeV have been obtained but are not completely stripped yet.

---

* Permanent address: Chiang Mai University, Thailand

** Permanent address: Centre d'Etudes de Bruyeres-le-Chatel, France

Phenomenological analyses have been successfully pursued. Deformed optical-model calculations for Iron and Copper have been submitted for publication, and a paper is near completion for $^{58,60}Ni$. The $^{116,120}Sn$ deformed optical-model calculations are completed. Preliminary spherical optical models have been investigated for ^{89}Y, ^{93}Nb and ^{208}Pb.

The analyzing power $A_y(\theta)$ measurements (which complement $\sigma(\theta)$ information) have been proceeding at a constant pace. We now have $A_y(\theta)$ data at 10 and 14 MeV for many of the same nuclei mentioned above. The major experimental breakthrough is the capability to obtain moderately high resolution data at 17 MeV, and much of the past year has been spent accumulating high accuracy $A_y(\theta)$ data at this energy. The analyses of the $A_y(\theta)$ data are continuing to lead to surprising results, the latest being a demonstration of the need for a complex (V_{so} + iW_{so}) term for n + ^{208}Pb at our neutron energies.

The few-nucleon studies, conducted in collaboration with W. Tornow of Tübingen, were confined during the last period to a convincing measurement at 14 MeV which determined that the size of the differences between $A_y(\theta)$ for $^2H(n,n)^2H$ and $^2H(p,p)^2H$ is smaller than that very recently reported. The new results are now sufficiently accurate to obtain a measure of the (n,n) and (p,p) differences and also to permit a sensitive test for three-nucleon-system calculations.

2. Facility Changes

There have been two major changes in the facility since the last annual report. The first is the installation of a high-energy-beam chopper installed between the high-energy end of the tandem Van de Graaff accelerator and the first beam deflecting magnet. The system is discussed in detail in the 1983 TUNL annual report. Use of this chopper has resulted in the production of 1.2 ns wide deuteron pulses at the deuterium gas target. The second change involves the construction of a second set of shadowbars between the neutron scattering sample and the entrance to the collimators of our two massively-shielded neutron detectors. The purpose of the material (pieces of copper) is to reduce the background from neutrons that are scattered by air molecules on the far side of the scattering sample.

3. Studies in the 1p Shell Between 7 and 17 MeV

The work on the differential cross section for ^{16}O between 9 and 15 MeV has been published in Nuclear Science and Engineering, 82, 393 (1982).

Differential cross sections for the elastic scattering of neutrons of incident energies 11, 14, and 17 MeV from ^{14}N and ^{9}Be were measured during the spring of this year. Beryllium nitride was used as a scattering sample, and pure Beryllium scattering was measured and subtracted from the beryllium nitride data to obtain the Nitrogen scattering data. Typical Beryllium, beryllium nitride, and Nitrogen difference spectra at neutron energy E_{lab} = 14 MeV are shown in Fig. A3-1.

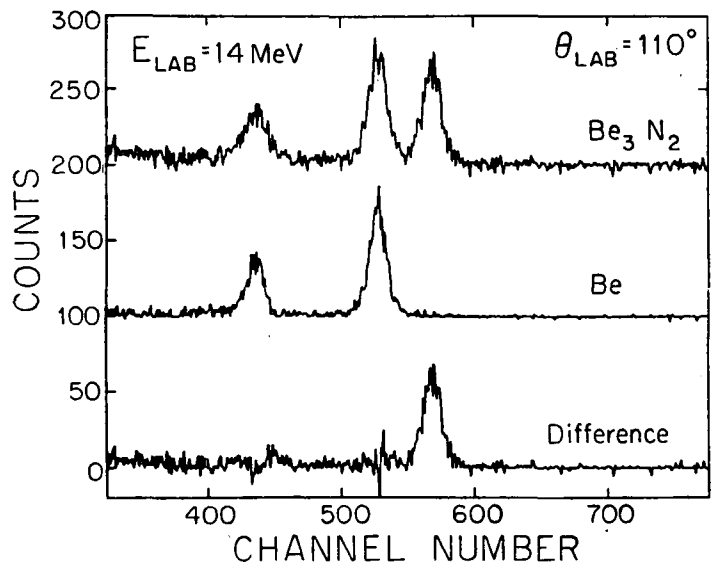

Fig. A3-1. Time-of-flight spectra at θ_{lab} = 110° and E_{lab} = 14 MeV. The nitrogen spectrum at the bottom is the difference of the two upper spectra.

The Beryllium data are already in final form. Measurements of both elastic scattering and inelastic scattering to the Q = -2.429 MeV state were obtained. The data at 11 and 14 MeV were used as a check on our previous measurements,[1] and the previously unavailable 17-MeV data have been used in Lane-consistent optical model parameterizations. The 11- and 14-MeV nitrogen data are also in final form; only uncorrected results are now available at 17 MeV. The corrected 11 MeV data are shown in Fig. A3-2 compared to the previous measurements of Bauer et al.[2] After the cross sections are in final form, optical model calculations will be performed.

---

1. H. H. Hogue et al., Nucl. Sci. Eng. 68, 38 (1978)
2. R. W. Bauer et al., Nucl. Phys. A93, 673 (1967)

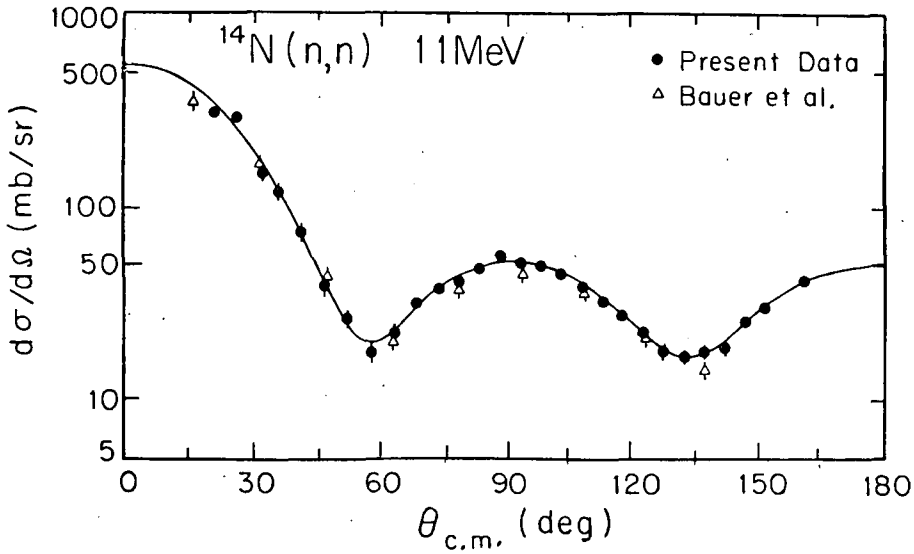

Fig. A3-2. Differential cross section for 11 MeV neutrons on ^{14}N.

The work on the optical model analysis of scattering of 7- to 15-MeV neutrons from 1p-shell nuclei has been accepted for publication in The Physical Review. Excerpts from the abstract follow:

"An optical model analysis of results from a program of neutron time-of-flight (TOF) measurements of elastic scattering from the 1p-shell nuclei is described.....Experimental methods and past results for neutron scattering from ^{6}Li, ^{7}Li, ^{9}Be, ^{10}B, ^{11}B, ^{12}C, ^{13}C, and ^{16}O are summarized.....Much of the neutron scattering data is well described by the spherical optical model (SOM), particularly for nuclei in which resonance structure is not prominent. However, SOM (available) parameters for heavier nuclei do not reproduce the data well. Parameter sets for the individual nuclei are presented along with the results of a global SOM search over 45 neutron scattering angular distributions for all 1p-shell nuclei. Volume integrals for the real and imaginary wells are compared to recent theoretical predictions. The SOM predictions for proton elastic scattering are compared to the available data for the T=0 nuclei. Coulomb correction terms to the real and imaginary potential well depths are investigated."

The final data from these experiments are available upon request from the National Nuclear Data Center and in two cases differ from our previously published results. Improvements in the multiple scattering codes were made after the ^{12}C data were originally reported and the new NNDC ^{12}C data set supersedes that published in Ref. 1. Also, the cross sections and Legendre polynomial coefficients for elastic scattering from ^{11}B are incorrectly interchanged in Ref. 2 for 9.69 and 9.96 MeV.

---

1. D. G. Glasgow et al., Nucl. Sci. Eng. 61, 521 (1976)
2. S. G. Glendinning et al., Nucl. Sci. Eng. 80, 256 (1982)

4. $^{27}Al(n,n)^{27}Al$ Cross Sections at 11, 14 and 17 MeV

Elastic and inelastic scattering angular distributions have been obtained for $^{27}Al(n,n)$ at 11, 14 and 17 MeV. The three inelastic groups for which yields were obtained are respectively the sum of the 0.84 and 1.01 MeV states, the 2.21 MeV state, and the sum of the 2.73, 2.98 and 3.00 MeV states. The angular distributions for 17 MeV are shown in Fig. A4-1. The lines are the results of Legendre polynomial fits to the data. The elastic scattering data have been used to extract optical model parameters. The inelastic scattering data have been successfully fit both via the excited-core and rotation-vibration models.

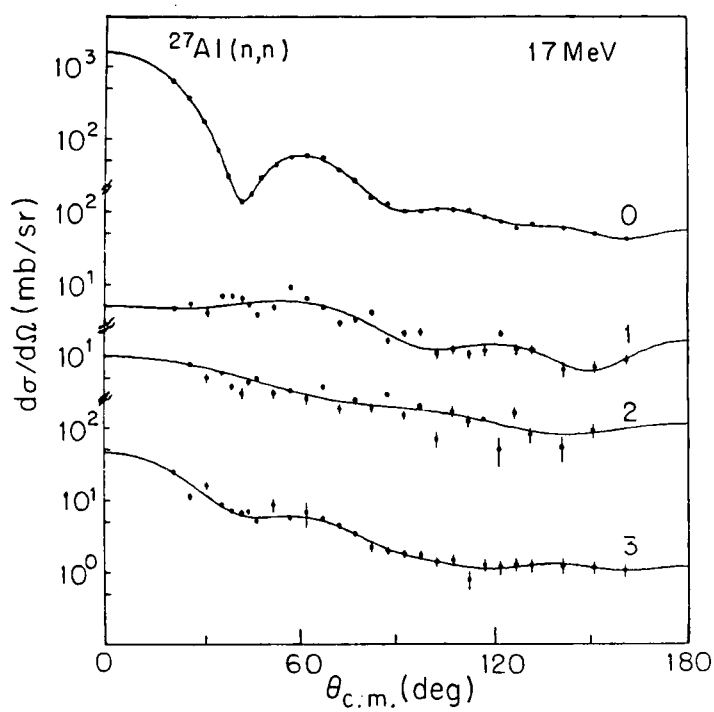

Fig. A4-1. Legendre polynomial fits to the 17 MeV angular distributions for neutron scattering from ^{27}Al.

5. ^{28}Si and ^{32}S Cross Sections

Cross-section measurements at 17 MeV have been added to our earlier data at 8, 10, 12 and 14 MeV for ^{28}Si and ^{32}S. Data for the ground state and first excited state have been stripped from the time-of-flight spectra. These data are being used in the coupled-channels (CC) calculations which are constrained to describe the $A_y(\theta)$ data from Section B. The goal is to obtain a model with a set of parameters which has a

smooth dependence on energy and which can be used to predict the $\sigma(\theta)$ for any neutron energy in the range from 8 to about 20 MeV. The Coulomb correction terms which connect (n,n) models to (p,p) models are also being studied. The nuclei ^{28}Si and ^{32}S, as well as ^{40}Ca mentioned below, are well-suited for this latter type of investigation as the asymmetry parameter $\varepsilon = (N-Z)/A$ is zero for these nuclei.

6. ^{40}Ca Cross Sections

The elastic scattering cross-section and analyzing power measurements for $^{40}Ca(n,n_0)$ at 9.9, 11.9 and 13.9 MeV have been published in Nuclear Physics A385, 373 (1982). This paper reports spherical optical model results and discussion of the Coulomb correction terms for (n,n) and (p,p) from ^{40}Ca. Also, ℓ-dependent potentials and Fourier-Bessel series description of the real central optical potential have been investigated and reported there. Additional measurements at 17 MeV have been made for (n,n_0) and at 14 MeV for (n,n') scattering for the first excited state. These data will complement the earlier analysis and, along with $A_y(\theta)$ data of Section B for $^{40}Ca(n,n')$, will provide the basis for a deformed optical model study.

7. Elastic and Inelastic Scattering from $^{54,56}Fe$ and $^{63,65}Cu$

The data and analyses of the 8 to 14 MeV $\sigma(\theta)$ for the isotopes $^{54,56}Fe$ and $^{63,65}Cu$ have been published in Nuclear Physics. An extension of the analysis which includes $A_y(\theta)$ data has been submitted to Physical Review. In order to make sure that the energy dependences of our models for ^{54}Fe have been properly characterized, we obtained additional data at 17 MeV. These new $\sigma(\theta)$ results have been put into final form and will be incorporated along with new $A_y(\theta)$ data at 17 MeV in the next stage of nuclear model studies. The 8 to 14 MeV $\sigma(\theta)$ data have been transmitted to the NNDC.

8. $^{58,60}Ni$ Cross Section

Results and analysis of $\sigma(\theta)$ for $^{58,60}Ni$ at 8, 10, 12 and 14 MeV for the ground and first excited states are being prepared for submission to Nuclear Physics. The analysis which involves $A_y(\theta)$ and $^{58,60}Ni(p,p)$ data, considers both a spherical optical model (SOM) and CC optical model. Additional (n,n) cross section data at 17 MeV have been obtained to test our model at this higher energy.

9. ^{89}Y and ^{93}Nb Cross Sections

Cross-section angular distributions for ^{89}Y and ^{93}Nb have been extended from the earlier set of 8, 10, 12 and 14 MeV to include results at 17 MeV. These data will be analyzed along with $A_y(\theta)$ using the spherical optical model. Some preliminary results suggest the need to include an imaginary spin-orbit term into the SOM for ^{89}Y in order to minimize chi-squared for the fit. Preliminary analysis of the 8 to 14 MeV data for ^{89}Y was shown at the Baltimore APS meeting.

10. $^{116,120}Sn$ Cross Section

The $\sigma(\theta)$ data at 10, 14 and 17 MeV for (n,n_0) and (n,n_1) for $^{116,120}Sn$ have been described in the Ph.D. thesis of Paul Guss. The $\sigma(\theta)$ data set will be complemented by new $A_y(\theta)$ measurements for ^{120}Sn at 17 MeV. A sample of the CC calculations for elastic and inelastic scattering from Tin were shown in the 1982 TUNL annual report, and a full description of the CC and SOM models is included in Guss' thesis. These $\sigma(\theta)$ results and the SOM and CC predictions are being prepared for publication.

11. ^{208}Pb Cross Section

As reported previously, we have been making SOM and CC calculations for ^{208}Pb from 10 to 17 MeV. The Mott-Schwinger calculations (and code) have been completed. A careful SOM study has led to the first evidence for the inclusion of a new spin-orbit term in models for neutron scattering. The abstract of a Brief Communication in Physical Review follows:

"The analyzing power $A_y(\theta)$ and differential cross section $\sigma(\theta)$ have been measured for elastic scattering of 10 MeV neutrons from ^{208}Pb. These data were analyzed with a spherical optical model which has a real spin-orbit potential with either a three-parameter conventional form or a one-parameter semi-microscopic form. The predictions with both spin-orbit potentials reproduce the data equally well, suggesting that fewer free parameters can be used in spherical optical model calculations. Including an imaginary spin-orbit term $W_{so}(r)$ in the optical potential greatly improves the fits to the $A_y(\theta)$ measurements and establishes the need for $W_{so}(r) \neq 0$ in the n + ^{208}Pb potential."

The energy dependent SOM analysis which spans 9 to 26 MeV is progressing well.

12. Monte Carlo Code EFFIGY

The multiple scattering codes for simulating neutron elastic scattering and inelastic scattering to discrete states (EFFIGY) has been fully documented. The code was exported to the neutron group at Ohio University and interaction with the OU group led to even more improved coding and documentation.

13. Neutron Elastic and Inelastic Scattering at Very Forward Angles (with R. E. Anderson, B. Carp, K. E. Nash)

A preliminary analysis of $\sigma(\theta)$ data obtained in the very-forward angular range from about 1.5^{o} to 9° has been made. Elastic scattering was studied for targets of Pb, Nb, C and Be, and inelastic to the first excited state for C and Be. To obtain the magnitude of $\sigma(\theta)$, the results are normalized to those for Pb. The angular range does not overlap with the region ($\theta < 1^{o}$) for which Mott-Schwinger scattering has a large effect on elastic scattering. No results were observed which could not be expected from standard nuclear models. Yet, this is the first "small-angle scattering" results available for inelastic scattering and the first elastic data at small angles for Nb. The Nb data will be included in the analysis disussed in Section A9 above. The size of the effort in the small angle scattering project has been small during the past nine months and no more $\sigma(\theta)$ measurements are planned for the immediate future. A progress report was given at the Baltimore APS meeting.

14. Detector Efficiency Calibration

The data for the relative efficiency of the main (4-meter and 6-meter) time-of-flight detectors which were obtained over a year ago have been analyzed. The measurement used $^{2}H(d,n)^{3}He$ reaction as a calibrated source of neutrons. For the high-energy region (9 MeV $< E_n <$ 18 MeV) an excitation function at 0° was measured in 200 keV steps for several simultaneous biases. For 2 MeV $< E_n <$ 9 MeV, an angular distribution with E_d = 6 MeV was obtained. A sample of the relative efficiency function for two biases (1 x Cs and 2 x Cs Compton edge) is shown in Fig. A14-1. It is hoped to compare these measured values to calculations with the efficiency code of G. Dietze of the PTB lab at Braunschweig, West Germany.

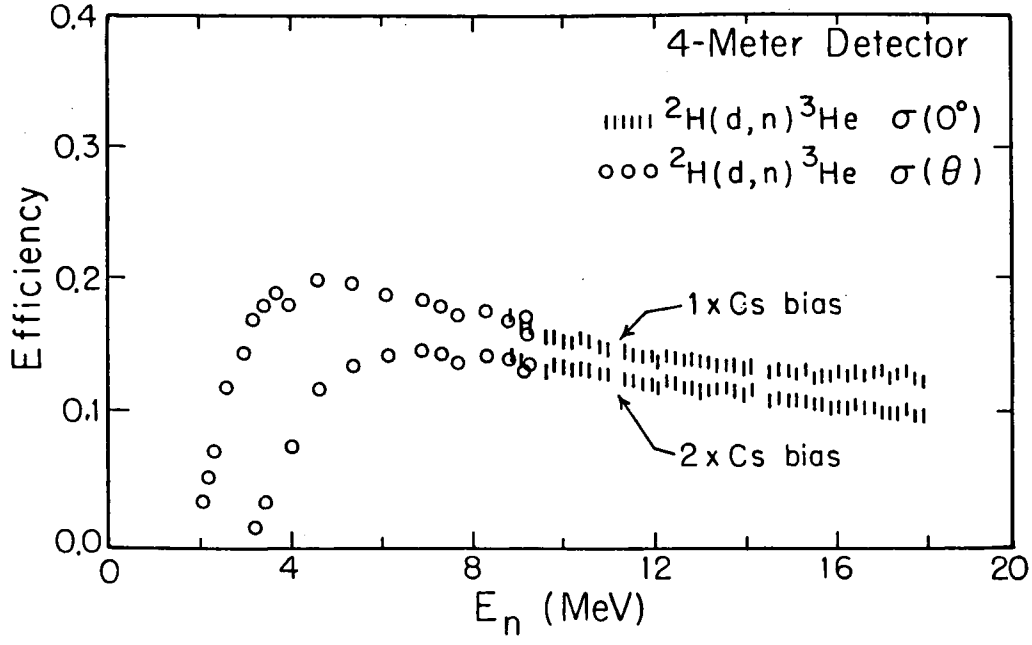

Fig. A14-1. Efficiency curves for biases of 1 and 2 times the pulse-height for the ^{137}Cs Compton edge.

B. NEUTRON POLARIZATION STUDIES

1. Overview (R. C. Byrd, J. P. Delaroche,[+] C. E. Floyd,[*] P. P. Guss,[**] G. M. Honore, C. R. Howell, K. Murphy, R. S. Pedroni, H. Pfutzner, M. Roberts, W. Tornow,[***] R. L. Walter)

Intimately tied to the usual neutron interaction cross sections are cross sections measured with incident polarized nucleons. The observables of this type that we have been interested in measuring are analyzing powers $A_y(\theta)$ and the various cross sections for polarized neutrons incident upon polarized targets. Some of the $A_y(\theta)$ data have been obtained for $(\vec{p},n)$ reactions, but most have been for $(\vec{n},n)$. In the latter case pulsed polarized neutrons are generated through the $^2H(\vec{d},\vec{n})^3He$ reaction at 0°, the reaction having been initiated with pulsed polarized deuterons. Time-of-flight techniques are used to measure both ground-state reactions as well as low-lying excited state reactions. The polarized target experiments which have just been initiated use the same nuclear reaction as the source of pulsed polarized neutrons.

Since the last report, new analyzing powers have been obtained for ^9Be, ^{12}C, ^{28}Si, ^{32}S, ^{40}Ca, ^{54}Fe, ^{58}Ni, ^{89}Y, ^{93}Nb and ^{120}Sn. For all these targets we have measured the complementary differential cross sections $\sigma(\theta)$. Much of the new data have been obtained at 17 MeV, our highest practical energy attainable at TUNL with the $^2H(\vec{d},\vec{n})^3He$ source reaction. We have also made the decision to obtain these data with the two TOF detectors at full flight path (4m and 6m) instead of the reduced path lengths used in our earlier measurements from 8 to 14 MeV. Use of the second shadow bar (Section A2) has greatly improved the cleanliness of our TOF spectra and our ability to measure $A_y(\theta)$ for $(\vec{n},n')$, the only such measurements ever conducted for medium-weight and heavy nuclei.

Analysis of the analyzing power data is leading to a better understanding of the spin-orbit interaction for the spherical as well as the deformed optical potentials. In addition, our Lane-consistent analysis of (n,n), (p,p) and (p,n) data is expected to give information on the isospin spin-orbit term, whereas the polarized target experiments will place limits on the spin-spin term. Our recent finding of the need for a W_{so} term (see Section A11) for neutron-nucleus scattering has introduced a

---

+ On leave from Service de Physique Neutronique et Nucleaire, Centre d'Etudes de Bruyeres-le-Chatel, France

* Now at the Dept. of Radiology, Duke University Medical Center, Durham, N. C.

** Now at the Dept. of Physics, College of William and Mary, Williamsburg, Virginia

*** On leave from the University of Tübingen, Tübingen, West Germany

complication into our analyses and caused a delay in the publishing of full reports of our studies. The global SOM code GENOA has now been modified to permit this W_{so} term to have a geometry-independent of V_{so}; this feature is important for obtaining the best fits to the $A_y(\theta)$ data (see Section A11). In another of our projects the Mott-Schwinger interaction which was incorporated into GENOA (in the Born Approximation) has been tested through an "exact" calculation using an optical model code written at TUNL in collaboration with R. Seyler of Ohio State, specifically for this purpose.

Multiple-scattering corrections to the data are important in the region of large $A_y(\theta)$ values and also in the region of the minima in $\sigma(\theta)$. For determining these corrections, the code JANE is employed. The documentation for this code has been greatly improved. Tests of the code for determining corrections in the first $\sigma(\theta)$ minimum for $^{28}Si(n,n)$ were made by measuring $A_y(\theta)$ in about 2° steps for two different source-to-scatterer geometries.

Although the polarization studies are important for neutron model development, specific details of the studies are not compatible with the purpose of the present report. A complete progress report on the studies is given in the TUNL annual report. Some of the most recent publications related to this work are listed below, however:

1. Analyzing Power and Differential Cross Section at 9.9, 11.9 and 13.9 MeV for $^{40}Ca(n,n)^{40}Ca$, Tornow, Woye, Mack, Floyd, Murphy, Guss, Wender, Byrd, Walter, Clegg and Leeb, Nucl. Phys. A385, 373 (1982)
2. The Analyzing Power for the $^2H(d,n)^3He_{g.s.}$ Reaction from 5.5 and 11.5 MeV, Guss, Murphy, Byrd, Floyd, Wender, Walter, Clegg and Wylie, Nucl. Phys. A395, 1 (1983)
3. Sensitivity of Neutron Scattering Properties to the Coupling to Giant Resonances, Delaroche, Guss, Floyd and Walter, Phys. Rev. C27, 2385 (1983)
4. Cross Section Measurement and Lane Model Analysis for the $^9Be(p,n)^9B$ Reaction, Byrd, Floyd, Guss, Murphy and Walter, Nucl. Phys. A399, 94 (1983)
5. The Analyzing Power $A_y(\theta)$ for $^{12}C(n,n_{0,1})^{12}C$ between 8.9 and 14.9 MeV Neutron Energy, Woye, Tornow, Mack, Floyd, Guss, Murphy, Byrd, Wender, Walter, Clegg and Wylie, Nucl. Phys. A394, 139 (1983)
6. Measurements of Analyzing Power for $^2H(n,n)^2H$ Scattering at 14.1 MeV and Comparisons to $^2H(p,p)^2H$, Tornow, Byrd, Howell, Pedroni and Walter, Phys. Rev. C27, 2439 (1983)
7. Comparison of Polarization and Analyzing Power for the $^9Be(p,n)^9B$ Reaction, Byrd, Lisowski, Tornow and Walter, Nucl. Phys. A404, 29 (1983)
8. Complex Spin-Orbit Potential for $^{208}Pb(n,n)^{208}Pb$ at 10 MeV, Delaroche, Floyd, Guss, Byrd, Murphy, Tungate and Walter, Phys. Rev. C28, 1410 (1983)
9. Spin-Orbit Potential Properties Derived from Measurements of Analyzing Powers for Neutron Scattering from ^{54}Fe and ^{65}Cu, Floyd, Guss, Byrd, Murphy, Walter and Delaroche, Phys. Rev. C28, 1498 (1983)

10. Comparison of Polarization and Analyzing Power for the $^{15}N(p,n)^{15}O$ Reaction, Byrd, Tornow, Lisowski, Murphy and Walter, Nucl. Phys. A410, 29 (1983)

A sample of the results of our combined cross-section and polarization program is given in Fig. B1-1.

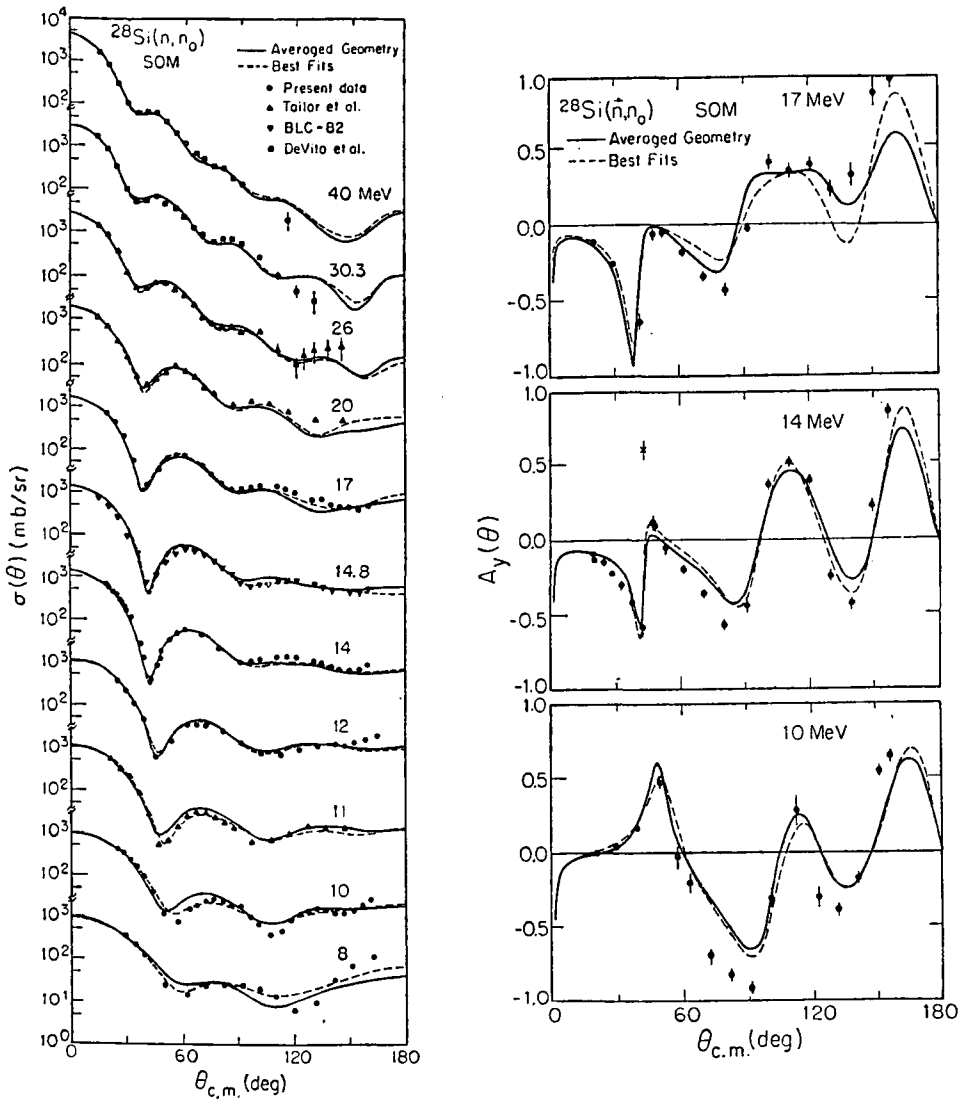

Fig. B1-1. Results of a spherical optical model parametrization for $^{28}Si(n,n_0)$.